ADVANCES IN PHYSICS, 2002, VOL. 51, NO. 6, 1379–1527

# Tube theory of entangled polymer dynamics

T. C. B. MCLEISH*

Polymer IRC, Department of Physics and Astronomy, University of Leeds, Leeds LS2 9JT, UK

[Received 1 November 2001; revised 29 April 2002; accepted 29 April 2002]

**Abstract**

The dynamics of entangled flexible polymers is dominated by physics general to many chemical systems. It is an appealing interdisciplinary field where experimental and theoretical physics can work closely with chemistry and chemical engineering. The role of topological interactions is particularly important, and has given rise to a successful theoretical framework: the 'tube model'. Progress over the last 30 years is reviewed in the light of specially-synthesized model materials, an increasing palette of experimental techniques, simulation and both linear and nonlinear rheological response. Our current understanding of a series of processes in entangled dynamics: 'reptation', 'contour length fluctuation' and 'constraint-release' are set in the context of remaining serious challenges. Especial attention is paid to the phenomena associated with polymers of complex topology or 'long chain branching'.

**Contents**



* e-mail: t.c.b.mcleish@leeds.ac.uk

*Advances in Physics* ISSN 0001–8732 print/ISSN 1460–6976 online 
http://www.tandf.co.uk/journals
DOI: 10.1080/0001873021015321 6

## 1. Introduction

The fascinating physics of flexible polymers flows from both necessity and beauty. Born of the rapid growth in synthetic polymer materials in the post-war years, the need to understand and control the processing of such highly viscoelastic liquids as polymer melts led rapidly to the fundamental investigations of Flory [1], and Stockmayer [2] and Edwards [3] building on work of Kuhn [4] (how large would macromolecules, linear or branched, be?), and Zimm [5] and Rouse [6] (how would such giant molecules move?). These pioneers were already using a beautiful notion that was to take hold of condensed-matter physics in the mid 20th century—that of *universality*, or the independence of physical phenomena from local, small-scale details. The emergence of universal properties is usually associated with 'critical phenomena' [7], since near phase transitions, the spatial scale of correlated fluctuations may hugely exceed molecular dimensions. Any properties that depend on these fluctuations (an example would be compressibility of a fluid near its critical point, and especially the *exponent* with which it vanishes as the temperature tends to

its critical value) will then be insensitive to molecular detail. In field theories of both condensed and high-energy matter, the field-fluctuations 'renormalize' microscopic constants into new emergent numbers on which the physics at coarser length scales (or lower energies) may be built (a famous example is the charge of the electron). Although there is at first glance no apparent neighbouring critical point in the case of polymeric fluids, both universality in exponents and renormalized quantities appear in abundance. Moreover, there is a natural large number associated with mesoscopic, rather than microscopic lengthscales. The defining feature of a polymer is, after all, its large 'degree of polymerization', $N$, the number of monomers linked together covalently to form the polymer chain. (The literature discusses interchangeably $N$ and the *molecular weight* $M$ of the chains, given in terms of the monomer molecular weight $m_0$ by $M = Nm_0$). At the most basic level of inquiry into polymer structure, experiments and simulations asking how the average end-to-end distance $R$ of a polymer molecule in solution depends on its degree of polymerization $N$, began to suggest a universal scaling behaviour

$$R \sim N^{\nu}, \tag{1}$$

with a 'Flory exponent' $\nu$ rather larger in solution $(\simeq 0.59)$ than the simple random walk value of 0.5 [8]. More phenomena reminiscent of other areas of condensed matter appeared at the level of many-body effects. In the dense limit of polymer melts and concentrated solutions, where chains are highly overlapped, the exponent $\nu$ reassumes the value of 1/2 of the ideal Gaussian random walk ('Gaussian' because the ensemble of spatial end-to-end vectors of the polymer chains is normally distributed). Closer inspection revealed this to be true above a 'screening length', introduced into polymer physics by Edwards [9]. The screening length $\xi$ itself may be directly measured by neutron scattering, and depends on concentration via another universal scaling exponent, related to $\nu$ [10]

$$\xi \sim c^{(-\nu)/(3\nu-1)}. \tag{2}$$

The picture we have build up so far is summarized in figure 1, where atomic detail at the monomer level is far below the resolution of the diagram. As the polymer concentration increases, so the screening length or 'mesh size' decreases. A typical strand of chain, whose end-to-end distance is $\xi$, dominates the monomer concentra-

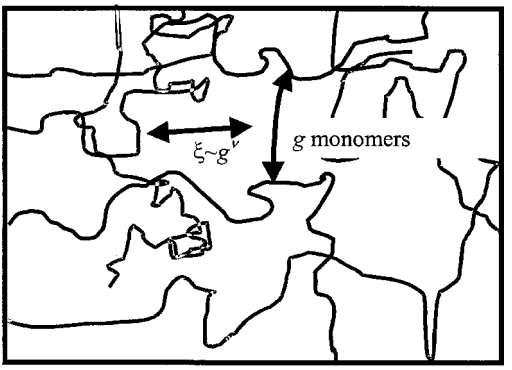


Figure 1. Schematic picture of universal structures of screening (overlap) length $\xi$ and the number of monomers $g$ that just spans $\xi$.

tion within the volume it spans. Both experimental and theoretical evidence of universality continued to build up. Even in the case of dynamics, the many-chain system of a polymer melt followed the ideal, local-dissipation theory of Rouse [5] (see below section 4.1.2) that assumed ideal Gaussian chains. It became clear that Rouse's result can be seen as a 'fixed point' of all theories of polymer dynamics in which linear connected objects are ideal and are subject to local dissipation (in dilute solution, far-field hydrodynamics destroys this locality [6]). For example, lattice models of polymer dynamics with local update rules renormalize to the continuum Rouse theory at large enough length scales [11].

It seemed as though the huge connectivity of macromolecules acts to freeze-in long-range order, even though there is no true thermodynamic transition nearby. Such suspicions were confirmed by the demonstration of direct isomorphisms of the calculation of statistical mechanical partition functions of polymers, both dilute and concentrated, onto idealized spin-lattice models of magnetism [8]. It is indeed the high molecular connectivity, as the inverse of the degree of polymerization, $N^{-1}$, that plays the part of proximity to the distance from a critical point in the spin model

$$N^{-1} \sim \epsilon \equiv \frac{T - T_c}{T_c}. \tag{3}$$

So by exhibiting physics in which an ensemble of macromolecules of polystyrene (PS) exhibits the same emergent behaviour as polyisoprene (PI) or polybutadiene (PB), following scaling laws, and tractable by application of statistical mechanical field theories [7], polymer physics drew together many of the strongest conceptual strands of the century.

More, however, has proved to be true in the realm of *topological* effects. The polymer melts of industrial polymer processing are very highly overlapped on the molecular level, where it becomes immediately apparent that molecular relaxation processes controlling elastic stress are prolonged to very long times indeed. All the important phenomenology is covered in Ferry's seminal survey of polymer viscoelasticity [12]. The central rheological experiment of stress-relaxation following a rapid step strain makes the point. For all high molecular weight flexible polymers in the melt state, the rubber-like elastic stress, $\sigma$, incurred on the step strain $\gamma$, first falls off rapidly, then is almost suspended at a 'plateau' level (defined by the material-dependent 'plateau modulus' $G_N^{(0)}$ defined in the usual way by $\sigma_{\text{plateau}}/\gamma$). At much longer times, increasing as a power of molecular weight substantially greater than 3, rapid relaxation resumes (see figure 2 for the form of this 'relaxation modulus' $G(t)$). Experiments restricted to the timescales of the plateau are hardly able to distinguish between the polymer melt and a rubber, in which the chains are permanently crosslinked to each other at very rare points, sufficiently for each chain to be permanently immobilized from large-scale diffusion. Conceptually, the absent 'crosslinks' were replaced in the minds of engineers and physicists alike by 'entanglements' [12]. These loosely-defined objects were assumed to represent the topological constraint that covalently-bonded molecular chains may not pass through each other. The effective distance between these objects could be calculated, employing rubber elasticity theory (see below), to deduce the degree of polymerization between entanglements $N_e$, or the equivalent 'entanglement molecular weight', $M_e$. The number $N_e$ consistently turned out to be of order $10^2$, indicating a length-scale for an 'entanglement spacing' of 50–100 Å, depending on the particular chemistry. This is highly significant for us, because it shows that small chains on

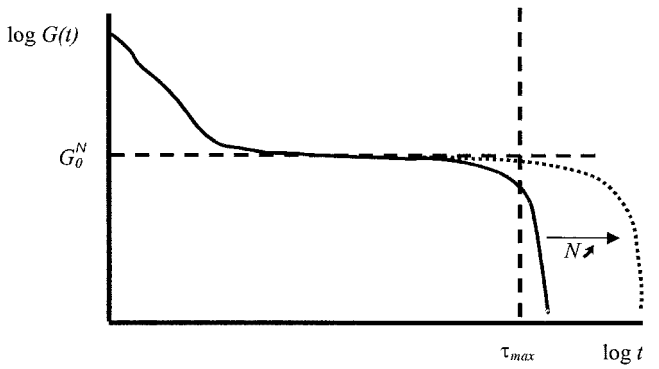


Figure 2. Stress relaxation of a polymer melt after a rapid, small, step strain. The dynamic modulus falls to a plateau value where it remains for a time $\tau_{\max} \sim N^{3.4}$.

the threshold of feeling topological interactions are real polymers, already long enough to show to a good approximation all the universal properties of statistical connected chains. It also suggests that the role of topology in highly-entangled $(N \gg N_e)$ polymer fluids has the potential to be treated universally. Further evidence of universality in entanglements came from experiments in which the polymers were diluted to a volume fraction $\phi_p$ by a compatible solvent. The apparent entanglement molecular weight $M_e \sim \phi_p^{-\alpha}$ where the scaling exponent $\alpha \simeq 1$ [10].

Other experiments had pointed to the existence of a topological feature at this coarse-grained scale of structure. Careful measurements on rubbers of controlled synthesis had shown that the shear modulus was higher for a network of long chains than a model incorporating crosslinks alone would predict [13]. Other 'trapped entanglements' on the same scale as the melt value of $N_e$ seemed to contribute to the elasticity. Advanced theories of rubber elasticity have been able to treat rubber networks in terms of the two distinct constraints of physical crosslinks and trapped entanglements [14, 15]. A second experimental approach, in the fluid phase, was the very natural one of investigating the dependence of melt viscosity $\eta$ (at fixed temperature) on molecular weight (or, more precisely, its weight-average, since almost no polymer sample is perfectly monodisperse). A remarkable universality emerged in accumulated experiments on very many different polymer chemistries [12]:

$$\left.\begin{array}{ll} \eta \sim M^1 & M < M_c \\ \eta \sim M^{3.4} & M > M_c. \end{array}\right\} \tag{4}$$

For each material, a critical molecular weight, $M_c$ emerged, above which the viscosity rises very steeply with molecular weight. Moreover, within experimental error, this explicitly dynamical observation was linked phenomenologically to the essentially static measurements of the plateau modulus by the correlation

$$M_c \simeq 2M_e. \tag{5}$$

This connection between essentially dynamic $(M_c)$ and static $(M_e)$ experiments, observed over a wide range of chemistries, is strong evidence that topological interactions dominate both the molecular dynamics and the viscoelasticity at the 10 nm scale in polymer melts (and at correspondingly larger scales for concentrated solutions).

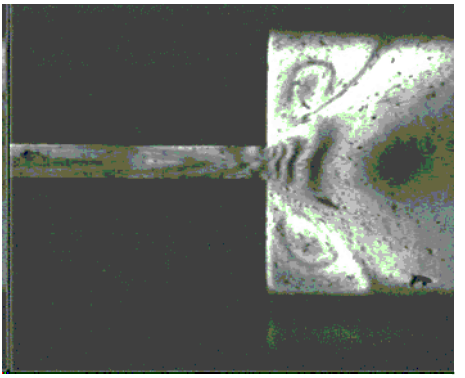

Figure 3. A branched Low Density Polyethylene melt flows into a contraction slit-flow from right to left, setting up large rotating vortices, in contrast to a melt of linear molecules. [Figure courtesy of P. D. Coates, University of Bradford.]

Without going beyond rheological measurements on bulk samples, there has long been other very strong evidence that molecular topology is the dominant physics in melt dynamics. This emerges from the phenomenology of 'long chain branched' (LCB) melts. These materials, commonly used in industry, possess identical molecular structure to their linear cousins on the local scale, but contain rare molecular branches. The density of branching varies from one branched carbon in every 10 000 to 1 in 1000. This level is chemically all but undetectable, yet the melt rheology is changed out of all recognition if the molecular weight is high enough [16]. Providing that $M \gg M_e$, the limiting low-shear viscosity may be much higher for the same molecular weight. Moreover in strong extensional flows (see section 3.3 below) the melt responds with a much higher apparent viscosity than in linear response. This phenomenon, vital for the stable processing properties of branched melts, is called 'extension hardening'. The effect is all the more remarkable because in shear flows, branched, as well as linear, melts exhibit a *lower* stress than would be predicted by a continuation of their linear response [17] (they are 'shear-thinning').

A fascinating example of the difference between linear and branched entangled melts is well known from flow-visualization experiments. Two polyethylenes with matched viscosities (and of course identical local chemistry) exhibit quite different flow-fields when driven from a larger into a smaller constriction (figure 3). The 'contraction flow' for the linear polymer resembles that of a Newtonian fluid, while that of the branched polymer sets up large vortices situated in the corners of the flow field. The understanding of a link between such differences in molecular structure and a macroscopic change in flow represents a considerable challenge, but no clearer evidence could point to the essential role of molecular topology. Slight changes to the topology of the molecules themselves give rise to qualitatively different features in the macroscopic fluid response.

Theoretical treatments of the dynamical slowing down beyond the entanglement scale have fallen into two classes. The first treats the physics as collective effects, without seeking to capture the topological nature of constraints explicitly. Starting with the Rouse theory, collective corrections introduced to the monomer mobility lead both to slowing down and to local anisotropy. An example is the approach of Williams and co-workers [18]. The second approach treats the entanglements

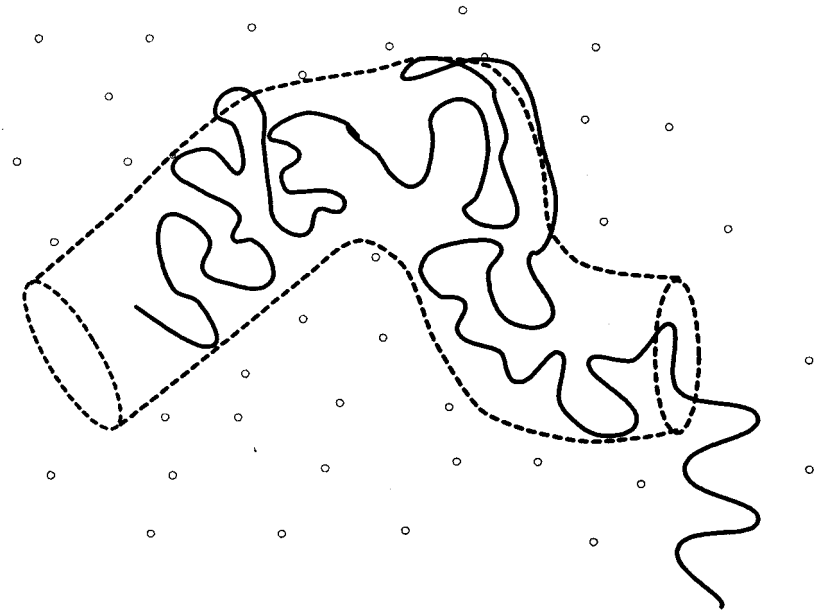

Figure 4. A tube-like region of constraint arises around any selected polymer chain in a melt due to the topological constraints of other chains (small circles) in its neighbourhood. [Diagram courtesy of R. Blackwell.]

phenomenologically, but as serious topological constraints. The most successful of these has been the *tube model*. The idea is to deploy the theoretical physicists' favourite strategy of replacing a difficult many-body problem with a tractable single-body problem in an effective field. In this case the 'single body' is the single polymer chain, and the effective field becomes a tube-like region of constraint along the contour of the chain. The tube is invoked to represent the sum of all topological non-crossing constraints active with neighbouring chains, and the tube radius, $a$, is of the order of the end-to-end length of a chain of molecular weight $M_e$. In this way, only chains of higher molecular weight than $M_e$ are strongly affected by the topological constraints (see figure 4). The tube was first invoked by Edwards [19] in an early model for the trapped entanglements in a rubber network. The consequences of the idea for dynamics were first explored by de Gennes [20], again in the context of networks. A free chain in a network would be trapped by the tube of radius $a$ defined by its own contour. This would suppress any motion perpendicular to the tube's local axis beyond a distance of $a$, but permit both local curvilinear chain motions and centre-of-mass diffusion along the tube. De Gennes coined the term 'reptation' for this snake-like wriggling of the chain under Brownian motion. The theory gives immediately a characteristic timescale for disengagement from the tube by curvilinear centre-of-mass diffusion. This disengagement time $\tau_d$ is naturally proportional to the cube of the molecular weight of the trapped chain (this arises from combining the Fickian law of diffusive displacement of length $L$ with time $\tau$, $\tau \sim L^2$, recognizing that path length $L \sim M$, with one extra power arising from the proportionality of the total drag to molecular weight). Very significantly, de Gennes also realized that a tube-like confining field would endow a dangling arm, fixed to the network at one

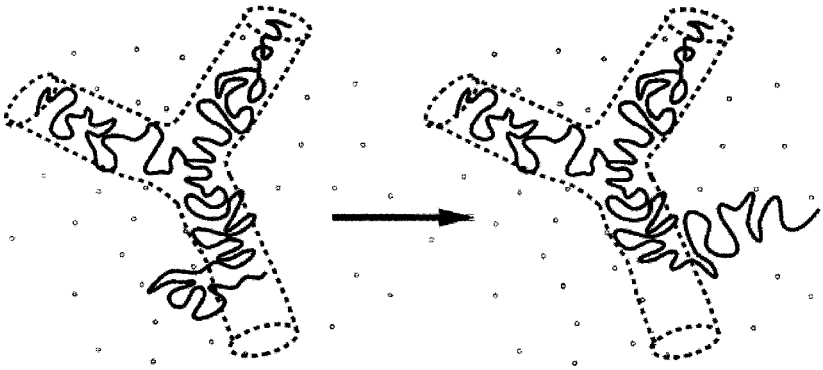

Figure 5. The process of arm retraction predicted by the tube model for the case of dangling entangled arms, as from the branch point of a star polymer. Unlike in reptation, reconfiguration of the outer parts of the arm occurs many times for one realxation of deeper segments.

end, or belonging to a star-shaped polymer in a network, with exponentially slow relaxations. In this topology reptation would be suppressed by the immobile branch point [21], and only exponentially-rare retractions of the dangling arm would disengage it from its original tube (see figure 5).

In the late 1970s, S. F. Edwards and M. Doi developed the tube concept into a theory of entangled melt dynamics and rheology for monodisperse, linear chains [22]. The work rapidly caught the attention of the community for a number of reasons. The first was that the underlying idea is so simple. The tube-field is much easier to conceptualize, and the approximation much clearer, than in approaches sometimes known as 'mode-coupling', in which the effective mean field is hidden in a dense forest of algebra. Secondly the tube-model made a parameter-free prediction for the most accessible nonlinear function of strain—the so-called 'damping function'. This is really an effective nonlinear shear modulus as a function of shear strain (see section 3.3 below). The prediction was in very good agreement with available data. Thirdly, Doi and Edwards were able, by making a mathematical approximation they called the 'independent alignment approximation' (IAA), to produce a *constitutive equation* in closed form of a recognizable type (see section 5.1.2). Rheologists had since the 1940s sought these general mathematical forms relating the local stress tensor of a viscoelastic liquid to its local strain history. Relations were written down using both differential and integral forms, using notions of frame-invariance and algebraic simplicity to constrain the huge space of nonlinear functionals that are possible [23]. The original Doi–Edwards formulation with the IAA took the form of an integral 'K-BKZ' equation [24, 25]:

$$\sigma(t) = \int_{-\infty}^{t} \mu(t - t')h(I_1, I_2)\mathbf{C}(t, t')\,\mathrm{d}t'. \tag{6}$$

where $\mathbf{C}(t, t')$ is the 'Cauchy' tensor-function of the strain between times $t'$ and $t$, with invariants $I_1$ and $I_2$, and $\mu(t)$ is a 'memory function', capturing the relaxation of stress after strain in a viscoelastic fluid [26] (the full K-BKZ form has a second term, but the essential structure is clear in equation (6)). This demonstrable connection from a non-trivial molecular model to an integral constitutive equation was an

important step in bringing the communities of physicists and chemical engineers closer together.

It is rather remarkable that the tube concept took such a hold in the following two decades in spite of some shortcomings of the early approximations that in retrospect are rather severe. The prediction that the viscosity $\eta \sim M^3$ rather than the observed $\eta \sim M^{3.4}$ was the mildest of them; in addition, the distribution of stress relaxation times in the response function $G(t)$ was much too sharp, and the prediction for steady shear flow inherently unstable. In strong shear, the model had all the confining tubes align in the flow direction, forcing unstretched chains within them to do the same, so that eventually the shear stress would *reduce* with increasing shear rate. That polymer melts do indeed exhibit instabilities resembling slip-flow kept this idea alive for a while [27], but it is now clear that polymer melts do not possess this constitutive non-monotonicity of response. The original suggestion that the way to handle polydispersity in chain length would be a linear superposition of response was seen to fail strongly as soon as experiments on controlled bimodal blends were performed [28]. Finally in early attempts to calculate the rheology of well controlled star polymer melts, rather large *ad hoc* changes were required to the tube model's dimensionless constants [29]. All along there remained a concern over even the validity of the tube in melts, even if it were accepted in the case of permanent networks. After all, in the melt the tubes themselves arise from constraints imposed by other chains which are also reptating. During the lifetime of a tube segment, therefore, some of the surrounding chains will typically release their contributing constraints by bringing one of their free ends into the tube segment's volume. This issue of self-consistency via 'constraint release' (CR) would require experiment, theory and simulation to sharpen, and is still an active issue at the time of writing (see section 4.2.5).

The period that has witnessed the experimental and theoretical examination of these and other important questions has also seen the publication of several extensive reviews of our subject (the situation prior to the development of the tube model is covered in an early review of Graessley [30]). Doi and Edwards' own book in 1986 [31] was usefully supplemented by a survey from Pearson [32] and a discussion of molecular topology by Klein [33]. A critical review of the developing experimental picture followed from Lodge and colleagues [34]. The status of linear and nonlinear response in 1996 was reported by Rubinstein and myself in the NATO ASI of that year [35] and with Milner we reviewed the special physics of branched molecules [36]. A still more recent review, that does more justice to the important Japanese literature than most and highlights the experimental and theoretical programme on dielectric spectroscopy, has been provided by Watanabe [37]. There are in addition a number of good introductory books for the researcher new to the field of molecular rheology, notably the classic texts from the Wisconsin school and colleagues [38] and the recent survey of complex fluids, including liquid crystal polymers and surfactant fluids, by Larson [39]. In the light of the above, the value of another review at this stage might be questioned. Yet, apart from the lack of discussion in the mainstream physics literature, which this review attempts to make good, the last three years have seen very rapid progress across an increasingly broad canvas of research. These advances are changing the quality and pace of the field and need to be considered together, rather than in isolation, as real bridges are built between the fundamental physics of entangled polymer fluids and actual industrial practice.

The first qualitative new feature is the explosive growth of experimental techniques able to probe polymer dynamics on the entanglement scale. No longer are we confined to the collective and macroscopic view of rheology, or even rheo-optical measurements [40, 41], but now have considerable accumulated data directly probing molecular motion from neutron spin-echo (NSE) [42–44] and nuclear magnetic resonance (NMR) data [46, 47, 48]. Dielectric spectroscopy is providing a complementary view of chain orientation dynamics to that of rheology, and small angle neutron scattering (SANS) of selectively deuterated material in quenched-flow experiments has started to reveal the nature of anisotropic structure on the lengthscale of the chain as a whole [49–51] under highly nonlinear response. Diffusion of polymers of varying architecture in different matrices is proving to be a sensitive test of co-operative relaxation of topology [52]. Dynamic light scattering as well as SANS on concentrated solutions has begun to test the consequences of theory for relaxation of composition fluctuations. This complements the information on chain orientation that tends to dominate the other molecular probes [53]. The efficacy of all these techniques is sharpened by the chemists' ability to synthesize monodisperse molecules of controlled architecture and deutero-labelling via anionic methods. The particular strengths of both the newer and older techniques is reviewed in section 3.

The second qualitative new feature of the last ten years has been the rise of the power of simulation. It is now possible to conduct molecular dynamics simulations of, for example, elastically connected Lennard–Jones polymers that contain 50 chains each of 10 000 monomers well into the regime in which entanglements dominate the dynamics [54], while a decade earlier the largest simulations feasible remained unentangled [55].

Thirdly, the growing quantity of data on branched molecules of controlled molecular weight and topology has provided severe tests of the tube concept at a level beyond that probed by linear chains [36]. The hierarchical nature of configurational relaxation at the molecular level in particular has been turned from speculation into orthodoxy. In the simplest case of entangled star polymers, the theory suggests that chains escape from their confining tubes not by reptation, which is suppressed by virtue of the immobile branch point, but by a process of *arm retraction*, present but largely eclipsed in the case of linear polymers (see figure 5). The effect on viscosity of replacing linear molecules with those of identical molecular weight, but of star topology, is striking: now

$$\eta \sim \exp\left[\nu(M_a/M_e)\right] \quad M_a > M_c \tag{7}$$

is the dominant form of the molecular weight dependence, rather than $\eta \sim M^{3.4}$, where $M_a$ is the molecular weight of the dangling *arm*.

Fourthly, as we have already hinted, the wealth of experimental and simulation data has sharpened the theoretical picture. Without exploding with new parameters, it has been possible to capture, in a single model, modes of entangled motion beyond pure reptation. In linear response *contour length fluctuation* (CLF, see section 4.2.4), the Brownian fluctuation of the length of the entanglement path through the melt, modifies early-time relaxation. Similarly, we anticipated that the process of *constraint release* (CR), by which the reptation of surrounding chains endows the tube constraints on a probe chain with finite lifetimes, contributes to the conformational relaxation of chains at longer times (section 4.2.5). Both the processes of CLF and CR contribute to the quantitative understanding of linear rheology, such that

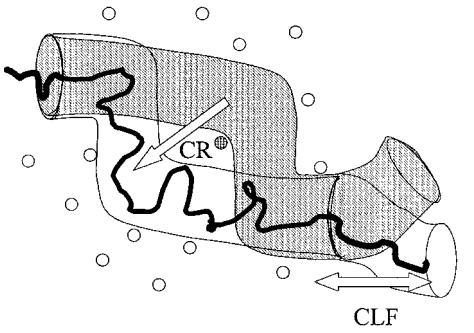


Figure 6. A cartoon of the processes of contour length fluctuation (CLF) and constraint release (CR) on a linear polymer in a constraining tube. In CLF the chain end retracts via longitudinal fluctuations of the entangled chain, but without requiring centre-of-mass (reptation) motion. Re-extension of the chain end may explore new topological constraints, reconfiguring the tube. In CR, an entanglement with neighbouring chains (shown hatched) may disappear, allowing effective conformational relaxation of that part of the tube, again without reptation of the test chain itself. In both cases the former tube configuration is shown dark, the new, light.

the $\eta \sim M^{3.4}$ law is no longer a mystery [56], but much of the newer data still need to be examined quantitatively as sensitive tests of the detailed physics, and many puzzles remain. We will refer to these processes continuously as we examine the potential of current experimental probes and theoretical treatments. For concreteness, they are visualized in figure 6. In strong deformations the additional processes of *chain stretch and retraction* (section 5.1) and *branch-point withdrawal* (section 5.2) emerge on the level of single chains (the latter exclusively in the branched case), and *convective constraint-release* (CCR) at the level of co-operative motion [57–59] (section 5.1.3).

Fifthly, a number of other theoretical frameworks have been proposed that do not invoke the tube concept directly [60–62]. Some of these are directly distinguishable in their predictions, others are not; but experimental groups producing new data have at times been in a quandary over which theory to compare with. Others begin with the tube idea, then make further approximations [63, 64]. Tools from dissipative hydrodynamics for discriminating at least between theoretical schemes that are thermodynamically permissible, and those that are not [65], have also been recently applied in the context of entangled polymeric fluids [66]. Although this review will focus on the tube model as the most developed case, we refer to other current approaches in the light of the new molecular-level data.

Sixthly, the fundamental work on entangled dynamics has progressed to such an extent that industry has begun to look intently at this programme of research to supply working tools in the development of new processes and products [67]. Activities range from using theory-interpreted rheology to deduce molecular weight distributions [68–70], to the identification of long chain branching (LCB) by rheological means [71], and even early attempts at prediction of extensional rheology in processing from models of the polymer synthesis [72]. Numerical solutions to the equations of motion derived for polymer melts are becoming an attractive industrial research tool.

Finally, the field has grown sufficiently in confidence for the serious debate of a number of new physical processes until now omitted from tube models.

Unsurprisingly, most of this conjectural ground lies in the domain of nonlinear response. As always the choice is between modifying the model and building an entirely new framework from scratch, but the tube approach has proved in the past to be a paradigm within which many second-order effects can be accommodated. A recurrent example is the question of local deformation of the tube-diameter in a bulk strain [73, 74]. Detailed considerations of local stress balance within topological interactions may be related to this idea [75]. The consequences of dropping of the assumption of high flexibility of all subchains has been explored by Morse in a series of papers reconstructing tube models for stiff polymers [76, 77]. Residual effects of local stiffness may go some way to explaining recent detections of *non-universality* in the path-length fluctuations of entangled chains, or equivalently in the relation between the transitional quantities $M_c$ and $M_e$ that we have already defined [78, 79]. These departures from universal behaviour are either worrying or interesting, depending on one's point of view, and are reviewed in a little more detail in section 6.5.

In this review, we aim to present the background necessary to understand the currently debated questions and provisional achievements. We will try to point out where to look for discriminating experiments and promising ideas. We first outline the molecular-coarse-grained paradigm that is assumed by almost every theoretical approach, based on the statistical mechanics of freely-jointed chains (section 2.1). This will provide us with a notational framework to review the particular strengths of current experimental techniques (including a well deserved mention—even for a physics journal—of some important chemistry). We present the Rouse model in modern notation at some depth since it recurs so frequently as a limiting theory (even the tube itself will become a Rouse object in advanced treatments of CR). The two classes of entangled dynamics: reptation in linear polymers (section 4.2.2) and arm retraction in branched polymers (section 4.3), then follow with applications to the linear response of systems with increasing topological complexity. The models are then extended to nonlinear response in shear and extensional flows (section 5.1), attempting to identify where current approximations work, and where they do not. We look briefly at some predicted consequences for complex flows (section 5.2.3), and finally revisit the question of fundamentals of tube theory and the origin of topological interactions.

Of course we shall also have to draw a line, however reluctantly and arbitrarily around the territory surveyed in this article. We shall be unable to treat the recent and remarkable advances in the cases of stiff, rather than flexible, chains and their application to liquid crystal polymers and biopolymers, for example. Nor can we treat at any depth the rich behaviour of polymer-like micellar systems and self-assembled polymers. Very likely these fields contain ideas that will prove essential to unravelling the problems currently presented by the case of flexible polymers, but that must be material for future reviews.

## 2. Polymers at the entanglement scale: the Gaussian chain

As we saw above, polymer physics in the fluid state is shaped by the notion of renormalization, or coarse-graining. Although it is possible to establish a formal mapping between the degree of polymerization, $N$, of a polymer chain, and the inverse distance $\epsilon^{-1}$ to a critical point in a spin-lattice model [8], it is just as easy to calculate directly correlation functions for connected chains possessing various local

rules for constraints and flexibility. One finds that, providing all interactions have finite range, chain statistics are indeed universal, becoming those of a random walk, up to a system-specific renormalization of the effective step-length for the walk [31]. This is the basis for the statistical mechanical theory of rubber elasticity [4, 13, 80], which we review briefly below. It will form the starting point for our review of the theory of *visco*elasticity and polymer dynamics. More importantly for the following section, it will provide us with a language in which to discuss the significance of experimental data at the molecular level.

Before going further, however, we should note nature's remarkable kindness in respect of the many-body problem of polymer melts. For it is of course manifestly untrue that all interactions between monomers of a chain are purely local—excluded volume constraints prevent simultaneous occupation of the same spatial volume by two monomers, no matter how far separated along a chain they might be! In dilute polymer solutions this long range interaction changes the correlations at all length scales; we say that the chains 'swell', changing the Flory exponent $\nu$ from 0.5 to 0.59. But in melts, polymer chains are highly overlapping (if the chains are random walks then the number of chains passing through the volume of gyration of a single one scales as $\sqrt{N}$). Two monomers in close contact, but not immediate covalently-bonded neighbours, are unlikely to be members of the same chain. The consequence is that chains become random walks once more, or equivalently that the long-range excluded volume interactions are *screened* [9]. The screening length, beyond which correlations are those of Gaussian chains, is of the order of the monomer dimension in the melt, but becomes larger in overlapping (or 'semidilute') solutions [10]. So models that renormalize the chemical detail of polymers into effective step lengths of random walks in Brownian motion will constitute an effective starting point for us.

Yet another difficulty might imperil the entire project in the case of entangled polymers. We already have the notion of topological interactions that dominate chain dynamics beyond a lengthscale (the tube diameter $a$) that also depends on the local polymer chemistry, but that are otherwise universal. This will only be true if the chains themselves are already long enough to be treated as random walks on the lengthscale $a$. A naïve expectation from the local structure in a melt fails this criterion miserably: the immediate topological constraints on a chain are only a monomer distance away on the neighbouring chains! However the tube arises (we shall return to this question at the end of the review), experiments tell us that the effective constraints on a segment of chain are happily far weaker than this. Sections of molecules that possess spans on a scale of the tube, or topological length $a$, are in practice already polymers. They have molecular weights of the order of the entanglement molecular weight $M_e$, defined above (and more formally in section 2.1.1). So a theory based on the dynamics and statistical mechanics of Gaussian random walks should still operate for entangled polymers. However, this is the least well controlled approximation of our approach, as it cannot be removed in the limit of large $N$. It may be expected to cause at least second-order difficulties. We will return to it later, in section 6.5.

### 2.1. *Statistical mechanics of polymer chains*

First we recap briefly the statistical physics of a polymer chain, modelled as a *random walk* in space and subject to some local rule for spatial links. An example is the freely jointed chain, in which the orientations of a set of linked rods are uncorrelated. The step length of the chain corresponds to the Kuhn length, $b$, of

the polymer (the shortest independently oriented segment length). It is not as small as a monomer length, but usually 4 or 5 monomers long.

For polymer statistics suppose the whole walk has $N$ links. Let the end to end displacement of an individual chain be $\mathbf{R}(N)$. From the theory of random walks: $\langle R^2(N)\rangle = Nb^2$ and $P(\mathbf{R})$ must have Gaussian form (from the law of large numbers, since each vector step is an independent random variable whose sum is $\mathbf{R}(N)$). So

$$P(\mathbf{R}) = \left(\frac{3}{2\pi Nb^2}\right)^{3/2} \exp\left(-3R^2/2Nb^2\right). \tag{8}$$

The macrostate of an ensemble of such chains is defined by the chain end-to-end vector $\mathbf{R}$. The microstates are the different specific paths through space that have $\mathbf{R}$ as their end-to-end displacement. Each individual path, or microstate of the chain, will be specified if the spatial position of each link is known. We will use the notation $\mathbf{R}(n)$ for the position of the $n$th link. The full time-dependence of the chain would then be described by the function $\mathbf{R}(n,t)$, extended to the two dependent variables of contour position $n$ and time $t$. The role of Brownian motion can be cast in the form of Langevin equations for $\mathbf{R}(n,t)$ (see the Rouse model, section 4.1.2), but here we exploit it as a generator of ergodic exploration of all chain configurations in the ensemble. The number of configurations with fixed end-to-end vector $\mathbf{R}$ is just the corresponding fraction of total microstates $\Omega(\mathbf{R}) = \Omega_{\text{tot}}P(\mathbf{R})$. Since the entropy of the walk $S = k_{\text{B}} \ln \Omega(\mathbf{R})$ we have $S(\mathbf{R}) = \text{const.} - 3k_{\text{B}}R^2/2Nb^2$. The conformational free energy of the chain $F(\mathbf{R}) = U - TS$ has $U = 0$ since there are no sources of internal energy. This yields for the free energy of a chain of fixed end-to-end vector $F(\mathbf{R}) = 3k_{\text{B}}TR^2/2Nb^2$. Finally we may derive the thermodynamic force (or 'Brownian tension') on the chain end-to-end vector as

$$f = -\nabla F(\mathbf{R}) = -\frac{3k_{\text{B}}T}{Nb^2}\mathbf{R} \tag{9}$$

and recognize a linear elastic spring law; i.e. a random walk polymer at finite $T$ is a Hookean spring with spring constant $\propto T/N$.

2.1.1. *Stress tensor*

Equation (9) will enable us to calculate the *stress tensor* and the *link orientation second moment tensor* in a dense polymeric fluid of flexible chains (where these two quantities are proportional) providing that the following conditions hold: (i) we know the instantaneous configuration of the chains at scales above some characteristic number $\tilde{N}$ of links, (ii) the configurations have achieved a *local* equilibrium for chain segments at smaller lengthscales than this, (iii) we may average over many subchains (of $\tilde{N}$ links) in a local volume large enough to define a macroscopic stress, but small enough to define uniform physical constraints on the polymer chains within it.

Recall that component $\sigma_{ij}$ of the stress tensor $\sigma$ counts the $i$th component of total force per unit area transmitted across a plane whose normal lies in the $j$th direction. Now consider a small cubic volume in a polymeric fluid of side length $L$ (figure 7).

It contains $\mathbb{C}/\tilde{N}$ subchains of length $\tilde{N}$, where $\mathbb{C}$ is the monomer concentration. The probability that one subchain of end-to-end vector $\mathbf{R}$ cuts a $j$-plane in the volume is just $R_j/L$ (the fraction of the sample length $L$ in the $j$-direction spanned by its end-to-end vector). The $i$th component of the force transmitted by this chain across the $j$-plane is, by equation (9), $3k_{\text{B}}TR_i/\tilde{N}b^2$. So the contribution to the total

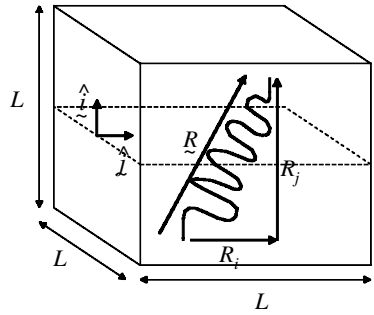


Figure 7. Contribution of a single chain segment to the stess tensor.

local stress from this subchain is $3k_BTR_iR_j/\tilde{N}b^2L^3$. The sum over all the strand segments may be replaced by the average $\langle \ldots \rangle$ over the ensemble multiplied by the number of subchains $\mathbb{C}L^3/\tilde{N}$, so that

$$\sigma_{ij} = \frac{3k_BT\mathbb{C}}{\tilde{N}^2b^2}\langle R_iR_j \rangle. \tag{10}$$

We will find it convenient to work with the continuous representation of the chains $\mathbf{R}(n,t)$ that maps the arclength position of the $n$th monomer onto its spatial position $\mathbf{R}$ at time $t$. Then we may replace $\mathbf{R}/\tilde{N}$ with $\tilde{N}\partial\mathbf{R}/\partial n$, bearing in mind that this notation implies a choice of subchain $\tilde{N}$ below which we do *not* take the usual limit of calculus (the Gaussian chain is formally non-differentiable in the limit $b \to 0; N^2b$ fixed). The formula for the stress tensor becomes the pleasingly simple

$$\sigma_{ij} = \frac{3k_BT}{b^2}\mathbb{C}\left\langle \frac{\partial R_i}{\partial n}\frac{\partial R_j}{\partial n} \right\rangle. \tag{11}$$

In polymeric fluids, this expression actually gives only the stress contribution from the polymer chain entropy; to make up the full stress tensor we add an isotropic pressure term. This is actually required in statistical mechanical theories of entropic elasticity to prevent the network of chains from collapsing—it arises physically from the incompressibility of the monomers. But this isotropic component of the stress does not couple to any of the coarse-grained degrees of freedom that concern us, and will not be measured by any of the rheological experiments we discuss below. Nor do we here treat other sources of stress that arise in the case of polymeric liquid crystals [31]. So, under these conditions for a coarse-grained ensemble of flexible polymers, the second moment average of equation (11) that governs the stress now needs to be calculated under appropriate assumptions for the dynamics. For example, it is sometimes possible to identify subchains containing $\tilde{N}$ monomers that have end-to-end distributions $P(\mathbf{r})$ fixed by external constraints (like a network when $\tilde{N}$ is the number of monomers between crosslinks) or by dynamics at a particular timescale (as in an entangled melt, when $\tilde{N}$ is the number of monomers between 'entanglements', $N_e$), but which are equilibrated at all smaller length scales. In this case the natural unit of arc length is the coarse-grained step length of the segments $\sqrt{\tilde{N}}b$. Writing $\delta nb = \delta s'\sqrt{\tilde{N}}$, the stress may be calculated from the known distribution of sub-chain vectors as:

$$\sigma_{ij} = 3k_B T \frac{\mathbb{C}}{N} \left\langle \frac{\partial r_i}{\partial s'} \frac{\partial r_j}{\partial s'} \right\rangle. \tag{12}$$

Each sub-chain contributes $k_B T$ of stress, distributed tensorially via the second moment of its orientation. The procedure we have sketched is equivalent to a 'virtual work' argument for the stress. In principle, polymeric fluids contribute both reactive and dissipative contributions to the stress, but unless the chains are very dilute, a regime that will not concern us, the former is greatly dominant and may be related directly to molecular configurations on the single chain level [31]. This result explains the joint definition of entanglement molecular weight, $M_e$ or $N_e$ and plateau modulus $G_N^{(0)}$ for, if the segments of chain deform affinely under small shear so that

$$\frac{\partial r_x}{\partial s'} \to \frac{\partial r_x}{\partial s'} + \gamma \frac{\partial r_y}{\partial s'},$$

the shear stress becomes just

$$\sigma_{xy} = k_B T \frac{\mathbb{C}}{N} \gamma,$$

and the shear modulus

$$G = k_B T \frac{\mathbb{C}}{N}, \tag{13}$$

where $N$ is the number of statistical segments in the subchain that remain unrelaxed after small-scale equilibration. In the case of entangled polymers, this can be attributed to an 'entanglement molecular weight', $M_e$ without any great specificity of theory, motivating finally the classical definition in terms of the melt density $\rho$ and plateau modulus of reference [12]:

$$G^{(0)}_{N,\text{Ferry}} = \frac{\rho RT}{M_e}. \tag{14}$$

However, we note here that an alternative definition, more informed by theory, has been suggested, allowing for the weaker constraints of an entanglement field when compared with real crosslinks [78]:

$$G^{(0)}_{N,\text{Graessley}} = \frac{4}{5} \frac{\rho RT}{M_e}. \tag{15}$$

We shall have more to say about definition of the plateau modulus in the following, and will strongly recommend the convention of equation (15) as it greatly simplifies the coefficients of many other expressions. This may also serve to remove the considerable confusion that has arisen in the literature from inconsistent use of either equation (14) or (15), and the inaccuracy of many measurements that has allowed the confusion to go unnoticed. We should also note that the two conventions (14) and (15) do contain a physical assumption, at least in the spirit of their link to rubber elasticity. The near-unity value of their coefficients favours the 'affine' model of rubber elasticity in which the crosslinks (here 'entanglements') deform affinely with the melt. This in turn is valid if the effective functionality of the entanglements (the number of chains that participate in it) is large. In networks of four-functional crosslinks, the fluctuations of the crosslink positions away from the affinely deformed positions would reduce the prefactor of the modulus by exactly 0.5 [81].

The self-similarity of the random Gaussian chains that constitute a polymer melt, and the arbitrariness of choice of lengthscale at which we label 'segments' ($\tilde{N}$ in

equation (12)) induces a choice of language to describe non-equilibrium states of the chain at lengthscales above and below the segment scale. Of course the *dynamical* differences in relaxation processes make the choice of $\tilde{N} = N_e$ appropriate (see below). However, once the segment scale is fixed, and the orientation distribution described at this lengthscale, any alignment of links at smaller lengthscales will be described as *chain stretch* [58], while at larger length scales it will be labelled *orientation*. This is because the description of orientation at the scale of $\tilde{N}$ invokes effective constraints on the Gaussian subchains at this scale also. As all internal degrees of freedom are relaxed, only the end-to-end vectors, or local stretch, remain. Nonlinear deformations will identify the role of the different dynamics of orientation and stretch induced by the presence of the tube-confining field at length scales beyond $N_e$.

2.1.2. *Dynamics*

In polymer solutions and melts the stress formula equation (12) above is always appropriate, given the validity of the three criteria above and the applicability of the Gaussian chain approximation. If suitable averages of the coarse-grained chain quantities $\mathbf{R}(n, t)$ are known, then not only the stress, but also other molecular quantities may be calculated. But there are important physical regimes in which the dynamics themselves differ qualitatively.

(i) *Unentangled chains* $(M < M_e)$. In the first regime topological interactions between chains are unimportant because the chains are not sufficiently overlapped. Note that this is the case even at remarkable degrees of *spatial* overlap: even in the melt, chains must be several hundred monomers long in order to see entanglement. The unentangled regime divides in to two subcases depending on whether or not long-range hydrodynamic interactions are important for the drag on the chains. If not (as in a melt) there is just local dissipation due to frictional forces as the chains slide past one another. Rouse [5] considered this simplest case as a model for dilute solution, but it actually finds its realization in low molecular weight melts! In solution the more complex issue of hydrodynamic interaction dominates. We will not deal with this regime in this review, but the relevant model was devized by Zimm [6] (see also references [31] and [38]). Here we will have a deeper reason for a thorough review of Rouse theory—it operates as the fundamental 'fixed-point' theory for all one-dimensional flexible, connected objects subject to local dissipation. Such a specification is met by the tubes of entangled melt theory themselves! In a self consistent picture, the conceptual tools of Rouse theory become essential not only for the 'bare' chains, but for their confining tubes as well. We consider some of the details below in section 4.1.2, but the central result is a longest 'Rouse-time' for configurational relaxation of the chain $\tau_R \sim N^2$.

(ii) *Entangled Chains* $(M > M_e)$: In this case the dissipation is local, on the scale of the entanglement spacing (whether in melt or concentrated solution, just as for Rouse chains above) but the chains' motion is severely restricted by the topological constraints of their surroundings—two chains may not cross each other. The mathematical formulation of the local drag needs to be supplemented by a model of the topological restrictions. This is the role of the *tube model* of Doi, Edwards and de Gennes (see below and reference [31]).

Chains with local (Rouse) friction are constrained at larger lengthscales by effective tube-like regions along their contours arising from the presence of other chains (see also figure 4) This regime also divides into two classes, but now depending on the topological structure of the chains themselves, i.e. whether they are linear or branched. Again we cover some details later, but note here that the dominant relaxation time is set by diffusive disengagment from the tube. This timescale $\tau_d \sim N^3$ for linear chains. The branched case offers a rich example of *hierarchical dynamics* in soft condensed matter [36], and produces exponentially slow disengagement times.

In the following experimental section we will see how various aspects of the polymer dynamics arise in the measured data, both microscopic and macroscopic. Labelled dynamic scattering experiments, for example, may measure a basic microscopic quantity: the average monomer displacement as a function of time $\phi_n(t) = \langle(\mathbf{R}(n,t) - \mathbf{R}(n,0)^2\rangle$ averaged over all chains. Some techniques average further over monomer positions, $n$, on the chains. Monomer displacement may be measured directly via NMR and neutron spin-echo in some circumstances, and by scattering indirectly. Collective diffusion emerges in the self-diffusion measurements of entire molecules. The most commonly measured macroscopic quantity is the linear rheological response $G(t)$ in the stress, and the components of its frequency-dependent Fourier transform $G'(\omega)$and $G''(\omega)$. We can see from the expression (12) for the stress, that these quantities are sensitive to the ensemble-average quantity

$$\left\langle \frac{\partial \mathbf{R}}{\partial n}\frac{\partial \mathbf{R}}{\partial n}\right\rangle.$$

So the coarse-grained description of the chain given by the stochastic chain paths $\mathbf{R}(n,t)$ and their averages may describe experimental observations. It is also a suitable language for theoretical development. In our review of tube theory in section 4 we will use an approach in which the Brownian motion is handled using a random thermal force on the chain monomers (a 'Langevin' equation) at the level of $\mathbf{R}(n,t)$. However, we will also find that in many cases it is possible to discuss the results up to prefactors using physical arguments that avoid detailed calculation.

## 3. Techniques and phenomenology

Focus on individual papers in the literature can lead to the conclusion that entangled polymer dynamics is a sub-field of rheology, or polymer processing, yet it has relied for its current level of achievement on a very wide range of techniques of materials preparation and analysis. It would simply not have been possible to build a molecular theory of entangled polymeric fluids on the basis of rheological measurements on semicontrolled industrial synthesis alone (it is quite remarkable how much had been deduced on a bulk of data harvested in this way, however, see for example the early discussion of long chain branching by Small [16]). To follow briefly an analogy, it is similarly possible to learn a lot about the outer planets by observing them optically through the Earth's murky atmosphere. But the ability to synthesize monodisperse, well controlled architectures in gram quantities, then to study them at both the molecular, nanoscale and bulk level in controlled conditions of deformation, is the equivalent in our field of the 'Voyager' missions to Jupiter and Saturn. In this section we first review briefly the polymerization techniques that have provided the clean materials that fuel current experimental developments. We then survey the

range of experimental methods that can now be brought to bear on the molecular–nanoscale–bulk chain of dynamic behaviour.

### 3.1. *Chemical synthesis of controlled topologies*

Nearly monodisperse (single molecular weight) polymers are a natural experimental requirement for molecular theories of polymer dynamics. As soon as substantial polydispersity is introduced, the number of variables also rises (think of the set of moments of the molecular weight distribution). Accurate values of the moments higher than the third are notoriously hard to acquire [82], even if a theory is sophisticated enough to account for them in a predictive way. It is far better to work with materials in which the polydispersity is reduced to a perturbative quantity. The breadth of the molecular weight distribution is usually summarized by the 'polydispersity index', $PI$, defined as the ratio of number-average and weight-average molecular weights. So in terms of the number distribution $f(M)$,

$$PI = \frac{M_w}{M_n} \equiv \frac{\int_0^\infty M^2 f(M)\,\mathrm{d}M}{\left(\int_0^\infty M f(M)\,\mathrm{d}M\right)^2}. \tag{16}$$

For a perfectly monodisperse material the $PI$ is 1. In the common 'free radical' polymerization route, every chain first begins growth, then chemically adds monomers until a random termination event fixes its molecular weight. Like all linear Markov processes (it is isomorphic to radioactive decay in time), the resulting distribution of chain lengths is exponential, giving a $PI$ of 2. Other polymerization processes, such as scission and 2-chain interactions, always broaden the distribution from this value. Industrial polyethylenes are common with $PI$s as high as 30. Even values of 2 would be ineffective tests for dynamical theories, since the lower molecular weights may act as unentangled solvent, and the occasional high molecular weight chains affect the elasticity of the melt out of proportion to their volume fraction. Fortunately, another family of polymerization methods, termed 'living polymerizations', is able to deliver much sharper distributions. In this 'batch' process, every chain begins growth on a single initiator molecule, then adds monomer onto a single 'living' end at a uniform mean rate until supplies are exhausted, or until the polymerization is quenched by addition of a terminator (which is sometimes a polar solvent such as methanol). Now the distribution is Poissonian, with very small normalized variance if the degree of polymerization is large. The most common version used to make model materials for experiment is anionic polymerization [83], indicating the charge on the living end. Polymers commonly prepared anionically are polystyrene (PS), polyisoprene (PI) and polybutadiene (PB), a useful series since they span a wide range of entanglement molecular weights ($M_e$ is 13 500, 4 500 and 1 600, respectively). Values of the $PI$ as low as 1.01 are routinely quoted, although in very clean polymerizations the true values may be even smaller, since this resolution is set by the separation columns used in characterization, rather then the intrinsic spread of molecular weights. Although it is not possible to prepare kilogram or tonne quantities of monodisperse material in this way, 10 g or even 100 g is possible, permitting even the relatively material-hungry measurements of nonlinear extensional flows to be attempted on model materials (see below).

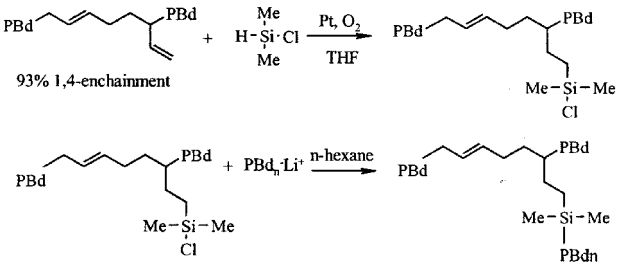


Figure 8. A reaction scheme for combs. Occasional pendant double bonds (vinyls) from anionically-polymerized PB are bound to chlorosilanes. These in turn act as coupling sites for separately synthesized arm material. [Coutesty of C. Ferneyhough [86].]

A word of caution is due on the use of $PI$ in very monodisperse materials, as the proximity to unity of these numbers can be deceiving. For narrow distributions of mean $M_w$ and standard deviation $\sigma_M$, equation (16) gives

$$PI \simeq 1 + \left(\frac{\sigma_M}{M_w}\right)^2, \tag{17}$$

so that $PI = 1.01$ still represents a 10% spread in the distribution. In the following we will therefore prefer to quantify polydispersity with the parameter $\epsilon$, defined so that $PI = 1 + \epsilon$. We shall see that there are slow dynamical processes, especially in branched polymers, that are very sensitive to polydispersities of even this magnitude.

The second great advantage of anionic methods is their ability to construct well-defined branched structures by controlled coupling reactions at the living chain ends. Chlorosilanes are typical coupling agents, with each living end (which hosts a metal ion from the initiator) reacting with a chlorine from the coupling molecule. Since it is possible to synthesize very complex chlorosilanes, many monodisperse chains may be joined to the same coupler, forming 'star' polymers of controlled functionality as high as 256 [84, 85]. More complex architectures may also be built from anionically-polymerized components. Starting with a difunctional initiator, two simultaneous chains will grow from the same point. The two living ends may then be chlorosilane-coupled to separately synthesized 'arms', to give the H-shaped structure that has been very significant in identifying the linear and nonlinear physics of branching [50]. As an illustration of what may be achieved, we give in figure 8 a reaction scheme for the synthesis of comb topologies from PB [86]. More complex architectures have been proposed and investigated, including 'pom-poms' [87] and arborescent polymers [88]. These will continue to set severe constraints on theoretical developments of the basic dynamical processes at the entanglement lengthscale.

More recently, serious attention has been paid to complex architectures of entangled polymers that are also polydisperse, but in a controlled and calculable way. If well entangled, monodisperse polymers are lightly crosslinked so that the links are truly uncorrelated, the resulting ensemble follows the statistical distribution of 'mean-field gelation' [89, 90]. Initially unentangled chains when crosslinked follow instead different 'percolation statistics' [90]. Both of these ensembles have power law polydispersity of the form

$$f(M) \sim M^{-\tau} f_c\left(\frac{M}{M_{max}}\right), \tag{18}$$

where $f_c(x)$ is a cut-off function at the maximum molecular weight of the ensemble. Recent rheological studies have followed both linear [91] and nonlinear [92] response of controlled randomly branched melts. All of these materials are in the '$A_3$' class of crosslinking of Flory (there is no preferred direction at any junction point in the clusters). Recently, another well controlled polymerization of the '$AB_2$' class has become available to experiment (in this case the three strands at each junction point may be divided in to two types, A and B, that react only with each other). This is the single-site metallocene family of materials. The reaction scheme bears some similarity with that of the comb materials described above in that growing chains on catalytic sites may be thrown off with pendant double bonds (like the living ends of the comb side-branches). These may be re-incorporated in an equivalent way to ordinary monomers at other chain growth sites, leading to tree-like families of molecules with self-similar structure [93, 94]. Remarkably, the entire family of structures is parameterized by only two numbers, which may be taken as a probability of meeting a branch point moving against the polymerization direction, $b^U$, and the mean degree of polymerization between branch points, $N_x$ [72]. The self-similarity implicit in the polymerization of the branched polymers generates recursion relations for their statistics in a natural way. Many are analytically soluble. As an example we quote here the bivariate distribution for the number-density of polymers containing $N$ monomers and $\beta$ branch points:

$$P(N,\beta) = \frac{N^{2\beta}}{N_x^{2\beta+1}\beta!(\beta+1)!}(b^U)^\beta(1-b^U)^{\beta+1}\exp(-N/N_x). \tag{19}$$

More complex reaction schemes that include chain-scission at present defy analytic enumeration of statistics, but may be amenable at least to stochastic simulation. This approach has been recently applied to low density polyethylene [95].

### 3.2. *Linear rheology*

The majority of experimental data on entangled polymer dynamics is accounted for by rheological measurements of linear response of stress to an imposed strain, or equivalents (details of the technique are available in a number of recent texts, such as reference [89], and a comprehensive survey of data in reference [12]). In a typical experiment, a small ($\simeq$1 g) sample of material is compressed between parallel circular plates. One plate is driven around its axis by small angles; the other feeds a torque transducer. Although the magnitude of the strain imposed on the material locally increases towards the perimiter of the plates, the displacement is controlled so that even the most highly strained material remains in linear response. An alternative, 'stress-controlled' arrangement imposes a fixed stress and measures the response in strain of the sample. In either case, the parallel-plate geometry imposes a simple shear deformation at all points within the sample.

#### 3.2.1. *Step-strain response and relaxation modulus*

At $t = 0$ a small step-strain $\gamma$ (usually shear—but in linear deformation the geometry is of no consequence up to a prefactor) is imposed and sustained. The resulting decaying stress $\sigma(t)$ is measured. If the material is in true linear response,

the limit of zero strain may be taken so that $\sigma(t) = G(t)\gamma$. The function $G(t)$ is the *relaxation modulus*, and is monotonically decreasing with time. In the case of entangled flexible polymers, the rubber-elastic expression for the stress from the statistical mechanics of the melt chains ((11) above) yields a direct interpretation of the normalized stress relaxation function in terms of the coarse-grained chain variables

$$G(t) = \frac{G_N^{(0)}}{S_{xy}(0)} S_{xy}(t) \quad \text{with} \quad S_{xy}(t) \equiv \left\langle \frac{\partial R_x(n,t)}{\partial n} \frac{\partial R_y(n,t)}{\partial n} \right\rangle, \tag{20}$$

where the average is taken over all chains and monomers in the chains. Polymer melts and solutions are naturally isotropic materials, in which $G(t)$ is a scalar function of time. We should make mention, however, of other cases in which the tensorial potential of stress relaxation is important. Lamellar, rodlike and other structural phases of surfactants and block co-polymers will have special directions in which measurements of $G(t)$ may give very different results [96]. Only random, polycrystalline samples of these materials recover isotropic rheology.

Very few materials exhibit single-exponential relaxation moduli (such a simple relaxation function is termed the 'Maxwell mode' in the context of rheology), but are often described in terms of an effective sum or integral of relaxation modes:

$$G(t) = \sum_{i=1}^{N} g_i \exp(-t/\tau_i) \equiv \int_{\tau=0}^{\infty} H(\tau) \exp(-t/\tau_i) \, \mathrm{d} \ln \tau. \tag{21}$$

The function $H(\tau)$ is known as the 'relaxation spectrum'. Its unique derivation from measurements of $G(t)$ is formally an ill-posed problem (it is very sensitive to noise in the data), but this can be regularized in practical cases, giving a function with considerably greater structure than $G(t)$ itself [97, 98].

The relaxation modulus may be measured directly, but this suffers from two major drawbacks: (i) the initial step-strain is never instantaneous, degrading measurements of short relaxation times; (ii) the signal-to-noise ratio at long times is very weak, degrading measurements of long relaxation times.

The same information contained in $G(t)$ may be extracted in a more robust way by other flow histories if the material properties are time-independent. That is, to each incremental strain $\mathrm{d}\gamma(t')$ applied prior to time $t$ there is a corresponding incremental stress given by $\mathrm{d}\sigma(t) = G(t - t') \, \mathrm{d}\gamma(t')$. We say that the material has Time-Translational Invariance (TTI, see reference [99]). Exceptions to this happy case are materials that are not in equilibrium, but which 'age' towards it on timescales longer than the length of the experiment [100]. Polymer melts with very long relaxation times, and which have been insufficiently annealed in the sample chamber before measurements begin, may exhibit ageing phenomena. These can take the form of spurious low frequency signals in materials, a question rather inadequately addressed in the literature.

### 3.2.2. *Frequency-dependent modulus*

The most common strain history used to extract information equivalent to $G(t)$ is the harmonic oscillation of strain $\gamma(t) = \mathrm{Re}[\gamma_0 \exp(\mathrm{i}\omega t)]$. Using TTI and equation (21) we write

$$\sigma_{xy}(t) = \lim_{\delta\gamma \to 0} \sum_{\delta\gamma} G(t - t')\,\delta\gamma(t')$$

$$= \mathrm{Re}\left[\int_{-\infty}^{t} G(t - t')\gamma_0 \mathrm{i}\omega \exp(\mathrm{i}\omega t')\,\mathrm{d}t'\right] = \mathrm{Re}\left[\gamma_0 G^*(\omega) \exp(\mathrm{i}\omega t)\right] \quad (22)$$

with the 'complex modulus' $G^*(\omega)$ defined by

$$G^*(\omega) = \mathrm{i}\omega \int_0^\infty G(t) \exp(-\mathrm{i}\omega t)\,\mathrm{d}t. \quad (23)$$

The form of equation (22) means that the stress will also be oscillatory at frequency $\omega$, but not in phase with the strain. If we write $G^*(\omega) = G'(\omega) + \mathrm{i}G''(\omega)$, then we can identify the real part, $G'$, as the in-phase (elastic) part of the modulus and the imaginary part $G''$ as the out-of-phase (dissipative) part. In general both will be frequency-dependent, crossing over from viscous (dissipative) behaviour at low frequencies (where $G'' > G'$) to elastic behaviour at high frequencies (where $G'' < G'$). We summarize these two ideal limits before giving examples.

The ideal Newtonian fluid has a shear stress that is simply proportional to the current shear rate. The constant of proportionality is the viscosity $\eta$. In the language of the complex modulus this yields a purely imaginary and linear function of frequency.

$$\sigma_{xy} = \eta \frac{\partial\gamma}{\partial t} = \eta \mathrm{i}\omega\gamma_0 \exp(\mathrm{i}\omega t) \Rightarrow \begin{cases} G'(\omega) = 0 \\ G''(\omega) = \eta\omega. \end{cases} \quad (24)$$

At the opposite material extreme, the ideal elastic solid has a shear stress that is simply proportional to the current shear strain. The constant of proportionality is the modulus $G_0$, giving a complex modulus that is just a real constant:

$$\sigma_{xy} = G_0\gamma = G_0\gamma_0 \exp(\mathrm{i}\omega t) \Longrightarrow \begin{cases} G'(\omega) = G_0 \\ G''(\omega) = 0. \end{cases} \quad (25)$$

Now we can interpret what the frequency-dependent experiment will give us in the simplest model of a viscoelastic fluid of a single relaxation time $G(t) = G_0 \exp(-t/\tau)$. The integral over $G(t)$ is readily done to yield

$$G'(\omega) = G_0 \frac{\omega^2\tau^2}{1 + \omega^2\tau^2}; \quad G''(\omega) = G_0 \frac{\omega\tau}{1 + \omega^2\tau^2}. \quad (26)$$

Note that the correct elastic and viscous behaviour are recovered at high and low frequency, respectively. The characteristic time emerges from this plot as the inverse of the frequency at which the curves cross (or the maximum in $G''$ in this case). The result for the terminal viscosity $\eta = G\tau$, is in fact general: equation (22) gives for an imposed steady flow the exact integral

$$\eta = \int_0^\infty G(t)\,\mathrm{d}t.$$

In consequence, it is always true that $\eta \approx G\tau$, where $G$ is an effective modulus and $\tau$ a characteristic relaxation time of the fluid.

More realistic examples are furnished by the elastic and loss moduli for a range of polymer-like materials. It is possible in many cases to extract effective information on relaxations covering many decades of frequency in polymers because of *time–temperature superposition* (TTS). For most polymers above both their melting point

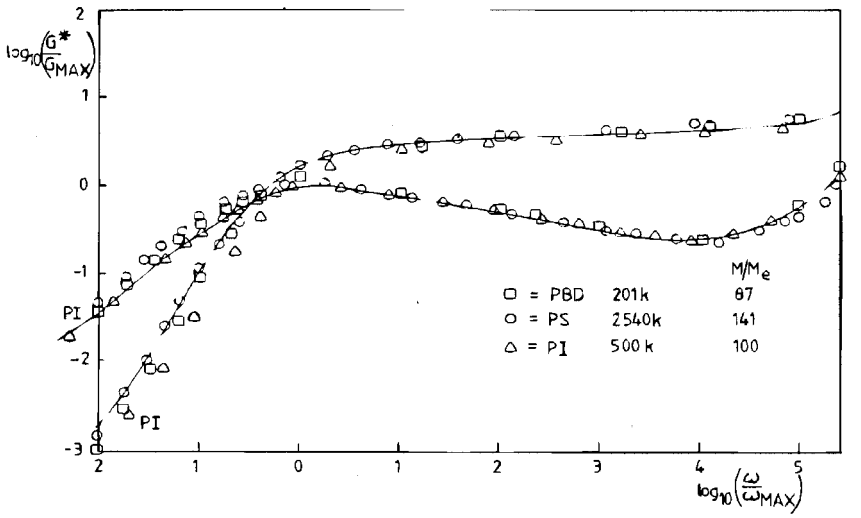


Figure 9. Linear viscoelastic moduli $G'$ and $G''$ as functions of oscillation frequency $\omega$, of monodisperse melts of polystyrene, polyisoprene and polybutadiene of similar degree of entanglement $(M/M_e)$.

and glass transition temperature, $T_g$, the timescales of *all* viscoelastic relaxations shift with temperature by the same factor $a_T = \exp[A/(T - T_0)]$, for material-dependent values of $A$ and $T_0$ (using the Vogel–Fulcher, or WLF form of the shift function [12]). By this method up to 12 effective decades in frequency are accessible for polymers with very low $T_g$, such as PI and PB, even though the experimental frequency range of mechanical oscillation available in the laboratory may not exceed four decades.

In figure 9 we show results for three chemistries of near monodisperse linear polymer melts, shifted by material-dependent values of $G_N^{(0)}$ and monomeric time-scale $\tau_0$ to give a near-superposition. Note that the data are, as usual for TTS experiments, plotted on a log–log axis in which the Maxwell model would give $G''(\omega)$ with slopes of 1 and $-1$ each side of the maximum. The slope in the data is much shallower on the right (for well entangled chains it is approximately $\omega^{-1/4}$, but in a few cases of very entangled chains such that $N/N_e \geq 600$, a region of $\omega^{-1/2}$ emerges). This indicates the presence of some shorter relaxation times, equation (21), but there is still clearly a dominant time at the crossover from viscous to elastic behaviour. The presence of a spectrum of higher relaxation times has been highly significant for detailed theories of linear chains. These subdominant dynamics also make themselves felt in the experimental scaling of viscosity with molecular weight, $\eta \simeq N^{3.4}$, which applies up to $N/N_e \lesssim 10^3$. Early suggestions based on such a broadening of the rheological relaxation spectrum, when compared with the Doi–Edwards model of a non-fluctuating chain in a fixed tube, correctly identified the main contributing effect as contour-length fluctuations [101, 102]. This has been confirmed more recently by more sensitive experiments using NMR and neutron scattering, as well as by more detailed theory (see below in section 4.2.4).

The second clear feature of the data above is the emergence of a near-plateau in the elastic modulus as a function of frequency. This is the famous historical signature of entanglements, and the value used to determine the entanglement molecular

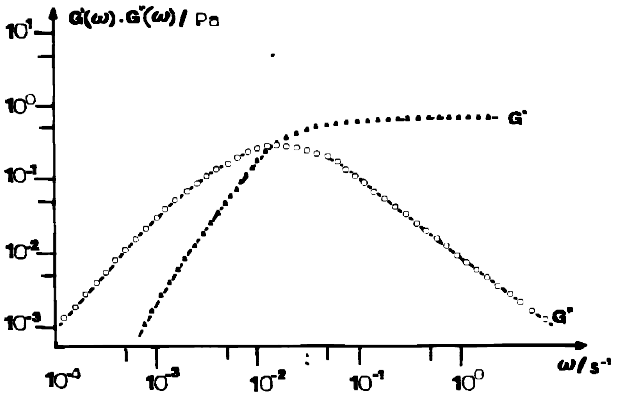


Figure 10. Near-Maxwellian behaviour of a worm-like surfactant solution CTAB. [From reference [104].]

weights $M_e$ of entangled solutions and melts via formulae such as equation (15). However, it is immediately clear that there is some ambiguity in the experimental determination of $G_N^{(0)}$. At all finite molecular weights, there is no regime of frequency at which a true plateau in elastic modulus can be measured. Various schemes to extract a value from the full relaxation modulus curve are also ambiguous because they depend on a choice of high-frequency cut-off [12]. As part of this review, we will argue strongly for the adoption of a limiting procedure for the definition of $G_N^{(0)}$, made in the light of theory.

There *is* a polymer-like system with a near-Maxwell behaviour: the family of self-assembled wormlike surfactant micelles. These entangled polymers support an additional dynamical process of breaking and reformation of chains, alongside the reptation form of molecular diffusion. This combination narrows the viscoelastic spectrum towards a single exponential [103]. In cases where the timescale for breaking is much faster than reptation, the relaxation time spectrum can be extremely narrow indeed. An example is given in figure 10. The asymptotic slopes of $G''(\omega)$ of $+1$ and $-1$ either side of the relaxation peak are now clear. Such systems of 'living polymers' also exhibit unusual features in their nonlinear rheology, and are currently helping to guide theories of nonlinear response, as we shall see in section 5.1.3.

A crucial test of theory that linear rheology can supply comes from increasing the number of structural variables in a melt by blending two monodisperse linear fractions together. When significant amounts of high and low molecular weight fractions, both themselves entangled, are blended, the frequency dependence can be striking, $G''(\omega)$ often exhibiting two peaks. Materials have been principally PS [105–108], and PB [109, 110]. Experiments have considered cases in which the higher molecular weight chains are 'self-dilute' or 'probes' (so would not entangle with each other were the lower molecular weight fraction to be replaced by a solvent) [111], and where both fractions provide contributions to the entanglement network [109]. In the probe case, the lower molecular weight species may act as unentangled solvent, as far as the terminal relaxation time of the higher fraction is concerned, but the conditions for this are subtle. A fuller review of the experimental picture than can be given here will be found in reference [37]. Historically, such experiments on linear rheology of blends first identified a difficulty with the assumption of a fixed

tube—such as would constrain polymer dynamics in a crosslinked network. Doi and Edwards [22] had suggested that the linear relaxation modulus in a melt should decay as the fraction of the occupied, or 'surviving' tube segments $\mu(t)$, since after a step strain only this fraction would impose orientational anisotropy on the chain segments occupying them. This would suggest a linear sum-rule for contributions of a blend to the relaxation modulus, yet the amplitude of the contribution from the higher molecular weight component of the blends often seemed to vary more in accord with the square of its volume fraction. Approximate and pragmatic rationalizations of this observation took the view that stress should be associated with binary interactions of strands [112, 113], an approach sometimes called 'double reptation' [114–116]. So, if $\mu(t)$ counts the remaining unrelaxed fraction of tube segments at time $t$, then double reptation just assumes that $G(t) = G_N^{(0)}[\mu(t)]^2$. This approximation, and its shortcomings, had in fact already been implied by the suggestion that the impermanence of entanglements in the melt case should be modelled by taking the tube itself as a Rouse-like object [110, 117]. We will see below (section 4.2.5) that double-reptation emerges as an approximation to such a more detailed theory of cooperative relaxation. The effect itself, that stress decays *faster* than the proportion of unrelaxed segmeents, while already evident in the rheological response, is even clearer when compared with dielectric measurements (see section 3.7 below).

Rheological measurements have proved particularly sensitive to changes in molecular topology on the scale of $M_e$ and above. Figure 11 compares $G^*(\omega)$ for a linear and 'three-arm star' architecture of polyisoprene melt, from reference [85]. In this architecture, only one carbon atom out of the $\sim 10^4$ present in the molecule carries a long chain branch, yet the response function is clearly qualitatively different from that of the linear polymer. The maximum in $G''(\omega)$ is now far from the cross-over, indicating a much broader superposition of relaxation modes over three orders of magnitude. This is also suggested from the form of $G''(\omega)$ itself—to reconstruct

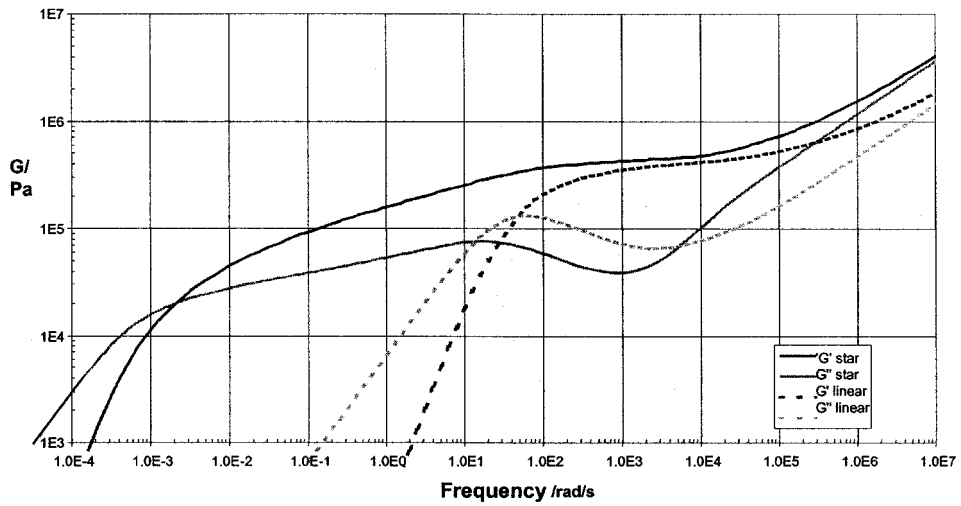


Figure 11. Comparison of $G'$ and $G''$ for monodisperse linear (broken lines) and star (continuous lines) polyisoprene melts [118]. The linear molecule and the *span* of the star molecule both comprise about 40 entanglements. Note the much broader range of relaxation times for the star polymer.

the broad, sloping shoulder of this function would require the superposition of Maxwell-like responses over three orders of magnitude in frequency. The terminal time is also much longer in the case of the star polymer, and no clear plateau emerges in $G'(\omega)$, even for high degrees of entanglement. In addition, comparison of star polymers of different molecular weight and arm number gives an astonishing result: the viscosity and terminal time is *not* dependent on the overall molecular weight of the stars, but only on the molecular weight of the *arms*, $M_a$ [119]. Moreover, the dependence is roughly exponential, in contrast to the power-law of linear chains, following $\eta \sim \exp(0.6\, M_a/M_e)$. All these radically different rheological signatures in star polymers are now very well attested [85]. We will examine the reasons for this critical effect of branching below, but from our entanglement-scale expression for the stress, equation (12), may deduce some features of the molecular picture directly. When the stress in the melt is of the order of the imposed strain multiplied by the plateau modulus, it comes principally from chain segments equilibrated at all lengthscales smaller than a tube diameter, but oriented at the tube scale by the deformation of the tube segments containing them. The qualitative result presented by the rheology of *linear* chains is, therefore, that tube segments remove their constraint on the orientation of chain segments at a single dominant timescale. In distinction, tube segments of an entangled branched arm are escaped by their chain segments at a wide range of timescales. The exponentially-growing terminal relaxation as the molecular weight of the star arms is increased, suggests that the slowest relaxations are topologically localized towards the branch point of the star, since it is always the passage of a free end that relaxed the topological constraints. The crucial dependence on arm-molecular weight only, strongly suggests that the relaxation of each arm is essentially independent of the others, motion of the branch point playing little role in stress relaxation.

More complex monodisperse branched polymers such as H-shaped melts [50, 122], 'pom-poms' [87] and combs [86, 123, 124] have been manufactured anionically and measured by linear rheology. In these cases clusters of relaxation process appear, in some cases as if the melts were composed of bimodal blends of linear chains. Like star polymers, the terminal times and viscosities are roughly exponentially-dependent on the length of the dangling arms.

When very long relaxation times are present in the stress relaxation with low amplitude, it is often better to apply a steady, or oscillating, controlled *stress* to the material, and measure the *strain*, rather than the reverse. The pattern of linear response functions (now of strain per unit stress) emerges just as in the strain-controlled case, with the time- and frequency-dependent *compliances* $J(t)$, $J'(\omega)$ and $J''(\omega)$ replacing the moduli $G(t)$, $G'(\omega)$ and $G''(\omega)$ [12]. This has been applied to great effect in the case of the highly branched, random low density polyethylene (LDPE) [125]. The limiting value of $J(t)$ as $t \to \infty$ is the 'steady-state recoverable compliance', $J_e^0$, and is weighted by the longest relaxations present in the viscoelastic material. This is clear from the sum rule [12]

$$J_e^0 = \frac{\int_0^\infty tG(t)\,\mathrm{d}t}{\eta_0^2}. \tag{27}$$

The physics behind this rule arises from the ideal experiment implied by the definition of $J_e^0$: a slow shear strain is continued until steady-state under a fixed

(and infinitestimal) stress. This is then removed, and the total reversed strain as $t \to \infty$ is just $J_e^0$. The integral in the numerator of equation (27) counts the accumulated stress driving the recovery, the denominator accounts for the viscosity that inibits the recovery. The dimensionless product $J_e^0 G_N^{(0)}$ is a useful additional measure of the width of the relaxation spectrum. It takes the value 1 for a single relaxation mode, and increases with the width of the relaxation spectrum. For monodisperse linear polymer melts, it has an experimental value independent of molecular weight, but for entangled star polymers the product increases linearly with molecular weight. This is a further illustration of the qualitative difference in the dynamics of branched and linear chains at the tube level, and of the hugely increased spectral width of relaxation processes in the branched case.

### 3.3. *Nonlinear rheology*

The coarse-grained molecular expression for the stress, equation (12), is applicable whenever the chain segments on the scale of entanglements, or tube diameters, are well-approximated by Gaussian chains, a criterion that may hold under even quite large deformations. This is because the chain configuration is only very weakly perturbed from equilibrium at the length scale of links. Such a local linearity condition applies for segments containing $\tilde{N}$ links in *macroscopic* extensions of up to a local strain of $\sqrt{\tilde{N}}$, which may be as large as 10 or more in entangled melts. This is well into a highly nonlinear range of response for the entanglement structure, even though the local sub-chains are still in linear response, and bearing a simple coarse-grained molecular interpretation! So rheology in highly nonlinear response is a promising tool for investigation of entanglement structure under high strains.

Three limiting cases of flow geometry are important to our study. They are (i) shear, (ii) uniaxial extension and (iii) planar extension. Perhaps they are best visualized as respectively the local deformations in the situations of sliding parallel plates, fibre-spinning and film-drawing respectively. It is worth becoming conversant with the usual mathematical description of nonlinear flows. The most convenient representation of a nonlinear material deformation is given by the deformation gradient tensor $\mathbf{E}(t, t')$ and its rate of change. $\mathbf{E}(t, t')$ describes the linear transformation of embedded vectors $\mathbf{X}(t') \to \mathbf{X}(t)$ under the deformation between times $t'$ and $t$ in the flow

$$\mathbf{X}(t) = \mathbf{E}(t, t') \cdot \mathbf{X}(t'). \tag{28}$$

The deformation rate, also a tensorial quantity $\mathbf{K}$ defines the time derivative of the embedded vector $\mathbf{X}(t)$, via

$$\frac{\partial \mathbf{X}(t)}{\partial t} = \mathbf{K} \cdot \mathbf{X}. \tag{29}$$

Since we may write $\mathbf{X}(t)$ in equation (29) terms of the original embedded vector $\mathbf{X}(t')$ using (28), we find that the deformation gradient and rate tensors are simply related by

$$\frac{\partial \mathbf{E}}{\partial t} = \mathbf{K} \cdot \mathbf{E}. \tag{30}$$

The deformation-rate gradient tensor $\mathbf{K}$ has familiar representations in Cartesian coordinates in our three fundamental flows:

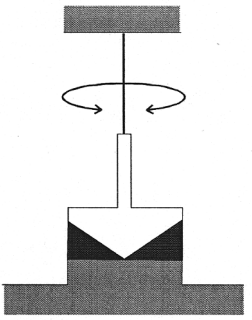

Figure 12. Schematic of a cone-and-plate shear rheometer.

$$\mathbf{K}_{\text{shear}} = \begin{pmatrix} 0 & \dot{\gamma} & 0 \\ 0 & 0 & 0 \\ 0 & 0 & 0 \end{pmatrix} \quad \mathbf{K}_{\text{uniaxial}} = \begin{pmatrix} \dot{\epsilon} & 0 & 0 \\ 0 & -\frac{\dot{\epsilon}}{2} & 0 \\ 0 & 0 & -\frac{\dot{\epsilon}}{2} \end{pmatrix} \quad \mathbf{K}_{\text{planar}} = \begin{pmatrix} \dot{\epsilon} & 0 & 0 \\ 0 & -\dot{\epsilon} & 0 \\ 0 & 0 & 0 \end{pmatrix}. \tag{31}$$

Rheometers are designed to impose either shear (relatively easy), or extensional flows (more challenging) on material. The latter pose a more difficult experimental problem, because of the need to respect the deforming free surfaces of the sample. Yet, as we shall see, properties of entangled polymers can be radically different in extension and shear. It is often important to measure both. A rotational device that generates a spatially-uniform shear flow is the 'cone-and-plate' rheometer (figure 12).

The cone is rotated at instantaneous angular velocity $\omega$. The material in the gap a distance $r$ from the axis has a velocity in the tangential direction that is fixed (in the case of non-slip boundary conditions) to zero at the bottom plate and $\omega r$ at the top plate. The local separation of the plates $h(r) = \alpha r$ where $\alpha$ is the angle at the base of the cone. So the local shear rate is $\dot{\gamma} = \partial v_\theta / \partial z = \omega r / \alpha r = \omega / \alpha$, a uniform shear field. This is especially important in nonlinear deformation, in which the material response may differ for different strains and strain rates. In the case of entangled linear and branched polymers, the key information yielded by nonlinear shear rheology is contained in the transient behaviour of the shear-stress $\sigma_{xy}(t)$ and normal stress $N_1(t) \equiv \sigma_{xx}(t) - \sigma_{yy}(t)$ on start-up of steady shear flow, and the following steady-state values. In particular the sizes and timescales of the commonly seen transient overshoots in both measurements is a strong discriminator of theories, especially when monodisperse materials are used. Examples of the shear-stress overshoots in an H-polymer melt are plotted in figure 13. In the case of monodisperse linear polymers, more data sets are available [126–128]. As the shear rate is increased, a maximum in shear stress appears at $\dot{\gamma}\tau_{\text{d}} \simeq 1$ at a strain of order 1. Increasing the rate further increases the peak stress, and decreases the time at which it appears. Over a range of shear rates, bringing the data sets together, we can say that the peak stress is reported to have a magnitude of $\sigma_{\text{peak}} = 0.73 \pm 0.1 G_N^{(0)}$. Beyond $\dot{\gamma}\tau_{\text{R}} \simeq 1$ it stays at $t_{\text{peak}} \simeq \tau_{\text{R}}$ and grows in magnitude. The peak in the normal stress only appears beyond $\dot{\gamma}\tau_{\text{R}} \gtrsim 1$. Experiments on bimodal blends of linear chains in start-up of steady shear can yield even more structure, including double peaks and under-damped

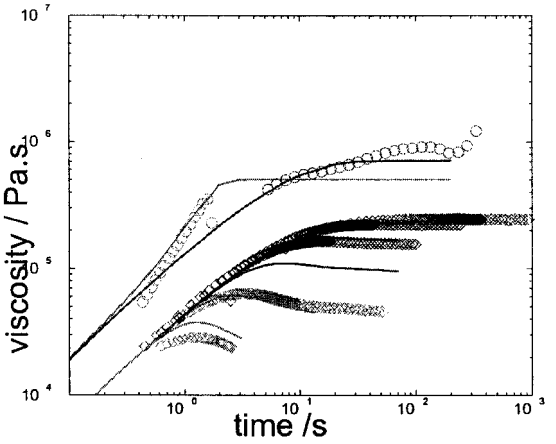


Figure 13. Time dependent shear (lower curves) and extensional (upper curves) stresses normalized by deformation rates over a range of rates for transient flows of a PI H-polymer melt [50]. The final data points at the low extension rate illustrate the difficulty of these experiments: the very thin thread at that point leads to noisy data. Lines are a nonlinear extension of a model discussed in the section on branched polymers below in section 4.3.3.

oscillations [129]. Even the steady-state values of $\sigma_{xy}(\dot{\gamma})$ and $N_1(\dot{\gamma})$ have important information on molecular origins of the response, especially for monodisperse polymers. When well-entangled, the shear stress shows a near-plateau between $\dot{\gamma}\tau_d \simeq 1$ and $\dot{\gamma}\tau_R \simeq 1$ of a magnitude of order $0.5G_N^{(0)}$, while the normal stress grows more slowly with shear rate in this region [130]. These complex responses are current, and difficult challenges for theory.

Extensional rheometers have been much harder to develop to a point at which good reproducible data is attainable. This is due, as we have seen, to the necessity of free surfaces over most of the sample in an extensional flow. It is also exacerbated by the requirement that material points separate exponentially with time, in contrast to shear flow. This is easy to see since in an extensional flow the extension rate, $\dot{\epsilon} = \partial v_z/\partial z$, implies that the velocity field in the flow direction $v_z = \dot{\epsilon}z$. But since a material point leaves the origin on a trajectory $z(t)$ in which, by definition $v_z = \mathrm{d}z(t)/\mathrm{d}t$ we have

$$\frac{\mathrm{d}z(t)}{\mathrm{d}t} = \dot{\epsilon}z \quad \Rightarrow \quad z(t) = z(0)\exp(\dot{\epsilon}t). \tag{32}$$

However, extensional rheology is an important independent measure of the nonlinear rheology of many materials. For example, branched entangled polymers (see below) may be strain-hardening in extension (the effective 'viscosity' defined as stress/strain-rate increases with strain), but strain-softening in shear. The existence of molecular effects that appear rheologically only in extensional flows, as well as the central role played by extensional flows in processing [131] have motivated the refinement of two designs of extensional rheometer. In 'filament rheometers', the material is stretched between two plates which separate at an exponential rate [132–135]. This maintains as far as possible a constant local extension rate in the material. In an alternative design, the sample is gripped and extended by two sets of rotating belts, one connected to a force transducer [136] (see figure 14) . This latter design has

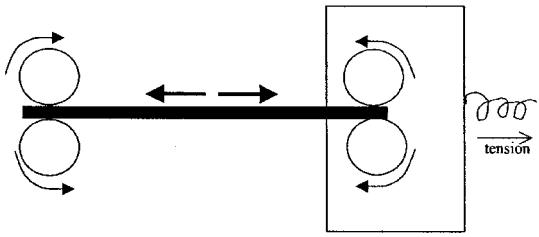


Figure 14. Schematic of a moving-belt extensional rheometer.

recently been commercialized, but the technique is by no means safe in the hands of anyone less than an expert [137]. An example of the extensional stress-growth of a model polymer melt using a 'Meissner' belt-rheometer is given in figure 13 (upper data) together with the transient shear response (lower data). Here the extensional stress difference $\sigma_{xx}(t) - \sigma_{yy}(t)$ divided by the extension rate $\dot{\epsilon}$ (the 'stress-growth coefficient' sometimes called 'transient viscosity'), is plotted against time. For the transient shear experiment we similarly plot $\sigma_{xy}(t)/\dot{\gamma}$. This way of representing data ensures that the curves superimpose at early times when the material is in purely linear response. The extensional data show strong 'hardening' at the higher of two extension rates, but none at the lower. In distinction, the shear responses at high rates are all softer than in linear response. In this case the polymer melt is composed of monodisperse molecules of identical (H shaped) branched structure [50]. This material is therefore an example that shows qualitatively different behaviour in shear and extension.

Harder still is the challenge of making quantitative measurements in strong planar extension. But this, too, has proved very important, at least in a transitionary period in which the prevalence of BKZ-type constitutive equations suggested that if the uniaxial and shear responses of material differed greatly, then the planar response should lie alongside the shear response, rather than the extensional. This is because the two-dimensionality of both shear and planar extensional flows induces the same invariant structure, see equation (6). In fact, experiments on LDPE in both tubular [138] and sheet [139] geometries have shown that the (hardening) stress-growth coefficients in planar flows are almost identical to those in uniaxial. This has had considerable impact on the development of molecular-based constitutive equations. In particular, it is possible to interpret the phenomena of extension hardening and shear thinning in the light of our comments in section 2.1.1 above. A lower shear stress than linear response (shear thinning) would imply, at the level $\tilde{N}$ of coarse-grained segments, orientation of chain segments but without stretching chain locally along the primitive path. This is because a model of affinely-convected and relaxing elastic subchains (the Rouse model, see section 4.1.2 below) exhibits a constant viscosity with shear rate in steady flow. A higher extensional stress than linear response, conversely, implies orientation with near-affine stretch (the same model predicts divergent chain stretch above a critical extension rate, leading directly to extension hardening). Although these remarks may be made independently of any specific model for the dynamics, an explanation of divergent and geometry-dependent dynamics for stretch and orientation does emerge naturally from tube models for both linear and branched polymers [140, 141].

An attempt to reduce the complication of experiments in which both strains and strain-rates are in nonlinear response (the double nonlinearity arises because the

dimensionless strain rates $\dot{\gamma}\tau_{\max} \gg 1$ as well as the strains $\gamma \gg 1$) has classically been made by taking the experimental limit of very fast 'step' strains, and looking at the response in stress as a function of strain only, comparing at fixed time following the step strain. The strain-dependent function that is the nonlinear extension of the modulus is called the 'nonlinear time dependent modulus' $G(\gamma; t)$. In shear it is defined by

$$G(\gamma; t) = \frac{\sigma(\gamma; t)}{\gamma}. \tag{33}$$

In many cases the dependence on time following the step strain $t$ is suppressed because no further time-dependence is seen after some time $\tau_k$ [142]. Such materials display 'time-strain separation' for $t > \tau_k$, so that

$$\sigma(\gamma; t) = \gamma h(\gamma) G(t) \tag{34}$$

so defining the 'damping function' $h(\gamma)$. In the case of monodisperse materials the damping function was observed to possess a universal, highly softening form (termed 'A-type' damping in a classic review by Osaki [143, 144]), before any theoretical suggestions that this might be expected on molecular grounds. Moreover, the molecular weight dependence of the time $\tau_k$ was found, in these cases, to grow with molecular weight as $\tau_k \sim M^2$. Suggestively, this is the same scaling as that of the timescale for stretch relaxation of a chain of molecular weight $M$ (recently other experiments by Archer have pointed to a longer timescale for separability of strain and time [145], but the discrepancy between Archer's and Osaki's results has yet to be explained). For very highly-entangled melts and solutions $(M > 50M_e)$, it is uncontested that a very rapid and severe reduction in the shear stress occurs, consistent with a flow-instability within the rheometer. Osaki has called this 'C-type' damping [142]. Polydispersity tends to reduce the severity of the strain dependence, as does branching and disentangling by lowering molecular weight or polymer concentration. The exception to this is the case of entangled melts of *star* polymers. These possess damping functions very similar to those of monodisperse linear polymers [146], and are both well accounted-for by the theoretical 'Doi–Edwards' damping function (see section 5.1 below and [31]). Damping function measurements of monodisperse complex architecture polymers have as yet yielded only small amounts of data, but there are indications that architectures such as the 'H' or 'pom-pom' can yield time-strain factorability separately in more than one region of time following a step strain [50]. In figure 15 we show an 'early time' and a 'late time' damping function extracted from a PI H-polymer melt, together with the 'Doi–Edwards' function seen in monodisperse linear polymers and stars, and stiffer 'early time' damping functions from a detailed tube model for this architecture (see section 5.2).

A final important experimental technique of nonlinear rheology is the simple but effective application of two strains of different magnitudes separated by a time interval $t$ that becomes a third parameter. Such 'double step shear' experiments have been applied to polydisperse melts [147] and to monodisperse linear melts [148]. The response from these experiments is a delicate measure of differential relaxation among topologically distinct strands. At a crude level, those segments that have equilibrated their orientation distribution between the two shears pick up only the second, reversed shear, while more slowly relaxing segments will respond to the net

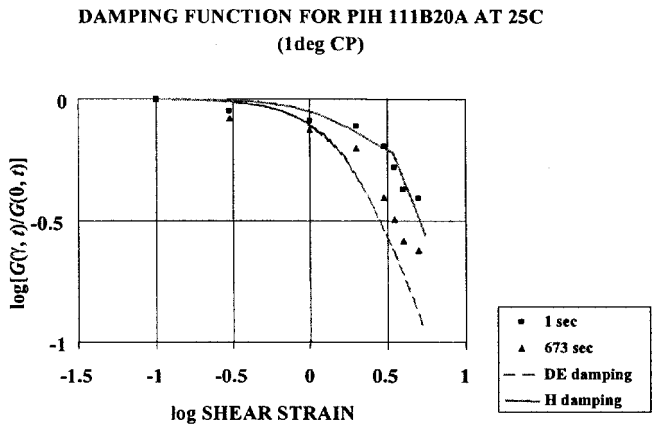


Figure 15. Damping functions observed in a PI H-polymer melt [50] at early and late times, in comparison with the highly shear-thinning Doi–Edwards damping function and a theoretical result for H melts.

deformation after the two shears. A careful accounting for the effect of double step shear within the tube model was made by Doi [32, 146] (and see section 5.2 below).

### 3.4. *Birefringence and dichroism*

Although rheology in both linear and nonlinear response has the double advantage of directness of technique and simplicity of interpretation in terms of a molecular description of polymer chains, it suffers from the inability to pick out the contribution of distinct subsets of chain segments. We might expect segments nearer the ends of entangled linear chains to reequilibrate their orientation, for example, faster than central segments, but the rheological signal simply sums over all segments, so is a poor test of this idea. The same can be said of other topologically non-equivalent segments such as those in the individual components of a polymer blend, or those occupying inequivalent positions in a branched polymer. It is also not always easy to measure the stress locally in a polymer, especially in a complex flow. A route to overcoming these difficulties is provided by the optical properties of polymer melts and solutions. Typically, a segment of polymer chain will possess an anisotropic polarizability with reference to the local chain axis. So a polymeric fluid with anisotropy of segment orientations will itself be optically anisotropic, causing (in the non-absorbing case) polarized light passing through the fluids to suffer a rotation of its plane of polarization. In other words, the tensorial index of refraction $\mathbf{n}$ will be non-trivial. However, $\mathbf{n}$ is just a second-rank tensor, and a bilinear function of the orientation distribution of bonds. These properties are shared by the stress tensor derived from rubber-elasticity theory, see equation (11) above. So the two are equivalent up to a constant and we have

$$n_{ij} = C\sigma_{ij}, \tag{35}$$

where $C$ is the 'stress-optical' coefficient. This relation can be derived from first principles [31] and even atomistic expressions given for the constant $C$. The relation is well attested by experiment in cases where the form birefringence is small and the relation between segment and bond orientation linear [150], though does break down under strong stretching, when the level of stress indicates significant perturbation of

the chain structure at the level of Kuhn segments [151]. In consequence, optical determination of the local stress tensor is now routinely used in evaluating simulations of complex flows [152, 153].The great advantage of optical methods is that experimental access to all components of the orientation (stress) tensor becomes available without the use of force-transducers on the boundaries of rheometer sample cells. Shear stress, first normal stress difference, and *second* normal stress difference $N_2 = \sigma_{yy} - \sigma_{zz}$ can be measured in nonlinear deformations such as step strains [40]. Although $N_2$ is much smaller that $N_1$ in the case of polymeric fluids (this is not the case in other complex fluids, especially those containing surfaces or membranes), it is none the less important in controlling some flow instabilities, including the Weissenberg effect [154], and is becoming an important discriminator of theory [155]. The ratio $N_2/N_1$under small deformations [40] and deformation rates [156] is close to a value of $-0.2$, falling rapidly at strains above 200%, although does not become as small as predicted by a tube theory without CCR.

Perhaps a more powerful application of optical methods, however, is the use of local chemical labelling. We will see below how the spatial and orientational dynamics of selected components of a blend or segments in a molecule may be extracted by neutron scattering and NMR by replacing selected hydrogen atoms in the polymer chain by deuterium. The same labelling can induce polarization-dependent absorption in the infrared region of the spectrum from C–D bond stretch. Called 'infrared dichroism', this signal allows the mean orientation of the chain backbone of the labelled segments alone to be measured [41, 157–159]. Two important physical observations have emerged from studies of this kind. The first is that topologically-distinct segments in entangled polymers carry different relaxation times and spectra of times, and that segments nearer chain ends do indeed tend to relax faster. The clearest example occurs in the case of star polymers, in which segments near the branch points relax very much more slowly than segments in the centre of arms, and even more slowly than central segments in linear polymers whose molecular weight is the same as the span of the star polymer [158]. A second, more subtle observation is that even when a rapidly relaxing segment has relaxed all possible contributions it can make to the elastic stress, by virtue of escaping from its original entanglements, it may still carry some anisotropy if it is in the presence of much slower, still oriented material [159]. This 'orientational coupling' has also been seen in labelled NMR experiments (see below), and conjectured to arise from small nematic chain–chain interactions or, more directly, from the excluded-volume screening interaction [160]. In either case, the presence of such an interaction does not affect the validity of the stress-optical law as a whole [161, 162] (note that this is *not* the case when there is finite macroscopic nematic order [31]), but means that *local* identification of contribution of segmental orientation to stress needs to be treated with caution.

Finally, optical measurements on blends of high and low molecular weight components show that a finite fraction of the anisotropy of segments in the long (slow) chains actually relaxes on the timescale of the short (fast) chains. This effect, alongside the observed volume fraction scaling of $G(t)$, motivates the introduction of the co-operative motion of CR (section 4.2.5 below).

### 3.5. *Neutron scattering*

For a considerable part of our story, rheological response (by direct or optical measurements of the stress) was the only tool available to test theories,

in spite of the concomitant predictions of molecular theories for aspects of chain configuration. The double challenge, shared by structured and complex fluids in general, is the requirement of a molecular probe sensitive to structure at the 10 nm scale, and with the ability to penetrate the bulk of a fluid sample. Both are met by thermal neutron scattering. Reactor and spallation sources are now able to provide neutrons with wavelengths and scattering angles that probe spatial correlations of scattering nuclei on lengthscales in the range 1–100 nm. This regime is ideal for probing polymers on the entanglement scale. Neutrons have considerable penetrating power into organic matter, as they are not charged. An extra very significant advantage is the large difference in scattering cross-section between hydrogen and deuterium nuclei. It is relatively easy to replace selectively hydrogen atoms with deuterium at polymer synthesis; so that, rather that probing only density fluctuations in a melt (which are very small), the scattering signal can be engineered to pick out correlations between the deuterium-labelled monomers only, in similar spirit to the IR dichroism experiments above. Experiments relevant to the study of entangled dynamics fall into two classes: (i) observations of the static structure under deformation and (ii) direct measurement of dynamics. We look in a little more detail at each in turn.

3.5.1. *Static structure factor by SANS*

A classic series of early experiments [163, 164] using admixtures of deuteriated and hydrogenated chains of monodisperse molecular weight distribution in an equilibrated melt were able to extract the 'single chain structure factor', $S(\mathbf{q})$:

$$S(\mathbf{q}) = \left\langle \frac{1}{N^2} \int_0^N \mathrm{d}n \int_0^N \mathrm{d}m \exp\{i\mathbf{q} \cdot [\mathbf{R}(n) - \mathbf{R}(m)]\} \right\rangle, \tag{36}$$

where the average is taken over the ensemble of chains. The 'scattering vector', $\mathbf{q}$, is related to the wavelength $\lambda$ and scattering angle $\theta$ of the neutron beam by

$$q = \frac{2\pi}{\lambda} \sin\left(\frac{\theta}{2}\right).$$

The experiment requires a finite fraction of all melt chains to be deuteriated while the remainder contain just hydrogen. It is possible to reduce the many-body exclusions of all the chains to a single-chain signal in this case, because of the strong validity of mean-field interactions in the limit of the polymer melt. Concentration fluctuations are very small, and all self-interactions of a chain (repulsive) are exactly screened by interactions with other chains [8]. The evaluation of equation (36) for the Gaussian chain model was first made by Debye [165]; the function that bears his name has the large scale asymptotics $S(\mathbf{q}) \simeq 1 - q^2 R_g^2/3$ and the small scale structure $S(\mathbf{q}) \simeq 1/\mathbf{q}^2$. Here

$$R_g = \frac{1}{N^2} \int_0^N \mathrm{d}n \int_0^N \mathrm{d}m \{[\mathbf{R}(n) - \mathbf{R}(m)]^2\}$$

is the 'radius of gyration' of the chain, and a measure of its overall spatial extent. The validity of the Debye function for singly-labelled chains, and the related family of scattering experiments using partially labelled chains (for which mean-field scattering calculations go by the name of the 'random phase approximation'—RPA) have been

well confirmed in experiment [166]. The important structure is picked up at length scales between a few monomers (1–10 nm) and the scale of a whole chain (100 nm). With cold neutron wavelengths of the order of a few angstroms, this requires measurement of the scattered signal at small values of the scattering angle (SANS).

The relevance of this technique to dynamics is not immediately apparent, but important results have been obtained by rapidly quenching labelled melts under conditions of flow so that the static structure factor may be examined in highly nonlinear response. It is typically impossible to perform the experiment in real time because of the limited intensity of neutron sources. Even using high-flux reactors, several minutes are needed to achieve a reasonable signal-to-noise ratio on an anisotropic response (in this most interesting case radial averaging loses vital information). Extensional measurements were first made by Boué [51]. The shear case for polystyrene was reported by Muller *et al.* [49]. The remarkable result suggested that the maximum degree of anisotropy, defined as the ratio of the effective radii of gyration in the flow and flow-gradient direction—$x$ and $y$ in the definitions of the shear rate tensor of equation (31)—did not exceed about 1.8, even for large deformations at rates such that $\dot{\gamma}\tau_{\mathrm{d}} \gg 1$. The observed anisotropy is represented by the contour-plot of figure 16. The upper figure is from flow such that $\dot{\gamma}\tau_{\mathrm{d}} \sim 10$, the lower two at $\dot{\gamma}\tau_{\mathrm{d}} \sim 1$. No greater anisotropy than the former can be achieved at accessible rates. Without detailed calculation, one might be surprized at this: using the tube model and assuming, as is standard [31], that the tubes deform affinely in the flow, would suggest that at very high strains the chain is constrained by just one highly sheared and deformed tube segment, now almost parallel to the flow direction. If the flow rate is small compared with the *stretch* relaxation of the chain (this requires $\dot{\gamma}\tau_{\mathrm{R}} \prec 1$), then it will occupy the same topological path length *via* continuous curvilinear retraction along the deforming tube, but even so a large anisotropy might be expected. If both tube length and widths are unaffected, but just oriented in the flow direction, the ratio $R_x/R_y$ might be expected to be of the order of the number of tube segments $N/N_{\mathrm{e}}$. In the case of the PS experiments, this would produce the very different pattern of the insert to figure 43.

A more complex experiment was performed on a monodisperse H-polymer melt under extensional deformation [50]. In this case the anisotropy of the scattering pattern (albeit from arm-end labelled chains) was greater than expected. Data sets on clean materials of this kind are still woefully few, and there is clearly a role for future experiments of this type (see, e.g. the recent results of reference [338]).

### 3.5.2. *Dynamic structure factor by NSE*

A direct measure of the dynamics of entangled chains is assessable via the technique of neutron spin echo (NSE). In this experiment the magnetic moment of the cold neutrons is exploited by a field set up by large coils around the sample so that their energy transfer is coded into their spin-rotation, and the energy and momentum of the scattered neutrons may be independently recorded. Fourier transforming the energy transfer gives the time-dependent correlation in the usual way. The final intensity depends on the motion of the scattering centres. Both incoherent and coherent signals may be independently accessed:

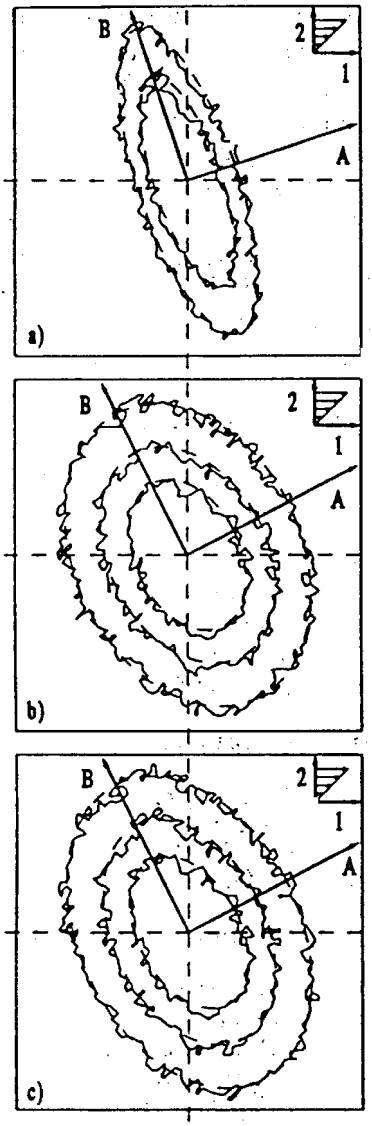


Figure 16. Isointensity SANS plots of the single-chain structure factor in the flow/gradient plane from the PS experiments of Muller *et al.* [49]. The shear stress of (*a*) was 4 times higher than (*b*) and (*c*); the total strains were 2.4, 2.8 and 4.0.

$$\left.\begin{aligned} S_{\mathrm{coh}}(\mathbf{q},t) &= \left\langle \frac{1}{N}^2 \int_0^N \mathrm{d}n \int_0^N \mathrm{d}m \exp\{\mathrm{i}\mathbf{q}.[\mathbf{R}(n,t)-\mathbf{R}(m,0)]\}\right\rangle \\ S_{\mathrm{incoh}}(\mathbf{q},t) &= \left\langle \frac{1}{N}\int_0^N \mathrm{d}n \exp\{\mathrm{i}\mathbf{q}.[\mathbf{R}(n,t)-\mathbf{R}(n,0)]\}\right\rangle \end{aligned}\right\} \tag{37}$$

providing information on single-monomer diffusion, and on monomer–monomer correlations respectively. Qualitatively, at small lengthscales where unentangled dynamics obtains, $\mathbf{S}_{\mathrm{incoh}}(\mathbf{q},t)$ falls off by Rouse motion in a near stretched-exponential manner [167],

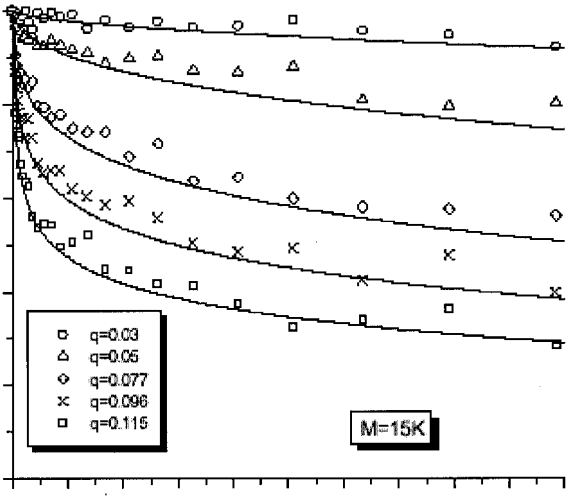


Figure 17. Neutron spin echo coherent decay for a monodisperse PE melt of molecular weight 15 000. The time axis runs from 0 to 200 ns, and the decays are normalized. Wave vectors $q$ are indicated in units of $\text{Å}^{-1}$. [Data courtesy of D. Richter [169].] Lines are theoretical predictions from a tube model with CLF (see section 4.2.4 below).

$$S_{\text{incoh}}(\mathbf{q}, t) = \exp\left[-(t/\tau_{\text{q}})^{1/2}\right] \tag{38}$$

but with a **q**-dependent timescale $\tau_q \sim q^{-2}$. This free decay is slowed down once the entanglement field is felt at times beyond the Rouse time of an entanglement strand $\tau_e$ (see figure 17). Such a motion was first detected in earliest applications of NSE [42, 43]. However, quantitative assessment of competing theories by NSE required the extension of available timescales to a few hundred nanoseconds, even for the most mobile and most entangled case of polyethylene (PE) [44]. Like $T_2$−NMR (see below in section 3.8) NSE is able to give direct, local dynamical information, sensitive to labelling schemes in a similar way. It is naturally more expensive, but does not suffer from the same difficulties of interpretation forced on the NMR data when slow dynamics break the simplifying 'second moments approximation'. However, fully quantitative treatments cannot escape the need to account for the more subtle processes of CLF and CCR. Even a standard expression from reptation [168], often used to interpret data, makes approximations that are not valid in the range of the data, and does not include important processes such as CLF, which have been essential in understanding much simpler data from rheology. A very recent data set on monodisperse polyethylenes, varying from just a few entanglements to nearly 200, has shown that at lower molecular weights CLF is essential in order to account for the data accurately (see figure 17 and [169]).

### 3.6. *Dynamic light scattering*

It is not immediately apparent that dynamic scattering experiments using optical wavelengths (also called photon correlation spectroscopy) would be a useful probe of molecular relaxations in entangled polymeric fluids since, at the much larger wavelength of light, all chain structure is too small to be resolved at any scattering angle. However, direct consequences of the relaxation of the entanglement network can be seen in semi-dilute solutions when there is optical contrast between the

polymer and solvent. In this case the local polymer density $\rho_{\text{pol}}(\mathbf{r}, t)$ fluctuates thermally. We may write the polymer density variables of the light scattering signal in terms of our coarse-grained chain representation $\mathbf{R}_\alpha(s, t)$ by summing over chains and contour coordinates:

$$\rho_{\text{pol}}(\mathbf{r}, t) = \sum_{\text{chains } \alpha} \int_0^N \mathrm{d}s\, \delta[\mathbf{r} - \mathbf{R}_\alpha(s, t)]. \tag{39}$$

Without entanglements the local composition fluctuations at low-$\mathbf{q}$ are suppressed by the osmotic pressure of the solution, and the scattering function $S_{\text{DLS}}(\mathbf{q}, t)$ decays via a co-operative diffusion constant in normal modes that are just harmonic in space with diffusive decay rates $\Gamma_q \sim q^2$:

$$S_{\text{DLS}}(\mathbf{q}, t) = \int \exp(-\mathrm{i}\mathbf{q} \cdot \mathbf{r}) \langle \rho_{\text{pol}}(\mathbf{r}, t) \rho_{\text{pol}}(\mathbf{0}, 0) \rangle \, \mathrm{d}^3\mathbf{r} \sim \exp(-D_{\text{coop}} q^2 t). \tag{40}$$

However, in the presence of entanglements, there is an additional elastic suppression of composition fluctuations. A fraction of the amplitude of the composition fluctuations may be 'frozen in' by the entanglements, according to the ratio of the osmotic $(K)$ and high frequency elastic $(G)$ moduli. This fraction of the light scattering signal may only decay with the spectrum of relaxation times of the entanglements themselves, producing a second 'slow mode' to the signal decay. The fingerprint of this mode is the non-diffusive dispersion relation $\Gamma_{\text{slow}} \sim \tau_{\text{d}}^{-1} \sim q^0$ where $\tau_{\text{d}}$ is a characteristic disengagement time for the entanglements. Qualitatively the response is now

$$S_{\text{DLS}}(\mathbf{q}, t) = \frac{K}{G + K} \exp(-D_{\text{coop}} q^2 t) + \frac{G}{G + K} \exp(-t/\tau_{\text{d}}). \tag{41}$$

The prediction of such a slow mode was made by Brochard and de Gennes [170] and observed in several semidilute systems [171, 172]. The quantitative theory was developed by Doi and Onuki [173] and Semenov [174], who has calculated both Rouse and reptative contributions to the slow modes, showing that the structure of the decay differs slightly in the two regimes $qR_{\text{g}} \ll 1$ and $qR_{\text{g}} \gg 1$. The full picture predicted is very complex, including a high-$q$ range in which the entangled mode timescale 'anomalously' *increases* with $q$. Experiments have confirmed that the slow relaxations match stress decay very accurately in both entangled polymer solutions [175] and entangled worm-like micelles [176], but there has yet to be a critical evaluation of the most complete current theoretical predictions. There has also yet to be an evaluation of this promising technique in cases where the relaxation of the entanglement network is expected to be temporally very polydisperse, such as in blends and branched polymers. Yet it has the advantage that the instrumentation and analysis of PCS signals is now developed to detect signals over many orders of magnitude in frequency in a simultaneous experiment. This dispenses with the need to exploit time–temperature superposition.

### 3.7. *Dielectric spectroscopy*

A technique rather analogous to rheology, yet with an important distinction in the way it sums over chain segmental correlations, is *dielectric spectroscopy* [37, 177]. If chain segments are associated with electric dipoles, then they will tend to align under the application of an electric field in a similar (and more direct) way to

alignment generated by the mechanical field in rheology. The induced polarization of the fluid is a sum over all molecular dipoles

$$\mathbf{P}(t) = \sum_i \mu_i(t) \tag{42}$$

and decays with a combination of fast local dynamics and also with the slow global dynamics of the chains, providing that the dipoles are correlated to the chain backbone. As in rheology, the experimental data may be acquired either by a pulse-probe technique, or by harmonic excitation. In the latter case the functions $\epsilon_0 - \epsilon'(\omega)$ and $\epsilon''(\omega)$ are the analogues of $G'(\omega)$ and $G''(\omega)$. Stockmayer has classified dipole-containing polymers into three cases [178]: A-type chains contain dipole moments along the chain backbone, B-type perpendicular and C-type attached to side chains. The best probes of slow entangled dynamics are naturally the A-type chains, of which by far the most exhaustively explored has been anionically-synthesized 1-4 PI. When the dipoles are all parallel to the chain, the normalized dielectric decay function $\Phi_d(t) = |\mathbf{P}(t)/\mathbf{P}(0)|$ can be written in terms of the coarse-grained chain variables $\mathbf{R}_\alpha(s,t)$ as [179].

$$\Phi_d(t) = \frac{1}{b^2}\left\langle \frac{\partial \mathbf{R}(n,t)}{\partial n} \cdot \frac{\partial \mathbf{R}(n',0)}{\partial n'} \right\rangle, \tag{43}$$

where, as in rheology (20), the average is taken over all chains and monomers. We note two vital distinctions, however, between equations (43) and (20): the rheological response of stress-decay is an *equal-time* correlation that is also *diagonal* in the matrix $(n,n')$ of monomer indices, while the dielectric response is a *two-time* correlation that also respects any off-diagonal correlations among the monomers. Since local dipoles add vectorially, the dielectric relaxation in the case of parallel dipole moments is simply a measure of the decay in correlation of the end-to-end vector of the chain, whereas the rheological time-dependent modulus measures the average decay of local segmental orientations. In the single idealized case of a chain diffusing in a fixed tube, the two functions $G(t)$ and $\Phi_d(t)$ are identical, since they both simply measure the fraction of original tube still occupied by chain $\mu(t)$ ([31] and see below section 4.2.2). However, experiments on entangled linear, monodisperse polymers comparing both rheology and dielectric relaxation [180, 181] have found that in *melts*, to a good approximation

$$G(t) \simeq [\Phi_d(t)]^2, \tag{44}$$

which is identical to the 'double reptation' or 'dynamic dilution' approximation introduced from rheological observations, and the co-operative relaxation suggested by labelled IR dichroism of blends. We will see later (section 4.2.5) how this can be rationalized by the 'constraint release' process. Just as in the rheological case, a well defined peak in $\epsilon''(\omega)$ is seen at the terminal time, followed by a region of the spectrum in which $\epsilon''(\omega) \sim G''(\omega) \sim \omega^{-1/4}$ (compare the reptation picture below of $\omega^{-1/2}$). In stark contrast, for non-entangled chains, dielectric and viscoelastic spectra differ widely: the rheology has $G'(\omega) \sim G''(\omega) \sim \omega^{1/2}$ above a frequency of $\tau_R^{-1}$ and 'terminal behaviour' tending to $G'(\omega) \sim \omega^2$ and $G''(\omega) \sim \omega^1$ below; but the dielectric response is still sharply peaked at the terminal time. As we will see, the unentangled chain dynamics can be represented in terms of normal modes spatially identical to those of a vibrating string. In orientational relaxation, the end-to-end vector (dielectric response) is dominated by the slowest such (Rouse) mode, but the stress

decay is equally distributed among all modes [182]. The molecular weight scaling of the terminal time exhibits, as it does in rheology, a transition from $\tau_{max} \sim M^2$ to $\tau_{max} \sim M^{3.5}$ at a critical molecular weight $M_c \simeq 2M_e$ [183].

The technique has proved powerful in the elucidation of blend dynamics, and is very sensitive to certain features, such as the molecular weight of an unentangled low molecular weight component in bimodal blend, in which the high-MW component is entangled [184]. Another case is the transition from reptation to constraint–release driven Rouse dynamics of self-dilute high-MW components as the molecular weight of the matrix component is reduced [37, 185]. The clearest picture of this transition arises in a comparison of rheological and dielectric data, since these are similar in reptative motion, but, as we have seen, differ markedly in Rouse motion. These data, again showing contrasting aspects of the dynamics to those of viscoelasticity, should still bear fruit in theories of constraint release, especially those exploiting another unique capability of the dielectric relaxation measurements of A-type chains: use of dipole inversion. Unlike the tensorial quantities of stress or birefringence, the dielectric signal is vectorial, so has the possibility of sign inversion by creating points along the chain at which the direction of the dipoles inverts. This may be done during the anionic synthesis by coupling living chains in non-polar solvents [186]. Watanabe has shown how measurements of identical chains, apart from their containing dipole inversions at $1, 2, 3 \ldots$ equally-spaced points, may permit calculation of the shape of the normal modes along the chain, independent of any particular theory [187]. The experimentally-determined modes corresponded closely to the pure harmonic functions predicted by Rouse and tube-model theories.

Perhaps the most surprising and informative recent application of dielectric spectroscopy has been the case of entangled star polymers [188, 189]. A 'dynamic dilution' theory, in which the tube gradually dilates as entanglements are released by other stars in the neighbourhood [190], accounts for the rheological response with remarkable accuracy (see section 4.3.2 below). However, although the theory also predicts the faster dielectric relaxations, as the terminal time is approached it goes badly wrong. In the recently examined case of star arms with 16 entanglements, the dielectric dissipation actually exhibits a Maxwell-like peak, while the rheological response continues to show a broad distribution of modes (see figure 18)! Other puzzles have emerged related to the terminal behaviour of star polymers, such as their self-diffusion constant (see below and [191]). Recent theoretical advances [192, 193] have suggested some explanations, but this topic has again assumed a rapid rate of development.

### 3.8. *NMR magnetic relaxation*

Another exciting direct probe of polymer dynamics is given by the whole family of techniques collectively known as nuclear magnetic resonance (NMR). In its guise as a technique in analytical chemistry, we are used to thinking of its principle regime as atomically-local in space and sampling GHz in frequency. However, time and spatial scales relevant to entangled dynamics have recently been explored by two other variants of this very adaptable technique. *Field-gradient NMR* (FGNMR) is essentially a method of spin-labelling monomers to extract information on spatial diffusion [45], so will be deferred to the next section. A direct measure of local orientational dynamics, on the other hand, capable of accessing timescales up to 100 ms or more is provided by the *transverse magnetic relaxation*, often referred-to as '$T_2$'. In this experiment, the spins on the sample's protons (or deuterons in the case

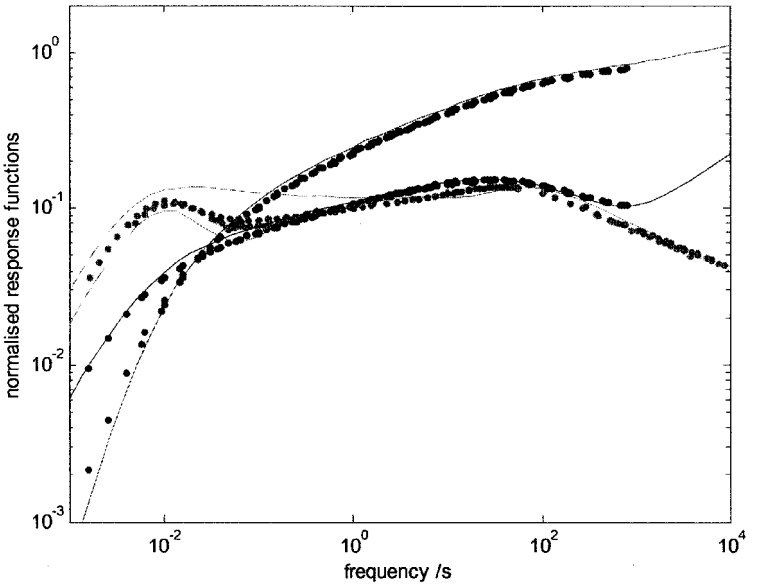


Figure 18. Dielectric and rheological data on a 6-arm PI star melt with $M_a/M_e = 16$. [Courtesy of H. Watanabe.] Curves associated with the lower two functions at low $\omega$ ($G'$ and $G''$) are predictions of the rheology by dynamic dilution [190], the upper (light) curve is its prediction for the upper data set for $\epsilon''(\omega)$. The peaked (light) curve is the prediction for $\epsilon''(\omega)$ of a theory in which dynamic dilution (see section 4.3.2) is arrested for the final third of the star arm, and all remaing reponse relaxed with the last entanglement.

of a labelled experiment) are first aligned with the applied field, then rotated by $\pi/2$ using a pulsed additional field. The resultant transverse magnetic moment, $M(t)$, relaxes principally by the dephasing of signals from protons (deuterons) in different magnetic environments. The direct experiment that measures $M(t)$ following the first pulsed field is called the 'free induction decay'. More complex pulse-sequences may be employed to filter out the effect of more than one type of C–D interaction. The main component of these local field variations is the proton–proton dipolar interaction and the deuteron C–D bond quadrupolar interaction respectively. The decay is sensitive to the local chain dynamics because these tend to average out, or anneal, the dipolar and quadrupolar interactions if they are fast, and leave them quenched if they are slow. So a rapid decay of $M(t)$ is the result of slow chain motion, and a slow decay arises when chain motion is itself rapid. Providing sufficient signal persists to a time $t$, dynamics of even small fractions of the effective local field variations can be detected. In terms of the molecular coarse-grained description of chains $\mathbf{R}(n,t)$ we are working with, the decay can be written, in the case of deuteriation [194]

$$M(t) = \left\langle \cos\left[\frac{3\Delta_b}{2b^2}\int_0^t \mathrm{d}t'\left(\frac{\partial \mathbf{R}(n,t)}{\partial n}\cdot\mathbf{L}\cdot\frac{\partial \mathbf{R}(n,t)}{\partial n}\right)\right]\right\rangle, \tag{45}$$

where

$$\mathbf{L} = 3\hat{\mathbf{B}}\hat{\mathbf{B}} - \mathbf{I} = \begin{pmatrix} 2 & 0 & 0 \\ 0 & -1 & 0 \\ 0 & 0 & -1 \end{pmatrix}, \tag{46}$$

where the matrix representation has the direction of the magnetic field $\hat{\mathbf{B}}$ in the $z$-direction. In equation (45) $\Delta_b$ is a renormalized quadrupolar interaction between the C–D bonds, averaged over all the dynamics faster that that of the fundamental Rouse unit, or Kuhn step length $b$. Brereton [195] has given solutions in the case of fast subsequent dynamics (in the sense that the entanglement dominated relaxation time $\tau_b$ of the renormalized bonds satisfies $\Delta_b\tau_b \ll 1$) and a path-integral solution for slow single-exponential dynamics when $\Delta_b\tau_b \succeq 1$ [196]. In the former, the 'second moments' approximation is valid [197]. This is equivalent to the assumption of Gaussian distribution of the stochastic quantities in equation (45) and gives

$$M(t) = M(0)\exp\left(-\frac{3}{2}\Delta_b^2\tau_b t\right). \tag{47}$$

Note that the dynamical averaging of the chain environment renders the NMR relaxation *faster* as the chain segment dynamics become *slower*. In this limit, the signal from both ideal Rouse and reptation dynamics is also single-exponential, $M(t) \sim \exp(-t/T_2)$, with relaxation times that depend on molecular weight in subtly different ways. For a Rouse chain the result is [195]

$$T_2^{\mathrm{Rou}} = \frac{\pi}{6\ln N\Delta_b^2\tau_b} \tag{48}$$

and in the case of reptation

$$T_2^{\mathrm{rept}} = \frac{\pi N_e}{18N\ln\left(\frac{N}{N_e}\right)\Delta_b^2\tau_b}. \tag{49}$$

These results have been tested against a series of PB chains above and below the entanglement threshold [46] (see figure 19). While qualitatively behaving as expected, there are still some puzzles with such experiments. Firstly, interpretation is not as clear as these clean results might lead us to hope, because of contour length fluctuations at the chain ends. An advantage of $T_2$-NMR makes this explicit: chain ends may be deutero-labelled at their ends, in which case $M(t)$ shows a free-Rouse

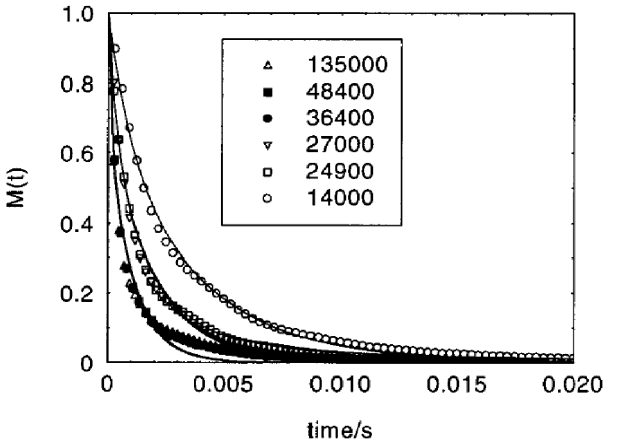


Figure 19. Decays of transverse magnetic moment measured on a series of linear polybutadienes of varying molecular weight. Lines are the second moment approximation applied to reptation dynamics. [Reproduced from reference [46].]

signal [47]. Secondly, the figure deduced for $M_e$ from the NMR experiments is high compared with rheology ($\sim$5000 as opposed to $\sim$2000) [46]. When the relaxation of entanglement segments conveys such slow dynamics on the chain that the second moment approximation breaks down, it is typically not possible to fit data with single exponentials. The formal solution in this case has recently been applied to the transverse signal from selectively labelled entangled star polymers [48]. Successively slower relaxation times were observed from the free end to the branch point of the star, as in rheology, but the very different (faster) absolute timescales recorded by this technique indicated the rather complementary views of chain motion taken by the two functions equations (45) and (11). Like NSE, the signal seems to be sensitive to the process of 'local reptation', in which chain segments sample new configurations by exploring neigbouring tube segments successively further from the originally occupied segment. This is a process that carries a rather small signal strength in rheological relaxation (see below) since it does not disentangle any material. Fully quantitative treatments of these promising experiments, made in the light of the theoretical models we review below, have yet to be done.

A recent imaginative application of signal coding in NMR on flowing melts has shown that the technique can extract the complete bond orientation tensor that also controls stress and birefringence, equation (11) [198, 199]. Inclusion of deuteriated benzene molecules in the melt provides a probe of the orientational state of the chains, filtered by spatial coding for particular regions of a Couette rheometer. A highly entangled ($Z \simeq 80$) polydimethylsiloxane gave a clear signal of a near-plateau in shear stress as a function of shear rate in the range $\tau_d^{-1} < \dot{\gamma} < \tau_R^{-1}$ (supporting the predictions of theories of convective constraint release, see section 5.1.3). The normal stresses were also measured, giving a clear signal of $N_2/N_1 = -0.1$ for shear rates up to $\dot{\gamma}\tau_d = 3$, after which the ratio dropped rapidly in absolute value.

### 3.9. *Diffusion measurements*

Theories of polymer dynamics make predictions not only for the relaxation of molecular configurations, but also for the simple spatial diffusion of the molecule as a whole, and, on a smaller scale, mean displacements with time of individual monomers. The most direct measurement is of the self-diffusion constant of the centre-of mass of the chains, $D_{CM}$

$$D_{CM} = \lim_{t\to\infty} \frac{\left\langle \frac{1}{N}\sum_{n=1}^{N}[\mathbf{R}(n,t) - \mathbf{R}(n,0)]^2 \right\rangle}{6t} \tag{50}$$

and its scaling with molecular weight. We note here (for derivations see below) that the Rouse unentangled theory gives $D_{CM} \sim M^{-1}$ and that pure reptation, without corrections for CLF or CR gives $D_{CM} \sim M^{-2}$. Several techniques for extracting $D_{CM}$ have been used on linear and star polymers of various chemistries. The evolution of original step-profiles in the concentration of hydrogenated and deuteriated versions of the polymer may be monitored by IR microdensitometry [200], by grazing-incidence neutron scattering [201], forward recoil spectroscopy [202] or by dynamic secondary ion mass spectroscopy [203]. The neutron reflectivity experiments 'SNR' give the greatest potential spatial resolution of all the methods, but at the cost of requiring model fitting to an assumed real-space profile. So scattering used in tandem with one of the real-space techniques can be particularly effective [204]. Centre-of-

mass diffusion of non-entangled and entangled melts has been measured for hydrogenated polybutadiene [201] and polystyrene [205, 206]. Early experiments on rather restricted data sets indicated that, in melts, the data in the entangled regime followed $D_{CM} \sim M^{-2}$ accurately, whereas in concentrated solution the scaling was more in accord with $D_{CM} \sim M^{-2.3\pm0.1}$ [207, 208]. This was of course a puzzle in the face of expectations that entangled dynamics should be universal in its scaling behaviour and functional form at comparable values of $M/M_e$, independent of dilution. It was also a concern to be reporting such a clean result as the pure-reptation form of $D_{CM} \sim M^{-2}$, when for the same materials rheology measured $\eta \sim M^{3.4}$ rather than the pure reptation result of $\eta \sim M^3$. The favoured explanation of the 3.4-law in terms of contour length fluctuations ought also to affect diffusion. But a recent survey of all the data on hydrogenated PB together, plus a new set of materials spanning the entire range of $1 < M/M_e < 1000$ by Lodge [52] has brought the melt results in line with those of concentrated solutions, suggesting $D_{CM} \sim M^{-2.3\pm0.1}$ in this range, with the suggestion of a cross-over to the pure-reptation power law at the highest molecular weights.

Diffusion may also be used to test the strength of the CR process by varying the degree of polymerization of dilute diffusing probe chain, $P$, with respect to that of the matrix chains, $N$ [209]. These results (on PS) still present something of a puzzle, since CR seems to dominate over reptation for molecular weights of the probe chain $P \succeq N^{2.5}$, an exponent not anticipated theoretically.

Just as in measurements of viscosity, the diffusion of star polymers [201, 210] gives a radically different, and stronger, dependence on molecular weight, also depending chiefly on the molecular weight of the star arms: $D_{CM} \sim \exp(\nu(M_a/M_e))$. The value of the order-unity constant $\nu$ in this expression depends crucially on the environment of the diffusing stars, and is much slower when this is a crosslinked network or high molecular weight melt than a homogenous melt of stars [201, 211], lending further evidence of the co-operative nature of entangled dynamics.

If the structure of an interface between differently labelled chains is measured at high resolution, and before the chains have had time to diffuse as much as their own radius of gyration, the diffusion can yield information about dynamics on a smaller scale. A recent study using triblock-labelled partially deuteriated PS was designed to give a 'ripple' profile of deuterium density only in the early stages of diffusion, and was able to differentiate critically between free Rouse motion, reptation, and other candidate theories of polymer dynamics [204]. Other techniques measure directly the early-time diffusion of labelled monomers on the chain. Both incoherent neutron spin echo and pulsed gradient spin echo NMR [45] have identified dynamics of $\phi_n(t) = \langle[\mathbf{R}(n,t) - \mathbf{R}(n,0)]^2\rangle$ that are sub-diffusive, a consequence of chain connectivity predicted by theory.

### 3.10. *Simulation*

An increasingly attractive addition to the experimental tools discussed above is the direct numerical simulation of entangled polymeric fluids. The great advantage of simulation, of course, is the ability to extract any desired data on the simulated system without the limitations imposed by experiment. All correlation functions (average displacements of individual monomers, selected bond correlation functions, specific trajectories of individual chains etc.) are accessible. However, there is one obvious hurdle that cannot be easily overcome—the simple issue of large numbers. We know that the phenomenon of entanglement requires the interaction of many

chains, since even a single entanglement strand of $N_e$ spans a volume containing $\sim N_e^{3/2}$ monomers, and data suggest that $N_e \sim O(10^2)$. In addition we are already aware that CLF reduces the efficacy of entanglement significantly for even quite long chains, so that a simulation volume containing sufficient chains to ensure that $N/N_e > 10$ seems a minimal requirement to explore entangled dynamics. Moreover, this minimum spatial scale, far larger than would be required to simulate adequately a simple fluid composed of monomers of the same structure, is accompanied by large temporal scales. We know from rheology that relaxation times for large chains can easily be of the order of hundreds of seconds, yet local molecular bonds re-orient within picoseconds. Or, more formally, while the CPU time for a simple fluids simulation scales as $N_{tot}$ (the total number of particles in the system), the time for the associated polymer simulation in which the monomers are concatenated into chains of $N$ requires a CPU time scaling as $N_{tot}N^z$. Here $z$ is a general dynamical exponent for the maximum relaxation time of the system (e.g. 3 for pure reptation), so that $\tau_{max} \sim N^z$. Representing the resulting 12 orders of magnitude or more of timescales in a computer simulation is a very long way beyond current capabilities. However, since we have seen that entanglement effects emerge at a coarse-grained level in polymers, with some indications of universal behaviour, we might expect that effective simulations would not have to be faithful to reality at the atomistic level. So in spite of the considerable difficulties, very great advances have been made by the use of coarse-graining [212], judicious choice of lattice methods [213], and Monte Carlo algorithms [213]. A recent and accessible review covers other aspects of soft condensed matter simulation as well as polymer statics and dynamics [214], but we will touch on results that provide challenges for the theoretical methods of the following sections.

Although the very long timescale of reptative stress–relaxation is prohibitive for even coarse-grained simulations, the tube model does have rather clear consequences for the non-Fickian diffusion of individual monomers on a chain at much earlier timescales than the reptation time. A monomer only has to diffuse a distance of the tube diameter $a$ before the constraint of the tube will modify all subsequent motion. This is accessible to simulation—in this the technique shares a similar timescale restriction with that of field-gradient NMR and NSE. A fundamental prediction is in the mean-square monomer displacements relative to the centre-of-mass displacement for monomers near the chain centre, $g_2(t)$:

$$g_2(t) = \langle [\mathbf{R}(n,t) - \mathbf{R}_{CM}(t) - \mathbf{R}(n,0) + \mathbf{R}_{CM}(0)]^2 \rangle, \tag{51}$$

where the average is taken over monomers far from chain ends. An important cross-over at the Rouse time of an entanglement strand, $\tau_e$, is predicted by the tube model:

$$g_2(t) = \begin{cases} 2b^2(t/\tau_0)^{1/2} & t < \tau_e \\ \sqrt{\frac{2}{3}}ba(t/\tau_0)^{1/4} & t > \tau_e \end{cases} \tag{52}$$

in terms of the monomer and tube diameters, $b$ and $a$, and a monomeric time $\tau_0 = b^2\zeta/k_BT$ (see below). The two non-Fickian (sub-diffusive) powers of 1/2 and 1/4 arise respectively from chain connectivity (a result of the unentangled Rouse model), and then beyond the entanglement time $\tau_e$ the additional constraint of random motion along a tube, which is itself a random walk. This is the motion sometimes called 'local reptation' [168]. A more coarse-grained measure of mean displacement,

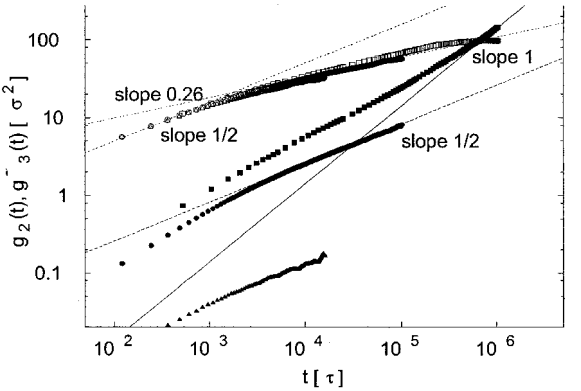


Figure 20. Plots of mean square monomer displacement (in units of the r.m.s. bond length $\sigma$) relative to the chain centre of mass $g_2(t)$ (open symbols) and the displacement of the chain centre of mass itself $g_3(t)$ (closed symbols) for three chain lengths from $N = 350$ to $N = 10^4$. The 'Rouse-in-a-tube' power laws of $t^{1/4}$ and $t^{1/2}$ respectively are clear for $t > 10^3$. [From reference [50].]

$g_3(t)$ is not expected to show this regime but is dominated by the outer segments of the chain:

$$g_3(t) = \langle [\mathbf{R}_{\mathrm{CM}}(t) - \mathbf{R}_{\mathrm{CM}}(0)]^2 \rangle = \begin{cases} (2a^2/N)(t/\tau_0)^{1/2} & \tau_{\mathrm{R}} > t > \tau_{\mathrm{e}} \\ (2a^2/N^2)(t/\tau_0) & t > \tau_{\mathrm{R}}. \end{cases} \tag{53}$$

It took some time for these cross-overs to be seen clearly in simulation, in retrospect because of the finite-size effect of CLF and the difficulty that lattice simulations have in approaching the dense limit (it is the vacancies on the lattice that provide opportunities for mobility). Early lattice simulations failed to see any evidence of the tube constraint [55], unless all structure below the tube diameter was discarded and the entanglement scale set to the lattice parameter [215], but a vectorized real-space molecular dynamics (MD) simulation by Kremer and Grest showed how off-lattice methods can reach higher effective densities without slowing the dynamics unacceptably [216]. The 'monomers' in the simulation were spheres interacting by Lennard–Jones potentials, and by Hookean springs along the chains. This landmark simulation saw clear evidence of a transition to the $t^{1/4}$ regime in the monomer diffusion (but without establishing a clear value for the exponent, since the chains of $N < 150$ were still only moderately entangled—$N/N_{\mathrm{e}}$ up to about 5). However, visualizations of successive configurations of individual chains within the simulation volume gave rather clear images of the tube-like regions of topological constraint. A more recent MD simulation has attained 50 chains of 10 000 monomers each, estimated to correspond to $N/N_{\mathrm{e}} \simeq 350$ and saw very clear cross-overs to the local reptation exponent of 1/4 [54] (see figure 20). It was also possible to deduce the value of $N_{\mathrm{e}}$ for the system from the induced stress and its decay after an imposed step-strain in the simulation. Some discrepancy arose in comparing the value deduced from the simulated plateau modulus of elasticity $N_{\mathrm{e,p}} \simeq 80$, with the value deduced from the monomer dynamics, $N_{\mathrm{e,m}} \simeq 30$, which has yet to be resolved. A similarly clear cross-over was observed in a non-equilibrium molecular dynamics (NEMD) simulation of Lennard–Jones spheres elastically coupled into chains of up

to 400 monomers [217]. This simulation introduced shear flow, so calculated viscosity as a response function rather than by equilibrium correlations, and was able to probe shear-thinning in nonlinear response. It also showed how simulation may be used as an important tool in understanding the possible provenances of non-universalities such as the ratio between $M_e$ and $M_c$ [78, 79], but found a strangely large value for $N_e$ when applying the experimentally observed scaling with the monomeric 'packing length' observed in reference [78] (see section 6.5). The issue of microscopic and macroscopic definitions of $N_e$ will concern us in the following, and is in urgent need of clarification.

Advanced lattice-based simulations, such as the 'bond-fluctuation' model have overcome some of the limitations of simple lattices [218], and have recently been able to simulate melts of chain of over 10 entanglements [219], and seen the relatively weak signatures of the tube-confined dynamics at the limit of high entanglement. Another recent study of melts of entangled ring polymers found both non-Gaussian statistics (with $R^2 \sim N^{0.83}$) and a terminal time for orientational correlations that scaled as $\tau_{max} \sim N^{2.5}$, intermediate between the results for Rouse and reptation motion of linear chains [220].

The terminal time itself, and its modifications due to CLF and CR have been accessed by Brownian Dynamics simulations that dispense with physically-realistic 'monomers' altogether. Of course, since CLF is itself, like reptation, a single-body effect, there is no need for a fully 3D real space simulation to arrive at numerical results for the fraction of chain escaped from the original tube, and for the viscosity/molecular weight relation under assumptions that the viscoelastic response is governed only by the surviving tube fraction. Stochastic simulations on an ensemble of 1D chains with internal Rouse modes that give the correct statistics for CLF will suffice. Several strategies have been employed to do this, either applying Markovian noise locally to coarse-grained segments of an entire chain (called 'reptons' by Rubinstein) [221], or correlated, non-Markovian noise to the end-to-end coordinate of the composite chain [222–224]. Naturally this method requires some subtlety in comparison with experiment for what is meant by the entanglement molecular weight in such abstract spaces as 1D spin models is not clear *a priori*, but a very similar cross-over from CLF-dominated to reptation-dominated stress–relaxation is indeed recovered.

An economic approach to many-chain coupling effects such as CR, and even nonlinear response in fast flows, is suggested by these 1D stochastic simulations. Rather than attempting a fully-3D simulation, one may explore effective, induced, couplings between the chains in the 1D ensemble. One version of this strategy [225], with a 'global' assumption of the effects of CR (see theoretical discussion below) has been compared with nonlinear measurements in fast flows and double step-strains [226]. A recent application has also achieved the terminal relaxation of mildly entangled star polymers in the linear regime [227]. A more promising approach using this type of 'intermediate simulation' identifies individual constraints between points on two chains in the ensemble and permits local rearrangements of entanglements as a consequence of CR modelled in this way [228]. A recent application of this approach to star polymers has identified a special mechanism by which the very slowest entanglements between two star arms may relax (a diffusion of the entanglement towards the free end of one of the star arms, from which it is then annihilated by CLF) [229]. This may help to explain the anomalous dielectric data on entangled stars also very recently published [189, 192].

Table 1. Summary of techniques for study of entangled dynamics.

| Technique | Coarse-grained chain correlation | Spatial scale | Timescale |
|---|---|---|---|
| Rheology | $S_{ij} \equiv \left\langle \frac{\partial R_i(n,t)}{\partial n} \frac{\partial R_j(n,t)}{\partial n} \right\rangle$ | — | $10^{-2}$–$10^{3}$ s |
| Optics | $S_{ij} \equiv \left\langle \frac{\partial R_i(n,t)}{\partial n} \frac{\partial R_j(n,t)}{\partial n} \right\rangle$ | — | $10^{-2}$–$10^{3}$ s |
| SANS | $S(\mathbf{q};t) = \left\langle \frac{1}{N^2} \int_0^N \mathrm{d}n \int_0^N \mathrm{d}m \cdot \exp\left[i\mathbf{q} \cdot (\mathbf{R}(n,t) - \mathbf{R}(m,t))\right] \right\rangle$ | 1–500 nm | — |
| NSE | $S_{\mathrm{coh}}(\mathbf{q},t) = \left\langle \int_0^N \frac{\mathrm{d}n}{N} \int_0^N \frac{\mathrm{d}m}{N} \cdot \exp\left[i\mathbf{q} \cdot (\mathbf{R}(n,t) - \mathbf{R}(m,0))\right] \right\rangle$ | 1–500 nm | 1–300 ns |
| | $S_{\mathrm{incoh}}(\mathbf{q},t) = \left\langle \int_0^N \frac{\mathrm{d}n}{N} \cdot \exp\left[i\mathbf{q} \cdot (\mathbf{R}(n,t) - \mathbf{R}(n,0))\right] \right\rangle$ | | |
| DLS | $S_{\mathrm{DLS}}(\mathbf{q},t) = \int \exp(-i\mathbf{q} \cdot \mathbf{r}) \langle \rho_{\mathrm{pol}}(\mathbf{r},t) \rho_{\mathrm{pol}}(\mathbf{0},0) \rangle \, \mathrm{d}^3\mathbf{r}$ | 1–$10^{2}$ μm | $10^{-6}$–$10^{3}$ s |
| DS | $\Phi(t) = \frac{1}{b^2} \left\langle \frac{\partial \mathbf{R}(n,t)}{\partial n} \cdot \frac{\partial \mathbf{R}(n',0)}{\partial n'} \right\rangle$ | 10–100 nm | $10^{-6}$–$10^{3}$ s |
| $T_2$-NMR | $M(t) = \left\langle \cos\left[ \frac{3\Delta_{\mathrm{b}}}{2b^2} \int_0^t \mathrm{d}t' \left( \frac{\partial \mathbf{R}(n,t')}{\partial n} \cdot \mathbf{L} \cdot \frac{\partial \mathrm{R}(n,t')}{\partial n} \right) \right] \right\rangle$ | 10–100 nm | $10^{-9}$–$10^{-2}$ s |
| SNR | $D_{\mathrm{CM}} = \lim_{t \to \infty} \frac{\left\langle \frac{1}{N} \sum_{n=1}^{N} [\mathbf{R}(n,t) - \mathbf{R}(n,0)]^2 \right\rangle}{6t}$ | 1–500 nm | $10^{-1}$–$10^{3}$ s |
| FGNMR | $\phi_{\mathrm{n}}(t) = \langle [\mathbf{R}(n,t) - \mathbf{R}(n,0)]^2 \rangle$ | 10–$10^{4}$ nm | $10^{-2}$–10 s |
| Simulation | All of the above | variable | variable |

### 3.11. *Summary of probes of entangled dynamics*

We have seen that the fields of experiment and simulation of entangled dynamics have grown from a restricted set of bulk measurements and coarse-grained tools to a large palette of subtle techniques that can probe polymer dynamics at a wide range of spatial and temporal scales. Different experiments acquire their signals from different correlations and averages of chain coordinates, and their application in parallel is a very powerful discriminator of theory. Clearly it is no longer adequate for the theoretician to predict the rheological response with a few free parameters! A fully molecular theory of polymer dynamics must be able to account for both tensorial (stress, birefringence, dichroism), vectorial (dielectric relaxation, NMR) in the orientational degrees of freedom, as well as spatial dynamics (NSE, DLS, diffusion) and structure (SANS) of entangled polymer chains. Before beginning our review of the structure of current tube theories themselves, we summarize the spatio–temporal scales as well as the correlations probed by the techniques that have guided the field so powerfully (table 1).

## 4. Tube theories in linear response

The special universal features of polymer dynamics, and especially those aspects controlled by entanglements and topological interactions, are manifestly emergent at a spatial scale larger than the strictly molecular. For this reason we have chosen in the discussion of experimental techniques in the preceding sections to adopt a coarse-grained description of the tube, in which the coordinates $\mathbf{R}(n, t)$ describe a section of the real polymer chain whose substructure we will not model, but which induces the properties of flexible Gaussian chains on all higher lengthscales. We now review the theoretical description of the dynamics of polymer chains at this level of coarse-graining. Before considering the entangled case when the tube potential becomes important, we review the Rouse model [5, 31] for the unentangled case. This serves a number of purposes beyond the important historical one: it gives us a framework for the real-space and normal mode descriptions of the more complex entangled cases and additionally provides the structure of an approximate theory of constraint release that we will use in section 4.2.5.

One additional introductory note about formalisms in stochastic dynamics is necessary. Brownian motion typically controls coarse-grained dynamics in soft matter, since the degrees of freedom at finer lengthscales that have been 'integrated out' provide the source of random forces with short correlation times on the larger scale explicit coordinates. Since the resulting dynamics will be inherently statistical, only average quantities will relate to experiment. There are two classic mathematical routes to the calculation of these averages (such as the quantities in table 1 of section 3.11). Either one may work with the entire distribution function for the stochastic quantities, $X_i(t)$, $\Psi(X_i, t)$, in which case the problem is cast into a set of partial differential equations (this is the Smoluchowski approach), or work with a set of ordinary differential equations for the $X_i(t)$ that include stochastic forcing terms with distributions of known moments (this is the Langevin approach). In this review we use the latter formalism. It is usually easier to solve, as well as providing a more transparent insight into the physics, though lacks the complete information available from the distribution functions. For more details, and the application of the Smoluchowski approach to linear polymers see reference [31]. For a Smoluchowski treatment of an entangled branched polymer see reference [230].

### 4.1. *Unentangled linear chains (the Rouse model)*

In this simplest fundamental model of polymer dynamics we make three key simplifying assumptions [5]. Their physical validity depends on the effectiveness of screening [9] of both static and hydrodynamic quantities in a melt. In the case of concentrated solutions, screening will not be operative at lengthscales below the mesh size $\xi$, but will hold at larger scales. But these contain the lengthscales of entanglement effects, so in the solution case also, coarse-grained local dynamics are expected to follow the Rouse model. The central assumptions are as follows.

(a) Gaussian chains: in which the force on a subchain segment $n$ is the net entropic force from its neighbours. In the continuum representation we have adopted, this is equivalent to a thermodynamic force at each point of the chain of

$$-\frac{\partial}{\partial n}\left(\kappa\frac{\partial \mathbf{R}}{\partial n}\right) = -\kappa\frac{\partial^2 \mathbf{R}}{\partial n^2} \text{ with } \kappa = \frac{3k_B T}{b^2}.$$

(b) Local drag: the drag force on a subchain segment comes from frictional drag against background without long range hydrodynamic effects of backflow (this works in melts where all long range mediated backflows are screened). This force is $\zeta\partial\mathbf{R}/\partial t$ with $\zeta$ a drag coefficient per segment.

(c) Brownian motion: a random force $\mathbf{f}(n,t)$ acts on each subchain with correlation times much faster than any polymer dynamics to be modelled by the theory.

#### 4.1.1. *A preliminary calculation: the Rouse-dumb-bell model*

Suppose for a moment that the drag is limited to two points, at the extremities of a subchain of $N$ step lengths, $\mathbf{R}_1$ and $\mathbf{R}_2$. This simplified model will help solve the full Rouse model below. The force balance for the two drag points is:

$$\left.\begin{aligned}\zeta\frac{\partial \mathbf{R}_1}{\partial t} &= \kappa(\mathbf{R}_2 - \mathbf{R}_1) + \mathbf{f}_1\\ \zeta\frac{\partial \mathbf{R}_2}{\partial t} &= \kappa(\mathbf{R}_1 - \mathbf{R}_2) + \mathbf{f}_2,\end{aligned}\right\} \tag{54}$$

with $\kappa = 3k_B T/Nb^2$ and $\zeta$ the drag coefficient of each of the two drag points. The random forces have correlations in time that are just delta-functions on the polymer timescale: i.e. $\langle \mathbf{f}_1(t)\mathbf{f}_1(t')\rangle_t = \eta_1 \mathbf{I}\delta(t-t')$, with $\eta_1$ a constant (and likewise for $\mathbf{f}_2$). This coupled system of equations is easily diagonalized with the following coordinates:

$$\left.\begin{aligned}\mathbf{R}_{CM} &= \tfrac{1}{2}(\mathbf{R}_1 + \mathbf{R}_2)\\ \mathbf{r} &= (\mathbf{R}_1 - \mathbf{R}_2).\end{aligned}\right\} \tag{55}$$

These represent the centre-of-mass motion of the molecule and the spatial separation of the drag points, respectively. In these variables the dynamical equations read:

$$\zeta_{CM}\frac{\partial \mathbf{R}_{CM}(t)}{\partial t} = \mathbf{f}_{CM}(t) \tag{56a}$$

$$\zeta\frac{\partial \mathbf{r}(t)}{\partial t} = -2\kappa\mathbf{r}(t) + \mathbf{f}_r(t), \tag{56b}$$

with new random forces defined appropriately in terms of the old ones:

$$\left.\begin{aligned}\mathbf{f}_{\mathrm{CM}}(t) &= \mathbf{f}_1(t) + \mathbf{f}_2(t)\\ \mathbf{f}_{\mathrm{r}}(t) &= \mathbf{f}_1(t) - \mathbf{f}_2(t)\end{aligned}\right\} \tag{57}$$

and $\zeta_{\mathrm{CM}} = 2\zeta$.

The first (centre-of-mass) coordinate is subjected to a history of random forces that generate random displacements. The final value of $\mathbf{R}_{\mathrm{CM}}(t)$ after such a history is clearly a sum of a large number of random variables; it will therefore have a Gaussian distribution. We recognize the physics of simple diffusion. The mean square displacement can be calculated by direct integration of the dynamical equation:

$$\begin{aligned}\langle R^2_{\mathrm{CM}}(t)\rangle &= \frac{1}{\zeta^2_{\mathrm{CM}}}\int_0^t \mathrm{d}t' \int_0^t \mathrm{d}t''\langle \mathbf{f}_{\mathrm{CM}}(t').\mathbf{f}_{\mathrm{CM}}(t'')\rangle\\ &= \frac{1}{\zeta^2_{\mathrm{CM}}}\int_0^t \eta_{\mathrm{CM}}\,\mathrm{Tr}\,(\mathbf{I})\,\mathrm{d}t' = 6D_{\mathrm{CM}}t,\end{aligned} \tag{58}$$

where the diffusion constant is given in terms of the noise by $D_{\mathrm{CM}} = \eta_{\mathrm{CM}}/2\zeta^2_{\mathrm{CM}}$. By the Einstein relation $D = kT/\zeta$ in one dimension, this sets the variance of the noise $\eta_{\mathrm{CM}} = 2kT\zeta_{\mathrm{CM}}$.

The second coordinate is the relative separation of the chain ends, and describes an overdamped Hookean spring with a Brownian exciting force. This time the solution is via the Green function

$$G(t-t') = \frac{H(t-t')}{\zeta}\exp\left[-(t-t')/\tau\right]$$

for the first-order ODE (56b)

$$\begin{aligned}\mathbf{r}(t) &= \mathbf{r}(0)\exp(-t/\tau) + \int_0^t G(t,t')\,\mathbf{f}_{\mathrm{r}}(t')\,\mathrm{d}t'\\ &= \mathbf{r}(0)\exp(-t/\tau) + \frac{1}{\zeta}\int_0^t \exp\left[-(t-t')/\tau\right]\mathbf{f}_{\mathrm{r}}(t')\,\mathrm{d}t',\end{aligned} \tag{59}$$

with $\tau = \zeta/2\kappa$ a relaxation time. The second moment calculation goes via the double integral (compare equation (58)):

$$\begin{aligned}\langle r(t)^2\rangle &= r^2(0)\exp(-2t/\tau) + \frac{1}{\zeta^2}\int_0^t\int_0^t \mathrm{d}t'\,\mathrm{d}t''\exp\left[-(2t-t'-t'')/\tau\right]\langle \mathbf{f}_{\mathrm{r}}(t')\,\mathbf{f}_{\mathrm{r}}(t'')\rangle\\ &= r^2(0)\exp(-2t/\tau) + \frac{1}{\zeta^2}\int_0^t \exp\left[-2(t-t')/\tau\right]\eta_{\mathrm{r}}\,\mathrm{Tr}\,(\mathbf{I})\,\mathrm{d}t'\\ &= r^2(0)\exp(-2t/\tau) + \frac{3\eta_{\mathrm{r}}}{4\zeta\kappa}\left[1-\exp(-2t/\tau)\right].\end{aligned} \tag{60}$$

Equation (60) says that the initial separation of the drag points is 'forgotten' in a characteristic time given by $\tau = \zeta Nb^2/6k_{\mathrm{B}}T$. As $t\to\infty$ we must recover the equilibrium value of the chain end separation, as given by the equipartition theorem:

$$\frac{\kappa}{2}\langle r(\infty)^2\rangle = \frac{\kappa}{2}\cdot\frac{3\eta_{\mathrm{r}}}{4\zeta\kappa} = \frac{3k_{\mathrm{B}}T}{2}, \tag{61}$$

so we find that variance of the noise in the separation variable must be $\eta_{\mathrm{r}} = 4k_{\mathrm{B}}T\zeta$.

4.1.2. *The Rouse chain*

Now we have the tools, we need to attack the Rouse model proper, in which frictional drag is uniformly distributed over all of the chain so that each monomer carries an effective drag of $\zeta_0$. The monomeric drag constant will parameterize all our theoretical models, setting the timescale for both Rouse and, subsequently, entangled motion. The balance of entropic, drag and random forces on the chain of $N$ subchains is the Rouse equation:

$$\zeta_0 \frac{\partial \mathbf{R}}{\partial t} = \frac{3k_B T}{b^2} \frac{\partial^2 \mathbf{R}}{\partial n^2} + \mathbf{f}(n,t). \tag{62}$$

The noise on each subchain is related to its frictional drag by the generalized Einstein relation as above:

$$\langle \mathbf{f}(n,t)\mathbf{f}(m,t')\rangle = 2\zeta_0 k_B T \mathbf{I}\delta(n-m)\delta(t-t'). \tag{63}$$

The Rouse dynamical equation (62) is diagonalized by the transformation:

$$\left.\begin{aligned} \mathbf{R}(n,t) &= \mathbf{X}_0(t) + 2\sum_{p=1}^{\infty} \mathbf{X}_p(t)\cos\left(\frac{p\pi n}{N}\right) \\ \mathbf{X}_p(t) &= \frac{1}{N}\int_0^N \mathbf{R}(n,t)\cos\left(\frac{p\pi n}{N}\right) \mathrm{d}n. \end{aligned}\right\} \tag{64}$$

The $\mathbf{X}_p(t)$ are the time-dependent amplitudes of the 'Rouse modes' of the polymer chain. These are just the (vector amplitude) Fourier modes of the chain path $\mathbf{R}(n,t)$ with respect to the arclength coordinate $n$. The choice of cosine modes arises from the effective boundary condition $\partial\mathbf{R}/\partial n = 0$ at $n = (0, N)$. This arises since the end subchains can support no elastic tension for they have no sources of drag or entropic tension on one side. We may re-write the dynamics in terms of the Rouse modes by replacing $\mathbf{R}(n,t)$ everywhere in the Rouse equation by their expression in terms of the mode amplitudes. The essential point is that the operator $\partial^2/\partial n^2$ becomes just $(p\pi/N)^2$ in the new modes. Then we operate from the left with the integral operator

$$\frac{2}{N}\int_0^N \mathrm{d}m \cos\left(\frac{p\pi m}{N}\right)$$

using the orthogonality result

$$\frac{2}{N}\int_0^N \cos\left(\frac{p\pi m}{N}\right)\cos\left(\frac{p'\pi m}{N}\right)\mathrm{d}m = \delta_{pp'}(1+\delta_{p0}).$$

Each mode amplitude is then found to obey a decoupled dynamical Langevin equation which reads (for $p \geq 1$):

$$\zeta_p \frac{\partial \mathbf{X}_p}{\partial t} = -k_p \mathbf{X}_p + \mathbf{f}_p(t) \quad \text{with} \quad k_p = \frac{6k_B T p^2 \pi^2}{Nb^2} \quad \text{and} \quad \zeta_p = 2N\zeta_0, \tag{65}$$

whereas the decoupled centre-of-mass mode $(p = 0)$ satisfies

$$\zeta_{CM} \frac{\partial \mathbf{X}_0}{\partial t} = \mathbf{f}_0(t); \quad \zeta_{CM} = N\zeta_0 \tag{66}$$

and undergoes simple diffusion. Each of the internal modes behaves exactly like the one internal mode of the dumbbell molecule we treated in section 4.1.1 above, with a noise term which can be calculated either by Fourier-transforming the spatial noise

terms, $\mathbf{f}(n,t)$, or by observing that their strength must be sufficient to maintain an energy equipartition of $k_BT/2$ per mode (for each Cartesian component). Either calculation gives

$$\langle \mathbf{f}_p \mathbf{f}_q \rangle = 2\zeta_p k_B T \mathbf{I} \delta_{pq} \delta(t-t'). \tag{67}$$

The key result for us is the time correlation function of the mode amplitudes, which is:

$$\langle \mathbf{X}_p(t)\mathbf{X}_q(t') \rangle = \mathbf{I}\frac{k_BT}{k_p}\delta_{pq}\exp(-|t-t'|/\tau_p). \tag{68}$$

Each mode has its own relaxation time $\tau_p = \zeta/k_p$ that decreases rapidly (as $1/p^2$) with mode index $p$. The longest of these relaxation times $\tau_1 = \zeta N^2 b^2/3\pi^2 k_B T$ has special significance. It is known as the *Rouse time*, and often given the notation $\tau_R$. It is the time for relaxation of the overall shape of the molecule (it is the relaxation time of the amplitude of normal mode with just one nodal point, $\cos \pi/N$), and is also the time taken by a Gaussian Rouse chain to diffuse its own radius of gyration.

4.1.3. *Monomer motion in the Rouse model*

What does the local motion of this model chain look like? We expect for short intervals that the chain contour may have adjusted locally, but retain a very similar global configuration (see figure 21). In order to answer this question, and to compare with local diffusion probes of NSE and FGNMR of unentangled dynamics, we need to calculate the correlation function $\phi_n(t) \equiv \langle [\mathbf{R}(n,t) - \mathbf{R}(n,0)]^2 \rangle$. The first step is to write it in terms of the Rouse modes whose dynamics we already know:

$$\begin{aligned}\langle (\mathbf{R}(n,t) - \mathbf{R}(n,0))^2 \rangle &= \left\langle \begin{array}{l} \left( \mathbf{X}_0(t) + 2\sum_{p=1}^{\infty} \mathbf{X}_p(t) \cos\left(\frac{p\pi n}{N}\right) \right. \\ \left. \quad -\mathbf{X}_0(0) - 2\sum_{p=1}^{\infty} \mathbf{X}_q(0) \cos\left(\frac{q\pi n}{N}\right) \right)^2 \end{array} \right\rangle \\ &= \langle (\mathbf{X}_0(t) - \mathbf{X}_0(0)^2 \rangle \\ &\quad + \left\langle \begin{array}{l} 4\sum_{pq} (\mathbf{X}_p(t)\mathbf{X}_q(t) + \mathbf{X}_p(0)\mathbf{X}_q(0) \\ \quad -2\mathbf{X}_p(t)\mathbf{X}_q(0)) \cos\left(\frac{p\pi n}{N}\right) \cos\left(\frac{q\pi n}{N}\right) \end{array} \right\rangle, \end{aligned} \tag{69}$$

Figure 21. A Rouse chain changes its configuration (from solid to dashed curve) locally but not globally in times shorter than $\tau_R$.

where the first term in the second expression is simple centre-of-mass diffusion. From the last section, we know all the correlations (and only those with $p = q$ are non-zero), so direct substitution gives

$$\phi_n(t) = 6D_{\mathrm{CM}}t + \frac{4k_{\mathrm{B}}T}{k_1}\sum_{\mathrm{p}=1}^{\infty}\frac{1}{p^2}\cos^2\left(\frac{p\pi n}{N}\right)[1 - \exp(-p^2 t/\tau_{\mathrm{R}})]. \tag{70}$$

The first term is just the centre-of-mass diffusion of the entire chain (with diffusion constant $D_{\mathrm{CM}} = k_{\mathrm{B}}T/\zeta_{\mathrm{CM}}$), the second the contribution from the internal modes. Now for times $t \ll \tau_{\mathrm{R}}$, the amplitudes of the modes in the sum decay slowly with $p$, so permitting us to replace the sum with an integral. Also we may average the $\cos^2$ function over monomers $n$ to obtain the approximation:

$$\begin{aligned}\phi_n(t) &\simeq 6D_{\mathrm{CM}}t + \frac{2k_{\mathrm{B}}T}{k_1}\int_0^{\infty}\frac{1}{p^2}[1 - \exp(-p^2 t/\tau_R)]\,\mathrm{d}p \\ &= 6D_{\mathrm{CM}}t + \frac{Nb^2}{3\pi^2}\left(\frac{t}{\tau_{\mathrm{R}}}\right)^{1/2}\alpha.\end{aligned} \tag{71}$$

Here

$$\alpha = \tfrac{1}{2}\int_0^{\infty} z^{-3/2}[1 - \exp(-z)]\,\mathrm{d}z \simeq 1.77$$

is a purely numerical constant. The result is remarkable: each monomer executes an 'anomalous' or sub-Fickian diffusion, such that its mean square displacement varies as $t^{1/2}$ rather than $t$ (as for ordinary diffusion). This behaviour persists until times longer than the Rouse time, after which each monomer is carried by the (faster) centre of mass motion of the whole molecule.

4.1.4. *A physical interpretation*

In some ways, the structure of the Rouse modes is misleading: although a perfectly correct diagonalization of the dynamics in linear response, they seem to imply longer range correlations along the chain than in fact exist. The sub-Fickian diffusion arises physically from the *absence* of such correlations. To diffuse a distance $\Delta\mathbf{R}_{\mathrm{n}}$, the $n$th monomer only requires its motion to be correlated with the $(\Delta\mathbf{R}_n)^2/b^2$ other monomers in the region spanned by $\Delta\mathbf{R}_n$. This arises as a straightforward consequence of their *connectivity*. All other monomers have motions *uncorrelated* with it, so cannot contribute to the effective drag for that motion, which by simple summation is therefore $\zeta_{\mathrm{eff}} = \zeta_0(\Delta\mathbf{R}_n)^2/b^2$. Thus from the law of normal diffusion and the Einstein relation $D_{\mathrm{eff}} = k_{\mathrm{B}}T/\zeta_{\mathrm{eff}}$, we obtain

$$\phi_n(t) = \langle(\Delta\mathbf{R}_n)^2\rangle \simeq D_{\mathrm{eff}}t \simeq \frac{k_{\mathrm{B}}Tb^2}{\zeta_0\langle\Delta\mathbf{R}_n^2\rangle}t \quad \Rightarrow \quad \phi_n(t) \simeq \left(\frac{k_{\mathrm{B}}Tb^2}{\zeta_0}\right)^{1/2}t. \tag{72}$$

The 'extra-drag' effect runs out of new monomers to add when the chain has diffused its own radius of gyration, which is at the Rouse time. After this all the drag comes from the entire chain, and all monomer motions become correlated as ordinary diffusion takes over. So a log–log plot of the monomeric mean displacement appears as in figure 22.

In the formalism of the calculation in Rouse modes, the successive decorrelation of each mode from its original amplitude does the job of this real-space argument

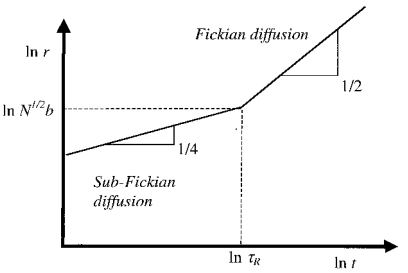


Figure 22. Monomer diffusion with time in the Rouse model.

when the mode wavelength is associated with the distance over which motion produces correlated drag.

4.1.5. *Stress relaxation in the Rouse model*

The (deviatoric) stress formula

$$\sigma_{ij} = \frac{3k_B T}{b^2}\mathbb{C}\left\langle \frac{\partial R_i}{\partial n}\frac{\partial R_j}{\partial n}\right\rangle$$

we derived above, equation (11), has a very simple representation in terms of the Rouse modes [31]

$$\sigma_{ij} = \frac{\mathbb{C}}{N}\sum_p \langle k_p X_{pi}(t) X_{pj}(t)\rangle, \tag{73}$$

where, on $X_{pi}$, the first suffix is the mode index and the second a Cartesian one. To find $G(t)$ we consider a step strain in shear of size $\gamma$. After the step is applied, all the $\mathbf{X}_p$ vector mode amplitudes just deform affinely (the Rouse equation (62) implies that in the limit of infinitely fast shear, the chain coordinates just follow the bulk deformation). Hence, immediately after the step strain at $t = 0$, the amplitude $X_{px}(0^+) = X_{px}(0^-) + \gamma X_{py}(0^-)$, so that the shear stress component becomes

$$\sigma_{xy}(0^+) = \gamma\frac{\mathbb{C}}{N}\sum_p \langle k_p X_{py}(0^+) X_{py}(0^+)\rangle = \gamma\frac{\mathbb{C}}{N}\sum_p kT. \tag{74}$$

Each mode then decays back to equilibrium anisotropy with its own time constant giving for $G(t) = \sigma_{xy}(t)/\gamma$:

$$G(t) = \frac{\mathbb{C}k_B T}{N}\sum_p \exp(-2p^2 t/\tau_R). \tag{75}$$

Again, for times $t \ll \tau_R$, the modes are effectively continuous and the sum is approximated well by the integral

$$\int \mathrm{d}p \exp(-2p^2 t/\tau_1) \approx \left(\frac{t}{\tau_1}\right)^{-1/2}.$$

So we find that, until a final crossover to an exponential decay beyond the Rouse time, the Rouse model has a relaxation modulus which is a power-law of $G(t) \sim t^{-1/2}$. From equation (23) we have then also $G'(\omega) \sim G''(\omega) \sim \omega^{1/2}$. This form can be seen, for example, in the high frequency parts of the polyisoprene linear and star rheology data we saw in figures 9 and 11.

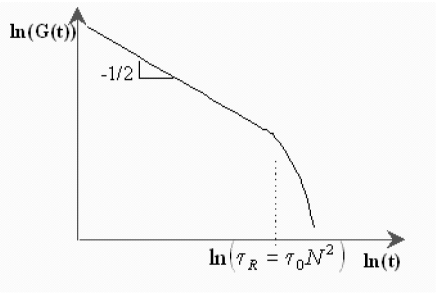


Figure 23. Stress relaxation in the Rouse model.

By analogy with the physics we used to understand the scaling of monomer diffusion, this behaviour can be understood simply from the result that the size of the modulus in soft matter is $k_B T \times$ (density of degrees of freedom) [39]. In this case, after a time $t$, we allot just $k_B T$ to each unrelaxed subchain. Such a chain contains $n(t)$ monomers where $n(t) \sim (\Delta \mathbf{R}(t))^2 / b^2 \sim t^{1/2}$. The number of such subchains decays as $t^{-1/2}$, giving $G(t) \sim t^{-1/2}$, until the sub-Fickian regime ceases at the Rouse time. In this case there are no larger subchains left to decorrelate, so there is a crossover to final exponential decay. The expected behaviour on a log–log plot is therefore as shown in figure 23. Note that the longest relaxation time scales with molecular weight as $N^2$, but the viscosity scales as $\mathbb{C} k_B T N$. This is because at the longest relaxation time that sets the value of the viscosity, the stress is carried only by the lowest Rouse mode; the density of these modes is just one per chain, or $\mathbb{C}/N$.

4.1.6. *Dielectric relaxation in the Rouse model*

As a final illustration of the application of the solution of the Rouse model, we calculate the prediction for the dielectric relaxation function $\Phi_d(t)$ in the case of A-type dipoles with all dipole moments directed in one direction along the chains (see section 3.7). As derived above in equation (43), the average may be written in terms of integrals along the chain contour to give a simple expression in terms of the correlation of the end-to-end vectors of the chains $\mathbf{R}_{ee}(t)$

$$\begin{aligned}\Phi_d(t) &= \frac{1}{\langle [\mathbf{R}(N,0) - \mathbf{R}(0,0)]^2 \rangle} \langle [\mathbf{R}(N,t) - \mathbf{R}(0,t)] \cdot [\mathbf{R}(N,0) - \mathbf{R}(0,0))] \rangle \\ &\equiv \frac{\langle \mathbf{R}_{ee}(t) \cdot \mathbf{R}_{ee}(0) \rangle}{\langle (\mathbf{R}_{ee}(0))^2 \rangle}. \end{aligned} \tag{76}$$

Now, using the normal mode description of the chains (64) we can write the end-to-end vector as

$$\begin{aligned}\mathbf{R}_{ee}(t) \equiv \mathbf{R}(N,t) - \mathbf{R}(0,t) &= 2 \sum_{p=1}^{\infty} \mathbf{X}_p(t) [\cos(p\pi) - 1] \\ &= 4 \sum_{p \text{ odd}} \mathbf{X}_p(t) \end{aligned} \tag{77}$$

so finally, using the equipartition amplitude distribution of mode amplitudes $\langle X_p^2(0) \rangle = Nb^2 / 6\pi^2 p^2$,

$$\Phi(t) = \frac{8}{\pi^2} \sum_{p \text{ odd}} \frac{1}{p^2} \exp(-p^2 t/\tau_R). \tag{78}$$

This is a rather familiar function in polymer dynamics—we will meet it again below in the calculation of the reptation prediction of the *viscoelastic* relaxation, but is perhaps more generally known as Fourier's solution of the diffusion equation in 1D with fixed value boundary conditions and constant initial condition. The corresponding dissipative part of the frequency-dependent modulus reflects the dominance of the longest relaxation time in equation (78) in that it is sharply peaked at $\omega = \tau_R^{-1}$, but falls off as $\omega^{-1/2}$ to the right of the peak.

4.1.7. *Experimental observations of Rouse motion*

It is very hard to obtain rheological data on unentangled polymers in the melt. This is due to the rapid relaxation times of the material, and the broad spread of the effect of more local, molecular mechanisms, that affect the stress relaxation modulus at higher frequency than the Rouse time [12]. Of the polymers normally prepared by anionic techniques, PI has the clearest rheological Rouse signature, but this is best seen in the high frequency part of the dissipative modulus in well entangled cases, e.g. [50], where $G'(\omega) \sim G''(\omega) \sim \omega^{1/2}$ for $\omega \gg \tau_e^{-1}$. In other cases, adding a free-Rouse function at high frequency to theoretical predictions for entangled modes only approximately accounts for the high frequency response—see, for example, reference [56] for PS, but note the error in this paper, which omits the factor 2 from the exponent in equation (75). In many polymers, there is also a strong dependence of the glass transition temperature on the density of free chain ends, which becomes more important as the molecular weight becomes small. So, for example, the predicted Rouse scaling of the centre of mass diffusion constant $D_{CM} \sim M^{-1}$ is usually not seen in raw data, since the monomeric mobilities are higher for the smaller chains. None the less, when corrected for these $T_g$ effects (to 'isofrictional states', approximately equal temperatures from the glass transition), unentangled chains do exhibit this scaling [200, 201].

More detailed information on unentangled chain motion is obtained from the relaxation spectrum and the structure of the eigenfunctions of the Rouse operator. We saw above that both of these were available from dielectric spectroscopy using A-type dipoles, including the technique of chemical dipole inversion. The experimental picture is intriguing: when self-dilute and unentangled probe PI chains are dispersed in a (chemically compatible) PB matrix that is itself unentangled, the dielectric relaxation function is indeed closely modelled by the Rouse prediction (78) [184]. Dipole inversion also indicates that the chain normal modes are very close to the predicted harmonic functions [187]. However, either allowing the PB matrix to entangle by choosing higher molecular weight polymers, or by measuring unentangled *homogenous* PI melts, leads to a broader mode distribution. In these cases $G''(\omega) \sim \omega^{-1/4}$ for $\omega \succeq \tau_R^{-1}$. In both cases, the experimentally determined eigenfunctions differ from the Rouse modes principally at the extremities of the chains (see figure 24). This would be consistent with a faster relaxation locally at the chain ends (see discussion of CLF in *entangled* chains below, where a very similar phenomenology arises) [231], but the reasons for this effect in unentangled melts are at present quite unclear.

Rouse motion predictions of the sub-Fickian monomer diffusion have been examined by NSE in melts of PE [232], PDMS [233] and PIB [234]. The conclusion

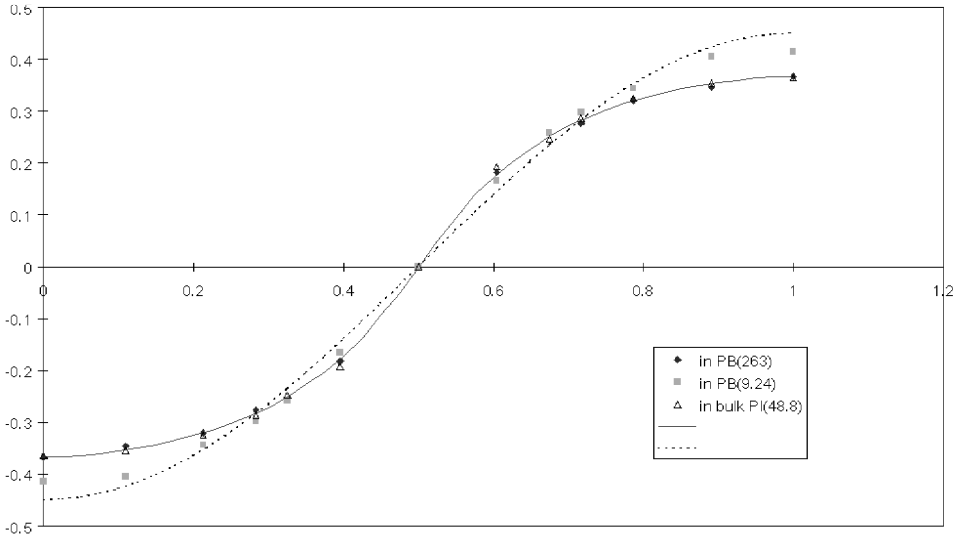


Figure 24. Form of the $p = 1$ dielectric relaxation eigenmode deduced from inverted dipole measurements. The dashed line is the Rouse mode. Data correspond to moderately entangled PI in a low MW PB matrix (close to Rouse form) and high MW PB and homopolymer PI matrices (perturbed from Rouse form). [From reference [177].]

of these studies was that the coherent structure factor out to 100 ns could be accounted for quantitatively by the Rouse model, but only in the regime of scattering vectors $q < 0.13\,\text{Å}^{-1}$. At higher $q$ (more local motions) the effective chain stiffness was higher than the Rouse model would predict, and as we might expect from fully molecular simulations [232]. There has been no report of special faster dynamics of chain ends at early times, but labelled incoherent NSE would allow this technique to explore the anomalies identified by dielectric spectroscopy.

A further complication arises from contributions to the stress that arise from local molecular features not represented by the flexible coarse-grained model we have adopted. The reorientation of monomers themselves, whose contribution to the stress is more usually associated with the glassy modulus at values of $\sim 10^9$ Pa may still contribute to the melt modulus in the Rouse region of the spectrum [235].

With these caveats in mind, and their implications for the physical assumptions made in the Rouse theory, we now consider how the model may be modified in the presence of entanglements.

### 4.2. *Entangled chains: the tube confining fields*

Now we consider the motion of a chain in a forest of topological constraints arising from its neighbours. The simple one-parameter theory for entangled chains that will be our working tool arises from the proposition that the local inability of one molecular chain to cross another leads to strong confinement for local motion lateral to its curvilinear path, but no confinement for motion parallel to it. The exception to this confinement is the behaviour of the chain ends, which are free to explore the melt without topological constraint. Furthermore, the lateral confinement is assumed to possess asymptotic freedom: the constraints are felt only beyond a localising length $a$. These assumptions are equivalent to picturing each chain in the melt or entangled solution to be surrounded by a tube, of radius $a$, that follows the

chain contour [19, 20] (see figure 4). As we have already seen, there is now considerable experimental and simulation evidence to support the tube assumption. In the case of concentrated solutions, the tube diameter will itself depend upon polymer concentration (in a way that is still not clarified; see section 6.4), but experimentally follows closely $a \sim \mathbb{C}^{-1/2}$). If the chain is itself a Gaussian random walk of $N$ subchains of effective steplength $b$, then the tube will also be a random walk, but coarse-grained to tube segment lengths of distance $a$. The number of chain steps in each tube segment is then $N_e = a^2/b^2$, and the curvilinear length of the tube is just $L_{eq} = (N/N_e)a = Nb^2/a$ (previous definitions of $M_e$ have introduced a factor of 4/5 into this relation, but we have here adopted a simpler convention for $M_e$; see section 4.2.4 below). This was also been termed the 'average primitive path length' by Doi and Edwards [22], who imagined freezing the positions of all chains but one, then increasing the tension in the test chain until it assumed the shortest possible length that respected the topological constraints upon it [236]. The primitive path is important because it controls the nature and timescales of all dynamics constrained by entanglements. Although the notion of a 'tube radius' is a rather inexact idea (and would depend both on definitions and the form of the confining potential), the notion of $a$ as the step length of the primitive path is well defined. The primitive path becomes a coarse-grained random walk of $Z = L_{eq}/a$ steps. $Z$ will henceforth become our standard dimensionless notation for molecular weight when entangled dynamics dominate. We note additionally that the instantaneous length of the primitive path $L$ is a *fluctuating* quantity: there will be sections of the chain on the lengthscale of $a$ that do not form a part of the primitive path, but instead belong to unentangled loops either within the tube or herniating from it. Polymer chain will execute continuous random dynamics of exchange between the principal path and unentangled loops. Termed 'kink defects' by de Gennes [20], the resulting curvilinear diffusion of chain length not on the primitive path, between entanglement regions of size $a$ was the motivation for the one-dimensional stochastic simulations of 'repton' dynamics we reviewed in section 3.10 [221].

4.2.1. *Statistics of the primitive path*

The lateral confining field is not the only component of the tube potential. In addition we require that the chain ends be subject to an effective tension that maintains the equilibrium path length of $L_{eq}$. Of course neither this component nor the local tube constraint are true equilibrium potentials since none of the uncrossability constraints in a melt is permanent. Instead they are effective potentials for dynamics on timescales between the fastest motion that detects many-chain constraints, and the time for complete escape of chains from their original tubes. The chain-end tension serves to generate an effective potential for the primitive path length, just as the tube generates an effective confining potential for lateral displacement of local segments of chain. The path length potential must localize the coarse-grained tube length around $Nb^2/a$, but we expect that the fluctuations around this value are important. One way to construct this potential proceeds by identifying a value for the effective end-tension. The free-energy gain due to the entropy of confinement of every entangled polymer segment is just $3k_BT$, equivalent to a tension of

$$f_{eq} = 3kT/a \tag{79}$$

along the entangled chain (we will see below that the prefactor of 3 guarantees our definition of the tube step length *via* the mean primitive path length $L_{eq} = Nb^2/a$). So the free energy change associated with doubly occupied tube, or unentangled loop, emerges naturally as just this tension multiplied by the distance translated curvilinearly along the tube, $a$. The chain tension arises in a physical way: at timescales short enough for the tube constraints to be effectively permanent, each chain end is subject to random Brownian motion at the scale of an entanglement strand such that it may make a random choice of exploration of possible paths into the surrounding melt. One of these choices corresponds to retracing the chain back along its tube (thus shortening the primitive path), but far more choices correspond to extending the primitive path. The net effect is the chain tension, sustained by the free ends. We can then write a potential $U(z)$ for the length of the primitive path $z$ by including both the (quadratic) curvilinear rubber-elastic term and the (linear) end-tension term as follows:

$$U(z) = \frac{3kT}{2Nb^2}z^2 - \frac{3kT}{a}z = \frac{3kT}{2Nb^2}s^2 + \text{const.}, \tag{80}$$

where $s = L_{eq} - z$ is the coordinate that measures the retraction of the free end from its equilibrium position. This quadratic potential [237] will determine the fluctuation dynamics of an arm of an entangled star polymer: it gives the free energy paid for a retraction of the free end a distance $s < L_{eq}$ along the tube. Whenever this happens, the subsequent equilibrium configuration, after re-extension of the arm, will have a renewed configuration for all chain segments occupying tube whose primitive path distance from the branch point is between $L_{eq} - s$ and $L_{eq}$. The effective potential in equation (80) generates a probability distribution function for fluctuations in primitive path length by insertion in a Boltzmann distribution:

$$P(L) \simeq \exp\left[-\frac{3}{2}Z\left(\frac{L}{L_{eq}} - 1\right)^2\right], \tag{81}$$

with $Z = L_{eq}/a$, the average number of tube segments in the primitive path. So in this approximation the distribution of primitive path lengths is Gaussian.

The primitive path has frequently been visualized in a lattice analogy. The set of tools available once the entanglement problem has been cast as a lattice calculation have also permitted calculations of the statistics of the primitive path that go beyond the Gaussian approximation of (80) [238–240]. By direct enumeration of distinct states of the lattice polymer, when the primitive path is defined by a coarser superlattice, numerical results for the potential in equation (81) can be obtained in the form [239]

$$P(L, L_{eq}, m) \sim \frac{1}{L_{eq}^{1/2}}\exp\left[-Z\bar{\phi}\left(\frac{L}{L_{eq}}, m\right)\right]. \tag{82}$$

Here $m$ is the integer size of the superlattice defining the primitive path. In two dimensions and for a simple square lattice, the function $\bar{\phi}(x)$ deviates from a simple quadratic by about 20% for extreme fluctuations of the primitive path to zero path length. However, other calculations [241, 242] extending the dimension and lattice structure, and making different assumptions for the boundary conditions for the set of recursion relations on $P(L, L_{eq})$ (they worked at $m = 1$), found that

$$\bar{\phi}\left(\frac{L}{L_{\rm eq}}, m\right) = \frac{\gamma}{2}\left(\frac{L}{L_{\rm eq}} - 1\right)^2 - \frac{1}{4\gamma L_{\rm eq}} \ln\left(\frac{L}{a} + \frac{1}{2\gamma}\right), \tag{83}$$

with $\gamma = (z-2)/z$. In this calculation, the correction to the quadratic part of the potential seems to vanish in the limit of high entanglement. However, a full 3D lattice calculation for arbitrary $m$ [243] came to different conclusions, finding that a 20% renormalization of the quadratic potential to lower values persists for deep retractions in the limit of large $m$, which presumably is the best model for highly flexible chains. This is in qualitative agreement with the 2D calculation of reference [238]. In this case, the $z$-dependence of the prefactor $\gamma$ to the dimensionless quadratic part of the potential is

$$\gamma = \frac{z(z-2)}{4(z-1)}, \tag{84}$$

which is also the result of references [240] and [244]. The conclusion from the lattice models seems to be that there remains a non-quadratic correction (downwards) to the full retraction potential of the order of 20% at large $z_0$ and large $N_{\rm e}$. However, there is an issue to settle in the mapping of the results of lattice models onto the asymptotics of the real-space chain, equation (81). One can either adopt the convention that $z = 6$ in the 3D case, in which case an additional factor of about 3 must be introduced into $\gamma$ in order to match the simple result (81), by arguing that the real chains are always 3D random walks. Alternatively [245], one can set the value of $z$ in order to recover the asymptotic result of the continuous tube model (81). From equation (84) we find $z \simeq 13$. Advocates of lattice calculations might claim that this indicates the unreliability of the calculation leading to equation (81), where $\gamma = 3$. On the other hand, a high co-ordination number for *topology* might well be much higher than that of, for example, random packing of spheres due to the large local Brownian fluctuations of the effective network. In this view, $z = 13$ is not unreasonable for the effective coordination number of tube segments at a chain end.

So the present state of primitive path statistics leaves both the magnitude of the quadratic fluctuations and the non-quadratic corrections open to debate in the case of continuous real space. We will see below that, although these corrections do not affect the equilibrium fluctuations involved in CLF effects on dynamics of linear polymers, they could be very important for branched polymers of moderate degrees of entanglement. These systems actually rely on such extreme fluctuations to relax their entangled conformations.

#### 4.2.2. *Linear polymers (1): reptation*

Now we consider the fundamental mode of motion of a chain in a confining tube whose ends explore the melt freely. At small times (for correlation functions) and small distances, the presence of the tube will not be felt, so $G(t)$ and monomer displacements at early times will be unchanged from their Rouse form. At later times (times after the Rouse time $\tau_{\rm e}$ of entanglement strands of chain of length $N_{\rm e}b$ that just span $a$) the tube *will constrain any piece of chain to the orientation of the piece originally present there, until the tube section is traversed by a free end.* This is itself determined by a one-dimensional stochastic dynamics along the tube contour. To identify the fundamental mode of entangled dynamics we make two further approximations (to be dropped later on) that will become exact asymptotically in

the limit of high molecular weight: (1) we coarse-grain the chain so that subchain dynamics on scales less than $a$ are averaged out (so setting the timescales to values larger than the Rouse time of an entanglement strand $\tau_e$), and (2) we ignore fluctuations in the primitive path (or contour length fluctuations, CLF). This leads to a simple stochastic formulation of these dynamics

$$\mathbf{R}(n, t + \Delta t) = \mathbf{R}(n + \Delta n, t), \tag{85}$$

with the random diffusive shifts $\Delta n$ selected from a Gaussian noise distribution satisfying

$$\langle \Delta n \rangle = 0; \quad \langle (\Delta n)^2 \rangle = \frac{2D_c a^2}{b^4} \Delta t. \tag{86}$$

Here $D_c = k_B T / N\zeta_0$ is the *curvilinear diffusion constant* arising from the summed drag of all the monomers in the chain. It is numerically identical to the centre-of-mass diffusion constant of the Rouse chain in equation (70). This is the one-dimensional dynamics we have already encountered pictorially as 'reptation' [20], and is simply the Brownian motion of the centre-of-mass coordinate of the chain confined to its primitive path. We note that an alternative, and more usual, description of the stochastic motion takes the variable of primitive path contour length, $s$, rather than monomer coordinate, $n$ [31]. We adopt $n$ here in order to keep the same level of chain description in Rouse and reptation dynamics. Reptation dynamics induce simple diffusion equations for functionals of the chain coordinates such as the experimental quantities of section 3. These can, as we have seen, be cast in the form of averages over functions of the chain coordinates $\langle f(\mathbf{R}(n, t)) \rangle$. Such a function will follow:

$$\langle f(n, t + \Delta t) \rangle = \left\langle f(n, t) + \Delta n \frac{\partial f}{\partial n} + \frac{(\Delta n)^2}{2} \frac{\partial^2 f}{\partial n^2} + O(\Delta t^2) \right\rangle, \tag{87}$$

from which the moments of $\Delta n$ produce under the limiting operation $\Delta t \to 0$:

$$\frac{\partial \langle f \rangle}{\partial t} = D_c \left( \frac{a^2}{b^4} \right) \frac{\partial^2 \langle f \rangle}{\partial n^2}. \tag{88}$$

The monomer diffusion, mechanical stress, birefringence, single chain scattering function and dielectric relaxation can all be cast in this form; the distinct solutions arising from the different boundary conditions in each case [31]. (In cases where more than one independent monomer argument arises, such as $f(n, n'; t) = \mathbf{R}'(n, t)\mathbf{R}'(n, t)$, the diffusion operator is induced on each contour variable in the equation for $\langle f \rangle$.) We review some important results for these quantities below, but observe here that an important new timescale emerges from the diffusive property of reptation and the length of the primitive path. To disengage all the chain from tube occupied at $t = 0$ (when a step-strain might be applied, or monomer positions labelled by NMR spin moments), the typical time follows the usual scaling of Fickian diffusion, and so is $\tau_d \approx N^2 / D_c$. Expressing the primitive path length $L_{eq}$ and the diffusion constant for reptation in terms of the parameters of the tube model gives the dependences on fundamental quantities as $\tau_d \approx N^3 b^4 \zeta_0 / k_B T a^2$.

We next review the results for important experimental quantities from the entangled reptation mode alone. The calculations correspond to specific choices for the function $f$ above, with the associated boundary conditions.

*Segmental diffusion*. A useful auxiliary function to work with [31] is

$$\phi(n,n';t) = \langle[\mathbf{R}(n,t) - \mathbf{R}(n',t)]^2\rangle, \tag{89}$$

from which the mean square displacement of a single monomer is just $\phi_n(t) \equiv \phi(n,n;t)$—cf. the Rouse calculation of equation (70). The initial condition is just the Gaussian chain result $\phi(n,n';0) = |n-n'|b^2$. The boundary condition arises from the assumption that the final entanglement strands are always uncorrelated and random, so always add the equilibrium increment of $b^2$ to $\phi$ with each step in $n$:

$$\frac{\partial}{\partial n}\phi(n,n';t) = \begin{cases} b^2 & n = N \\ -b^2 & n = 0. \end{cases} \tag{90}$$

The solution is expressed in the eigenmodes of equation (88) with zero-gradient boundary conditions (the finite gradients of equation (90) are assumed by subtracting the initial condition) to give for the diffusion of a single monomer at $n$:

$$\phi_n(t) \equiv \phi(n,n;t) = \frac{2}{Z}D_c t + \sum_{p=1}^{\infty}\frac{4L_{eq}a}{p^2\pi^2}\cos^2\left(\frac{p\pi n}{N}\right)\left[1 - \exp\left(\frac{-p^2 t}{\tau_d}\right)\right]. \tag{91}$$

The solution now sets exact prefactors in the expression for the 'disengagement time' $\tau_d$

$$\tau_d = \frac{N^3 b^4 \zeta_0}{\pi^2 k_B T a^2}. \tag{92}$$

We note the structural similarity between this and the result for Rouse monomer motion given by equation (70). Both give non-Fickian mean square displacements going as $\phi_n(t) \sim t^{1/2}$ for times less than a certain characteristic time ($\tau_R$ for Rouse motion and $\tau_d$ for reptation), and ordinary diffusion beyond that, as each monomer is convected by the centre of mass of the molecule. However, the behaviour arises for completely different reasons. In the Rouse chain the sub-Fickian motion is due to growing correlations of displacement along the chain away from the probe monomer, so increasing the effective drag. In reptation, the drag is constant, but a Fickian diffusion along the tube is reduced to sub-Fickian motion in real space, since the tube is itself a random walk.

In fact, the tube model predicts a regime in which both these contributing factors combine to produce a very slow monomer displacement such that $\phi_n(t) \sim t^{1/4}$. This is also seen in experiments using NSE and FGNMR, and is an effect of contour-length fluctuation from the Rouse modes longitudinal to the tube, which are important in the regime $\tau_e < t < \tau_R$. These are not constrained by the tube in the same way that lateral modes are. We examine ways of treating them in section 4.2.4 below.

*Tube survival: rheological and dielectric response*. Another example of the function $f(n,t)$ that will assist both as a concrete example and as a calculation aid is the 'tube survival probability'. We have seen that the tube conveys its original local orientation on any segment of chain that lies within it. This persists until the topological constraint of the tube is annihilated by the arrival of a chain end. For this reason, when pure reptation is the dominant mode, we expect some experimental signals to depend only on the fraction of original tube segments that have not yet been visited by a chain end, usually denoted $\mu(t)$. An example is the stress decay after

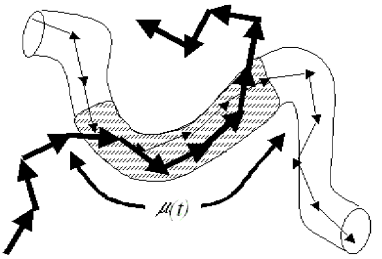


Figure 25. A reptating chain has retained only the shaded tube segments from those defining the chain at $t = 0$. The constraints at $t$ induce correlations of the current chain segments and their dipoles (bold arrows) with those of the original chain configuration (light arrrows) only *via* the surviving tube segments, constituting a fraction $\mu(t)$ of the originals.

a step strain at $t = 0$. The only chain segments possessing orientation at time $t$ correlated with that of the ensemble at $t = 0$ will be those occupying surviving tube segments, so we expect $G(t) \sim \mu(t)$ for pure reptation. Similarly, the dielectric response of A-type chains without dipole inversion will also be proportional to $\mu(t)$, since only chain occupying these tube segments will have a dipole moment correlated with the moment at $t = 0$ (see figure 25). For this reason, it is sometimes commented that *stress (and dielectric moment) is carried by the surviving tube*. Because we know that the dominant relaxation time for escape from the tube is $\tau_d$, we expect, for timescales between $\tau_e$ and $\tau_d$ (a range that grows with $N^3$!), a near-plateau in $G(t)$, with an amplitude of $G_0 \simeq \mathbb{C}k_BT/N_e$, and a similar plateau in $\Phi(t)$, of amplitude 1. Without further calculation, we can see that the tube model with the reptation mode alone in a fixed tube contour has $G(t)/G(0) = \Phi(t) = \mu(t)$, so that in the entangled case, the stress and dielectric decay function should be proportional (we recall that this is by no means the case for the Rouse model of unentangled dynamics). This is qualitatively the case for monodisperse linear chains [180, 181].

To calculate $G(t)$ more precisely within the tube model, we calculate a more general function of the survival probabilities for segments of original tube during stress relaxation. In the frame of the *chain*, these behave as an ensemble of diffusers on the curvilinear coordinate $x$ with diffusion constant $D_c$ that are absorbed by boundaries at 0 and $L$. So if $\Psi(x, x', t)$ is the probability that a tube segment initially at position $x'$ on the chain has diffused to $x$ at time $t$ without being visited by a chain end, it will obey:

$$D_c \frac{\partial^2 \Psi}{\partial x^2} = \frac{\partial \Psi}{\partial t} \tag{93}$$

with $\Psi(x, x', 0) = \delta(x - x')$ as an initial condition and $\Psi(0, x', t) = \Psi(L, x', t) = 0$ as boundary conditions.

This is equivalent to the Fourier problem of heat diffusion through a slab with cooled faces. We may express the simpler tube survival probability $p(s, t)$, that the tube segment at primitive path co-ordinate $s$ has survived to time $t$ as an integral over starting positions for the segment:

$$p(s, t) = \int_0^L \Psi(s, s', t)\, \mathrm{d}s'. \tag{94}$$

To solve these we expand in the normalized eigenfunctions $\vartheta_p(x) = (2/L)^{1/2}\sin(p\pi x/L)$ (for integer $p$) that obey the boundary conditions:

$$\Psi(x, x', t) = \sum_{p=1}^{\infty} u_p(t, x')\vartheta_p(x). \tag{95}$$

Substituting in the differential equation gives the time dependence of the coefficients $u_p(t) = u_p(0)\exp(-p^2 t/\tau_d)$. This gives us now an exact expression for the disengagement (reptation) time $\tau_d$

$$\tau_d = \frac{L^2}{\pi^2 D_c} = \frac{N^3 b^4 \zeta_0}{\pi^2 k_B T a^2}. \tag{96}$$

The final ingredient is the initial amplitudes of the eigenfunctions in the survival probability

$$u_p(0) = \int_0^L \vartheta_p(s)\Psi(s, x', 0)\,ds = \left(\frac{2}{L}\right)^{1/2}\sin\left(\frac{p\pi x'}{L}\right).$$

So the final solution for the local survival probability is

$$\Psi(x, x', t) = \sum_{p=1}^{\infty}\frac{2}{L}\sin\left(\frac{p\pi x'}{L}\right)\sin\left(\frac{p\pi x}{L}\right)\exp\left(-\frac{p^2 t}{\tau_d}\right) \tag{97}$$

and the total tube survival probability is just proportional to the integral over all starting positions $x'$ and all final positions $x$

$$\mu_{DE}(t) = \int_0^L dx\int_0^L dx'\Psi(x, x', t) = \sum_{p\ \text{odd}}\frac{8}{\pi^2 p^2}\exp\left(-\frac{p^2 t}{\tau_d}\right). \tag{98}$$

As expected, the result is nearly single-exponential, certainly in qualitative accord with the data shown in section 3.2.2. However, the prediction for the density of higher modes is less than that experimentally seen—it is simple to show by approximating the sum for the modulus with an integral, that $G''(\omega) \sim \omega^{-1/2}$ at frequencies higher than $\tau_d^{-1}$. We have met the function $\mu_{DE}(t)$ before—it is just the Rouse model prediction for the *dielectric* relaxation of *unentangled* melt chains. So, even though the experimental results show a slightly broader maximum in $\epsilon''(\omega)$ than predicted by pure reptation alone, the observation that $\epsilon(t)$ is *unchanged* in form (when a rescaling in time is made) [37] is an exact prediction of the pure reptation model. This agreement must however be a conspiracy of different effects, because the $\omega^{-1/4}$ scaling of $\epsilon''(\omega)$ to the right of its peak cannot be due to the same reason in both unentangled and entangled chains. Crossing the entanglement threshold has very great qualitative consequences for rheology, however. The predicted change from the very broad, scaling–function Rouse response of $G(t) \sim t^{-1/2}\exp(-2t/\tau_R)$ to the near-exponential form of $\mu(t)$ is, as we have seen, observed. What remains to be understood is why, in experiment, $G(t) \sim [\Phi(t)]^{1+\alpha}$ with $\alpha = 1$ rather than 0, and why both $G''(\omega)$ and $\epsilon''(\omega)$ fall away as $\omega^{-1/4}$ rather than as $\omega^{-1/2}$ for $\omega > \tau_d^{-1}$.

We have not discussed the predicted values for the prefactor in the expression $G(t) \sim \mu_{DE}(t)$, which one would naturally identify with the plateau modulus $G_N^{(0)}$, but defer this until we have treated contour length fluctuations, since without them no quantitative link to experiment such as the value of $G_N^{(0)}$ can be made.

One important modification to reptation theory was made for the case of 'living polymers' in which the chains rapidly break and reform while their spatial dynamics proceeds [103, 246]. If the chemical dynamics is much faster than the curvilinear diffusion, or more formally when $\tau_{\text{break}} \ll \tau_{\text{d}}$, where $\tau_{\text{break}}$ is the mean waiting time for a break to occur in a chain of mean length, then a tube segment is typically relaxed by a 'reptation-reaction' process. The segment waits until a break appears in the chain occupying it near enough to diffuse to it before it recombines with another chain end. This removes any dependence of the relaxation times on a chain coordinate; all segments are equivalent. So the stress decay is pure-exponential. This explains the intriguing data we saw above (figure 10).

*Dynamic scattering function.* The form of the coherent dynamic scattering function (equation (37) above) for pure reptation alone was calculated by Doi and Edwards [31], again from the reptation diffusion equation, to give the effect of escape from the tube alone, $S_{\text{esc}}(\mathbf{q}, t)$:

$$S(\mathbf{q}, t) = S_{\text{esc}}(\mathbf{q}, t) \equiv \sum_{p=1}^{\infty} \frac{2\mu N}{\alpha_p^2(\mu^2 + \alpha_p^2 + \mu)} \sin^2 \alpha_p \exp\left(-\frac{4D_{\text{c}}\alpha_p^2 t}{L^2}\right), \tag{99}$$

where $\mu = (q^2 N b^2/12)$ and $\alpha_p$ are the roots of the equation $\alpha_p \tan \alpha_p = \mu$. It is very difficult to test this prediction, because the assumptions under which entangled chain dynamics are dominated by the pure reptation mode are those of very long chains, and for timescales longer than the Rouse time $\tau_{\text{R}}$. These are mutually exclusive when the current constraints of timescale of the NSE technique impose themselves. Fluctuation effects both locally along the chain [168] and at the chain ends [247] effectively dominate the experimental signal (see section 4.2.4 below). However, both references [31] and [168] state that $S_{\text{esc}}(\mathbf{q}, t)$ is dominated in the region within the molecular volume, $qR_{\text{g}} \gg 1$, by the surviving tube fraction, i.e. that

$$S_{\text{esc}}(\mathbf{q}, t) \simeq \frac{12}{q^2 b^2} \mu_{\text{DE}}(t). \tag{100}$$

In fact, this approximation is only good at timescales comparable to the reptation time [169, 247], which is never accessed by NSE. The reason for this can be appreciated by referring to figure 25. The chain material escaped from the tube (segments in the unshaded region) may not contribute at all to the rheological or dielectric response, since they are orientationally relaxed. However, they are still *spatially* correlated with the monomers on the chain at $t = 0$ by virtue of connectivity. An alternative analytic approximation to the calculation of $S_{\text{esc}}(\mathbf{q}, t)$, that recognizes these contributions as a starting point, was given for the case of star polymers [248], and has been applied to NSE data on linear polymers [169].

4.2.3. *Some comments on Rouse and reptation dynamics*

The existence of modes with shorter relaxation times than the longest reptation time, arises from the greater rapidity with which tube segments originally near a chain end are lost, compared with those near the middle of the chain. The calculation here ignores all fluctuations of the total entangled path length of the molecule, so would not be expected to estimate this contribution accurately. It turns out that this approximation is directly related to the difference between the cubic dependence of $\tau_{\text{d}}$ on $N$ predicted above and the experimentally observed $\tau_{\text{d}} \sim M^{3.4}$. An accurate

calculation of these fluctuations becomes necessary to make any progress at all with entangled branched polymers (see section 4.3)

The two types of polymer dynamics presented here have established themselves as rather fundamental. For example, at long enough lengthscales, the dynamics of an unconstrained random walk with *any* local rule for its motion becomes equivalent to the Rouse description [11, 31]. Similarly, reptation arises quite generally in the constrained case of one-dimensional random walks of chain-like objects (another example is to be found in the high temperature mobility of the chains in polyethylene crystals! [249]).

Moreover the two dynamics are 'orthogonal' in their natural mathematical representations: Rouse modes do not diagonalize reptation dynamics and *vice versa*. This may lead to some confusion—since at first sight the eigenfunctions of the Rouse equation (when written for the local segmental orientation $\partial \mathbf{R}(n,t)/\partial n$), and those for the tube-survival probabilities in reptation, take the same form of $\cos(p\pi n/N)$ (see equations (64) and (95) above). This restricted case has been exploited in an approximate theory of constraint-release effects on dielectric relaxation [250]. However, the Rouse modes do not diagonalize the operation of the stochastic reptation moves on $\mathbf{R}(n,t)$ itself [59]. This is the fundamental object: if its dynamics and those of its correlation functions are known, in whatever theory, then simultaneous predictions of several measurable signals, from scattering to rheology, can be made. Indeed, in real polymer melts and entangled solutions both of these limiting cases of dynamics seem to coexist. This is because the tubes themselves are not permanent objects, but are subject to local rearrangement as constraints from neighbouring chains are released. Without this additional CR relaxation mechanism, the tube model overpredicts the alignment of chains in a strong shear flow, and severely underestimates the shear stress at high shear rates. Recent work (see below in section 5.1.3) is developing a formalism in which the chains *reptate* within tubes that behave as *Rouse* objects, and promises to be a powerful description of melts at high shear rates.

### 4.2.4. *Linear polymers (2): contour-length fluctuation (CLF)*

We have seen that the crude model of a chain without any internal dynamical degrees of freedom, but relaxing by the reptation mode only, has some severe drawbacks in the face of detailed experimental data. This is in spite of its remarkable success in grasping the qualitative outlines of entangled dynamics of linear chains. Close comparison of complementary experiments with theory has already suggested the two additional degrees of freedom that a quantitative theory must allow the chains to explore. In this section we review the 'single-body' effect of 'contour-length fluctuation' (CLF), in the next, the 'many-body' effect of constraint-release. We should clarify at the outset what we mean by CLF. Because linear rheology has historically produced the greatest weight of data indicative of the importance of internal chain modes, even when well entangled, the term has usually meant the restricted sense of 'contour length fluctuations of the primitive path length'. This is because it is only the CLF of the ends of the chain that affect the tube-segment survival probabilities that in turn affect both rheology and dielectric relaxation (see section 4.2.2). However, CLF more generally transports segment material from one tube segment to the next along the primitive path by virtue of the curvilinear, unconstrained modes of the chain throughout the interior of the primitive path. Such motion, which is independent of the reptative diffusion of the

centre-of-mass coordinate, has direct signatures in the dynamic structure factor and monomer displacement. (It turns out that it can also be detected in careful measurements of rheology!) So by CLF we will refer to all such curvilinear segmental motion, examining attempts to calculate its effects on the key experimental quantities.

The fundamental assumption in most treatments of CLF is that the entangled chain undergoes Rouse dynamics in the curvilinear coordinate along the contour of its primitive path [102]. That is, we work in a new coordinate $s(n,t)$, the projection of the full chain coordinate $\mathbf{R}(n,t)$ along the primitive path, and write

$$\zeta_0 \frac{\partial}{\partial t} s(n,t) = \frac{3k_B T}{b^2} \frac{\partial^2}{\partial n^2} s(n,t) + f(n,t); \quad \frac{\partial}{\partial n} s(n,t) = \frac{L_{eq}}{N} \quad \text{at} \quad n = 0 \text{ and } N \quad (101)$$

in analogy with the Rouse equation (62). The distinction is that the boundary conditions on this entangled Rouse chain have to respect the equilibrium mean length of the primitive path, and the consequent equilibrium tension $f_{eq} = 3kT/a$ borne by the chain at the tube ends (see section 4.2.1). The model is motivated by the physics of screening (the friction is local and independent of topology) and the inability of entanglements to affect motion that does not attempt to violate topological constraints, such as curvilinear motion along the tube contour. There have been a number of approximate treatments of equation (101) to treat the experimental probes at our disposal, with considerable success. However, it is still a challenge to formulate a proper cross-over from the curvilinear entangled Rouse form of (101) to the free Rouse dynamics of (62) that must hold for lengthscales smaller than the tube diameter $a$. We also note that this formulation includes the statistics of primitive path lengths far from equilibrium we discussed in section 4.2.1, in the Gaussian approximation (80).

*Segmental diffusion*. CLF motion strongly affects the tube model prediction for the segmental diffusion function $\phi_n(t)$. Once the entanglement field is encountered at $t = \tau_e$, each segment is then constrained to diffuse along the primitive path, but not immediately with the centre-of-mass diffusion constant $k_B T/N\zeta_0$. This cannot be the case until $t = \tau_R$, by which time information on the connectivity of the entire chain has been able to diffuse to the probe monomer *via* expression (101). Instead, for $\tau_e < t < \tau_R$, the effective friction grows with the Rouse scaling of $t^{1/2}$, so that the mean square displacement of a monomer along the primitive path $\langle [s(n,t) - s(n,0)]^2 \rangle \sim t^{1/2}$. By putting $\phi_n(t) \equiv \langle [\mathbf{R}(n,t) - \mathbf{R}(n,0)]^2 \rangle \simeq s(n,t)a$ (by the properties of the random walk of the tube) we find that $\phi_n(t) \sim t^{1/4}$ in this time regime. Cross-overs from $t^{1/2}$ to $t^{1/4}$ and from $t^{1/4}$ to $t^{1/2}$ are predicted at $\tau_e$ and $\tau_R$ respectively. An exact calculation of the prefactors would employ Wick's theorem and the assumption of Gaussian distribution of $\mathbf{R}(n,t) - \mathbf{R}(n,0)$, since the exact solution of expression (101) for $\langle [s(n,t) - s(n,0)]^2 \rangle$

$$\langle [s(n,t) - s(n,0)]^2 \rangle = 2D_{CM}t + \frac{4Nb^2}{3\pi^2} \sum_{p=1}^{\infty} \frac{1}{p^2} \cos^2 \left( \frac{p\pi n}{N} \right) [1 - \exp(-p^2 t/\tau_R)] \quad (102)$$

permits the direct calculation of $\phi_n^{(4)}(t) \equiv \langle [\mathbf{R}(n,t) - \mathbf{R}(n,0)]^4 \rangle$.

The rather rich sequence of regimes for the segmental diffusion (see figure 26 and compare with the simulation results of figure 20) became rapidly a rather famous prediction of the tube model. Yet it had to wait for advances in FGNMR [45],

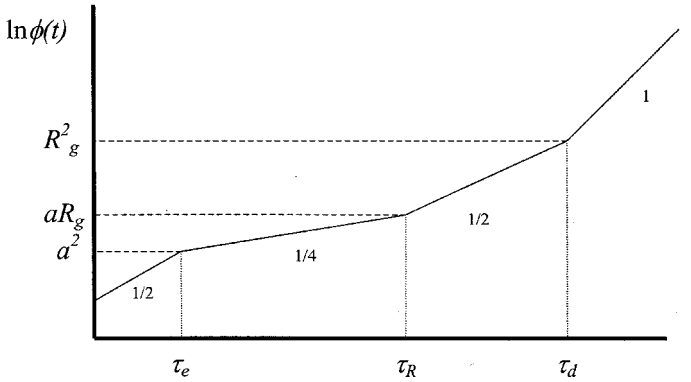


Figure 26. Qualitative tube model predictions for the segmental diffusion function $\phi_n(t)$ in logarithmic coordinates. Gradients are marked alongside the curve.

incoherent NSE [251] and simulation [54] in order to establish the 'local reptation signature'of the $t^{1/4}$ regime between $\tau_e$ and $\tau_R$. FGNMR is rather restricted, yet by judicious choice of polymer molecular weight and concentration in semi-dilute solution, has situated the 'NMR window' at the cross-over timescales. The NSE measurements, on the other hand, were made on the most densely entangled melt, PE, in order to bring the cross-over at $\tau_e$ into the NSE window. Such measurements can also yield direct results for the associated spatial scales. There is some interesting discrepancy between the value for $a$ found by incoherent NSE, and the coherent result below [251].

*Linear rheology and dielectric spectroscopy*. The effect of CLF on these two functions is mediated in two ways: (i) by its effect on the surviving tube fraction, and (ii) by its effect on the distribution of monomers between tube segments. No other modifications arise, providing that we allow tube segments to relax only by the passage of a chain end (no CR). We first examine the effect on the number of surviving tube segments. For times earlier than the Rouse time $\tau_R$, the chain ends will partake of the curvilinear Rouse motion, travelling a contour distance $\bar{s}(0,t) \sim a(t/\tau_e)^{1/4}$. This is initially a faster way to pass, and relax, tube segments than the reptative diffusion of $s_{CM}(t) \sim Za(t/\tau_e Z^3)^{1/2} = Z^{-1/2}a(t/\tau_e)^{1/2}$ (we recall that $Z = L_{eq}/a$ is the number of tube segments in the primitive path). By equating the effect of the local and reptative contributions to the path length traversed, we find that the reptation mode dominates after $t \sim \tau_R \sim Z^2\tau_e$. This is, of course, just the cross-over at $t = \tau_R$ between the two associated non-Fickian diffusion regimes of figure 26. The consequence is that, by the time stress is relaxed by reptation, local motion via CLF of the chain ends has already served to equilibrate the orientation of a fraction of outer segments given by $\bar{s}(0,\tau_R)/L \simeq Z^{-1/2}$. Chain reptation now needs only to relax the remaining (central) parts of the primitive path. So an estimate of the corrections to quantities related to tube survival combine a renormalized reptation time:

$$\tau_d = \tau_d^{(0)}[1 - \bar{s}(0,\tau_R)/L]^2 = \tau_e Z^3[1 - C_1 Z^{-1/2}]^2 \tag{103}$$

with a renormalized modulus

$$G_{rep} = G_N^{(0)}[1 - C_1 Z^{-1/2}] \tag{104}$$

obtained by subtracting the contribution lost rapidly by CLF. For the time being, where we discuss only CLF, we will not attempt to modify the modulus further (some crude treatments of CR would put $G_{\text{rep}} = G_N^{(0)}[1 - C_1 Z^{-1/2}]^{\alpha+1}$ at this stage, where $\alpha$ is the exponent with which the entanglement molecular weight decreases with polymer concentration). The calculation of the $O(1)$ constant $C_1$ is not straightforward, as the chain end motion results from the sum of the fluctuations of all the interior Rouse modes, and the stress relaxation depends not on the mean motion of the chain ends, but on their *extremal* excursions. It is the *first* passage of a chain end that is assumed to relax the constraint of a tube segment on the chain. Doi invoked a functional minimization scheme to calculate a lower boundary for $C_1$ [101, 102] of 1.47. The resulting form for the viscosity , $\eta \simeq G_N^{(0)} \tau_e Z^3[1 - C_1 Z^{-1/2}]^3$ could produce the apparent $\eta \sim Z^{3.4}$ power law, but not to the same degree of entanglement $(Z \simeq 600)$ as the experiments, displaying a cross-over to $\eta \sim Z^3$ nearer to $Z = 100$. This approximation was naturally by itself unable to predict the spectrum of stress relaxation expected from CLF, but this could be estimated in several ways.

The one-dimensional stochastic simulations we reviewed above in section 3.10 [220, 222], and lattice simulations that permit CLF [221], were able to account for the dominance of fluctuations up to the remarkably high value of $Z$ seen in experiments. Simulations are not constrained to work with mean behaviour, but can gather statistics on the extremal end fluctuations. It became clear that part of the $Z^{3.4}$ behaviour arises from the contribution to the stress of segments relaxed by CLF rather than reptation, from calculations of $G(t)$ including CLF. An approximation for the entire relaxation spectrum can be made by associating an expected relaxation time $\tau(s)$ with the segment of primitive path a curvilinear distance $s$ from the chain end [52]. For times $\tau \ll \tau_R$, the monomer displacement from internal Rouse motions of equation (102) can be written

$$\langle [s(0,t) - s(0,0)]^2 \rangle \simeq \frac{4a^2}{3\pi^{3/2}} \left(\frac{t}{\tau_e}\right)^{1/2} \tag{105}$$

as discussed first by Doi [102]. Inverting this relation gives an approximation for the typical time for a segment at $s$ to be visited by the free end via curvilinear Rouse motion:

$$\tau_{\text{early}}(s) \simeq \frac{9\pi^3}{16} \frac{s^4}{a^4} \tau_e. \tag{106}$$

When $s$ is large enough that the reptation time (self-consistently determined as the time to diffuse the remaining contour length of the chain) is shorter than $\tau_{\text{early}}$, the relaxing segment is assigned the reptation time itself as its local relaxation time. This procedure generates a function $\tau(s)$ that asymptotes to $\tau_{\text{early}}$ for $s$ within $Z^{-1/2}L$ of the chain ends, and to $\tau_{\text{rept}}$ in the centre. Now assuming that the ensemble of segments with original primitive path coordinate $s$ relaxes with a single mode at these characteristic timescales, a form for the relaxation modulus is suggested:

$$G(t) = G_0 \frac{1}{L_{\text{eq}}} \int_0^{L_{\text{eq}}} \exp\left[-t/\tau(s)\right] \mathrm{d}s. \tag{107}$$

Here we expect the prefactor $G_0$ to be rather larger than a typical experimental determination of the plateau modulus, because it includes stress lost during the rapid

CLF process. This approximate approach is flawed in two central assumptions. Firstly the hope that equation (106) gives a good estimate of a first-passage time is unfounded (recent stochastic simulations indicate that these mean times scale only approximately with $s$ with a rough power law closer to $s^3$ [247]). Moreover, it is easy to show (see the appendix) that such inversion procedures are very dangerous in this context. Secondly the assumption that their distribution is single-exponential, is also wrong. This has motivated explorations of other phenomenological approaches [114, 115], but these fail other experimental tests. In spite of this, the approach gives a good account of the $\omega^{-1/4}$ domain of the functions $G''(\omega)$ and $\epsilon''(\omega)$, as well as of the $M^{3.4}$ scaling of viscosity [56]. The procedure has also been used as an ingredient in the development of schemes designed to make quantitative predictions of viscoelasticity without solving detailed PDEs or making large scale simulations [58, 63, 128].

A better approach to the issue of chain-end segments lost by CLF avoids the assignment of a single $\tau(s)$, tempting though this is, but observes that the scale-invariance possessed by the Rouse equation allows one to write down an exact asymptotic result for the surviving tube fraction at early times. The Rouse equation of motion (62) is invariant under the transformation

$$t = \lambda t'; \quad R = \lambda^{1/4} R'; \quad n = \lambda^{1/2} n' \tag{108}$$

so that all relevant lengths scale as $t^{1/4}$. So the fraction of unvisited tube segments must behave, for early times, as

$$\mu(t) = 1 - \frac{C_\mu}{Z}\left(\frac{t}{\tau_e}\right)^{1/4}. \tag{109}$$

An expansion of this kind, including terms of higher powers of $Z^{-1/2}$ induces universal renormalizations of $\tau_d$ and $G^{(f)}$ as in equations (103) and (104), as functions of $Z$ only. Here is a good example of the close interaction of theory with simulation, for the values of the coefficients $C_\mu$ and $C_i$ in such an expansion may be determined in a 1D stochastic simulation (current results for $C_\mu$ in (109) above indicate that $C_\mu = 1.5 \pm 0.02$). Results from stochastic simulations for the renormalized quantities $\tau_d$ and $G^{(f)}$ given recently [247] are shown in figure 27. The tube model with reptation and CLF also makes a prediction for the front-factor of $G(t) \sim G_{rep}\mu_{DE}(t)$, which we would naturally identify with the plateau modulus $G_N^{(0)}$ (but this needs great care—as we have seen, the plateau modulus is both an experimentally defined quantity, and one on which there is no currently agreed method for its extraction!). Moreover, the fraction of the original chain actually relaxing by a reptative terminal process, the renormalized $G_{rep}$, is not independent of $Z$, as we have seen. Were the primitive path a series of crosslinks at a mean separation of $a$, the shear modulus from equation (13) would simply be the 'entanglement modulus'

$$G_e = k_B T \frac{\mathbb{C} b^2}{a^2} = k_B T \frac{\mathbb{C}}{N_e}, \tag{110}$$

but even at the inception of the tube model, it was realized that the most important difference between crosslink and tube constraints is that the tube allows chain material rapidly to pass from one tube segment to neighbouring segments to equilibrate the contour length density of monomers [31]. This is also an effect of

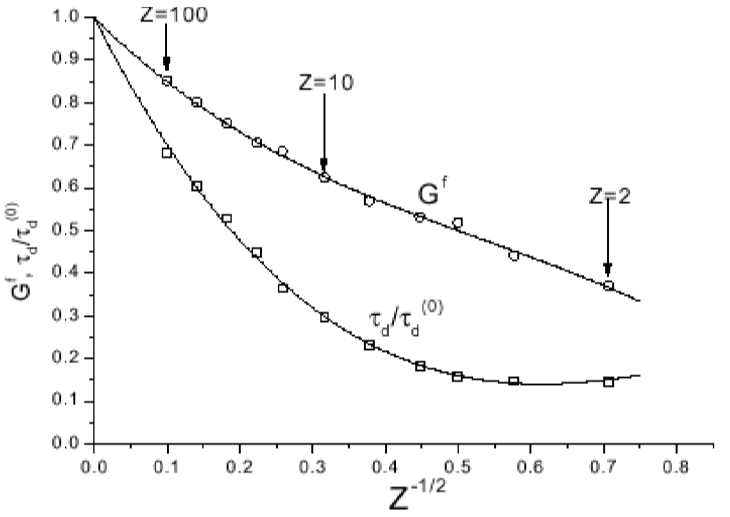


Figure 27. Results of a one-dimensional stochastic simulation on the values of reptation time (lower curve) and plateau modulus (upper curve) renormalized by CLF, as a function of number of entanglement segments $Z$ of the chain, plotted against $Z^{-1/2}$.

CLF, of course, but acts in addition to the loss of tube segments, rather it redistributes chain from tube segments less stretched by the deformation to those stretched more. We note, additionally that this contribution of CLF affects stress only, not the relaxation of type-A dielectric dipoles. To calculate the effect on the stress we rewrite equation (11) as

$$\sigma = \frac{\mathbb{C}}{N_e}\langle f\mathbf{uu}\rangle, \tag{111}$$

where $f$ is the local tension along the chain $(= 3k_BT/a$ in equilibrium) and $\mathbf{u}$ is the orientation of a tube segment. On applying the strain $\mathbf{E}$ to the ensemble of segments of $N_e$ subunits and orientations $\mathbf{u}$, the stress generated in the putative crosslinked network is

$$\sigma = \frac{\mathbb{C}}{N_e}\langle f(\mathbf{E}\cdot\mathbf{u})(\mathbf{E}\cdot\mathbf{u})\rangle \quad \text{with the shear asymptote } \sigma_{xy} = \frac{\mathbb{C}}{N_e} f_{eq}\cdot\frac{1}{3}\gamma, \tag{112}$$

where the average is taken over original orientations $\mathbf{u}$. Now after the local tension is equilibrated along the chain once more (in linear response there is no perturbation of the global tension) the stress will now only arise from a pre-averaged tension of $f_{eq}$ throughout all segments, and weight segmental orientations according to the number of monomers they contain, which in turn is proportional to their (normalized) deformed length $|\mathbf{E}\cdot\mathbf{u}|/\langle|\mathbf{E}\cdot\mathbf{u}|\rangle$. The final result is

$$\sigma = \frac{\mathbb{C}}{N_e} f_{eq}\left\langle \frac{|\mathbf{E}\cdot\mathbf{u}|}{\langle|\mathbf{E}\cdot\mathbf{u}|\rangle}\frac{(\mathbf{E}\cdot\mathbf{u})}{|\mathbf{E}\cdot\mathbf{u}|}\frac{(\mathbf{E}\cdot\mathbf{u})}{|\mathbf{E}\cdot\mathbf{u}|}\right\rangle, \tag{113}$$

$$= \frac{\mathbb{C}}{N_e} f_{eq}\frac{1}{\langle|\mathbf{E}\cdot\mathbf{u}|\rangle}\left\langle \frac{(\mathbf{E}\cdot\mathbf{u})(\mathbf{E}\cdot\mathbf{u})}{|\mathbf{E}\cdot\mathbf{u}|}\right\rangle, \tag{114}$$

with the shear asymptote of $\sigma_{xy} = \frac{\mathbb{C}}{N_e} f_{eq}\cdot\frac{4}{15}\gamma$.

So, by comparing equations (112) with (113), we see that the redistribution of segments in linear response from a step strain renormalizes the modulus downwards by a factor 4/5. This is the origin of the variant definitions of the plateau modulus (see section 2.1.1). This factor, and its powers, has plagued recent theories of rheological response that need to make quantitative predictions. This is because, if the entanglement molecular weight is defined from the plateau modulus without acknowledgement of this renormalization, then the factor needs to be reintroduced in the calculation of $L_{eq}$ from $M$ and $M_e$. Perhaps the most helpful set of definitions, that avoid misleading and tiresome repetitions of this quantity, is to keep the notion of the 'entanglement modulus', $G_e$, from which

$$G_e \equiv G(\tau_e) = \frac{\rho RT}{M_e}. \tag{115}$$

This allows a tube model prediction of the plateau modulus

$$G_N^{(0)} = \frac{4}{5} G_e, \tag{116}$$

with the caveat that this quantity can only be extracted from experiment by a careful limiting process involving measurements on several molecular weights. So, for example, we might suggest the following definition of the experimentally determined $G_N^{(0)}$

$$G_N^{(0)} = \lim_{Z \to \infty} \{G[t = (\tau_d \tau_R)^{1/2}]\}. \tag{117}$$

With these definitions we have also $Z = N/N_e$ and $L_{eq} = Za$. The definition suggested by equation (117) is, however, still extremely formal and unlikely to be of value at realistic values of $Z$. It may prove more valuable in future to focus on values of $G_e$, one fifth of whose value is relaxed before the limiting value of the plateau modulus is recorded.

Until very recently it has not been clear how this 1/5 of the stress recorded at the entanglement Rouse time [for $G_e = G(\tau_e)$] is relaxed. It might be thought that it occurs within a few multiples of $\tau_e$, since contour length equilibration typically involves segment exchange between closely neighbouring tube segments. However, a careful application of the curvilinear Rouse equation for CLF shows that this contribution to the stress decays with the standard Rouse form for *one*-point correlations (the relaxation time of the $p$th mode is $\tau_R/p^2$, not $\tau_R/2p^2$), and containing only the entangled Rouse modes of low index up to $p = Z$ [247]:

$$\sum_{p=1}^{Z} \exp(-p^2 t/\tau_R). \tag{118}$$

This contrasts also with conjectures that the one free curvilinear Rouse mode not constrained by the tube carries just 1/3 of the Rouse stress [56]—the amplitude is just the 1/5 of the Rouse stress evaluated by the counting argument for equilibrated segment density. This helps us to see in part why the true plateau modulus is so elusive—stress decay from path length equilibration (sometimes assumed to have been completed before the plateau stress is reached), continues right up to $\tau_R$, well after the time at which CLF effects on chain-end retraction are making considerable inroads into the surviving tube fraction!

Finally we can assemble together the results of the most complete treatment of CLF we have for rheological response

$$G(t) = G_e\left[\frac{1}{5Z}\sum_{p=1}^{Z}\exp\left(-p^2t/\tau_R\right) + \frac{4}{5}\mu(t) + \frac{1}{Z}\sum_{p=Z+1}^{N}\exp\left(-2p^2t/\tau_R\right)\right], \qquad (119)$$

where $\mu(t)$ is the tube survival fraction calculated from the universal curves (fitting functions for them exist [247]), and the last factor counts free Rouse stress decay at very early times. It has a high frequency modulus that counts $k_BT$ per unit volume from every monomer, so is approximately $N/Z$ times greater than the entanglement modulus at $t \to 0$. The role of CLF is strongly to moderate the slopes of the $G''(\omega)$ curve, introducing a slope of $-1/4$, as seen in experiments, to the right of the peak, and delaying the emergence of the pure reptation slope of $-1/2$ until very high $Z$ (cf. figure 29). The longitudinal relaxations affect predictions of the shape and position of the minimum in $G''(\omega)$ seen at higher frequency. Even this degree of refinement does not, however, do the justice intended to experimental results. In particular the 'reptation peak' in $G''(\omega)$ is always sharper in theory than in experiment [52], and the terminal time overpredicted. Another important process must also be included. To this we turn in the next section, after looking at the aspects of CLF accessible to diffusion measurements and neutron scattering.

*Self-diffusion.* CLF speeds up self-diffusion in relation to the pure-reptation picture. This is because the fundamental real-space jump of the chain occurs at the renormalized reptation time given by equation (103) and its higher-order expansions. The distance diffused per jump also reduces by the primitive path relaxed by CLF prior to reptation, but the two effects do not cancel. The renormalized diffusion constant becomes [191]

$$D_{self} = \frac{R_{eff}^2}{\tau_d} \simeq \frac{Za^2(1-2C_1Z^{-1/2})}{\tau_e Z^3(1-2C_1Z^{-1/2})^2} = D_{self}^{(0)}(1-2C_1Z^{-1/2})^{-1}. \qquad (120)$$

The detailed calculations compare well to to collected data on the molecular weight scaling of self-diffusion constants [52], resembling a power-law relation of the form $D_{self} \sim Z^{-2.4}$ up to $Z > 300$.

*Dynamic structure factor.* The role of CLF affects the dynamic structure factor in two ways, just as it does the rheological response: via local motion in the tube driven by curvilinear Rouse motion, and via tube orientational relaxation at the chain ends. The effect of local motion generates a new term in $S(\mathbf{q}, t)$ that comes into play at high values of $q$, calculated by de Gennes [168]:

$$S_{loc}(\mathbf{q}, t) = \exp\left[-\frac{t}{\tau_{loc}(\mathbf{q})}\right]\operatorname{erfc}\left[\frac{t}{\tau_{loc}(\mathbf{q})}\right]^{1/2} \quad \text{with} \quad \tau_{loc}(\mathbf{q}) = \frac{12\zeta_0}{k_BTb^2q^4}. \qquad (121)$$

The inherent scaling $\tau \sim q^{-4}$ reflects the monomer displacement $\phi_n(t) \sim t^{1/2}$ in the Rouse-dominated regime within a tube radius. Since the typical NSE timescale range includes local unentangled motion, it is essential to include this relaxation of the structure factor by internal modes. The complete expression, combining local and tube-escape contributions, is

$$S(\mathbf{q},t)=\left[1-\exp\left(-\frac{q^2a^2}{6}\right)\right]S_{\rm loc}(\mathbf{q},t)+\left[1-\exp\left(-\frac{q^2a^2}{6}\right)S_{\rm esc}(\mathbf{q},t)\right]. \qquad (122)$$

Naturally, in the limit of large $Z$, the separate effect of CLF on the chain-end contribution makes proportionately less impact on the total chain structure factor. However, this asymptote is also reached rather slowly, and chain-end effects have been seen in experiment and simulation up to $Z=100$ [44, 169, 252]. Even at current extended correlation times for NSE, however, it is not possible to evaluate the predicted form of $S_{\rm esc}(\mathbf{q},t)$ from the reptation mode (99). This is because even for quite short chains, the Rouse time is still beyond the NSE window, which means that $S_{\rm esc}(\mathbf{q},t)$ is always dominated by CLF effects. The best current level of approximation uses the exact result (109) to give a characteristic primitive path co-ordinate $x(t)=(C_\mu/2N)(t/\tau_{\rm e})^{1/4}$ from the chain ends, up to which tube segments will have been vacated at time $t$—we note that this is a much better defined average quantity than the inverted $\tau_{\rm early}(s)$ of equation (106). The correlations required to produce $S_{\rm esc}(\mathbf{q},t)$ are calculated by assuming a random reconfiguration for all relaxed chain, and tube-confinement for unrelaxed chain [248]. The structure factor depends only on the primitive path coordinate separating relaxed from unrelaxed chain, and reads, [169]

$$S_{\rm esc}(\mathbf{q},t)=\frac{N}{2\mu^2}[2\mu+\exp(-2\mu)+2-4\mu x(t)-4\exp(-2\mu x(t))+\exp(-4\mu x(t))]. \qquad (123)$$

The main assumption in this calculation is uniqueness of the chain coordinate partitioning the CLF-relaxed outer segments of chain. This could be improved upon by integrating over a simple distribution. In fact this level of treatment is already rather good: the curves compared with NSE data in figure 17 were produced by using this approximation for $S_{\rm esc}(\mathbf{q},t)$ in equation (122), and without a change of parameters (including a molecular weight independent tube diameter) accounted for the NSE coherent signal over a range of molecular weights in PE $(10<Z<200)$.

A crucial corollary of this result is that, when CLF chain-end fluctuations are accounted for, phenomena that have previously been attributed to a wider tube diameter at low molecular weights [253] no longer demand such a variable $a(Z)$. This has consequences for theories of the tube itself, supporting conclusions from experimental trends in plateau moduli that local chain stiffness and bulk are the determining factors of entanglement density [78, 79], rather than the density of chain ends. Future extensions of the 'NSE window' beyond the Rouse time would be very attractive tests of the spatial consequences (as opposed to the chain-orientational) of the cross-over to reptation-controlled relaxation. This is also the regime in which the structure factor would become a test of constraint release (CR), to which we now finally turn.

4.2.5. *Linear polymers (3): constraint-release (CR)*

We have seen strong experimental evidence that, in polymer melts and entangled solutions, the rheological, optical and dielectric responses, and so by implication the spatial chain configurations, are not simply those of an ensemble of chains in a corresponding ensemble of fixed tubes. Rheology alone, when applied to carefully prepared bimodal blends of linear chains, shows that the form and frequency of the relaxation of the high molecular weight component depends on the molecular weight

[111] and concentration [107] of the lower, even when this is itself entangled [110]. Similarly, the amount of stress relaxed at the relaxation timescale of the lower molecular weight component is a greater proportion of the total stress than its volume fraction [110]. Star polymers entangled dilutely with an entangled linear polymer matrix relax in a completely different way to the exponentially-slow processes they follow in a star homopolymer melt, instead following more closely a retarded Rouse-like relaxation [254, 255]. The measured value of the self-diffusion constant of the probe component of a bimodal blend depends on the molecular weight of the matrix component, unless this is very much higher than the probe molecular weight [209].

Yet, as we have anticipated (see figure 6 and related discussion), there is good reason to expect that the topological constraints that define the tube for a given chain possess a finite lifetime themselves, that is itself a function of the molecular weight and architecture of the chain(s) responsible for the constraints. Since dynamic events do not propagate beyond a very short screening length in concentrated solutions and melts [31], such 'constraint release' events can only result in local reorganization of tube constraints. Moreover, because the equilibrium structure of the melt is preserved, the tube diameter will not be perturbed by CR events (but see below for cases in which CR generates an effective tube dilation): new constraints will typically arrive at the same rate at which the old ones depart. So the tube itself becomes a random walk subject to local rearrangements. This is sufficient to conclude that the tube-fields around entangled chains behave dynamically like Rouse polymers [11], a conjecture first made by Graessley [30, 256, 257]. It also points to the need for at least one additional dimensionless parameter in tube theories that include CR. This lies in contrast to the addition of extra 'one-body' processes we considered above under the banner of CLF. These did not introduce any new physics to the basic tube model, but really amounted to reinstating the local Rouse-chain dynamics that were discarded in calculations of the effects of the reptation mode alone. In contrast, the 'many-body' process of CR, although asymptotically inducing Rouse dynamics on the tube, depend on a detailed knowledge of the local physics of entanglements to quantify their magnitude. We might conjecture that the disappearance of a neigbouring chain by reptation or CLF from the neighbourhood of a tube segment on a test chain would induce a local stochastic jump of the segment through a distance of order $a$. But with what prefactor? At the very least we require this dimensionless number in order to make quantitative predictions from calculations assuming such a 'Rouse tube' picture. We might also hope that it is a universal number, independent of molecular weight and detailed chemistry of entangled polymers, but this hope might itself prove idealistic given the coherent way in which chain ends will be responsible for correlated CR events in their vicinity [33].

Later we shall review the predictions of a quantitative theory of CR that calculates experimental quantities assuming a range of values of such a CR coupling constant, which we shall define and call $c_\nu$. However, independent of the exact value of $c_\nu$, we can explore the qualitative outlines of Rouse tube CR. In a monodisperse melt, the tubes will behave as chains of $Z$ segments each of which has a local relaxation time of $\tau_d \simeq \tau_e Z^3$ (in the limit of large $Z$—for realistic values we might write in view of the effect of CLF $\tau_d \simeq \tau_e Z^{3.4}$). So the fundamental CR relaxation time of the tubes will be the corresponding Rouse time, $\tau_{CR} \simeq \tau_e Z^3 \cdot Z^2 \sim Z^5$. This is much longer than the reptation time itself, so we do not expect the self-diffusion

constant in homopolymers to be affected strongly by CR. For the same reason in this case, neither do we expect the dielectric relaxation $\epsilon(t)$, to acquire CR effects, since a Rouse object weights the relaxation of its end-to-end vector strongly with the terminal time; see equation (78). The stress-relaxation is much more sensitive, however, because of the broad spectrum of relaxation times inherent in Rouse dynamics. An estimate of the stress-relaxation function due to combined reptation and CR combines a tube–Rouse relaxation $R(t)$ with the survival probability of unrelaxed chain segments within the tube, $\mu(t)$, in a product form [258]

$$G(t) \simeq G_N^{(0)} \mu_{\mathrm{DE}}(t) R(t), \tag{124}$$

with

$$\mu_{\mathrm{DE}}(t) = \frac{8}{\pi^2} \sum_{p \text{ odd}} \frac{1}{p^2} \exp\left(-p^2 t/\tau_{\mathrm{d}}\right) \tag{125}$$

and

$$R(t) = \frac{1}{Z} \sum_{m=1}^{Z} \exp\left(-2m^2 t/Z^2 \tau_{\mathrm{d}}\right) \simeq \left(\frac{t}{\tau_{\mathrm{d}}}\right)^{-1/2} \quad \text{for } \tau_{\mathrm{d}} < t < \tau_{\mathrm{CR}}. \tag{126}$$

Evaluating each of the factors in (124) at the reptation time yields (in the limit of large $Z$), $\mu_{\mathrm{DE}}(\tau_{\mathrm{d}}) \simeq 0.3$ and $R(\tau_{\mathrm{d}}) \simeq 0.6$. So the same order of magnitude of stress relaxes via CR as by reptation in the region of the reptation time. It is to this fact that we can ascribe the success of the 'double reptation' approximation of CR [112–114].

$$G(t) \simeq G_N^{(0)} [\mu_{\mathrm{DE}}(t)]^2. \tag{127}$$

In fact, the simple quadratic form of (127) does quite well quantitatively [258] as an approximation to the product of (124), but suffers from the oversimplification of employing just a single relaxation time for constraint release. In reality, constraints possess a distribution of mean lifetimes, depending on whether they arise from interactions with chain centres or chain extremities. We will review the current schemes used to account for such a distribution below (section 4.2.5), but next consider the informative case of bimodal blends.

*CR in bimodal blends*. Blending two monodisperse polymer fractions creates a family of entangled polymeric fluids with very rich properties and variety. The experimental data now available is, as we have seen, extensive; for a recent and comprehensive survey see reference [37]. But the idea has also proved a very useful conceptual tool in the development of the tube model, particularly in regard to CR. The parameter-space of blends containing even two components is already large, spanned by the three dimensions of $Z_1$, $Z_2$ , the number of entanglement strands in the low and high molecular weight components, and $\phi_1$, the volume fraction of the lower molecular weight component. Two general studies a decade ago made different assumptions to determine whether the high molecular weight component was constrained to a tube or not. Doi *et al.* [259] chose a global criterion to define a regime of 'tube dilation', while Viovy *et al.* [260] made a more convincing local assumption of CR jumps of a constant diameter tube. The latter idea is that a chain 'feels' a tube if the lateral motion of a chain segment on it is faster than the lateral motion of the Rouse motion of the tube itself. If the free-chain motion should generate a displacement as great as that of the tube only after motion somewhat greater than the bare tube diameter, the subsequent constrained dynamics can take

place in a 'dilated' tube. This idea was first introduced in the context of linear polymers by Marrucci [261]. Although this picture of tube dilation has proved to be valid in cases of branched polymers (see below), reference [260] found that in bimodal linear blends the long chains are always entangled in a bare tube of diameter $a$ as long as $Z_1 > 1$.

Yet the subsequent behaviour still possesses a rich diversity of physics. The long chains' terminal relaxation may be determined by any one of three processes: (1) reptation from their bare tubes; (2) Rouse relaxation by CR of the bare tubes; (3) reptation of the Rouse bare tube by CR in a 'supertube' defined by the long chains alone. Since all of these processes occur, whichever gives the shortest relaxation time is the dominant one, determining the form of the relaxation and terminal time. To decide between the first two, we simply need to evaluate the faster of the tube Rouse time $\tau_{CR} = \tau_e Z_1^3 Z_2^2$ and the bare reptation time of the long chains $\tau_{d2} = \tau_e Z_2^3$. The ratio between the two, sometimes referred to as the 'Graessley–Struglinski' parameter $r_{GS}$ is

$$r_{GS} \equiv \frac{\tau_{d2}}{\tau_{CR}} = \frac{Z_2}{Z_1^3}. \tag{128}$$

As $r_{GS}$ increases past 1, the tube Rouse relaxation becomes longer than the reptation time of the long chain in the tube. The prediction on the form of the relaxation modulus in the terminal zone is that this should be pure Rouse-like, of form (75), for all $r_{GS} < 1$; then adopt a truncated Rouse relaxation for higher values, for which the $t^{-1/2}$ relaxation of the tube is interrupted by the reptation process of the chain. A series of experiments on PS blends in which the long chains are self-dilute confirmed this prediction qualitatively, with departures from a pure Rouse terminal zone beginning for $r_{GS} \simeq 0.1$ [28, 107, 111]. An approximate calculation of the relaxation modulus function, that follows essentially the product form of equation (124) gave additionally a good account of the form of $G(t)$ in the range $0.004 < r_{GS} < 5$ [37].

An additional parameter comes into play as the longer chains are increased in concentration: for when non self-dilute, they may constrain each other by effective tubes arising from their mutual entanglements irrespective of the density of entanglements with the short chains. We introduce

$$\tilde{Z}_2 = Z_2 \phi_2^{\alpha} \tag{129}$$

where $\alpha$ is the dilution exponent (which depends on the details of how the tube arises from topological invariants, but we recall has a value close to 1), which is the number of entanglement segments of the long chains in 'supertubes' defined only by their mutual entanglements. When $\tilde{Z}_2 > 1$, the Rouse-tube motion generated by CR events from short chain reptation has carried the lateral displacement as far as the diameter of the supertube $\tilde{a} = a\phi^{\alpha/2}$, then further Rouse-tube motion is not possible. Instead, the orientational relaxation must proceed by reptation, but here there are two alternatives. Either the chain can reptate in its bare tube (as for the dilute case with $r_{GS} > 1$) or the Rouse-tube *itself* may effect a more rapid relaxation by the third of the processes—its own reptation by CR events from short chains within the supertube. Whichever is the faster process is a subtle payoff between the shorter primitive path offered by the supertube and its greater effective frictional drag. The timescale $\tau_{trep}$ for 'tube reptation' may be estimated from the CR timescale for a supertube entanglement strand $\tau_{\tilde{a}} = Z_1^3 \phi_2^{-2\alpha} \tau_e$:

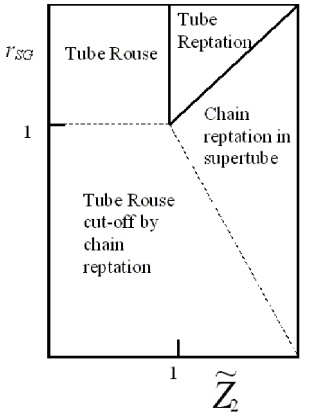


Figure 28. Regimes of dynamical behaviour in bimodal blends in terms of the parameters $r_{SG}$ and self-entanglement of the long chains $\tilde{Z}_2$ (which incorporates dependence on $\phi_2$). Solid lines denote change of expression for the terminal time, dashed lines of the modulus. [From reference [260].]

$$\tau_{\text{trep}} \simeq \tau_a \tilde{Z}_2^3 = Z_1^3 Z_2^3 \phi_2, \tag{130}$$

where we have taken $\alpha = 1$. This process therefore only dominates when $\tau_{\text{trep}} < \tau_{\text{d2}}$, so requires a window of concentrations for the long chains such that $\phi_2 < 1/Z_1^3$ (so that tube reptation is faster than chain reptation) and $\phi_2 > 1/Z_2$ (so that the long chains are self-entangled). This regime only exists, of course, providing that $Z_2 > Z_1^3$. Not surprisingly, this regime has yet to be accessed strongly by experiment. There is some evidence in the blend series of reference [111] that tube reptation may just be modifying tube Rouse relaxation in the case of the higher concentration of probe chains and at the transition molecular weight of the matrix chains, predicted in this case to be $\simeq 10^5$, but more experimental evidence is needed. It is an important case conceptually, however, because it conspires to mimick the alternative picture of tube dilation [259]. The terminal relaxation is produced by a renormalized reptation (of the bare tube) in dilated supertube. It has been tempting to write down the dilation proposition as a starting point on several occasions, but this is an example (we will see that we expect the case of star polymers to be another) in which it may actually be derived from a more detailed treatment of CR locally. We summarize the regimes of different physical behavior in the two-dimensional space of $r_{SG}$ and $\tilde{Z}_2$ in figure 28.

At the scaling level of this section, we note finally that the assumption that the fundamental timescale for CR jumps in bimodal blends scales as $Z_1^3$ (or even a more nuanced $Z_1^{3.4}$) can be called into question experimentally and theoretically. Probe rheology [254], and probe diffusion studies [209] find that the jump times seem to scale with $Z_1$ more as $Z_1^{2.4}$, although the exponent deduced from available data does depend critically on how the data is treated. Carefully weighting data from the CR-dominated regime leads to exponents nearer $Z^3$ [37]. In any case, the CR jump events seem to be faster than would be predicted by assuming that each reptating chain gave rise to just $Z_1$ entanglements. Klein has suggested [33] that CR events may be correlated—since chain A is highly overlapped with chain B, it may be responsible for more than the $Z_A$ entanglements of a mean-field picture. A conjecture that the number of entanglements that are candidates for CR events between two chains is

proportional to the volume of overlap of their tubes [262] compares favourably with the diffusion experiments, but a detailed calculation of effects on the relaxation spectrum has yet to be made.

*Self-consistent CR.* There are clearly limits on the degree of close experimental comparison that can be derived from scaling approaches such as that of the last section. CLF is completely ignored in spite of the essential way in which it accounts for dynamics at all realistic degrees of experiment. But equally, simple product forms of the type of (124) do not do justice to the distribution of CR timescales expected from even a monomodal melt, let alone bimodal blends or more complex polydispersity. The method introduced by Rubinstein and Colby currently represents the most quantitative approach to date [110]. In this method, the relaxation spectrum of the tube $R(t)$ is made self-consistent with the tube survival relaxation spectrum $\mu(t)$, which itself can contain the effects of CLF and polydispersity. First $\mu(t)$ is converted to a relaxation spectrum $P(\epsilon)$:

$$\mu(t) = \int_0^\infty P(\epsilon) \exp(-\epsilon t)\, \mathrm{d}\epsilon \tag{131}$$

then the Rouse problem is solved for the case of chains selecting their local mobilities at random from the distribution set by $P(\epsilon)$, giving a density of states of Rouse relaxation modes $M(\epsilon)$. This uses Sturm's theorem and a numerical method due to Dean [263]. Finally the tube Rouse relaxation is determined

$$R(t; c_\nu) = \left\langle \int_0^\infty \frac{\mathrm{d}M(\epsilon)}{\mathrm{d}\epsilon} \exp(-\epsilon c_\nu t)\, \mathrm{d}\epsilon \right\rangle. \tag{132}$$

For clarity, the standard, Rouse relaxation function at high frequency, $R(t) \sim t^{-1/2}$ is generated by a density of states $\mathrm{d}M(\epsilon)/\mathrm{d}\epsilon \sim \epsilon^{-1/2}$. In equation (132) we introduce the dimensionless constant $c_\nu$ that couples the rate of CR events to the rate of tube segment jump rates [247]. In treating bimodal PB blends in the chain-reptation regime with $\tilde{Z}_2 > 1$, this procedure gave a very impressive degree of accord with experiment [110], in spite of the use of a poor approximation to CLF. The main residual difference between experiment and theory was a consistent under-prediction of the weight of stress relaxation due to short-chain reptation. Recent calculations using the asymptotically exact result (109) for the CLF contribution gave a good account of monodisperse PS and PB data from the terminal zone into the local free-Rouse regime.

In figure 29 we review the way that each of the main physical processes of pure reptation, CLF, CR and longitudinal chain equilibration is predicted to contribute to the relaxation modulus of a monodisperse linear melt at a high degree of entanglement. In these calculations [247], the CR parameter $c_\nu$ was set to 1. A comparison to PS data on $G^*(\omega)$ of this theory is given in figure 30. We note that CLF is essential for understanding the form in the region of the minimum of $G''(\omega)$, and of its slope, and that CR is essential for capturing the smoothed form of the maximum at the terminal time. In consequence, even the renormalized reptation time reduced by CLF, equation (103), is not itself the terminal rheological relaxation. It is itself further affected by the high Rouse-tube CR modes.

With this degree of refinement of theory it becomes possible for the first time to investigate by rheology or dielectric relaxation the possible non-universalities suggested by the packing-length parameter [78, 79] (see section 6.5). The conclusions

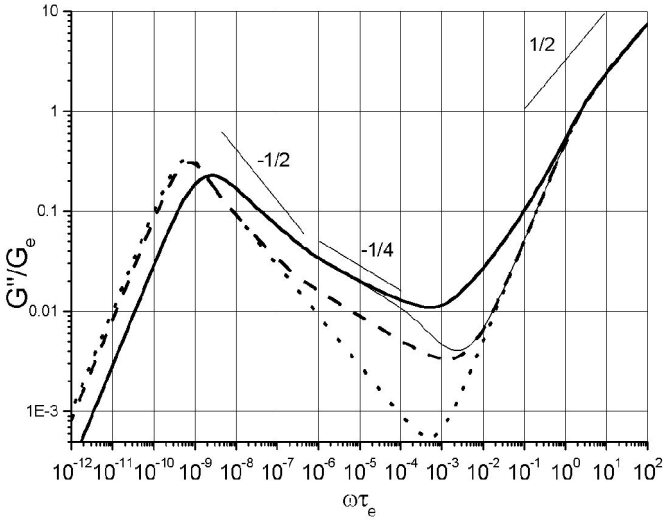


Figure 29. Predicted contribution of effects of $G''(\omega)$ for a linear melt with $Z = 800$. Dotted: pure reptation plus free-chain Rouse; dashed—with chain end CLF; thin sold—with CR; thick solid—with CLF longitudinal chain equilibration.

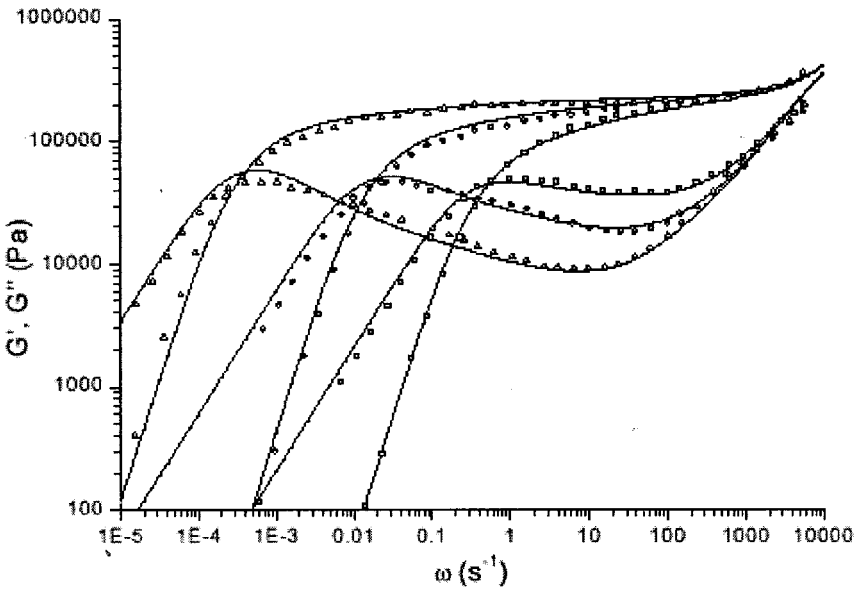


Figure 30. Comparison of the tube theory including CLF, longitudinal modes and CR with $c_\nu = 1$, to data on PS from reference [264]. Molecular weights are 290k, 750k and 2540k [247].

will have to wait for experiments on high packing-length materials, themselves difficult to synthesize in monodisperse, stable form. But in advance of these conclusions, we may anticipate that a still more careful theory for CR may be necessary. The Rouse-tube picture, while correct in outline, and even permitting a degree of self-consistency, is still not quite faithful to the physics of the underlying model. For the Rouse-like tubes do not relax with a *frozen* set of mobilities chosen

from the modes of $\mu(t)$ of the surrounding chains. Rather an individual entanglement segment may exchange its CR lifetime from one jump to the next.

It is high time to turn to the arena in which the effect of CR is most clearly brought into view, indeed in which it is no longer perturbative at all—the case of entangled polymers of higher topology than linear. For it has been said that the really striking success of the tube model is to be found in its capacity to explain the counter-intuituive rheology of star polymers, to which we now turn.

### 4.3. *Entangled branched chains*

From the earliest years of our programme of research, the special phenomena arising in the case of long chain branched polymers have acted as severe tests of theoretical developments. First noted in the context of industrial branched polymers [16], early experiments on anionically polymerized star polymers [84, 119, 120, 265] showed that the distinct rheology we noted above (section 3.2.2) arose also in well-defined monodisperse architectures. In the following we begin with the fundamental case of star polymers, and follow the developments of the tube model to make predictions for rheology, dielectric spectroscopy and diffusion. As a preliminary, we will need to extend the treatment of CLF we began above to the case of very deep fluctuations of the primitive path. We will then develop an approximation to CR necessary for entangled stars, whose tubes possess an exponentially-broad range of CR timescales, finally extending the model to cover data on more complex architectures, both monodisperse and random in their topology. Other qualitative effects emerge in the nonlinear rheology of more general branched polymers. We defer considerations of nonlinear predictions of the tube model to section 5.2.

#### 4.3.1. *Experimental rheology of star polymers*

We have already seen the great difference made by introducing a branch point into the molecules of a polymer melt to the relaxation modulus (section 3.2.2) . This induces equally remarkable differences in the way the terminal viscosity varies with molecular weight in the case of star polymers. Instead of the $M^{3.4}$ dependence of linear polymers, the viscosity increase is dominated by an exponential growth. Comparison between different chemistries indicates that it is the number of entanglements along the star polymer *arms* that dominates universally:

$$\eta \sim \exp(\nu' M_a/M_e), \tag{133}$$

where $M_a$ is the molecular weight of a single arm of the star and $\nu'$ a first order coefficient. More remarkably, the number of arms affects neither the viscosity nor the relaxation spectrum [85] (providing that this is not more than 30 or so, when new low-frequency effects and structures do arise [53, 266]). When the viscosity is plotted against the *span* molecular weight, defined as twice the arm molecular weight (see figure 31), the viscosity is always greater than that of the analogous linear melt. Of course, when the viscosity is plotted against the total molecular weight, the result for star (or more highly branched) polymers is lower than that for the linear material of the same total molecular weight (the branched molecules at equal $M$ are more compact, and posses fewer entanglement strands in their span). But eventually the exponential growth of the star melt viscosity overwhelms that of the linear in even this convention. When diluted in a good solvent, an exponential dependence on polymer concentration is also seen [267]. This very sensitive dependence on the entanglement environment appears again in tracer diffusion measurements [210]. The

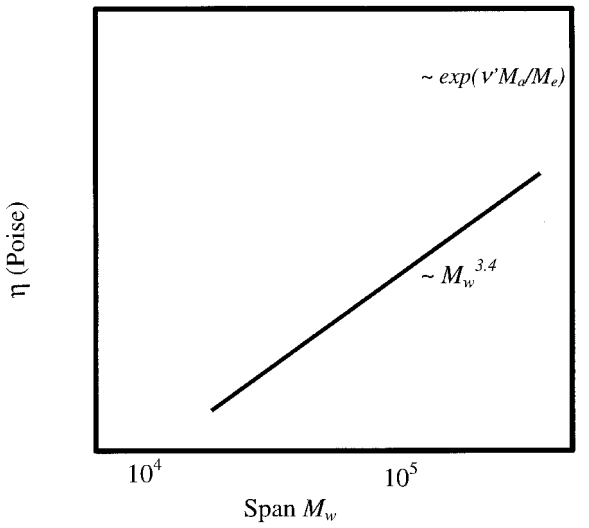


Figure 31. Viscosity versus span (twice arm) molecular weight for a series of PI star melts of arm-number from 4 to 33. Linear polymer result shown by the light line. [From reference [85].]

tracer diffusion constant of entangled stars is also exponentially dependent on the arm molecular weight, in the same manner as equation (133), and furthermore the values of $D$ can be many orders of magnitude smaller in an immobile matrix than in a homopolymer star melt.

The rheological relaxation spectrum itself is vastly broader for star polymer melts than linear chains. This is true of both rheological [85] and dielectric response [188]. As the molecular weight of the arms is increased, so the near-plateau of relaxation modes represented by $G''(\omega)$ grows towards lower frequencies with the same exponential dependence as the viscosity (see figure 32).

We have seen how the tube model can account qualitatively (see figure 5) for these observations. The key observation is that the branch point of a $q$-armed star within the confining potential of the tube is *localized* [21] to a region of order $a$ in size. This is a consequence of the equilibrium tension $f_{eq}$ induced by the tube in timescales faster than all disengagement processes. The reptation of the branch point along any one of the arms' confining tubes by a primitive path distance $s$ would require an entropic fluctuation of free energy of magnitude $f_{eq}(q-1)s = (3k_BT/a)(q-1)s$. We will see that this is typically far greater than the free energy barrier posed to independent retractions of individual arms. The one exception is in the case of lowest $q = 3$ [33], when co-operative displacements of the branch point reduce the viscosity slightly from the universal form for higher arm numbers. However, the mechanism for configurational (and stress) relaxation is unchanged—tube segments must be visited by chain ends. In entangled star polymers this can only happen by CLF; the chain forms unentangled loops along and emerging from the tube so that the free end retraces the tube contour before re-emerging into new tube. In so doing, all previously occupied tube from the free end to the point of deepest retraction of the free end is reconfigured. Clearly shallow retractions will happen much more frequently than deep retractions—this is the origin of the huge spread in relaxation times—and the deepest retractions themselves

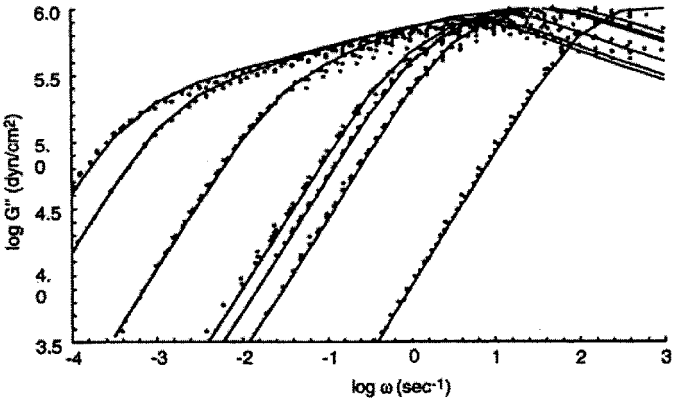


Figure 32. Data on series of PI star polymers from reference [85] and corresponding theoretical predictions using the theory of reference [190]. In order of decreasing frequency of the terminal times, the arm molecular weights $10^{-3}M_a = 11, 17, 37, 44, 48, 95$ and 105.

will become extremely rare as the molecular weight of the arm increases. This is the origin of the molecular weight dependence of the retraction times in the data of figure 32 and the slow diffusion of stars in section 3.9, since terminal processes such as viscosity and diffusion will require retraction of arm ends to within one tube diameter of the branch point. In the language of the primitive path (section 4.2.1), this corresponds to an extreme fluctuation of the primitive path to zero, which we have seen is exponentially unlikely in the number of entanglements $Z_a$ of the arms, equation (81). We therefore find immediately the qualitative prediction that viscosity and diffusion will be exponentially slow in the degree of entanglement of the arms [237].

$$\eta \sim \frac{1}{D_{\text{self}}} \sim \exp\left(-\nu Z_{\text{arm}}\right) \tag{134}$$

with $\nu = \nu_Q \equiv \frac{3}{2}$ for a quadratic potential (see section 4.2.1). More quantitative treatments require a calculation of the dynamics of Brownian motion in a deep potential well, which we consider in the next section.

4.3.2. *A tube model for star polymers*

To develop the theory we will need the rate for the escape time of a single degree of freedom (e.g. diffusing particle) over a barrier. Calculations have often written $\tau_{\text{esc}} \simeq \tau_0 \exp\left(U/k_B T\right)$ [21, 237], where $U$ is the barrier height and $\tau_0$ some local microscopic hopping rate. This is often good enough, but there are times when the pre-factors to the expression will be important. Both exact and approximate expressions based on a famous approach developed by Kramers [268, 269] are so important here, that we review the basic structure of the problem briefly in the appendix. The result for the mean first passage time for a diffusing particle (of self diffusion constant $D$), released at $s = 0$ to attain a point $s$ within a potential $U(s)$ is

$$\tau(s) = \frac{1}{D}\int_0^s \mathrm{d}x' \exp\left[U(x')\right] \int_{-\infty}^{x'} \mathrm{d}x \exp\left[-U(x)\right], \tag{135}$$

which can be approximated when the gradient of $U(s)$ is finite as

$$\tau(s) \simeq \frac{\exp[U(s)]}{DU'(s)} \left(\frac{2\pi}{U''(0)}\right)^{1/2}. \quad (136)$$

The first term in this product is an approximation to the first integral of (135) (valid when $U$ is large); the second term similarly approximates the second integral. We have seen (section 4.2.1) that we can write a potential $U(s)$ for the length of the primitive path $s$ inwards from the equilibrium value by including both the (quadratic) curvilinear rubber-elastic term and the (linear) end-tension term. We will find it convenient to redefine the potential acting on a fractional co-ordinate $0 < x < 1$ along the arm primitive path (so that complete retractions correspond to $x = 1$). In this case the potential becomes:

$$U(x) = k_B T \nu_Q Z_{arm} x^2. \quad (137)$$

This quadratic potential will determine the fluctuation dynamics of an arm of an entangled star polymer: it gives the free energy paid for a retraction of the free end a distance $x < 1$ along the tube. Whenever this happens, the subsequent equilibrium configuration will have a renewed configuration for all chain segments occupying tube whose primitive path distance from the branch point is between $1 - x$ and 1. We bear in mind that there may be corrections to the quadratic potential of order 0.1 that will make a difference to the rate of deep retractions [239]. The other major assumption in this approach to star-arm dynamics is that only the slowest Rouse mode acts as an effective dynamical variable for deep retractions. This assumption seems appropriate, since Rouse modes of index $p$ have effective elastic potentials that vary as $p^2$; see equation (65). However, the higher modes may renormalize the barrier-hopping timescales [269, 270], and may be required in future, more accurate, theories of branched polymers.

Once such approximations have been made, the observations above can be rapidly turned into a semi-quantitative theory for star-polymer stress-relaxation [21] which is amenable to more quantitative refinement [271]. The key observation is that the diffusion equation for stress-release, which arises in linear polymers via the passage of free ends out of deformed tube segment, is now modified in star polymers by the potential of $U(s)$. Apart from small displacements of the end, the diffusion to any position $s$ along the arm will now need to be activated and so is exponentially suppressed. Each position along the arm, $x$, will possess its own characteristic stress relaxation time $\tau(s)$ given by the average first passage time of the diffusing free end to $s$. The effective diffusion constant, $D$, of the Brownian particle we can identify as the Rouse diffusion constant of the arm, modified by a factor 2 since the mean displacements of monomers in deep retractions are proportional to their distance from the branch point. In the figure of the appendix, the curve for $U(x)$ is the quadratic potential given by the tube model by a fixed environment; simple substitution of the arc-length potential into the general result (136) gives a dominant exponential term to the longest relaxation time $\tau(1)$ of

$$\tau_{late}(1) = \frac{\pi^{5/2}}{\sqrt{6}} \tau_e Z_{arm}^{3/2} \exp(\nu_Q Z_{arm}) \quad (138)$$

(NB the prefactor is not insignificant!), where $\tau_e$ is the Rouse time of an entanglement segment. We have chosen the notation $\tau_{late}(x)$ to distinguish this expression from the result for rapid retractions $\tau_{early}(x)$. The difference between that result and this new form for deep CLF retractions is generated by the significant

free-energy penalty in the star case. The exponentially suppressed retractions were not seen in the case of linear polymers we considered above because the reptation mode dominates for precisely those retractions $(x > Z^{-1/2})$ that become exponentially suppressed. The relaxation modulus in the star melt can then be written

$$G(t) = G_N^{(0)} \int_0^1 p(x,t)\,\mathrm{d}x, \tag{139}$$

where $p(x,t)$ is the survival probability of the tube segment at the fractional coordinate $x$ (the probability that it has not been visited by the free end before time $t$). In the limit of high potential barriers $U(x)$ the form of $p(x,t)$ becomes proportional to $\exp[-t/\tau(x)]$ in an approximation that is asymptotically exact [269]. This form of $p(x,t)$ is well approximated for highly entangled arms by a step function in $x$: consider the state of relaxation at any time $t$ intermediate between the relaxation time of the first entangled segments near the end of the arm and the core-segments of the star. At $t$ some internal segment will typically be just in the process of reconfiguration via its first 'visit' by the free end. This segment will have an arc-length coordinate $x$ given by $\tau(x) = t$. All segments exterior to the segment $x(t)$ given by the inverse of the function $\tau(x)$ are almost certain to have relaxed, because their relaxation timescales are exponentially shorter, while segments nearer to the core are conversely almost certainly unrelaxed.

Unfortunately, although qualitatively promising, this version of the theory fails disastrously at the quantitative level. A glance at the polyisoprene $(M_e = 5\,000)$ star data above (figure 32) will suffice: the sample with the longest arm molecular weight (105 000) is predicted to carry an exponential term for the terminal time of approximately $10^{18}$. Yet this must describe roughly the width of the 'relaxation shoulder' in $G''(\omega)$ in the figure, which is only 6 decades broad. Pearson and Helfand [271] accommodated this anomaly by allowing the preexponential factor $\nu$ in equation (137) to take on experimentally adjusted values, finding $\nu = 0.5$ to fit the data well (using our definition of $M_e$). However, the problem lies with the need to account for 'constraint release'—described as a correction in the case of linear polymers in section 4.2.5, but which in the case of star polymers becomes quite dominant, rather than simply a large perturbation. Fortunately it is sometimes much simpler to treat in the case of star polymers, as we see in the next section.

*Hierarchical constraint release in star polymer melts: tube dilation.* The much more significant contribution of constraint release to the dynamics of entangled star polymers in comparison with linear polymers arises from the very broad distribution of relaxation timescales we have discussed above. Fortunately, the same breadth of timescales provides a simple way of calculating the effect [190, 272]. As a consequence of the exponential separation of relaxation timescales along a star arm, by the time that a given tube segment $x$ in the population is relaxing, all segments of tube $x'$ such that $x' < x$ (nearer a chain end) have renewed their configurations typically many times. So chain segments at $x$ and nearer the star cores *do not entangle* with these fast segments at the timescale $\tau(x)$ and beyond. Alternatively we can say that the tube is dilated due to this effective dilution of the entanglement network: fast relaxing segments act as solvent for the slower relaxing ones. Such an idea applied to constraint-release in linear polymers is problematical [36] because of the dominance of the near-single relaxation time for

CR events of $\tau_d$. We recall that even in the case of bimodal blends, only very special circumstances permit the long chains to relax in a dilated tube in which the short chains act as solvent. However, the exponentially-broad spectrum of CR relaxation times permits the limit of tube dilation to apply in the case of stars, and branched polymers generally. In the following we calculate the spectrum of relaxation times, then show its self-consistency.

The new information necessary to make this approach quantitative is the dependence of the effective entanglement molecular weight on the concentration, $\Phi$, of unrelaxed segments. This is known from experiments on dilution of polymer melts by theta-solvents to be approximately $M_e(\Phi) = M_{e0}/\Phi^\alpha$ (with $\alpha = 1$ and $\alpha = 4/3$ two popular choices [36]), which corresponds to the approximately quadratic concentration dependence of $G_0 \sim \Phi^{\alpha+1}$. At any stage in the relaxation dynamics of a melt of identical star polymers, therefore, when a segment $x$ is currently relaxing for the first time the effective entanglement molecular weight is $M_e(x) = M_{e0}/(1-x)^\alpha$. This means that the effective number of entanglements along the arm is reduced at this timescale to $Z_{arm}(x) = Z_{arm}(1-x)^\alpha$. To recompute the relaxation times $\tau(x)$ with the dynamic dilution assumption we consider the activated diffusion in a *hierarchical* way. To retract from $x$ to $x + dx$, the attempt frequency is $\tau(x)^{-1}$ and the activated probability for this diffusive step is $\exp\{(-1/kT)[U(x+dx; M_e(x)) - U(x; M_e(x))]\}$ where the notation for $U$ indicates that the running value of the entanglement molecular weight is kept. Taking the limit of $dx$ small gives the differential equation

$$\frac{dU_{eff}}{dx} = \frac{\partial U}{\partial x}[x; M_e(x)], \tag{140}$$

where the dependence on an $x$-dependent value for $M_e$ arises from the 'dynamic dilution' of the tube increasing the effective value of $M_e$. Taking the dilution exponent $\alpha = 1$, this is simply $M_e(x) = M_{eo}(1-x)^{-1}$. Integration of this equation leads to an effective renormalization of the potential $U(x)$ which, if we make the choice of $\alpha = 1$, is now a cubic in $x$:

$$U_{eff}(x) = \nu Z_{arm}\left(x^2 - \tfrac{2}{3}x^3\right). \tag{141}$$

The terminal time and viscosity are dominated, as we saw above, by the potential at complete retraction $U_{eff}(1)$. This is now given by $1/2(M_a/M_e)$, in much closer agreement with experiments. The formula for the relaxation modulus also needs modifying since each element of chain $ds$ contributing to the stress relaxation now does so in an environment diluted by $(1-x)$, so picks up this factor within the integrand as a coefficient of $p(s,t)$. The general result is

$$G(t) = G_N^{(0)} \int_0^1 \frac{\partial G}{\partial \Phi}\frac{\partial \Phi(x)}{\partial x} \exp\left[-\frac{t}{\tau(x)}\right] dx, \tag{142}$$

with $\tau(x)$ calculated from the full expression for barrier-hopping equation (135), but using the dilated effective potential $U_{eff}(x)$. The shape of the relaxation spectrum predicted by this procedure does indeed fit rheological data on pure star melts better than the quadratic expression calculated for stars in permanent networks [53, 190, 273], especially when corrected for at high frequencies by a cross-over to unactivated tube loss by Rouse-like motion, $\tau_{early}(x)$, near the free end:

$$\tau(x) \simeq \frac{\tau_{\text{early}}(x)}{\exp\left[-U_{\text{eff}}(x)\right] + \tau_{\text{early}}(x)/\tau_{\text{late}}(x)}, \tag{143}$$

where a good approximation for $\tau_{\text{late}}(x)$ from equation (135) is

$$\tau_{\text{late}}(x) = \left(\frac{\pi^5}{6}\right)^{1/2} \tau_e Z_{\text{arm}}^{3/2} \frac{\exp\left[U_{\text{eff}}(x)\right]}{\left[x^2(1-x)^2 + \dfrac{2}{3\pi Z_{\text{arm}}}\right]^{1/2}}.$$

Care should be taken in the use of these approximations, however, as their asymptotic regime of validity is quite slowly reached [274]. It is usually quite possible to calculate with the exact expression (135) numerically.

*Criterion for dynamic dilution*. A criterion that accounts for the regimes of validity of such a tube dilation simplification compares the rates of self-diffusion of monomers on chain segments relaxing on a timescale $t$ with the rate of tube widening given by the dilution hypothesis [36, 275]. This is identical to the criterion used to identify the effective diameter of the tube in bimodal blends considered above [260]. If the first is greater than the second, then the diluting tube acts as the effective topological constraint, and tube dilation, or 'dynamic dilution' is valid. If not, then the chain relaxation is not impeded by the tube and the approximation fails. So, implementing this criterion for star arm retraction, if $x$ is some label for chain material which relaxes at time $\tau(x)$, the physical criterion for dynamic dilution can be written

$$\frac{1}{\langle r^2(t)\rangle}\frac{\mathrm{d}\langle r^2(t)\rangle}{\mathrm{d}t} > \frac{1}{a^2(\Phi(t))}\frac{\mathrm{d}}{\mathrm{d}t}a^2(\Phi(t)). \tag{144}$$

Using the Rouse result for the sub-Fickian monomer displacement (71), the left hand side of equation (144) is just $1/(2t)$. In the case of star polymers, using the approximate result for $\tau(x)$ from equation (143) and $a^2(\Phi(t)) \sim [a^2(\Phi(t))]^{-1}$, the criterion becomes:

$$x(1-x)^2 > \frac{2}{3}\frac{1}{Z_{\text{arm}}} \tag{145}$$

for the choice of $\nu = \nu_Q$ in the primitive path potential. The condition of equation (145) is satisfied for $x > 2/(3Z_{\text{arm}})$; i.e. when the chain first feels the original undiluted tube, and for $x < 1 - (2/3Z_{\text{arm}})^{1/2}$. This is typically very close to the core of the star, and corresponds to a 'disentanglement transition' when the tube dilates faster than the remaining unrelaxed star arm can follow it by Rouse-like constraint release. The contribution of this small amount of unrelaxed material obeying effectively unentangled dynamics near the terminal time contributes very little to the relaxation modulus.

*Experimental assessment of tube dilation model in star melts*. The curves through the experimental points in the data for $G''(\omega)$ on the PI stars above (figure 32) were calculated via this scheme [273], and fit the experiments using literature values of the two fitting parameters required, $\tau_e$ (a horizontal shift on the figure) and $G_N^{(0)}$ (a vertical shift). Other chemistries of star melts are equally well accounted for by this approach [53, 274, 276]. The great strength of this remarkably powerful theoretical framework is that in principle, only these two parameters are required for all molecular weights and topologies of a single chemistry, so that the theory is very constrained.

Rather stringent tests are supplied by bimodal blends involving a monodisperse star-polymer component. Rheological results are available on the cases of star–star [274, 275] and on star–linear [275, 278] blends. The highly cooperative nature of tube-dilation CR in star arm retraction leads to a remarkable prediction in the case of polydisperse stars (of which bimodal blends are the simplest case). A strong *motional narrowing* occurs: the slower component relaxing exponentially faster in the presence of the faster than it does in a homopolymer melt, and the converse for the smaller. As an immediate result [272], the terminal time of the blend carries a form of exponential dependence on arm molecular weight that is identical to that of the homopolymer, but with $Z_{\rm arm}$ replaced by its weight average so that

$$\tau(1) \sim \exp\left(\frac{\nu}{3}\langle Z_{\rm arm}\rangle_{\rm w}\right).$$

The detailed relaxation of each component in the blend is calculated by a transformation from the fractional path length coordinate of species $i$, $x_i$, to the coordinate $z_i = Z_{a,i}^{1/2} x_i$ in which the calculation of the renormalized potential becomes universal. Predictions of the resulting theory for $G^*(\omega)$ and data from [277] are given in figure 33, together with a comparison spectrum of a linear monodisperse PI. Both the relaxation times and the detailed forms of the response function clearly vary exponentially with the relative fraction of the two components, yet the two-parameter theory captures the complete behaviour. A similar picture emerges in the case of star–linear blends, with the subtlety that, after the reptation time of the linear component, a regime of stress-relaxation that is pure Rouse tube (rather than tube dilation) sets in. This is because the remaining star component is not able immediately to explore the wider tube formed only by its self-entanglements; the criterion for the tube dilation limit fails until the wider tube is encountered by lateral excursions of the Rouse tubes [275].

However, not all the possible experimental probes support the predictions of a theory invoking maximal tube dilation. When the self-diffusion of monodisperse stars is compared with their rheology, it is possible to examine the dilation of the tube at the terminal time rather carefully [191, 279]. The product $\eta D_{\rm self}$ cancels the exponential dependence of the two dynamical quantities, leaving only the pre-exponential dependencies on $Z_{\rm arm}$. In the case of diffusion, the additional physical assumption in a calculation of $D_{\rm self}$ is the size of the hop made by the branch point. The natural assumption to make for the jump length if tube dilation holds is the value of the tube diameter at the disentanglement transition we identified above at $x < 1 - (2/3Z_{\rm arm})^{1/2}$. Such an assumption gives $\eta D_{\rm self} \sim Z_{\rm arm}^{-1/2}$, but if the hops take place in the bare undiluted tube, the prediction is the much steeper $\eta D_{\rm self} \sim Z_{\rm arm}^{-3/2}$. The data of reference [201] are very clear: the scaling with $Z_{\rm arm}$ is much closer to the undiluted result than the dilated case, although the prefactor indicates that the typical jumps are larger than the bare value of $a$ by a factor of about 3.

The self-diffusion also introduces a dependence on the number of arms, unlike the rheology. This is because, independently of the spatial and temporal scale of the diffusive hops, the only effective moves will be made when the arms are locally arranged colinearly, as pointed out by Rubinstein [280]. The predicted dependence on the number of star-arms $q$ in a lattice model is

$$D_{\rm self}(q) \sim \frac{[1 + (z-1)(q-1)/2]z!q!}{(z+q-1)!}, \qquad (146)$$

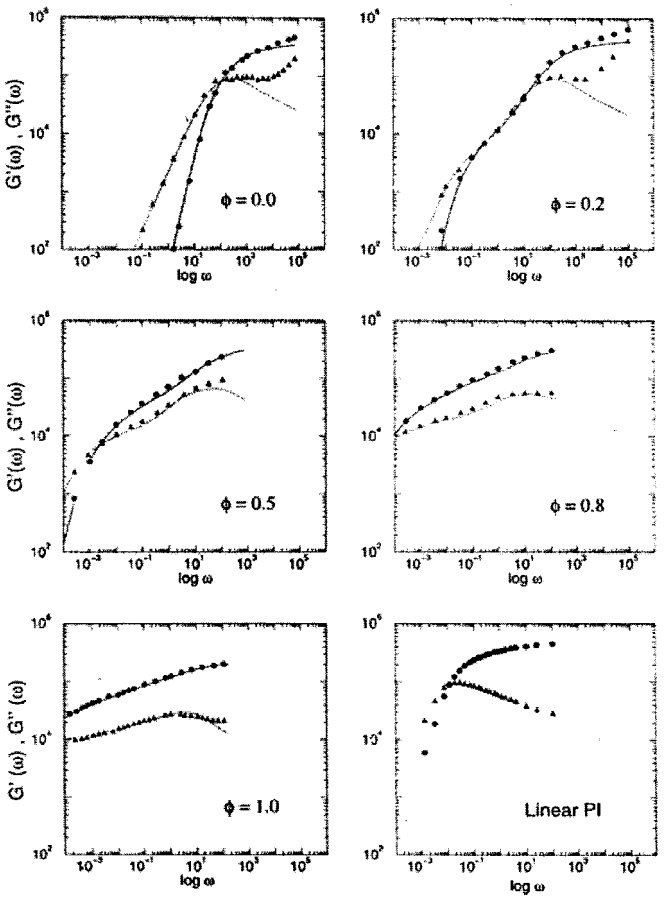


Figure 33. Linear rheology on blends of a pair of PI three-arm star polymers of arm MW 144 000 and 28 000 together with the tube theory (curves) with values of $G_N^{(0)}$ and $\tau_e$ set by the monodisperse materials and the choice of dilution exponent $\alpha = 1$. Volume fractions of the high MW star are shown. Data from a linear polymer is shown for comparison.

where $z$ is the functionality of the lattice (we expect $z > 6$ in three dimensions). This relationship may be modified in a melt, where one might expect the simple $D_{\text{self}} \sim 1/q$ from an addition of effective drag, but is followed well by experiments on diffusion of variable arm-number stars [281]. We note that this prediction is independent of the validity of tube dilation called into question by the results on the product $\eta D_{\text{self}}$.

A purely rheological experiment that is nonetheless sensitive to the diffusive properties of the branch point is the relaxation of a melt of three-arm stars with one arm shorter than the other two. If considerably shorter, the retraction of the third arm permits further orientational relaxation by reptation of the remaining linear object, albeit slowed down by the larger effective drag of the branch point. Recent studies of just such series of PEP [282] and PI [283] stars confirmed the accuracy of the dynamic dilution theory for nearly-symmetric stars, but found that short arms of just a few entanglements contribute to the drag to a much greater extent than predicted.

Perhaps the most powerful test of CR and effective tube dilation, as we have seen in the context of linear polymers, is dielectric relaxation on A-type dipole chains. This is because, to a good approximation, the dielectric relaxation function measures the surviving tube fraction directly (at least at timescales shorter than the CR Rouse time of the tube) so that $\epsilon(t) \sim \mu(t)$, while the rheological relaxation function picks up any CR relaxation function of the tube itself $G(t) \sim \mu(t)R(t)$. Since, for the case of full tube dilation we have $R(t) = [\mu(t)]^{\alpha}$, where $\alpha$ is the modulus dilution exponent ($\alpha \simeq 1$), we predict

$$G(t) \sim [\epsilon(t)]^{\alpha+1} \tag{147}$$

when tube dilation holds. We saw above [180, 181] in section 3.7 that this holds experimentally for entangled linear chains. This we would expect to be approximately true, since for Rouse tube CR the value of $R(t)$ when $t \simeq \tau_d$ is of the same order as the value of the reptation decay function $\mu(t)$ itself. We might therefore expect it to be followed even more closely in star melts, if tube dilation is indeed rigorously true in that case. However, recent results indicate a departure from the tube dilation prediction for $x \gtrsim 2/3$ [188] for $Z_{arm} = 8$. Increasing $Z_{arm}$ to 16 makes the picture even clearer (see data of figure 18). Although the rheological response indicates the apparent continuation of tube dilation beyond $x = 2/3$, the dielectric relaxation for this final 1/3 of the arm is almost mono-modal at the terminal time, showing a clear peak in $\epsilon''(\omega)$!

*Tube dilation in stars: a second look.* Even without the experimental difficulties as soon as one goes beyond rheology, the original treatment of dynamic dilution in stars reviewed above [190, 272] leaves some important questions unanswered, and is based on a physically intuitive, but non-formal, treatment of the Kramers problem. In particular it leaves the physical interpretation of the effective potential unclear, does not examine the effect of several modes contributing independently to retraction, and does not appear to visit the problem of the balance between effective primitive path length and effective drag. In this context, it is dangerous to assume that the range of validity of tube dilation demonstrated within such an approach is the right one.

A recent re-appraisal of the original calculation of the effective potential $U_{eff}(x)$ has applied a more formal application of the Kramers' result (135) to the hierarchical series of retractions and showed that $U_{eff}$ is composed of a pseudo-static and a dynamic component [192]. The first is a true renormalized entropic potential $U_{dil}$, diluted with the effective solvent of relaxed outer segments

$$U_{dil}(x) = k_B T \nu Z_{arm} x^2 (1 - x), \tag{148}$$

while the second is the expected renormalized drag, arising from the need to incorporate all faster CR events into current retractions of the *tube* to relieve the next unrelaxed segment in the hierarchy (like the Rouse tube CR picture, it is the tube itself that carries the retraction dynamics as if it were a polymer chain and underpins the dilation calculation). The renormalized drag can be represented as an effective coordinate-dependent diffusion coefficient for the Kramers' problem

$$D(x) = D_0 \exp\left(-\frac{\nu Z_{arm} x^3}{6}\right), \tag{149}$$

with $D_0$ the bare Rouse diffusion coefficient for the retracting arm. Now,

$$U_{\text{eff}}(x) = \frac{D_0}{D(x)} U_{\text{dil}}(x), \tag{150}$$

which has the property of monotonically increasing with $x$, even though the diluted potential for retractions to $x$, $U_{\text{dil}}(x)$, possesses a maximum, and has the value 0 at both $x = 0$ and $x = 1$. The exponentially slow dynamics can be attributed to the *potential* for small values of $x$, but as $x$ approaches 1, and the entanglement field becomes more and more dilute, the slow dynamics arise more from the renormalized *drag*. So continuity of the physical picture is maintained right up to diffusive timescales, on which there is of course no tube field at all, but simply branch points executing diffusive hops generated by the exponentially large friction of their arms. The problem with a single-mode picture is sharpened: (149) is larger than the result of direct calculations of $D$.

Now it is possible to test the tube dilation hypothesis by offering the star arms at each stage of the retraction hierarchy several co-operating choices of tube diameters from the bare value (minimizing drag at the expense of a steep potential) to the maximally-diluted one (minimizing the potential for further retraction at the expense of requiring a large renormalized drag). In effect this is a saddle-point solution to a high-dimensional Kramers formulation of the tube segment relaxation. At each stage of retraction $x$, the star melt is free to choose coordinates $\tilde{x}(x)$ so that the effective tube diameter for the next retraction is $a(1 - \tilde{x})^{1/2}$ and the diffusion constant $D(\tilde{x})$. The function $\tilde{x}(x)$ is chosen to minimize the tube segment disengagement times, since all such processes are open to the system to explore.

The result of this calculation is that the assumption of maximal dilution is indeed a close approximation for star melts and melts containing a finite fraction of more slowly-relaxing material (higher molecular weight polymers or deeper segments of more complex branched polymers), so that $\tilde{x}(x) = x$ [192] is the best choice in a single-mode approximation. However, when the driving potential for retractions is now assigned to $U_{\text{dil}}$ rather than $U_{\text{eff}}$, the former criterion for tube dilation (144), which must be independently applied, fails at the maximum of $U_{\text{dil}}(x)$. No longer is maximal tube dilation self-consistent; assuming that the largest possible tube diameter were explored beyond the maximum in $U_{\text{dil}}$ would create a potential that would drive further retractions much faster than the rate of tube dilation. Intriguingly, the mutual failure of this double-criterion for tube dilation occurs at $x = 2/3$ (taking the quadratic value $\nu_{\text{Q}} = 3/2$ for $\nu$), which coincides with the departure of the dielectric data from the dilation result (147). In addition, if the diffusive hops of the branch point are taken within a tube diameter of the dilated value at $x = 2/3$, the observed scaling of $\eta D_{\text{self}}$ can be accounted for (the dependence on $Z_{\text{arm}}$ of this dilated tube is just the same as that of the undiluted tube, since $a(2/3) = a(0)(1 - \frac{2}{3})^{-\alpha/2}$).

In further support of a more subtle dynamics of the final 1/3 of entangled star arms, a recent coarse-grained simulation has modelled entanglements between an ensemble of star arms as a complementary ensemble of 'slip-links', with stochastic dynamics of creation and annihilation that follow the retraction potential of equation (137) [229] (see figure 34). It is possible to account for both stress and dielectric relaxation in the simulation by keeping track of the total surviving number of links (stress) and the distance to the furthest surviving links from the branch points (dielectric relaxation). The simulation recovered at least qualitatively the observed departure of the two response functions from the tube dilation result.

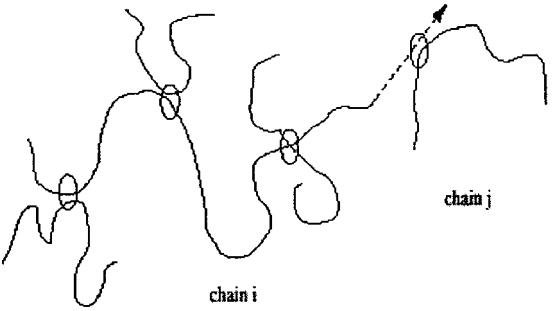


Figure 34. A schematic representation of the slip-link simulation of reference [229]. Spatially local pairwise interactions of star arms $i$ and $j$ are described by links that are annihilated by diffusing to free ends, and created at random, so increasing primitive paths with the potential of equation (137).

Moreover, it suggested a form for the typical terminal dynamics that suggests how the rheology may continue to mimick full tube dilation while the dielectric relaxation accrues a final, single relaxation time. The last segments to relax are those neighbouring to a branch point, but entangled (via a slip-link) with other similarly deep segments. Instead of waiting for a full retraction of one of the arms (which would take as long as the terminal time of a star polymer in a permanent network), these 'recalcitrant links' relax instead by themselves diffusing along the arm of one of the stars to meet a shallower and more favourable retraction from its free end. So the simulation seems to capture two modes of retraction acting simultaneously. The implication in real-space is that material nearer to the branch point than the recalcitrant link continues to explore wider and wider tubes (apparent tube dilation for stress) while the single end-to-end vector (carrying only a fraction of the stress but all the dielectric response) is forced to wait for the true terminal time. The peaked curve closely matching the dielectric data of figure 18 was calculated using this assumption for the dynamics beyond $x = 2/3$, together with full dilation for the rheology.

*Temperature effects.* A final intriguing anomaly of the experimental rheology of star polymers occurs in a range of hydrogenated polyolefin materials. It has long been known that the temperature dependence of LCB PE melts can be quite different from the linear versions, even if the branch points are quite dilute [284]. More striking still are experiments on PE star polymers made by the hydrogenation of anionically synthesized PB star polymers [285–287], which exhibit an enhancement of the apparent activation energy, $E_a$, for viscoelasticity (this is measured from the terminal region, so that, far from $T_g$, $\eta \sim \exp(E_a/RT)$). Moreover, the component of $E_a$ additional to the value recorded for linear PE melts is experimentally proportional to the arm molecular weight $M_a$. The monodisperse star architecture provided sufficient detail in the relaxation spectrum to determine additionally that the extra activation energy applies only to the lowest frequency zone of $G^*(\omega)$, precipitating a failure in these materials of time–temperature superposition. A wide survey of different chemistries [287] has unearthed a correlation of this 'thermo-rheological complexity' in star polymers (and other LCB topologies) with the coefficient of thermal expansion of the molecular $R_g$ in theta solutions [288]. The situation with regard to PI is at present rather unclear [289].

A possible explanation for this unorthodox behaviour, and in particular the stark difference between the $E_a$ values of linear and star polymers, was advanced by Graessley in the light of the tube model's appeal to deep retractions in the entanglement release of star arms [290]. Only for star relaxation are highly looped local configurations of the chain necessary. These are the 'kinks' of unentangled chain that proliferate to reduce the primitive path, and contain a mean radius of curvature of order $a$. If a real enthalpic energy penalty is paid for such tight turns of the chain, then the retraction potential must contain an enthalpic as well as entropic part. One source for such a term arises from local molecular conformations; to create an unentangled loop, a subchain segment must contain a higher proportion of '*gauche*' states than '*trans*'. If gauche states carry a higher energy (this is the case for PE), then the extreme retractions of star arms indispensible to stress relaxation carry this energy cost multiplied by the number of unentangled loops. It can be shown that this is also, on average, proportional to the original primitive path $L_{eq} \sim M_a$.

A quantitative calculation based on this idea was recently shown to be in reasonable accord with the data [245]. A lattice model of the primitive path (see section 4.2.1) was taken, with the modification that 'hairpin' returns of the chain on the lattice cost an energy $\Delta$, which becomes the new parameter of the model. In the continuum limit, the only modification to the quadratic potential for the primitive path length is a temperature dependency of $N_e$ so that $N_e = N_{e0} f(\Delta/k_B T; z)$. The cost of agreement was the adoption of a value for $M_e$ in the *dynamic* expressions that was about twice the value required for the *static* property of $G_N^{(0)}$; and even when this was done the level of agreement was considerably poorer than in the case of thermorheologically simple star melts. We have seen that this is a high price to pay within our theoretical scheme. The calculation is not straightforward, however, because there will be a coupling between the energy ascribed to a kink, and the conformations accessed by the retracting arm. In the limit of a very high energy kink, a zero primitive path state can in principle be attained with only one unentangled loop, the rest of the chain adopting a 'hairpin' configuration. Even PE melts clearly have their molecular retraction configurations strongly perturbed by the enthalpic contribution. In this case the primitive path potential can be strongly non-quadratic, becoming much weaker for deep retractions [245]. This is clearly an area of current research that would benefit from further series of well defined materials in hydrogenated PB at least, possible venturing into more complex topologies (see below).

*The future for the stars.* Clearly the current state of theory, even for star polymers, is in rapid development. This is in spite of the considerable strides taken in dealing with, for example, the complex case of star–linear blends. The issues raised by the recent dielectric data and simulations are a reminder of the fearful complexity of the problem that we are inclined to forget, after working with extreme simplifying approximations such as self-averaged tube dilation. But there are lessons to be learned from more complex architectures still, even before all the current uncertainties are cleared. In some cases we might even expect a simplification. For example the worrisome non-monotonicity in the diluted potential for star-arms, $U_{dil}(x)$, that gave rise to the loss of the tube dilation limit for CR in monodisperse stars, does not exist if a fraction of more slowly relaxing material $\phi_b$, is present. For in that case, using quadratic potentials,

$$U_{\rm dil}(x) = \frac{3Z_{\rm arm}}{2} x^2(1 - \phi_{\rm a} x), \tag{151}$$

where the fraction of arm material $\phi_{\rm a} = 1 - \phi_{\rm b}$. For all $\phi_{\rm a} < 2/3$, this potential has no maximum, and maximal tube dilation is in principle permitted for all $0 < x < 1$ [192]. This encourages us to look at the simplest case of such materials: monodisperse melts whose molecules contain a fraction of dangling arms attached to a long backbone segment rather than a single branch point. This case of the H-polymer we will treat in some detail, as it constitutes a rather fundamental approach to branched polymers in general. This will be true in nonlinear response as well as linear.

4.3.3. *H-polymers and combs*

The attraction of the H-polymer melt is that the idea of hierarchical relaxation by arm retraction, and the consequent renormalization of the effective degree of entanglement of the melt, generalizes in an appealing way to this architecture. For just as the long time picture of an entangled star polymer melt is an ensemble of branch points with rapidly-moving 'clouds' of retracting arms, providing exponentially high drag, so the H-shaped polymer at long timescales becomes just an ensemble of the crossbar sections moving against drag concentrated at the attachment points of the arms (see figure 35). Before making any lengthy calculations, therefore, we can see that the early-time dynamics will be similar to that of star melts (apart from the presence of slow crossbar material), and that the late-time dynamics may even be reptation of the effectively linear crossbars in supertubes defined only by their mutual entanglements. A very similar picture will present itself in the case of entangled combs, with the difference that the effective late-time drag will be located at the branch points along the comb backbone.

An early set of data on H-polystyrenes by Roovers [122] was obtained on a series of molecular weights with equal amounts of material in each arm $M_{\rm a}$ and crossbar $M_{\rm b}$. Three important observations were made:

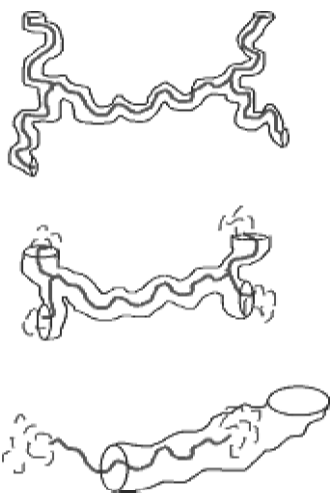

Figure 35. Depiction of the stages (i), (ii) and (iii)/(iv) in the relaxation of an H-polymer melt outlined in the text. Arm-length fluctuation precedes crossbar reptation in a progressively widening tube.

(i) The presence of the crossbar segment did indeed provide relaxations at lower frequencies than a melt of pure stars (of matching $M_a$) would have had;
(ii) for most of these polymers the low frequency contribution appeared Rouse-like, having $G''(\omega) \sim \omega^{1/2}$ before the terminal time, with the highest molecular weights suggesting the emergence of a new low frequency peak;
(iii) plotting log $\eta$ against the arm molecular weight $M_a$ gave a straight line (i.e. exponential dependence like that of stars) but with a higher slope than that of star polymers, so that $\eta \sim \exp(\nu Z_{arm})$ with $\nu > 0.5$.

However, PS has a large value of $M_e$ of about $18\,000\,g\,mol^{-1}$, so molecules of reasonably high molecular weight are still not highly entangled. A subsequent initial theoretical approach to the H-polymer problem [230] predicted a much more marked peak in $G''(\omega)$ at low frequencies if the crossbars were sufficiently well entangled to be forced to reptate at long times. This is a strong condition since the only entanglements available to the crossbars at long times are those with other crossbars. All arm material would disengage from the entanglement network on much faster timescales than any motion of the crossbars. The theory also conjectured a new process in nonlinear deformation with associated predictions for neutron scattering (see section 5.2). All of these predictions require a more heavily entangled polymer as a test material. These were the motivations behind the synthesis and analysis of a series of H-polyisoprenes (PI) [50, 291]. PI has a much lower value of $M_e$ of 3 800—5 000 $g\,mol^{-1}$ depending on microstructure, and a low glass transition temperature. The first property allows H-polymer melts with a much greater degree of entanglement and a wider range of relaxation times to be synthesized using reasonable molecular weights; the second permits experimental access to the longest relaxation times that arise. In these circumstances, the rheological spectra do indeed show remarkable features at different timescales, in particular in $G''(\omega)$, that seem to be identified with the relaxation of arms (fast) and crossbar (slow) [50] (and see figure 36). Similar features have arisen in polybutadiene 'pom-pom' architecture polymer melts (in which more than two arms are attached at each extremity of the molecular crossbar; see figure 47 and section 5.2.2 below) [87] and entangled combs [86, 123, 124].

*Tube model theory of H-polymers.* As briefly discussed above, the goal of our theoretical development will be to make quantitative the insight that the existence of the tube constraint gives rise to a dynamical hierarchy of relaxation events in melts of entangled H-polymers. We consider linear stress-relaxation in this section (for nonlinear response see section 5.2). As before, the implementation of the tube model for stress-relaxation requires us to focus on the dynamics of the free ends of the polymer architecture in question, for it is generally true that stress is lost from a tube segment when a free end diffuses past it. We take the dynamical processes that progressively liberate tube segments in the H-polymer in order of timescale. They are represented pictorially in figure 35.

STAGE (i): At early times (following a small step strain) stress will relax by path-length fluctuation in the dangling arms. Just as for star polymers these fluctuations will be controlled at very early times by rapid Rouse motion of the chain end along the tube.

STAGE (ii): The rapid pathlength fluctuation crosses over to an exponentially-slow 'activated diffusion' for the deeper arm fluctuations. The effective tube diameter

grows continuously and self-consistently throughout this regime, and the crossbars remain immobile.

STAGE (iii): After the star-like arms have completely retracted, the physical picture for the molecules changes to consider the mobility of the crossbars in widened tubes defined only by their mutual entanglements. All of the effective friction is concentrated at the branch points. The rapidly fluctuating arms provide drag that far outweighs the sum of monomeric drags along the crossbars. Initially, stress is lost from crossbar segments via free independent diffusion of the branch points along the tube (analogous to the early curvilinear Rouse motion of the free arm ends).

STAGE (iv): The free curvilinear diffusion of the chain ends is suppressed when pathlength fluctuations become slowed by the effective elastic potential (so thinking of the crossbar as a 'two-arm star' [56]). Central portions of the crossbar are relaxed by reptation. This is the slowest contribution to the linear stress relaxation.

The strategy for turning this physics into a quantitative theory requires two steps:

(1) We must calculate a hierarchy of timescales $\tau(x)$ in terms of an arc coordinate or coordinates, $x$, that trace through the molecular segments from the extremities to the centre. For example, in simple star polymer melts with monodisperse arms, $x$ takes the value 0 at the chain ends and increases to 1 at the core where the arms meet. A more general arc coordinate $x$ has elsewhere been termed the *seniority* in the context of an arbitrary branched polymer [292] (and see below).

(2) We then write a form for the effective modulus of an entanglement network diluted to a concentration $\Phi(x)$ where $G(\Phi) = G_N^{(0)}\Phi^{\alpha+1}$. $\Phi(x)$ is the concentration of unrelaxed material when segments with coordinate $x$ are just relaxing (i.e. at the timescale when tube segments at $x$ are just being reached by free ends for the first time). These are the assumptions of the 'dynamic dilution' or 'tube dilation' hypothesis we used above for simple star polymers, linear polymers with fluctuations, and their blends. Then an expression for the relaxation modulus $G(t)$ may be written from the general expression (142) above.

Without loss of generality we may choose limits on $x$ that are convenient. For H-polymers it is natural to divide the arc coordinate into two sections: $x_a$ runs along the arms from the ends to the branch points $(0 < x_a < 1)$ and $x_b$ runs from the branch point to the middle of the crossbar $(0 < x_b < 1)$. Now equation (142) becomes:

$$G(t) = G_N^{(0)}(\alpha+1)\left\{\int_0^1 \phi_b^{\alpha+1}(1-x_b)^\alpha \exp\left[-t/\tau_b(x_b)\right] dx_b + \int_0^1 (1-\phi_a x_a)^\alpha \exp\left[-t/\tau_a(x_a)\right] dx_a\right\}. \quad (152)$$

Here $\phi_a$ and $\phi_b$ are the volume fractions of arms and crossbar respectively. The first term comes from the contribution of crossbar material and the second from the relaxation of the dangling arms. In each integral, the term in round brackets represents the effective concentration of unrelaxed entangling network surrounding a segment relaxing on a timescale $\tau_{a/b}(x)$. An important check on expressions such as (152) is the 'sum rule' that $G(0) = G_N^{(0)}$, but this is ensured by generating

terms from each level of the hierarchy from equation (142). The derivation of these relaxation timescales for the dangling arms and for the crossbar follow analogous routes to the calculations of the star polymers and blends. Details can be found in reference [50]. Here we draw attention to a few key features of the physics.

STAGE (ii): It is easy to see, for example, that the potential well for the arm fluctuation is deeper and steeper than for pure star polymers, due to the fraction of crossbar material that behaves as permanent network for the relaxing arms. In this way, this fraction of arm material enters into the exponent for the longest relaxation time among arm retractions. The generalization of equation (151) to general dilution exponent $\alpha$ gives

$$\tau_a(1) \sim \exp\left[3Z_{arm}\left(\frac{1-\phi_b^{\beta}(1+\beta\phi_a)}{\beta(1+\beta)\phi_a^2}\right)\right],$$

where $\beta = 1 + \alpha$ and $\phi_b = 1 - \phi_a$. The mean first-passage time for diffusers over such a potential barrier as $U_{eff}(x_a)$ can be calculated analytically for all $x_a$ in terms of integrals over the potential [50]. But even at this level of our analysis we notice one very important physical consequence of the co-operative nature of the arm relaxations. The longest relaxation time of the arms is exponentially dependent not only on the number of entanglements on each arm $Z_{arm}$, but also on the arm fraction $\phi_a$. Increasing the amount of material in the crossbars, which acts as a permanent network throughout the relaxation of the free arms, greatly extends the slowest mode of the arms. So star-arms attached to crossbars of an H-polymer melt would be expected to exhibit exponentially slower relaxation times than when attached to simple branch points as in a melt of pure stars. This is the reason for Roover's early observation [122] that the 'viscosity enhancement' of dangling arms (over the value they would have as linear polymers) was much greater in his H-polystyrenes than in the corresponding stars. The theoretical value of $\nu \simeq 1.5\nu_Q$ for those materials (in which $Z_b = Z_{arm}$) is consistent with the experiments.

STAGE (iii): When the path length of the dangling arms eventually fluctuates to zero, corresponding to the free end retracing a path through the melt to the branch point itself, the branch point may make a diffusive hop through the melt. At this timescale of $\tau_a(1)$, the tube diameter is set only by other crossbars (if maximal tube dilation is valid, which is currently predicted to be the case providing $\phi_a < 2/3$, as we saw above) so has a value $a^* = a_0\phi_b^{-\alpha/2}$. There is a slight uncertainty in the $O(1)$ number that relates the timescale of the hop to the mean hopping distance (just as in the case of diffusion of star polymers). This introduces a further (universal) dimensionless constant into the model, by writing the effective curvilinear diffusion constant of the branch point as

$$D_{bp} = \frac{p^2 a^{*2}}{2q\tau_a(1)}.$$

The new constant $p$ is the fraction of the current tube diameter $a^*$ jumped on average by a branch point at each jump time $q\tau_a(1)$. The dependence of the effective drag of the branch point on $q$ in a melt is taken as simply proportional in this approximation. In fact we expect $p$ to be rather smaller than one from the nature of the projection of spatial diffusion onto the curvilinear tube, and a value of $p^2 = 1/12$ was found for the PI materials of reference [50] (though this is misprinted in the original paper as $1/6$).

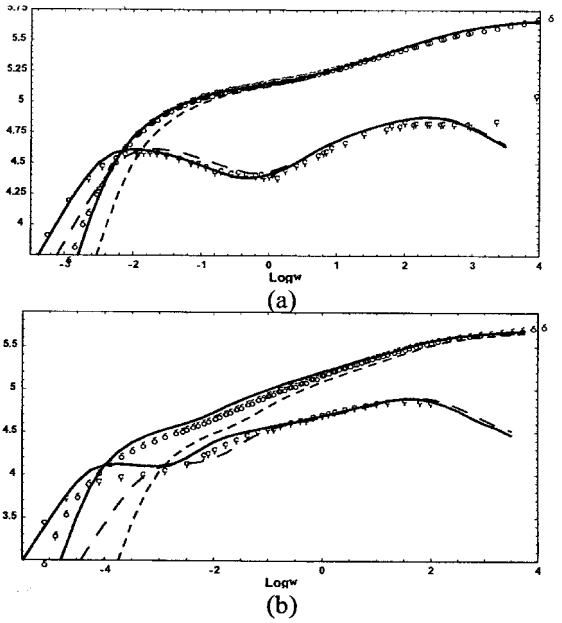


Figure 36. Experimental and theoretical complex moduli for the two H-polymers of the table. Fitting parameters of $G_N^{(0)}$ and $\tau_e$ were consistent with literature values and $p^2 = 1/12$. Polydispersity corrections were omitted to produce the dashed curves.

STAGE (iv): Tube segments at the extremities of the crossbar, just as for linear polymers and star arms, are lost sooner by CLF than by reptation, but in the case of the H-polymer, the expression for $\tau_{\text{early}}(x_b) \sim x_b^2$ rather than $x_b^4$, since the diffusion is dominated by drag on the branch points rather than diffused over the crossbar. The non-Fickian Rouse form does not arise. A cross-over formula for the spectrum of relaxation times is constructed in an analogous way (for details see reference [50]). A final cross-over to the reptation time of the crossbars is also required, since their central sections will typically have star-like fluctuation times much longer than the centre-of-mass reptation mode of stress-relaxation available to them (but not available to dangling ends of Hs or star polymers). The reptation time is determined by the time taken for the crossbar to diffuse the curvilinear length not already relaxed by fluctuation, so is given by the self-consistent set of relations (for a more detailed derivation of the prefactor see the derivation of the general 'pom-pom' equations below in section 5.2.2)

$$\tau_d = \frac{4}{\pi^2 p^2} q\tau_a(1) \cdot \phi_b^{2\alpha}(1 - x_c)^2 Z_b^2$$

$$\tau_b(x_c) = \tau_d.$$

The results of this procedure, which introduces no new parameters into the theory, apart from the $O(1)$ number $p$, may be compared with the linear rheological spectra for real entangled H-polymers. Figures 36($a$) and 36($b$) show the frequency-dependent moduli calculated from the scheme outlined above for two values of arm and crossbar molecular weights. The prominent 'shoulder' feature at higher frequencies in $G''(\omega)$ is a clear signature of the arm relaxations; its logarithmic

Table 2. Comparison of polymers H110B20A and H110B52A.

| Polymer | $Z_a$ (ch), (fit) | $Z_b$ (ch), (fit) | $\epsilon_a$ (ch), (fit) | $\epsilon_b$ (ch), (fit) |
|---|---|---|---|---|
| H110B20A | 4.5, 5.2 | 27.7, 28.9 | 0.01, 0.01 | 0.13, 0.13 |
| H110B52A | 13.0, 13.6 | 27.7, 28.9 | 0.02, <0.01 | 0.13, 0.13 |

width increases with the arm molecular weight. The low frequency peak comes from the crossbar: lengthening the crossbar takes the peak to lower frequencies, while reducing it both speeds up the crossbar relaxation and weakens the magnitude of the peak as the volume fraction $\phi_b$ reduces, and with it its contribution to the modulus. So the H-polymer spectrum we expect contains features reminiscent of the spectra of both star (a broad shoulder in $G''(\omega)$) and linear polymers (a well-defined peak in $G''(\omega)$) at the frequencies corresponding to the inverse relaxation time of the structural components that resemble them (arms and crossbar, respectively). Plotted alongside the data are predictions from the tube model outlined above. The molecular weights of the arms and crossbars for each in terms of $M_e$ are given in table 2, together with the polydispersity indices $\epsilon = M_w/M_n$ for all these components. Each parameter is given as determined by GPC and light scattering (ch) and by the rheological molecular model (fit).

Two salient points emerge immediately from the data on these well controlled model structures. The first is that the triple structure of free Rouse behaviour ($\sim\omega^{1/2}$) at high frequencies, a broad peak of widely-spread relaxations from the dangling arms at intermediate frequencies, and a narrow peak from crossbar relaxation at low frequency, is ubiquitous. Lengthening the arms of the H-polymer does indeed broaden the 'shoulder' feature in the relaxation modulus and 'dilute' the prominence of the terminal peak. The second is that, for H-polymers, accounting for polydispersity is very important indeed. The dashed lines in figure 36 give the model predictions in the absence of polydispersity; the solid lines are the predictions when even small polydispersity ratios of order 0.01 are assumed in the calculation. The reason for the strong effect is the exponential dependence of the branch-point diffusion constant $D_{bp}$ on the arm molecular weight. Even small increases in $Z_a$ can greatly influence $D_{bp}$, and consequently the reptation time of the crossbar. Even when the polydispersity is small, however, its effect is difficult to calculate [283]. There are two opposite tendencies: the motional narrowing of the self-entanglements of the arms works to reduce the effect of polydispersity, while their entanglements with the slow crossbar material increases it. When the volume fraction of crossbar material is significant, these two effects can be cast into an approximation for the terminal time of the arms, which, up to exponential factors, becomes

$$\langle \tau_a(1) \rangle \approx \exp\left(\frac{\nu\phi_a\bar{Z}_a}{3}\right)\exp\left(\nu\phi_b\bar{Z}_{arm} + \frac{\nu^2\phi_b^2\bar{Z}_a^2\epsilon_a}{2}\right).$$

(NB an approximation accounting only for the second effect was used in reference [50].) The rheological results are certainly consistent with measured values of the polydispersity and this calculation. We should also note that the anomalously slow diffusion noted in the case of asymmetric stars does not arise in the H-polymer experiments.

Very similar observations were made in the case of 'pom-pom' architectures [87]. The theoretical development reviewed above applies without change to this architecture, since the number of arms attached at each end of the crossbar, $q$, has been kept variable. A more subtle calculation would be required, however, for asymmetric pom-pom melts, in which either the $Z_a$ or $q$ or both differed at each end. This investigation lies in the future, but we may conjecture that a scheme such as that used for asymmetric stars would be required. Branch points may adopt individual timescales at which their physical role renormalizes from pinning points to sources of high drag. A general scheme on these lines for arbitrary architectures has recently been proposed by Larson [293].

The case of comb melts is very similar to that of high-$q$ pom-poms, with the exception that the drag on the comb backbone section is distributed at all branching points with dangling arms, rather than concentrated at the end. The evidence of several studies supports the exponential separation of relaxation modes of the entangled arms via deep CLF, combined with either renormalized Rouse or reptation dynamics for the backbones, depending on whether they are self-entangled or not $(Z_b\phi_b^\alpha \lesssim 1)$ [86, 123, 124, 294]. The theoretical application of the tube model to the case of combs has supported this at the quantitative level [86, 295]. Both comb and pom-pom melts have an additional degree of freedom over the H-polymer in the number of arms, which allows independent tuning of the backbone fraction $\phi_b$ from the arm molecular weight. So the terminal modulus $(\sim\phi_b^{\alpha+1})$ and relaxation time, $\sim\exp(\nu Z_a)$, can be independently set by the molecular architecture. Combs and pom-poms differ theoretically only in the consequences of the spread of drag along the backbone. If the CLF contribution to the backbone relaxation requires the coherent motion of several branch points, the linear-chain relation $\tau_{\text{early}}(x_b) \sim x_b^4$ becomes more appropriate than the pom-pom form $\tau_{\text{early}}(x) \sim x_b^2$. This alters the experimentally observed distribution of modes at intermediate times [86].

4.3.4. *Complex topologies: the seniority distribution*

Beyond comb and pom-pom architectures lie an infinite family of more complex topologies that are also, in principle, amenable to the rules of the tube model. The picture of hierarchical retraction dynamics with dynamic dilution can be generalized in a straightforward way to arbitrary topologies of branched polymers. For structures with many branch points a simplification is to treat the relaxation in discrete stages, calculating the timescales at which arm retraction has penetrated to each layer of segments. At each stage the effective topology of the molecule simplifies: all faster relaxing (outer) segments relax much faster than the current timescale, so are not part of the entangled network for longer timescales, but instead dilute the current value of $M_e$ and so the tube diameter, $a^*$. In an arbitrary branched molecule, entangled in a melt, any segment will be relaxed by deep, renormalized retraction from whichever of the two trees it is connected to relaxes first. This special statistic (equivalent to the longest path to the exterior of the molecule within the relaxing tree, measured in topological steps between branch points) has been termed the *seniority* of the segment [296]. An example of assignation of seniorities on a randomly branched molecule is given in figure 37. The distributions of seniorities in a melt uniquely determines the entangled dynamics in linear response if the chain sections between branch points are monodisperse. For example, the Cayley tree of $n$ layers of branching, and of branch points of functionality $f$ [297], contains $f^n$ segments in its outermost layer and $(f^{n+1}-f)/(f-1)$ segments altogether. The

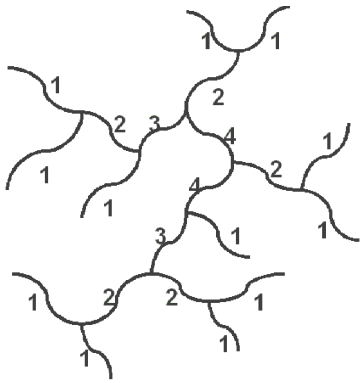

Figure 37. Illustration of the assignation of seniority values to topologically distinct subchains in a branched molecule. [After reference [72].]

effective concentration of unrelaxed segments after $m$ levels have relaxed is $C(m) = (f^{n-m+1} - f)/(f^{n+1} - f) \simeq f^{-m}$ when $n$ is large. Solving the star-arm-like retraction from level $m$ to level $m+1$ with the approximation that the effective concentration at level $m$ is valid throughout that stage of the hierarchy gives the set of induction relations

$$\tau_{m+1} = \tau_m \exp\left[\frac{\nu}{2}(Z_x)f^{-m}\right]$$

which have the solution $\tau_m = \tau_0 \exp\left[\nu Z_x((1-f^{-m})/(1-f))\right]$. Here $\nu$ is the principal path parameter ($\gamma/2$) of section 4.2.1 and $Z_x$ the (bare) number of tube segments between branch points on the tree. At this level of approximation we may also take $G(t) \simeq G_0[C(m(t))]^{\alpha+1}$. This leads to the logarithmic form of stress relaxation

$$G(t) = G_0 \ln\left(\frac{\tau_{\max}}{t}\right)^{\theta}, \tag{153}$$

where $\tau_{\max}$ is the (finite) relaxation time for $\tau_m$ as $m \to \infty$, and $\theta$ is a 'topological exponent' with a value of $1 + \alpha$ in this case. It turns out that other, less regular, tree-like structures also have this form, but with different values for $\theta$. For example, the ensemble of randomly branched trees just at the classical mean-field gelation point has $\theta = 3 + \alpha$ [296]. A more careful treatment of the Cayley tree case, including the fast CLF contributions, has recently been given [298].

If the subchains between branch points are polydisperse, the timescale hierarchy and seniority hierarchy are not equally ordered. But an important consequence was noted very early in application of tube models to branched polymers [299]: if the rheology is dominated by single, long, dangling arms in the presence of a network (so that CR is moderated) and if the polydispersity is exponential in form, i.e. $P(Z_a)\exp(-Z_a/\bar{Z}_a)$, then the exponentially rare presence of very long arms is countered by their exponentially long relaxation times to give an effective power-law relaxation

$$G(t) \sim t^{-u} \quad \text{with} \quad u = u(\nu, Z_a) \simeq \frac{1}{\nu Z_a}.$$

This is approximately true in the case of the mean-field gelation ensemble [296], where, near the percolation threshold (where an incipient gel forms [300], the prediction for the apparent dynamic exponent that is valid for several decades of the logarithmic form of equation (153) is $u = \gamma/(\nu Z_x)$ (note that this is actually

*independent* of the topological exponent $\theta$, so is of general application to highly branched entangled polymers). The prediction that a strongly entangled gelation ensemble would exhibit effectively power-law relaxation is amusing, because this is also the Rouse result for unentangled percolation clusters [90, 301, 302]. In this case the result is independent of $Z_x$:

$$u = \frac{d_f(\tau - 1)}{d_f + 2} \simeq 0.67$$

where $d_f$ is the fractal dimension of the clusters (expected value 2 in 3D percolation ensembles) and $\tau$ the exponent of the power-law molecular weight distribution function (expected value 2.2 in 3D percolation). This prediction is in accord with experimental results on crosslinked systems with $Z_x < 1$ [303]. Crosslinking linear chains that are already entangled, however, does indeed lead to a much more striking enhancement of viscosity, consistent with the exponentially slow retraction mode of dangling arms [304, 305]. Recent experiments on reacting monodisperse precursor polymers have shown that careful crosslinking of linear segments using a urethane condensation technique does indeed create a much more slowly relaxing melt when $Z_x > 1$, and that, for the systems so far explored up to $Z_x = 13.6$, the dynamic exponent $u \simeq 1/Z_x$ with a prefactor close to unity [306, 307]. The comparable work using a polycondensing polyester system found equally good agreement, but with a prefactor closer to 0.5 [91]. Fully quantitative theoretical treatments of the entangled gelation ensemble are still to be made; arguably the time for such a careful analysis is ripe now that clean data are becoming available.

A more readily accessible system is now available in the form of the long-chain-branched metallocene catalysed ensemble [93, 94] (see section 3.1). In the ideal circumstances of a continually stirred steady-state reaction with vinyl-incorporation of branches, the topological distribution of molecules is a well defined one-parameter family [72]. The resulting seniority distribution is different from that of random gelation. This is due to the special, directional, way in which molecules are synthesized. The relaxing retraction that frees any given segment is far more likely to come from the direction opposite that of the molecule's prior synthesis at the catalyst site! This is due to the greater number of routes through the molecule that end with a chain end in that direction (in the synthesis direction there is only one—the final terminating monomer). The challenge for theory is the same, however, as from the earlier randomly crosslinked experiments, in that the molecular weight of the segments between crosslinks is exponentially distributed. One way of accounting for this is to insert a discontinuity in the assignation of local relaxation times in terms of path length from the molecule's extremities $\tau(x)$. This is the basis of a recent suggestion by Larson of a framework in which to make approximate (numerical) calculations of linear rheology for arbitrary admixtures of architectures [293].

Perhaps the most practical result of this and other more phenomenological approaches to the rheology of random entangled melts is the description of how the zero shear rate viscosity depends on the fraction of branched monomers per molecule, taken at fixed molecular weight. Figure 38 gives the result for the cases of stars, and two families of combs, for a total number of entanglement strands per molecule of $\simeq 100$. The maximum value of viscosity quite generally corresponds to a value of about one branch-point on average in each molecule. In this case the terminal time $\tau_{max} \sim \exp(\nu Z_a)$ takes the greatest it can, while maintaining a majority of molecules branched. At lower branching frequencies the entangled arms are

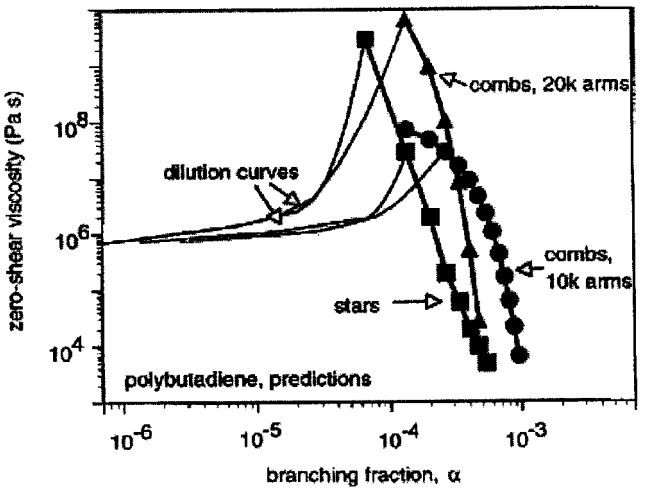


Figure 38. Predictions of the approximate tube model theory of Larson [293] of the dependence of viscosity on fraction of branch points per molecule at fixed molecular weight of 200 000 for the case of PB at 25°C. Both comb and star cases are indicated (each arm of the star accounting for a branch point).

longer, but become diluted by the reptating linear fraction. At higher branching content the terminal times falls exponentially with $Z_a$. This strong dependence on $Z_a$ has been turned recently into analytic methods for the characterization of LCB in *unknown* melts [71, 308]. In the latter case, the dependence of the zero-shear viscosity on polymer concentration, $\eta(\phi_p)$ at levels near the melt can be turned into a quantitative evaluation of $Z_x$. For example, in the case of LCB single-site catalysed metallocenes, the senority–rheology calculation gives

$$\frac{d}{d\phi_p}\ln\eta\big|_{\phi_p=1} = \nu Z_x \frac{1}{2}[1-(1-b_U)(1-2b_U)]^{\alpha}\left(\frac{1}{1-2b_U}\right).$$

The topological parameter $b_U$ is the probability that a randomly chosen segment is attached to a branch point rather than a dangling end at the direction from which polymerization proceeded. It is generally in the range 0.1–0.2 for commercial materials, and is independently measured by $M_w$ of the ensemble. So, once $b_U$ is known and $(d/d\phi_p)\ln\eta|_{\phi_p=1}$ measured, $Z_x$ can be determined directly. This is a very promising industrial application of a molecular understanding of LCB melts, since at just the low concentrations of branching that are typical of some of the newer materials, the ability of dilute solution methods to detect, let alone characterize, the branching becomes very difficult.

## 5. Tube theories in nonlinear response

It became clear in the early development of the tube model that it provided a means of calculating the response of entangled polymers to large deformations as well as small ones [31]. We recall that this is because strong nonlinearities at the level of the tube correspond to weak perturbations from the melt or solution equilibrium structure at the local, bond lengthscale. Some predictions, especially in steady shear flow, led to strange anomalies as we shall see, but others met with surprising success. In particular the same step-strain experiment used to determine $G(t)$ directly in shear

is straightforward to extend to large shear strains $\gamma$. We saw above that in many cases of such experiments on polymer melts both linear and branched, monodisperse and polydisperse, the experimental strain-dependent relaxation function $G(t, \gamma)$ may be factorized, equation (34), for all times $t > \tau_k$, a material time constant [142]. For the longest relaxation times of the material, the nonlinear viscoelastic response in step strain factorizes into a time dependence identical to that of linear deformations $G(t)$, and a strain dependence $h(\gamma)$, which is known as the 'damping function'. In particular, linear polymer melts have a rather weak nonlinear elasticity, in which the effective modulus falls rapidly with strain in a universal way (except, paradoxically, when the degree of entanglement becomes very large [71, 309], when it is weaker still, and probably due to elastic instabilities in the deformation field). In fact it was the success in accounting for the universal damping function that drew attention to the tube model as a powerful simplifying tool, rather than the linear rheological response. This, as we have seen, requires a rather subtle treatment of fluctuations (CLF) and cooperative effects (CR) to operate quantitatively, which appeared considerably later.

The challenge within our programme is to follow up the consequences of the tube model for the nonlinear rheology of branched polymers—would such a theoretical framework lead to any understanding of the special behaviour of, for example, LDPE in complex flows? We build up our tools as before in the context of linear polymers.

### 5.1. *Linear polymers in nonlinear deformations*

When large nonlinear deformations are made, we need additional assumptions within the tube model on how the tube itself deforms with the bulk strain. The simplest, and original assumptions are that:

(1) the tube contour deforms affinely,
(2) the tube diameter remains unchanged,

although other assumptions are possible [310, 311] (and see below). The first may be motivated on the grounds that, by definition, the tube diameter sets the scale below which non-affine deformation of chains dominates. More advanced models [312] and simulations [313] of rubber-elastic networks do indeed confirm that at least the topological *constraints* on chains follow an affine deformation on average. The main challenge to such an extension is the possibly increased significance of elastic inhomogeneities at large strains. The second assumption is less compelling, but is motivated by the observation that the local configuration of chains is not greatly different from that at equilibrium even at large strains due to the fact that $N_e \gg 1$ (but see section 6.4 below).

When these assumptions are made, an additional mechanism for stress-relaxation arises within the tube model, beyond those we considered in section 4.2—that of retraction (see figure 39). When a random walk chain is embedded randomly in a deforming incompressible medium, the contour length of both chain and tube is initially increased by the rapid strain, independent of deformation [31]. This is true in spite of the larger proportion of segments (roughly perpendicular to the major axis of uniaxial strain) that are initially compressed (by $\sim 1/\sqrt{\lambda}$) rather than extended by the strain. The segments more parallel to the axis are extended to a greater extent $(\sim \lambda)$, leading to an overall extension on average (but see section 6.1 for a discussion of the possible pitfalls of the average over chain segments implied by the use of this result). However, when the strain stops, the stretched chain now supports a greater

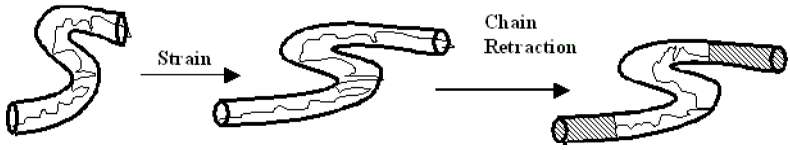


Figure 39. The nonlinear process of chain retraction within the tube model. Segments of affinely deformed tube are rapidly vacated (shaded) via internal Rouse modes as the chain regains a primitive path length of $L_{eq}$.

curvilinear tension at its centre than the equilibrium tension $f_{eq}$ still applied to its ends by their entropic exploration of the surrounding entanglement network. So the chain retracts back along the deformed tube until its curvilinear tension returns to equilibrium, which will be achieved when it regains its equilibrium contour length. This process happens much faster than reptation for $Z \gg 1$ because no diffusion of the centre of mass of the molecule is required. Instead the retraction dynamics take the form of *forced* (rather than stochastic) curvilinear Rouse motion so the contour length relaxation follows the Rouse form $L \sim t^{-1/2}$ cut-off at the Rouse time $\tau_R$.

We now use this to calculate the stress in the melt after the retraction has occurred. In fact this process was implicit in our calculation of the internal chain distribution of equation (113). When summing over entanglement strands to calculate the stress, we saw that the length of an entanglement strand is increased by a factor $|\mathbf{E}\cdot\mathbf{u}|$ where $\mathbf{u}$ is the unit vector along the strand and $\mathbf{E}$ the strain tensor. The other modification is to the concentration of entanglement strands. The retraction process means that the same proportion of original entanglement strands are lost as the length retracted, so the concentration of elastic segments is reduced along each chain by the factor $\langle|\mathbf{E}\cdot\mathbf{u}|\rangle^{-1}$. Note that this approach requires a pre-average of segment orientations $\mathbf{u}$ along *each* chain. We may do this because a well entangled chain samples democratically from all orientations in its tube segments. However, the rate at which this self-averaging is attained with $Z$ has yet to be assessed critically (see section 6.1 below). On average, the increased primitive path length $\langle|\mathbf{E}\cdot\mathbf{u}|\rangle$ is then positive definite and grows (in shear) as $\gamma^2$, so the retraction mode is only activated in nonlinear deformations. With this in mind we recall that the final result for the stress-tensor is

$$\sigma = \frac{\mathbb{C}}{N_e} f_{eq} \mathbf{Q}_{DE}(\mathbf{E}) \quad \text{where } \mathbf{Q}_{DE}(\mathbf{E}) = \frac{1}{\langle|\mathbf{E}\cdot\mathbf{u}|\rangle}\left\langle \frac{(\mathbf{E}\cdot\mathbf{u})(\mathbf{E}\cdot\mathbf{u})}{|\mathbf{E}\cdot\mathbf{u}|}\right\rangle. \tag{154}$$

The averages may be written in spherical polar coordinates as angular integrals, which are simple to evaluate numerically, and in some cases have analytic forms.

### 5.1.1. *Step-strain: properties of the* $\mathbf{Q}$*-tensor and consequences*

In the two classic viscometric deformations of simple shear and extension, the appropriate components of $\mathbf{Q}(\mathbf{E})$ have very different behaviour. For small shear strains $\gamma$, the shear stress depends on the component $Q_{xy}$, which has the linear asymptotic form $\frac{4}{5}\gamma$. This prefactor is the result of the loss of 1/5 of the affine stress by CLF redistributions of chain. For large strains, however, $Q_{xy} \sim \gamma^{-1}$, and therefore predicts strong shear thinning. Physically this comes from the entanglement loss on retraction and the alignment of the remaining tube segments into the plane of the shear—away from the '$x$–$y$' direction in which they contribute

maximally to the shear stress. In extension the relevant experimental component is the difference $Q_{xx} - Q_{yy}$. This is linear with extensional strain $\gamma$ at low strain, but in this geometry asymptotes to a constant (15/4) at high strains because segments orient into the direction in which they contribute to the stress. The behaviour of the $\mathbf{Q}$-tensor in shear gives directly the damping function from its definition so that $h(\gamma) = (15/4)Q_{xy}(\gamma)/\gamma$.

*Damping function*. The Doi–Edwards shear damping function is plotted in the usual convention in figure 40. It is very close to results on monodisperse entangled solutions and melts [40, 314]. Very significantly the same result is observed for entangled stars as for linear polymers (though unentangled polymers and polymers of more complex LCB exhibit a weaker departure of $h(\gamma)$ from a constant). This might be expected as the curvilinear arm retraction is just as uninhibited in stars as in linear polymers, although we might imagine that segments trapped between two branch points on the same molecule might indeed support more elastic stress at higher strains.

The suggestion that strange behaviour arising in step shear strains from very entangled fluids might arise from elastic instability is inherent in the highly strain-softening of the Doi–Edwards prediction. Once the retraction mechanism is over, the shear-stress as a function of shear strain $\sigma(\gamma; t > \tau_k)$ is non-monotonic, achieving a maximum at $\gamma \simeq 1$ and thereafter decreasing as $\gamma^{-1}$. Regarded as an elastic solid, such a material is unstable to local perturbations of shear strain. It would be predicted to adopt a banded structure of coexisting phases, each on a stable branch of the response. The very weak apparent elastic response of entangled polymer fluids with $Z > 50$ [144, 315] is consistent with the appearance of such instabilities [316].

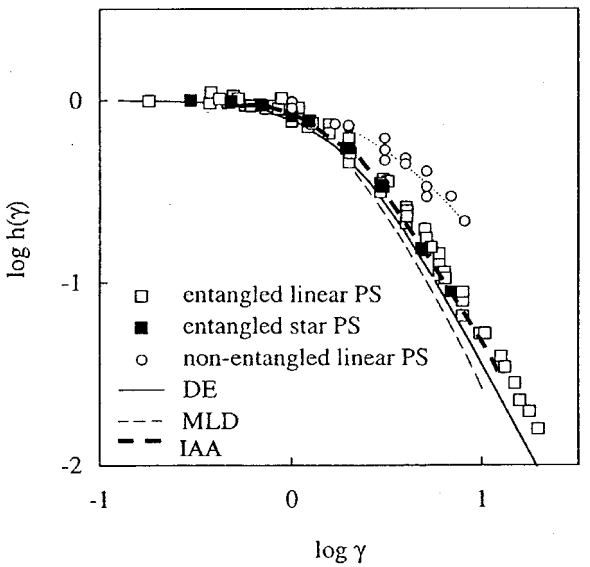


Figure 40. Shear damping functions measured from entangled linear [143] and star [146] PS solutions with $5 < Z < 50$. Solid and light dashed curves are the Doi–Edwards result and an approximation to the effect of convective constraint release [58]. The heavy dashed curve is the result of the IAA approximation. [Figure adapted from reference [37].]

Yet, although such shear banding has been observed directly in steady shear flow of worm-like micellar fluids, it remains to be observed in either steady or step flows of fixed-chemistry entangled polymers.

*Small angle neutron scattering*. The strong strain-softening predicted by the tube model for rapid step deformations is naturally a reflection of the physical alignment of the chains. This has a direct prediction for the SANS responses in both shear and elongation (see section 3.5.1). The experiment requires a very rapid quenching of the melt after the application of the strain, so that an adequate exposure to neutrons is possible with the chain configurations frozen. In shear, affine convection of tube segments coupled with chain retraction must align the chains so that once $\gamma \succ Z^{1/2}$, the radius of gyration parallel to the flow increases by this ratio: $R_{g\|} \simeq R_{g0}Z^{1/2}$ (the primitive path is deformed from a random walk to a directed path of length $Za$). In directions perpendicular to the flow, the chain dimensions would retract to the order of the tube diameter, so that $R_{g\perp} \simeq a$. In practice we expect especially the latter result to be destroyed by the rapid CLF from the chain ends, which quickly contribute to enlarge $R_{g\perp}$, but a high degree of anisotropy in the scattering pattern should in principle be attainable. This is not in accord with the only experiments available in shear (on partially labelled PS quenched after large step shears) [49], which recorded a maximum attainable anisotropy as shear was increased, measured by $(R_{g\|}/R_{g\perp})^2 \lesssim 3$.

In uniaxial extension, similar experiments on PS with very rapid quenching hoped to see the retraction dynamics contributing a further reduction of $R_{g\perp}$ after its affine compression by $\lambda^{-1/2}$ (with $\lambda$ the principle deformation ratio) [51]. That this was not observed is probably due to a combination of the low degree of entanglement of PS, and the strong role of CLF, for which there was no adequate expression at the time of that experiment. It remains to revisit these rare and hard-won data sets in the light of more sophisticated theory (see section 5.1.3 below). But in any case, the idealized 'step strain' is never really attained: there are always relaxation processes fast enough to resolve the timescale of the initial strain, so we must consider the case of continuous nonlinear flow.

### 5.1.2. *Constitutive equations for continuous flow*

The step-strain experiments discussed above furnish the simplest example of a strong flow. Many other flows are of experimental importance: transient and steady shear, transient extensional flow and reversing step strains, to give a few examples. Indeed the development of phenomenological constitutive equations (these calculate the present stress tensor $\sigma(t)$ as a function of the strain of the material $\mathbf{E}(t, t')|_{t'<t}$ at all past times $t' < t$), to systematize the wealth of behaviour of polymeric liquids in general flows, has been something of an industry over the past forty years [26]. We cannot review the details of these many formulations here, but it is useful to bear in mind the structure of the two main families of differential and integral constitutive equation. The differential constitutive equation takes the form

$$\frac{\partial}{\partial t}\sigma(t) = H(\sigma(t), \tau, \{\alpha_i\}), \tag{155}$$

where the operator $\partial/\partial t$ is one of a set of co-rotational derivatives that rotate the principal axes of the stress tensor with the flow. $H$ is a function that contains both linear and nonlinear terms in the stress (it always contains a term in $-\sigma(t)/\tau$,

generating stress-relaxation with time constant $\tau$). Other terms typically require a set of dimensionless numbers $\{\alpha_i\}$. In practice, the broad set of relaxation times observed in commercial polydisperse polymers are modelled by a superposition of contributions defined by equations such as (155). While the differential constitutive equation needs solving either analytically or numerically, the integral constitutive equation has an explicit form:

$$\sigma(t) = \int_{-\infty}^{t} \mathbf{Q}(\mathbf{E}(t, t'))\mu'(t - t')\,\mathrm{d}t', \tag{156}$$

where we have chosen to separate the strain behaviour from the relaxation function $\mu(t)$ (this is not a necessary restriction, see equation (6), but is usually chosen to match the experimentally observed separation in step strains). At first sight it is surprising that even such general formulations should work at all, given the molecular picture we have built up so far. The differential form implies that the stress tensor behaves as an 'inertial manifold'—a minimal set of dynamical variables that do not require the addition of any further state-variables to define the dynamical system. Yet we know that in polymeric liquids the stress (and other experimentally determined quantities) arise from at least the coarse-grained molecular chain variables $\mathbf{R}(n, t)$, and that the mapping $\mathbf{R}_\alpha(n, t) \rightarrow \sigma(t)$, or even from the distribution function $P(\mathbf{R}_\alpha(n, t)) \rightarrow \sigma(t)$ is many-to-one. We must expect to follow the dynamics of other structural variables in some cases in order to calculate even the stress. It goes without saying that calculation of, for example, $S_{\mathrm{coh}}(\mathbf{q}, t)$ in nonlinear flows will require keeping at least the correlation function $\langle \mathbf{R}_\alpha(n, t)\mathbf{R}_\alpha(m, t)\rangle_\alpha$. It is also clear that chain segments at different positions on a polymer chain (in particular at different distances from a chain end) may possess very different relaxation times, and yet remain strongly coupled by the connectivity of the chain. This connectivity is very important in the nonlinear process of chain retraction we reviewed above, yet is not reflected in the form of equation (155).

The integral constitutive family, on the other hand, has a familiar form—as the *solution* to convected PDEs or ODEs describing complex fluids with slow variables (such as model-H for phase separation) [317, 318]. They bear a simple physical interpretation: the stress (in this case) is a sum over elements 'born' at time $t'$, surviving to time $t$ with a probability $\mu'(t - t')$, and contributing to the response with a value of $\mathbf{Q}(\mathbf{E}(t, t'))$ when they do. Although this is a good physical picture for the fate of Brownian composition fluctuations in a two-component fluid subject to flow, it is not clear that it should generalize to entangled polymeric fluids, again because of the connectivity of the chains. Tube segments are indeed 'born' by the exploration of the entanglement network by chain ends, but they are then convected and diffused along chains in a way that is highly dependent on the configuration that the chains already have. The problem of hidden variables is also evident here: although often spoken in terms of 'material memory', polymer melts have no intrinsic memory other than their present structural state. In other fields of physics, integral forms such as (156) arise from explicit integration over 'fast variables', but this brings us to the same impasse as with the differential forms—why should the stress tensor contain enough information on the system to be able calculate its own future dynamics?

*The IAA for linear chains: an integral constitutive equation.* It is important to note that it is not possible to derive a constitutive equation from the tube model in

closed form without making rather uncontrolled mathematical assumptions—indeed this suggests that the space of non-Newtonian constitutive behaviour is rather larger than that spanned by compact sets of differential or integral equations. In order to project the tube model onto one of the familiar forms above (famously the separable integral or 'K-BKZ' equation [24, 25]) required the 'independent alignment approximation' (IAA) [22, 31]. Regarding figure 39 above, we see that continuity on the chain induces a shift of *chain segments* against the background of *tube segments* during the retraction. A chain segment that before the strain had a primitive path distance $\tilde{s}$ from the centre of the chain, occupies after retraction the tube segment originally occupied by the segment a primitive path distance $s$ from the chain centre, where

$$\tilde{s} = \int_0^s |\mathbf{E} \cdot \mathbf{u}(s')| \, \mathrm{d}s'. \tag{157}$$

Here $\mathbf{u}(s')$ is the unit tangent vector along the tube segment at primitive path coordinate $s'$. This in turn induces the non-local transformation rule for the local orientations

$$\tilde{\mathbf{u}}(\tilde{s}) = \frac{\mathbf{E} \cdot \mathbf{u}(s)}{|\mathbf{E} \cdot \mathbf{u}(s)|}. \tag{158}$$

The non-locality is technical to treat (but see below), so an initial approximation (IAA) [22] was to ignore the coordinate shift $s \to \tilde{s}$, and put $s = \tilde{s}$ in equation (158). The significant pay-off is that now an explicit integral equation can be written for the stress in the form

$$\sigma(t) = 5G_N^{(0)} \int_{-\infty}^{t} \mathbf{Q}^{IAA}(\mathbf{E}(t, t')) \mu'_{\mathrm{DE}}(t - t') \, \mathrm{d}t', \tag{159}$$

where the tensor $\mathbf{Q}^{\mathrm{IAA}}$ differs slightly from the non-approximated $\mathbf{Q}_{\mathrm{DE}}$ [31]. The difference that the IAA makes to the shear damping function is shown in figure 40, where we also observe that the approximation approaches the data closer than the full calculation. The IAA preserves information on the original orientation of the chain ends that physically is lost during the retraction process, and amounts to retracting each tube segment by the same amount to preserve the equilibrium contour length of the chain, shrinking the chain affinely. When the original conformation is at equilibrium, we might expect such a drastic move not to be very serious; it amounts to choosing segments from a different realization of an equilibrium ensemble from the one explored by the physical chain. On the other hand, we might expect it to fail rather badly when the configuration of the chain before a deformation was *not* an equilibrium one. This can be achieved by an earlier, but partially relaxed, strain in a 'double step strain' experiment. We have seen that reptation, but especially CLF, equilibrates the orientation of the outer segments of an entangled chain much faster that the more central ones. If this occurs between two periods of more rapid strain, then an IAA calculation will account erroneously for the occupation and later deformation of equilibrated tube segments that are in reality vacated during the second strain. This gives some insight straight away into a general problem with K-BKZ equations, namely that they perform poorly in double step strains (this is particularly true of *reversing* strains, in which the second shear carries the opposite sign of the first). In spite of this, perhaps the feature of the tube model that first won it attention from the rheological community was this derivation

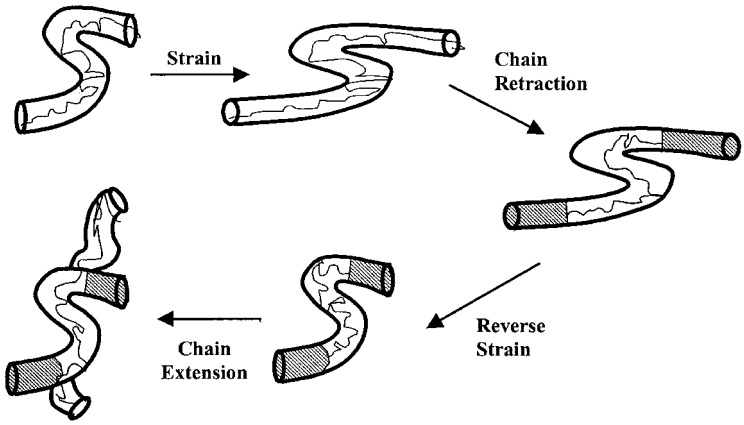


Figure 41. A second, reversed, shear follows an initial deformation. Chain segments at the extremities feel only the second strain, segments at the centre feel both. Addtionally the second strain generates new tube, since the primitive path length of the occupied section *decreases* during this strain as it is returned to the original equilibrium configuration.

from molecular considerations of a constitutive equation that had become established as standard in the chemical engineering community.

*Double step strains*. Without attempting to calculate a full constitutive formulation without using the IAA, it is possible carefully to account for retraction, relaxation and re-occupation of tube segments during a double step strain. The general form was given by Doi [31, 149]. The algebraic form of the result is complex, but in essence counts the contributions from the new processes we see if we extend figure 39 to a second, reversing, strain. Several new features arise. Firstly, segments of chain near the ends that have found new, equilibrium tubes following the first strain, feel only the second, reversed strain (figure 41). Original tube segments near the chain centre, and never vacated, feel only the sum of the strains. Additionally, new tube segments are actually *created* by the second strain, since the primitive path actually decreases during it (it is returning to an equilibrium configuration from an extended one). The chain seeks always a primitive path length of $L_{\rm eq}$, so must create new tube in a process opposite to that of retraction.

A careful set of entangled solution experiments [148] on high molecular weight PS showed that this careful treatment of the tube model in nonlinear response gave very close predictions of the experimental data for step shears of up to $\gamma \sim 10$, while the KBKZ form underpredicted the stress by up to an order of magnitude.

The Doi–Edwards KBKZ equation had another strong failing, however, in that it predicted a non-monotonic dependence of the steady-state shear stress on shear rate $\sigma_{xy}(\dot{\gamma})$. This arises from the same strong alignment of the chains we considered above, in a qualitative appraisal of the single chain structure factor. It is the corollary for flow of the $\gamma^{-1}$ *strain* dependence of the elastic response on step shear and retraction. More rapid reptative loss of tube segments from chain ends moderate the non-montonicity so that $\sigma_{xy}(\dot{\gamma}) \sim \dot{\gamma}^{-1/2}$ for $\dot{\gamma}\tau_{\rm d} \gg 1$, but no experiment has conclusively shown that the resulting shear-banding instabilities occur in entangled

polymers, in spite of their clear observation in other fluids [319]. A first attempt at circumventing this problem might be to avoid the IAA, which we now consider.

*Avoiding the IAA in continuous flow.* The essential picture of stress arising from occupied and deformed tube segments carries over naturally to the case of continuous flow. Tube segments are born at chain ends, are carried by diffusion along the chain during which time they are stretched and oriented, and die when they are passed again by a chain end. As we saw above, this insight leads directly to a formal integral expression for the stress (or other functions that depend on the survival probability of tube segments). However, we anticipate that the *kernel* of the integral is not the fixed and separated product of the IAA KBKZ equation (159). An integro-differential scheme to calculate the time-dependent kernel was derived by Doi [320]. We can motivate the result by the means of a survival probability function, similar to the $p(s,t)$ of equation (94) but in the form of $p(s,t,t')$, the probability that a segment born at time $t'$ still exists at time $t$ at contour coordinate $s$ along the occupying chain. The reptation diffusion equation (88) for $p$ is now modified by the *convection* of the chain past the tube segment by the flow as well as by the curvilinear diffusion. We assume here that the flow rates are less than the inverse retraction time so that the chain length is constant. If $v(s)$ is the relative velocity of tube and chain (due to the extension of the tube by the flow past the constant-length chain), then equation (88) becomes

$$\left(\frac{\partial}{\partial t} - D_c \frac{\partial^2}{\partial s^2} + v(s,t)\frac{\partial}{\partial s}\right) p(s,t,t') = 0, \tag{160}$$

where $v(s,t)$ arises from summing the extension rates of all the segments from the centre of the chain to the point $s$. If any segment has an orientation $\mathbf{u}$ then its local rate of increase in length, if deformed affinely in the flow, is $\boldsymbol{\kappa} : \mathbf{uu}$, where $\boldsymbol{\kappa}$ is the velocity gradient tensor. If we take the limit of high $Z$, so that each chain pre-averages over segment orientations, we may write the sum over segmental stretch for $v(s,t)$ in (160) in terms of the ensemble average orientations as

$$v(s,t) = \int_0^s \boldsymbol{\kappa}(t) : \langle \mathbf{u}(s',t)\mathbf{u}(s',t)\rangle \, \mathrm{d}s'. \tag{161}$$

The probability distribution $f(\mathbf{u},s,t)$ for the local segment distribution is related to the contribution from the ensemble of segments at $s$ to the total stress. It is calculated self-consistently from the survival probability function by letting the surviving tube segments be deformed by the total deformation tensor over their lifetimes, $\mathbf{E}(t,t')$:

$$f(\mathbf{u},s,t) = \int_{-\infty}^{t} \mathrm{d}t' \int \mathrm{d}^2\mathbf{u}' \delta(\mathbf{u} - \mathbf{u}') \mathbf{E}(t,t') \cdot \mathbf{u}' \frac{\partial}{\partial t'} p(s,t,t'). \tag{162}$$

The stress tensor can finally be written as

$$\sigma(t) = \frac{15}{4} G_N^{(0)} \int_{-L/2}^{L/2} \mathrm{d}s \int \mathrm{d}^2\mathbf{u} \cdot \mathbf{uu} \cdot f(\mathbf{u},s,t). \tag{163}$$

This full set of self-consistent equations is clearly very difficult to solve even numerically, and few serious studies have attempted this level of treatment, but they have been shown to perform better in large amplitude oscillatory flows than the

IAA [321, 322]. A difficulty is that, even at this level, chain stretch (defined as a flow-induced increase in the primitive path length) is not taken into account. This will only be valid for highly-entangled polymers when $\tau_d \gg \tau_R$, since stretch is likely to become important when $\dot{\gamma}\tau_R \sim 1$. The model predicts as a result *no* overshoot in the transient of normal stress in shear flow, $N_1(t;\dot{\gamma})$, but an overshoot in the shear stress at a nearly constant strain. These predictions are qualitatively in accord with experiment when $\dot{\gamma}\tau_R \ll 1$ . However, the removal of the IAA does *not* remove the non-monotonicity in the shear stress with $\dot{\gamma}$.

*Theories of chain stretch*. We already have the theoretical tools which will allow the relaxation of the assumption of vanishing chain stretch in nonlinear response, for the stretch and relaxation of the chain in the primitive path under flow is no more than an extension of the curvilinear Rouse formulation we developed for CLF in linear response, equation (101). The difference is that the dynamical equation is now forced by the drag on the chain of convecting tube, passing chain segments with the local velocity $v(s,t)$ (we adopt here again a convention in which primitive path coordinates are measured symmetrically from the centre of the chain). So we find

$$\zeta_0\left(\frac{\partial}{\partial t}s(n,t) - v(s,t)\right) = \frac{3k_BT}{b^2}\frac{\partial^2}{\partial n^2}s(n,t) + f(n,t). \tag{164}$$

The local stretch of the chain $\partial s/\partial n$ may now increase beyond its equilibrium value of $a/N_e$. If it does so, then the stress is increased in two ways. Firstly, the chain tension is higher by one factor of $\lambda(n) = (N_e/a)\partial s/\partial n$. Secondly, the primitive path is longer than at equilibrium, by the same factor, so that the stress becomes

$$\sigma(t) = \frac{15}{4}G_N^{(0)}\int_{-L/2}^{L/2}[\lambda(s)]^2\,ds\int d^2\mathbf{u}\cdot\,\mathbf{uu}\cdot f(\mathbf{u},s,t), \tag{165}$$

where the formulation may take either tube $(s)$ or chain $(n)$ variables. This scheme, and a simpler approximation to it, in which the stretch is taken to have a single value for the whole chain, was introduced by Marrucci and Grizzuti [323] (for an application of a similar idea to branched polymers, see section 5.2.2) and developed by Pearson and co-workers [140]. The stretch variable has a natural (and single) relaxation time at $\tau_R$ in the simple model, and a Rouse spectrum of relaxation times in the continuous-coordinate version. It successfully captures the growth of an overshoot in $N_1(t)$ as $\dot{\gamma}\tau_R$ is exceeded, together with the increase in magnitude of the shear-stress maximum, and its displacement towards a constant *time* close to $\tau_R$, rather than at a constant *strain*. It also illustrates the sometimes essential role of structural variables other than the components of the stress tensor. The scalar $\lambda(t)$ or scalar field $\lambda(s,t)$ becomes essential in describing entangled chains in fast flows, following its own dynamics, and becoming an ingredient in the stress tensor.

However, any hope that chain stretch would remove the non-monotonic shear stress response is unfounded. There are other physical processes at play that serve to reequilibrate chain segments faster than reptation, CLF or retraction can do. Building on the experience of linear response, we might look at how CR is modified in strong deformation. This will also guide towards increasing our account of dynamical variables in nonlinear response back towards the minimal set of the coarse-grained chain configurations, so that other experimental observables than the components of stress lie within the theory.

5.1.3. *Convective constraint release (CCR)*

We have seen that two related anomalies of the tube model have remained stubbornly resistant to efforts to include even the subtle aspects of chain stretch and chain connectivity in strong flows: the phenomenon of shear thinning is greatly overpredicted, resulting in a non-monotonic variation of shear stress with shear rate, and the anisotropy of the single chain structure factor in shear is predicted to increase up to a factor of $Z^{1/2}$. The maximum in the flow curve is not seen in experiments on well characterized polymer melts and entangled solutions [130] (although it does seem to be present in entangled worm-like surfactant solutions [319], see below). Nor is the high chain anisotropy seen in SANS experiments in shear [49]. The problem clearly arises from the spurious perfect alignment of the tubes along the flow direction predicted by any model that allows only affine convection of tube segments. In an attempt to relax this simplification in a physical but simple way, Marrucci [57, 324] proposed a new type of constraint release arising from the convection of surrounding chains by the flow, which he called convective constraint release (CCR). We have seen that in linear response, the arrival of a neighbouring chain end at a confining tube for a test chain allows a local reconfigurational relaxation of that chain segment (see figure 6). Without flow, the CR-generating events were caused by reptation or CLF of the neighbouring chains as aspects of their Brownian motion (these processes have been termed 'thermal CR' [37]). However, we have seen that in strong flow a forced, non-stochastic motion of chain ends enters *via* the process of chain retraction. Now, at least when the chain stretch is only marginally perturbed from equilibrium, and possibly beyond into the stretching regime, the rate of tube-loss from retraction grows proportionally with the bulk deformation rate, so is a candidate for finite configurational relaxation towards equilibrium. Moreover, since the rate of the CCR relaxation process follows the bulk deformation rate, continuous relaxation of the tube contour is achieved however fast the flow! Such 'convective constraint release' becomes increasingly important with shear rate and at some point should dominate the chain motion.

Marrucci [57] suggested that CCR be taken into account by correcting the reptation time by a term proportional to the chain retraction rate

$$1/\tau = 1/\tau_{\mathrm{d}} + \beta \mathbf{K}(t) : \langle \mathbf{u}(t)\mathbf{u}(t) \rangle, \tag{166}$$

where $\mathbf{u}$ is the tangent vector of the primitive path, $\mathbf{K}(t)$ is the shear rate and $\tau_{\mathrm{d}}$ is the reptation time—we recognize the double-contraction as proportional to the relative velocity of chain and tube in equation (161). The $O(1)$ number $\beta$ is necessary for the same reason as the equivalent constant $c_\nu$ we introduced in linear response CR: the number of CR events required for each local tube reorientation is unknown.

Mead *et al.* [58] developed this approach to CCR in a similar way in a set of constitutive equations for the tube orientation tensor and chain stretching. When $\dot{\gamma}\tau_{\mathrm{R}}$ is large and both chain-stretch and CCR are operating, it is necessary at this level to redistribute the effect of CCR from orientational relaxation at low $\dot{\gamma}$ (*via* renormalizing the effective reptation time as in (166)) to relaxing the *stretch* at high $\dot{\gamma}$. The (MLD) set of equations in the approximation (in which primitive path coordinates are ignored) reads

$$\left.\begin{aligned}
\frac{\partial}{\partial t}p(t,t') &= -\left(\frac{1}{\lambda^2(t)\tau_{\mathrm{d}}} + f(\lambda)k_{\mathrm{CCR}}\right)p(t,t') \\
\mathbf{S}(t) &= \int_{-\infty}^{t} \frac{\partial p(t,t')}{\partial t'}\mathbf{Q}_{\mathrm{DE}}(\mathbf{E}(t,t')) \\
\frac{\partial}{\partial t}\lambda(t) &= \mathbf{K}(t):\mathbf{S}(t)\lambda(t) - \left(\frac{1}{\tau_{\mathrm{s}}} + \frac{k_{\mathrm{CCR}}}{2}\right)[\lambda(t)-1] \\
k_{\mathrm{CCR}} &= \mathbf{K}(t):\mathbf{S}(t) - \frac{\dot{\lambda}}{\lambda}.
\end{aligned}\right\} \tag{167}$$

The rate of CCR, $k_{\mathrm{CCR}}$, is the mean retraction rate: the difference between the chain stretch and the tube stretch rates, and $f(\lambda)$ is a 'switching' function (between orientation and stretch relaxation by CCR) that has $f(0) = 1$ and $f(\lambda) \to 0$ as $\lambda \to \infty$. A much more sophisticated version in which path length coordinates are retained allowed adoption of CLF at the same level as equation (106) [58]. These approaches predict a final plateau of the steady state shear stress as a function of shear rate, and can achieve a good fit with data on $\sigma_{xy}(\dot{\gamma})$ and $N_1(\dot{\gamma})$ over a range of shear rates, but the plateau is approached from above for any reasonable value of the parameters $\beta$, i.e. the stress maximum is *still* present! The version without stretch requires $\beta \simeq 3$ to avoid the maximum, but this is hard to reconcile with the much smaller values required in linear response. A further drawback of these approaches is that information on the structure of the entangled chains is lost by allowing CCR to affect only the global stress relaxation time. This still leaves unexplained an important data set on the single chain structure factor in a sheared melt probed by small angle neutron scattering (SANS) [49]. A recent assessment of the MLD theory using entangled monodisperse and binary-blend PS solutions confirmed that the introduction of CCR was essential to capture the steady-state values and rates at which overshoots appeared, but found the magnitude of the overshoots in $\sigma_{xy}(\dot{\gamma})$ and $N_1(\dot{\gamma})$ to be consistently underpredicted. Non-spatial stochastic simulations have also introduced CCR *locally* on chains in the same way as in reference [325], yet also predicted a weak stress maximum. This seems to be because the way CCR is introduced in all these cases serves to reduce the stress from the Doi–Edwards result. Real chains seem to find a way to *increase* it. Yet it is clear that CCR is of overwhelming importance and dominates the dynamics and configuration of entangled linear chains at high flow rates.

A recent, more detailed approach to this problem (for non-stretching chains) treats CCR at a nearly equivalent level to CR (making only the approximation of a single frequency of CR events, rather than respecting the distribution), by keeping the coarse grained coordinates of the chain, and allowing CCR events to generate local Rouse jumps of the tube [59, 326]. The idea is to retain full information about average chain trajectories instead of working indirectly with dynamic equations for the stress and orientation tensor. This approach also allows quantitative predictions about the single chain scattering function $S(\mathbf{q})$, and to develop a *local* description of CCR events. The main assumptions of the first version of the theory (valid when there is no chain stretch) are: (i) that CCR operates locally in reorienting chain segments both into and away from the flow direction, and (ii) that neither the number of entanglements per chain $Z = M/M_{\mathrm{e}}$ nor the tube diameter $a$ changes. The first assumption endows the tube itself with a Rouse-like motion in which the

local hopping rate is coupled to the global deformation rate via a single new parameter. The second (constant length) assumption introduces a difference from ordinary Rouse-chain motion, and limits the range of validity at first (but see below) to $0 < \dot{\gamma} < 1/(\tau_e Z^2)$.

No single set of variables will be able to diagonalize the essential entangled modes of motion, namely (i) chain reptation, (ii) chain retraction, (iii) tube-length fluctuation and the new mode (iv) Rouse-tube motion. However, the theory is conventionally cast in a real-space notation for the tube trajectory $\mathbf{R}(s,t)$ and its tangent curve $\mathbf{R}' \equiv \partial\mathbf{R}/\partial s$, functions of curvilinear distance $s$ from along the tube and time $t$. Our chains are monodisperse containing $Z$ entanglements of tube diameter $a$. The (stochastic) equation of motion becomes

$$\begin{aligned}\mathbf{R}(s,t+\Delta t) = \mathbf{K}\cdot\mathbf{R}\Delta t + \mathbf{R}(s+\Delta\xi(t),t) \\ + \Delta t\left(\frac{3\nu}{2}\frac{\partial^2\mathbf{R}}{\partial s^2} + \mathbf{g}(s,t)\right) \\ + \Delta t\lambda\left(\frac{Z}{2} - s\right)\frac{\partial\mathbf{R}}{\partial s}.\end{aligned} \tag{168}$$

The first term describes affine convection of the tube segments. The second is the well known reptation form in which the noise term has a variance related to the curvilinear diffusion constant $D$, $\langle\Delta\xi(t)\Delta\xi(t')\rangle = 2D\delta(t-t')$. The third term describes the new Rouse motion of the tube. It has exactly the same form of deterministic and stochastic noise terms as the usual Rouse equation for chains, equation (62), and they are coupled by the same fluctuation–dissipation relation. However the rate $\nu$ is not controlled by temperature, but by the rate of CR from other chains. Counting the entanglement release rate of all chains from retraction and reptation gives a self-consistent relation $\nu = c_\nu(\lambda + 12/\pi^2 Z^3\tau_e)$ where $\lambda$ is the retraction rate of the chain, set by the constant-length condition

$$\int_0^n |\mathbf{R}'|\,\mathrm{d}s = Za.$$

The number $c_\nu$ is, as in linear-response CR and early versions of CCR the one new parameter in our theory; $c_\nu = 1$ would correspond to one constraint release event giving rise to one local hop of an entanglement segment. We might therefore expect a rather smaller value than this, given the $O(10)$ number of chains involved in an entanglement [78]. The fourth term accounts for the retraction of the chain within the tube in a pre-averaged approximation in which the relative velocity of chain and tube increases linearly from the chain centre at $s = Z/2$. The retraction rate $\lambda$ appears again as a prefactor. It is also possible to add a fifth term in a representation of CLF [59]. Stochastic breathing-mode retractions of the chain end replace the tangent vector at $s$ with a stochastic vector $\mathbf{u}$ chosen randomly from the unit sphere (with a careful choice of the correlation $\langle\mathbf{u}(s)\mathbf{R}'(s')\rangle$). The rate of this process $1/\tau(s)$ is the same as that calculated for the local stress relaxation of entangled star-polymer arms [56]. Its inclusion allows the nonlinear theory to reduce to a quantitative theory for the chain dynamics in linear response.

The real-space Langevin representation (168) is convenient for describing the physics, but not for performing calculations. More useful is the matrix of Fourier-transformed (tensor) second moments of the chain tangent vectors $\mathbf{R}'(s,t)$ defined by

$$(c_{pq})_{\alpha\beta} \equiv \frac{6}{Za^2}\int_0^n\int_0^n \mathrm{d}s\,\mathrm{d}s'\,\sin\left(\frac{p\pi s}{n}\right)\sin\left(\frac{q\pi s'}{n}\right) \times \langle(\partial R_\alpha/\partial s)(s,t)(\partial R_\beta/\partial s)(s',t)\rangle - (\delta_{pq})_{\alpha\beta}. \quad (169)$$

The average over the ensemble of trajectories renders the dynamics of the $\mathbf{c}_{pq}$ deterministic, while retaining the ability to calculate both the full deviatoric stress tensor

$$\sigma_{\alpha\beta} = \frac{c}{N_e}\sum_{p=1}^{Z} p^2(c_{pp})_{\alpha\beta}$$

and the single chain structure factor $S(\mathbf{q})$, which has a similarly computable but more complex expression. The real-space dynamic equation (168) induces a first order equation of motion for the $\mathbf{c}_{pq}$ of the form

$$\frac{\partial}{\partial t}(\mathbf{c}_{pq}) = (\mathbf{K}+\mathbf{K}^{\mathrm{T}})\delta_{pq} + \mathbf{K}\cdot\mathbf{c}_{pq} + \mathbf{c}_{pq}\cdot\mathbf{K}^{\mathrm{T}} - \left(\frac{1}{Z^3}\right)\left(1 + c_\nu\frac{3\pi^2}{2}\lambda\right)(p^2+q^2)\mathbf{c}_{pq} + \frac{8}{\pi^2 Z^3}\sum_{p',q'} M_{pp'}M_{qq'}\mathbf{c}_{p'q'} + \lambda\left(\sum_{p'}\bar{M}_{pp'}\mathbf{c}_{p'q} + \sum_{q'}\bar{M}_{qq'}\mathbf{c}_{pq'} - \delta_{pq}\mathbf{I}\right) \quad (170)$$

where $M_{ij}$ and $\bar{M}_{ij}$ are tensors whose components are simple algebraic functions of the indices [59]. The retraction rate $\lambda$ is chosen to keep the mean square contour length constant, which becomes equivalent to the simple condition $\sum_p \mathrm{tr}\,\mathbf{c}_{pp} = 0$. A decoupling approximation is applied to averages of $\lambda$ and $\mathbf{R}$ to derive the equation of motion.

Setting $c_\nu = 0$ in this scheme generates a non-monotonic shear stress response in steady flow, closely following the standard Doi–Edwards prediction, but adding a small amount of local CCR such that $c_\nu > 0.06$ removes the shear stress maximum entirely; instead the shear stress tends monotonically to a plateau at high shear rates (see figure 42 for results in the large $Z$ limit—for smaller $Z$ the response is very nearly the same, with shifts to $G_0$ and $\tau_d$ from rapid end-fluctuations). Increasing the rate of local CCR continues to enhance the shear stress at high shear rates, while decreasing it at low rates. The transient approach to the steady state exhibits a maximum for $\dot{\gamma}\tau_d > 1$, as observed in experiment. The opposite behaviour at low and high shear rates can be understood from the way CCR operates: at low rates the tube configurations are nearly isotropic so the additional relaxation mechanism simply speeds up the return to equilibrium, reducing the stress. However at high rates the tubes are nearly aligned in the flow direction in the absence of CCR; introducing it generates random buckles in the tube contour that protrude distances of order $a$ in the flow gradient direction. Subsequent deformation of these buckles generates in turn immediate contribution to shear stress, which is therefore larger than without CCR. Omitting this symmetry can lead to problems. It is tempting, but incorrect, to permit CR events to smooth local tube contour but not to roughen it [224]. In fact at shear rates $\dot{\gamma} \sim \tau_d^{-1}$ there is only weak perturbation to the melt structure on the length scale of an entanglement strand, so there is no reason to suppress the natural symmetry of tube-Rouse motion incorporated in equation (168). Moreover the level of coupling of chain retraction to CCR indicated by values of $c_\nu \simeq 0.1$ corresponds to $O(10)$ retracting chains per tube-Rouse hop. This

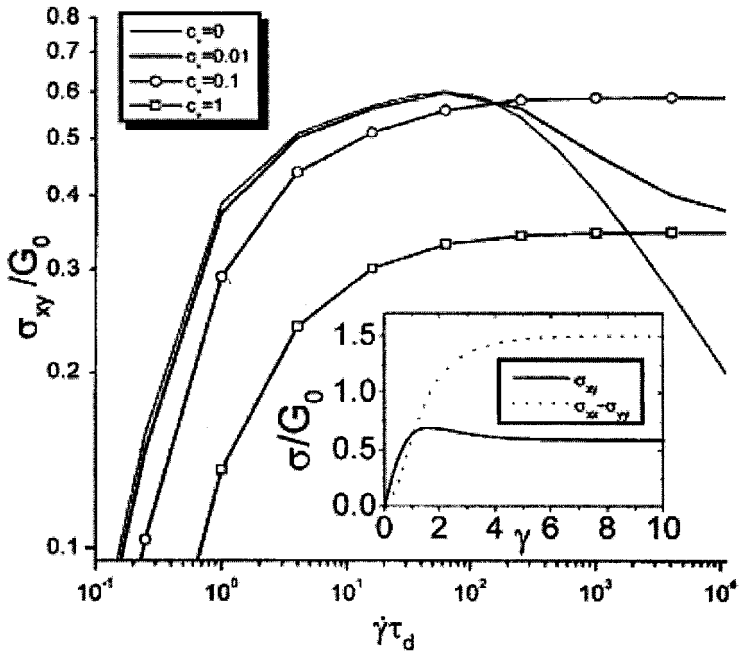


Figure 42. Predictions of the local CCR theory for the steady-state values of shear stress with shear rate for various values of the CCR parameter $c_\nu$. The inset displays the predicted shear stress and normal stress transients in the limit of high shear rate (but with no stretch) for $c_\nu = 0.1$ [59].

compares favorably with the universal number of chains involved in a single entanglement [78].

A typical structure factor computed from this theory is shown in figure 43. Constraint-release drastically changes the overall picture from tube theory without CCR: the degree of orientation decreases, and the $q$-dependence of the orientation angle appears; contour lines of $S(\mathbf{q})$ at smaller $q$ are more oriented in the flow-gradient direction than at larger $q$.

To compare these results with neutron scattering experiments, we can extract various quantities including the characteristic dimensions $R^2_{\max}(\dot{\gamma})$ and $R^2_{\min}(\dot{\gamma})$ in the major and minor principal directions, as well as the $q$-dependent alignment angle $\beta(q, \dot{\gamma})$ between the major principal axis contours of $S(\mathbf{q})$ and the flow $(x)$ direction. These quantities summarize the changes in dimension and orientation of typical chain conformations as a result of the flow, assuming that the contours of $S(q)$ are elliptical. The dependences of $\beta$ on both $q$ and $\dot{\gamma}$ are shown in the inserts to figure 43, and are in qualitative agreement with existing experiments [49]. In particular both experiment and this theory agree that the mean square radius of gyration in the flow direction never grows by more than a factor of three (see also figure 16), and local CCR is able simultaneously to account for the chain anisotropy and the rotation of the principal axis of the scattering pattern with $q$. The latter is a striking feature of the data, and is a direct consequence of the local Rouse 'buckling' of the tube, and the convection of the perturbed structures so formed to longer length scales by the flow. This is just the same process that led to the erasure of the shear stress maximum discussed above.

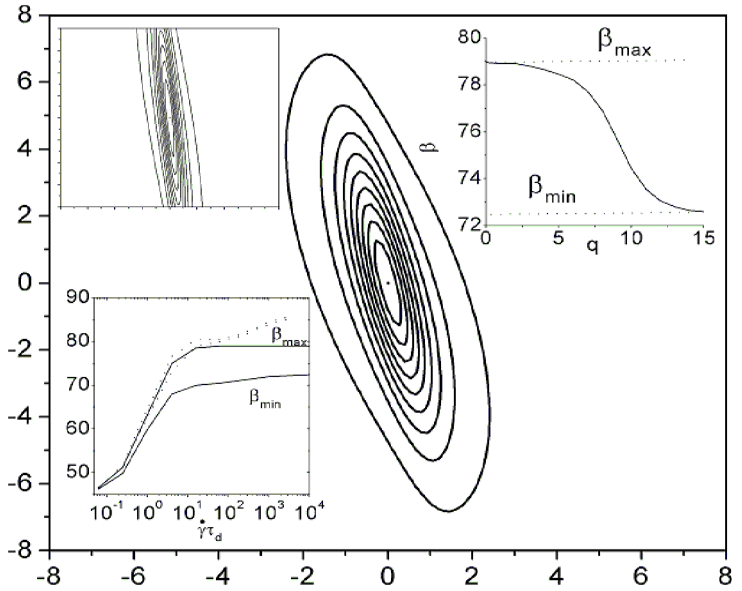


Figure 43. Steady-state scattering patterns calculated from a theory allowing CCR and original Doi–Edwards (insert top left). The axes of $q_x$ and $q_y$ are in units of the inverse tube diameter $a^{-1}$. Other inserts indicate behaviour of the angle of the principal axis with shear rate and $q$.

Local CCR calculations can be modified for the case of living polymeric micelles [103, 326]. In this case local CCR is much less effective in removing the stress maximum than in the case of polymer melts; the maximum persists until a value of $c_\nu \simeq 0.3$. So in the physically reasonable range $0.06 < c_\nu < 0.3$ this theory is able to account for the simultaneous absence of a stress maximum in melts and its presence in living micelles.

The addition of chain stretching is a natural next stage to the theoretical development of a contour-variable account of CCR, just as in the single-mode approximations of references [57] and [58]. This can be done at the level of the Langevin equation for the contour coordinates $\mathbf{R}(n,t)$, equation (168), by adding a term that accounts for the curvilinear motion of monomer driven by local gradients in chain tension (itself proportional to the local stretch $\mathbf{R}'(n,t)$). This now replaces the term previously keeping the tube length constant in (168). The stochastic equation in $\mathbf{R}(n,t)$ (168) acquires a new term that reads

$$\mathbf{R}(n,t+\Delta t) = \cdots + 3D_c Z \frac{(\mathbf{R}''\cdot\mathbf{R}')}{|\mathbf{R}'|^2}\mathbf{R}' + \cdots$$

and is supplemented by an expression for the CCR rate $\nu = c_\nu \lambda$, where the retraction rate is counted from the rate of tube loss at the chain ends [327]. Calculation proceeds in the same way as in the non-stretching case by passing to the Fourier representation of the tensor correlation functions of $\mathbf{R}(n,t)$. This more complete model predicts a near-plateau of $\sigma_{xy}(\dot\gamma)$ between $\dot\gamma\tau_{\rm d}$ and $\dot\gamma\tau_{\rm R}$, and an increase proportional to $\dot\gamma^{1/2}$ beyond that (so that the 'shear-dependent viscosity' $\eta(\dot\gamma) \sim \dot\gamma^{-1/2}$ (see figure 44). As with the non-stretching case, decoupling approximations are required to derive closed equations for the necessary correlation functions

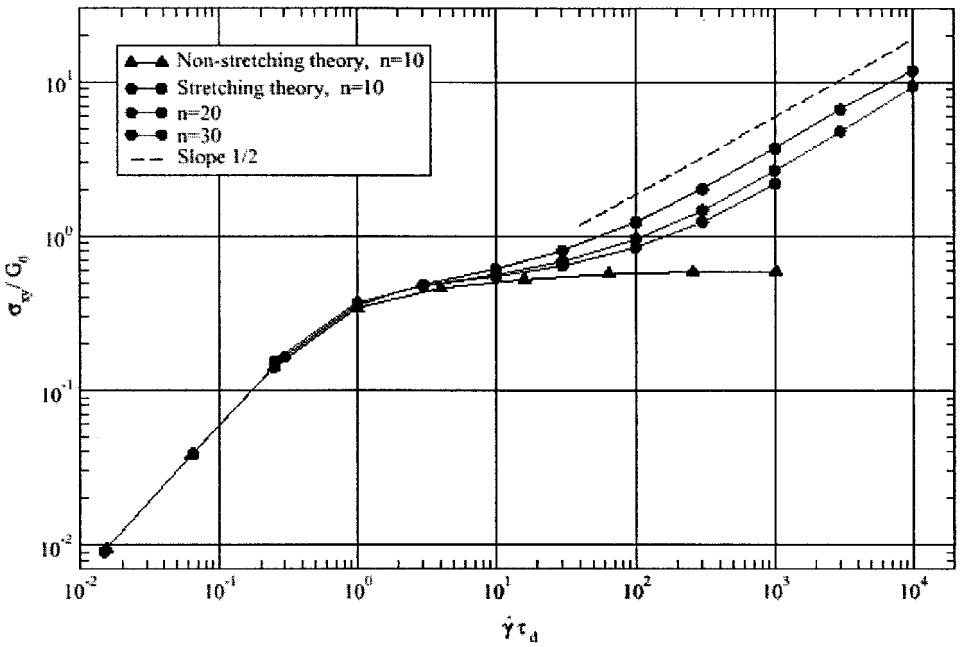


Figure 44. Predictions of the local CCR model with chain stretch using $c_\nu = 0.1$ for values of $Z = 10, 20, 30$. A comparison to the non-stretching version is given.

$\langle \mathbf{R}(n,t)\mathbf{R}(m,t)\rangle$. The quality of these approximations can be checked by simulation, but also by thermodynamic consistency (see section 6.3). One issue concerning the possibility of new physics should, however, be raised in theories of CCR that are both local and nonlinear. In fast flows, the primitive path length of the chain can be far greater than at equilibrium. This introduces (at least) two choices into a theory at this level for the *density* of CR events along the chain. We might assume either that the number of constraints along the chain were constant independent of stretch (so that the long CR Rouse relaxation time is independent of the flow rate and stretch). Alternatively, we might suppose that constraints of this dynamic kind are met at constant contour density along the principal path. In this latter case, the CR Rouse relaxation is actually increased quadratically with chain stretch. Of course this choice touches deeply on the local physics by which the entanglement field arises. A detailed comparison of this model (and its variants) with data from both transient rheology data as well as SANS chain structure factors will guide the next developments of theory.

We should note a recently discovered connection between the local CCR theory and the Marrucci and MLD versions without explicit chain coordinates. If only the lowest Fourier mode (tube Rouse eigenfunction) in the full theory is retained, $\mathbf{c}_{11}$ in equation (170) above, then a constitutive equation equivalent to the use of equation (166) results

$$\boldsymbol{\sigma} = \mathbf{K}\cdot\boldsymbol{\sigma} + \boldsymbol{\sigma}\cdot\mathbf{K}^{\mathrm{T}} - \frac{2}{\tau_{\mathrm{d}}}(\boldsymbol{\sigma}-\mathbf{I}) - \frac{2}{3}\,\mathrm{tr}\,(\mathbf{K}\cdot\boldsymbol{\sigma})\boldsymbol{\sigma} - \beta(\boldsymbol{\sigma}-\mathbf{I}))$$

but with an *expression* for $\beta$ in terms of the physical parameters of the full model ($\beta = 3\pi^2 c_\nu$). The large prefactor of $3\pi^2$ in this ostensible $O(1)$ number perhaps

indicates why such a large value is needed to overcome the shear stress maximum in that model. The stretching case gives an interesting 'single mode' equation under similar treatment, whose consequences are yet to be explored, but which indicates again the utility of molecular thinking even in the derivation of 'toy' models for phenomenological application.

We have come a long way from the early reptation-only approximations, keeping also the subtler entanglement modes of CLF, CR, CCR, chain stretch and retraction in the model, able to describe not only bulk properties but also mean chain configurations at the tube scale $a$ and above. However, there are still physical effects that may be just as important unaccounted for, and there has yet to be a proper assessment of the self-averaging approximations of all theories that work with the dynamics of a mean chain, rather than taking the average after solving the dynamics of a many chain ensemble. But, just as in the case of linear response, a key test of a theory that is topological in essence, is to examine the cases of more complex molecular topology. We now turn to the nonlinear response of branched polymers.

### 5.2. *Long chain branching in nonlinear response*

A current challenge for molecular rheology is the continuous nonlinear flow of highly branched polymers [17, 26, 328]. The central issue as we have seen (section 3.3) is that in both uniaxial and planar extensional flows, LDPE is strain-*hardening* [138] (stress grows faster than linearly with strain over some range of strain and time, in a time-dependent flow), while retaining a *softening* characteristic in shear. It has proved impossible to fit simultaneously all the flow behaviour of LDPE with existing integral-type phenomenological constitutive equations, of similar form to equation (156), even qualitatively [329]. From our discussion above, we must assume that this is because such equations rely on employing restrictive functionals of the flow history to calculate the stress, considered as the primary dynamical variable. Although this approach guarantees frame-invariance by making their kernel functions depend only on invariants of the strain history, trouble arises because planar extension and shear posses the same invariant structure of the strain tensor $\mathbf{E}$ (arising from the two-dimensionality of the flows). However, the insights of the special molecular features of long-chain-branched polymers under high strain make a molecular approach doubly appealing. In particular we will find that chain stretch has a special role to play in entangled branched polymers, and introduces a further distinct molecular mode of dynamics, that we term 'branch point withdrawal'.

#### 5.2.1. *Stretch and branch-point withdrawal (BPW): the priority distribution*

The process of chain retraction can be applied to more complex topologies of entangled polymers under the same assumptions discussed for linear polymers [230, 292]. In the case of star polymers retraction may proceed just as for linear chains, and the damping function is expected to be of the universal 'Doi–Edwards' type. This has been confirmed experimentally [146]. However for polymers with higher levels of branching the situation is different. In spite of being stretched along its contour by a large bulk strain, a segment one level further into a branched molecule than the outermost arms cannot in general retract, because this would mean drawing those outer segments into its tube. It may only do this when its tension exceeds the sum of the (equilibrium) tensions in the impeding arms. This criterion in turn is only met beyond a critical strain. This strain will be proportional to the number of arms attached at the outermost branch point, because of the Hookean elastic response of

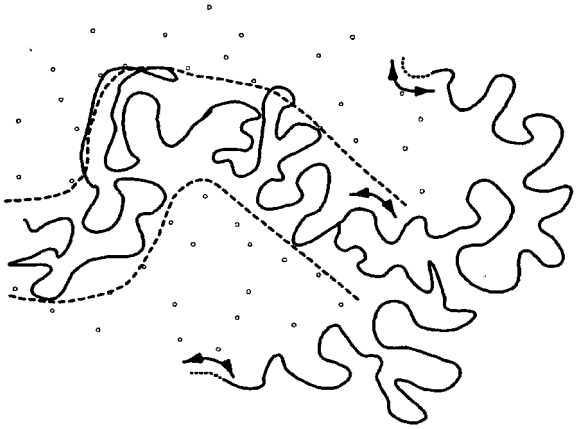

Figure 45. The process of branch-point withdrawal: a segment with greater than equilibrium tension pulls attached dangling arms some distance into its own tube, thus shortening their effective entangled path length.

the chain's entropic tension. This process is illustrated in figure 45 for a local entanglement structure composed of two dangling arms joined to a deeper segment of seniority 2 (see section 4.3.4). When a bulk strain is applied, the primitive path length of the tube containing the seniority-2 segment increases in length by the strain-dependent function $\langle \mathbf{E} \cdot \mathbf{u} \rangle_u$. Since, for small deformations, the branch points are trapped at the confluences of their tubes, the seniority-2 segment is stretched by the same amount and its entropic tension increased in proportion. When the tension $f = \langle \mathbf{E} \cdot \mathbf{u} \rangle_u f_{\text{eq}}$ equals the sum of the equilibrium tensions of the dangling arms, and not before, the arm configuration may be partially collapsed and the branch points withdrawn into the tube originally occupied by the crossbar.

In a manner akin to the hierarchical relaxations in a highly branched polymer, this new form of retraction via 'branch-point withdrawal' also happens hierarchically, though as a function of strain rather than time. A segment sited two levels into the molecule may only retract when its tension exceeds that of all the first level segments attached to it, and so on. As a consequence of this balance of entropic tensions, the strain at which any segment withdraws its outermost branch-point (and so the functional form it contributes to the strain dependence of the stress) just depends on the number of free ends at the edge of the tree it is connected to. Just as in the seniority distribution, there are in general two such trees: in this case it is the one that first permits BPW that determines the critical strain (we recall that any segment in a branched polymer is connected to two trees). This statistic (of the lesser number of free ends of the two trees) has been termed the 'priority' distribution [292], in analogy with the 'seniority' distribution which controls the relaxation times (see figure 46). In general a branched molecule has different seniority and priority distributions—a knowledge of the former is required to predict the linear stress-relaxation function, of the latter to predict the nonlinear strain response. A general formula giving the damping function in terms of the priority distribution of an arbitrarily branched melt is given in reference [292], where results for a range of topologies from Cayley trees to combs is given. In the case of the percolation ensemble, for example, the priority distribution is a universal power-law with

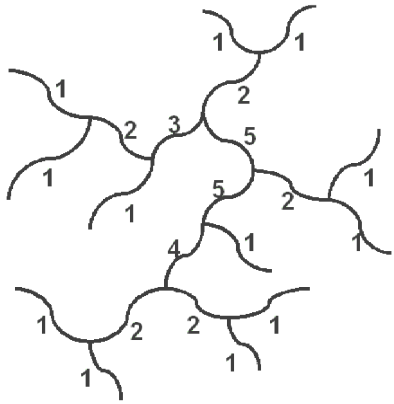


Figure 46. The same topology of molecule as in figure 37, labelled this time with the segment *priorities*.

exponent $-3/2$. It is generally true that $h(\gamma)$ for all classes of branched polymer lie above the Doi–Edwards result for linear chains.

An important, and startling, prediction is that for most monodisperse branched structures, time–strain factorability will in general be lost, although there may be regimes of timescales between the stretch relaxation of one seniority and the orientational relaxation of the next, during which a local separability can define a 'time-local' damping function. As we already saw for the important example of the H-polymer structure, a melt of the model polymer in figure 35 will behave as a diluted and slowed down system of entangled linear chains at times much longer than the longest relaxation time of the arms. So the nonlinear response in step strain at these timescales must be described by the (much more thinning) Doi–Edwards damping function! The strain response exhibits a higher effective modulus at short times than at long times in nonlinear step strain, with a discontinuity in the gradient of the 'early time' damping function, corresponding to the critical strain for onset of BPW. The difference in the two stress responses is connected by the timescales of stretch relaxation of the crossbar section, inhibited by the exponentially large drag at the branch-points arising from the star-like arm retractions.

Experiments on H-polymer melts have confirmed this expectation [50] (for the damping function results see figure 15), together with a subtle and interesting feature: the stretch relaxation time depends itself rather strongly on strain. The higher the strain, the sooner is the transition from a rubbery response to a Doi–Edwards-like strain thinning. For high strains beyond the level at which branch-point withdrawal occurs this is not difficult to understand, as the dangling segments which control the effective drag on the branch-points are smaller. However, even at smaller strains the branch-point will tend to withdraw the dangling arms by up to one entanglement length. This is not a minor perturbation to the effective drag on the branch-point because of its exponential dependence on the dangling primitive path length (we recall the underlying dynamics are those of an entangled star arm). This subtle partial retraction is, however, the sort of conjecture that requires more than rheological measurement to confirm satisfactorily. In this case, small angle neutron scattering on quenched strained samples was able to contribute direct structural

evidence that small translational rearrangements of branch points do occur for all strains [50].

Given the clear observation of non-factorable $G(t,\gamma)$ in model monodisperse branched polymers, the puzzle which then arises is to explain why the highly branched LDPE *does* exhibit time–strain factorability [330]. Experiments and calculations on branched melts with controlled polydispersity will be the next stage, since it is known that summing the response of intrinsically non-factorable rheological models with a sufficiently broad range of relaxation times can lead to an overall response that is indistinguishable from a factorable one [328].

5.2.2. *Branched polymers—a minimal model with stretch*

We are now ready to combine the new physics arising in the case of branched topologies for a model, monodisperse, polymer in nonlinear response. We seek to develop a full constitutive equation for arbitrary flow histories. For a first case we need to remove the complications of polydispersity in molecular weight and topology, but must have sufficient complexity to capture the new phenomena of uniform segment stretch and branch point withdrawal suggested by the tube model. This has recently proved a very effective line of attack on the general problem of LCB entangled viscoelasticity, since the physics may be checked against model architectures [50, 141, 331], while supplying theoretical structures that may be generalized and applied directly to commercial polymers [151, 332–334]. From the considerations above on step-strain response, it will be clear that monodisperse star polymers do not satisfy our requirements since they possess no segment without a free end. We recall that all the arms of an entangled star polymer retract as linear chains. So a more fruitful choice is a family of architectures based on the H-polymer, but with a variable number of arms, $q$, attached symmetrically to each end of the crossbar portion. Such 'pom-pom' polymers permit us to explore the notion of 'degree of branching', contained in $q$, while keeping simplicity of structure [87, 151]. The other structural parameters will be the number of entanglements of the crossbar $Z_b = M_b/M_e$ and arm $Z_a = M_a/M_e$, as illustrated in figure 47. Because of its generic nature, we will review the nonlinear theory of entangled pom-pom polymers in some detail, before covering applications and subsequent developments more briefly. Further simplifications may be made if restriction is made to the *first* nonlinearities that appear in the viscoelastic response. From our review of the H-polymer melt in linear response above, a direct generalization of the outlines of a theory to the pom-pom architecture is trivial. The arms relax by retraction, in the presence of the effectively permanent crossbar segments, and the branch-points themselves

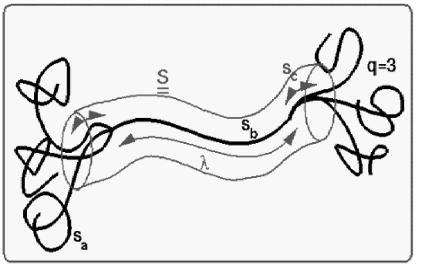


Figure 47. Schematic diagram of the pom-pom molecule illustrating structural parameters and dynamic variables.

behave as slow diffusers whose fundamental step time is given by the first-passage time for arm retraction. The only modifications required from the H-polymer results are: (i) an account of the number of arms in the crossbar volume fraction and (ii) an increase in the effective drag coefficient of the branch points so that $\zeta_b \sim 1/q$. So the slowest relaxing segments in the melt (by typically exponentially large ratios) are the crossbars themselves. The nonlinear response of the melt will be dominated by the crossbars at deformation rates at which the arms are hardly perturbed from equilibrium for most of their length. So for a first theory of nonlinear response we ignore the contribution to stress from the tube occupied by the arms (apart from a trivial addition of the linear viscoelasticity, calculated similarly to equation (152)), and concentrate solely on the crossbars. The only exception to this is required when deformation rates are so high that branch-point withdrawal occurs, when the strain-induced renormalization of the arm drag will require some new physics to quantify BPW. This theory will be valid for timescales $\tau > \tau_a$, or alternatively deformation rates $\dot{\epsilon} < \tau_a^{-1}$.

In this regime (see figure 35 above) the molecules become topologically *linear* polymers, entangled in the diluted tubes arising from crossbar entanglement alone, but with special dissipation: all the effective drag is located at the extremities of the chains. In nonlinear response this drag will depend on the state of deformation itself via BPW. The polymers will therefore reptate, with a near single-exponential relaxation modulus, and stretch curvilinearly within their tubes. The stretch may be represented as the simple scalar ratio of current path length $L$ to equilibrium length $L_0$, $\lambda = L/L_0$. In this regard they resemble entangled versions of the simple 'dumbbell' models of dilute polymer solutions, except for the variability of drag, which we shall see overcomes many of the shortcomings of those earlier phenomenological models [38]. Curvilinear stretching will affect the stress contributed per molecule in the two ways we saw in the case of linear polymers with chain stretch. Firstly, since the segments are Gaussian chains, stretch increases the effective chain tension, so increasing each component of the stress tensor in proportion. Secondly, a stretched crossbar will have an increased primitive path, contributing additionally as the number of tube segments of length $a^*$ that it spans. The (unit trace) geometry of the stress tensor $\mathbf{S}$ will, as in all tube models, be given by the second moment average of the tube-segment orientations $\mathbf{u}$, $\mathbf{S} = \langle \mathbf{uu} \rangle$. A final contribution arises from arm material dragged into tube once occupied by crossbar segments. A we have seen, this occurs once the crossbar has attained its maximum stretch. A convenient measure is the time-dependent number of entanglement segments so withdrawn, $Z_c$. These segments are aligned with the crossbar tube, but *not* stretched, so only carry one factor of the stretch. So, as the orientation moment (controlled by reptation), the stretch (a measure of curvilinear retraction) and the withdrawn arm length will vary with time, the stress has the structure

$$\sigma(t) = G[\lambda(t)]^2 \mathbf{S}(t) \left( 1 + 2 \frac{Z_c(t)}{L_0 \lambda(t)} \right), \tag{171}$$

where $G$ is an effective modulus. In a monodisperse melt of real pom-pom architecture polymers, the effective modulus $G$ depends on the true plateau modulus of the polymer $G_N^{(0)}$ and the volume fraction of crossbar material, since at the relevant timescales, arm material is acting as a diluent. If $\beta = 1 + \alpha$ is the dilution exponent (taken variously as 2 or 7/3) then we have $G = \frac{15}{4} G_N^{(0)} \phi_b^\beta$. No further reduction in variables is possible than that of equation (171), apart from the good

approximation in which the last term, representing stress from aligned arm material, is discarded. Doing this does not change the special factorized structure of the stress. In particular it will not be possible to write a closed equation for the stress tensor itself; instead we need one dynamical equation for the orientation, and one for the (scalar) stretch. We now review the derivation of dynamical equations for the three structural variables $\mathbf{S}(t)$, $\lambda(t)$ and $X_c(t)$.

*Orientation tensor* $\mathbf{S}(t)$. The time evolution of the orientation of tube segments under flow may be treated itself at a number of levels, for example choosing whether or not to incorporate CCR. Without it, as in the original treatment of the model, the discussion is identical to that for linear polymers. It leads to the same 'sum-over-history' solution as an integral over the birth at time $t'$ (rate $\tau_b^{-1}$), survival to time $t$ (by reptation, approximated by single-exponential decay with rate $\tau_b^{-1}$) and deformation of tube segments (described by the deformation tensor $\mathbf{E}(t, t')$):

$$\mathbf{S}(t) = \frac{4}{15}\int_{-\infty}^{t} \frac{\mathrm{d}t'}{\tau_b} \exp\left[-(t-t')/\tau_b\right] \mathbf{Q}_{DE}(t, t'), \tag{172}$$

with $\mathbf{Q}_{DE}(t, t')$ the Doi–Edwards tensor of equation (154).

A differential approximation, which retains the qualitative character of the integral result, but is quantitatively considerably more shear-thinning, is useful for intensive computations such as in finite-element solvers for complex flow geometries [152, 331]. It functions by calculation of an auxiliary tensor $\mathbf{A}(t)$, satisfying

$$\frac{\mathrm{D}}{\mathrm{D}t}\mathbf{A} - \mathbf{K}\cdot\mathbf{A} - \mathbf{A}\cdot\mathbf{K}^{\mathrm{T}} = -\frac{1}{\tau_b}(\mathbf{A} - \mathbf{I}) \tag{173}$$

then projecting onto a unit-trace tensor (this is an approximation to the molecular process of retraction) to find the approximation for $\mathbf{S}(t)$:

$$\mathbf{S}(t) = \frac{\mathbf{A}(t)}{\mathrm{trace}(\mathbf{A}(t))}. \tag{174}$$

The essential feature captured by this approximation is the asymptotic form in shear that $S_{xy} \sim \dot{\gamma}^{-1}$. This is important in controlling the behaviour of stretch in shear flows, as we will see below. In cases where the differential approximation is compared with real data, it is important to note that the expression for $G$ changes to $G = 3G_0\phi_b^{\beta}$. Other differential approximations have recently been applied, and other choices are necessary if the second normal stress difference $N_2 = \sigma_{yy} - \sigma_{zz}$ is to be non-zero [153].

The relaxation time for orientation may be left as a free parameter if the system of equations is considered as a general constitutive equation to be explored, but if related to specific molecular architectures, may naturally be derived from them. In terms of the primitive path of the crossbar, $L$, and the curvilinear diffusion constant $D_c$, $\tau_b$ follows the reptation expression $\tau_b = L^2/\pi^2 D_c$. We already have $L = Nb^2/a$ and $a^2 = N_e b^2$, giving $L^2 = a^2 Z_b^2$. The diffusion will be dominated by the diffusion constants of the two branch points $D_b$ so that $D = D_b/2$ (the drag of each is additive). These in turn may be calculated from the ansatz that diffusive 'hops' of the branch points are permitted by arm retraction. In fact the physics of this hop-entanglement-release process is currently under intensive discussion as there is (as we have seen in section 4.3.2) strong evidence that the process is much slower than a simple physical reasoning would suggest, at least in asymmetric star polymers.

However, here we take the simplest assumption as for the H-polymer, that the hop length is a finite fraction $p$ of the dilated tube diameter, $a^* = a\phi_b^{-\alpha}$, and that the diffusion is reduced in proportion to the number of dangling arms $q$, giving $D_b = (ap\phi_b^{-\alpha})^2/(2q\tau_a)$ and

$$\tau_b = \frac{4q\tau_a\phi_b^{2\alpha}Z_b^2}{\pi^2 p^2}. \tag{175}$$

Note that although this is a *reptation* time, it scales as $Z_b^2$, not $Z_b^3$, because the effective drag arises from the branch-points only, and is independent of $Z_b$.

*Stretch ratio* $\lambda(t)$. To derive the dynamical equation for the stretch we employ the same notion as above, that each branch point is a source of effective drag $\zeta_b$, via an Einstein relation $\zeta_b = k_B T/D_b$. The branch point diffusers are also subjected to drag from stretching tube around them, and from the entropic elasticity of the chain connecting them.

If the chains are sufficiently long, then the relative curvilinear velocity of the chain and tube at the branch point may be replaced by its ensemble average, which is $L/2\langle \mathbf{K} : \mathbf{S} \rangle$ . This assumes that the centre of the crossbar is at rest on average. The entropic spring applies curvilinear forces of $\pm 3L/Z_b\phi_b^{\alpha}a^{*2}$ on each branch point, and they are additionally subject to the normal tube-end tension of $3k_BT/a^*$. Writing the curvilinear coordinate of each diffuser as $x_i$ with $i = 1, 2$,

$$\zeta_b\dot{x}_1 = +\frac{3k_BT}{a^*} + \zeta_b x_1\langle \mathbf{K} : \mathbf{S} \rangle - \frac{3k_BT}{Z_b a^{*2}}(x_1 - x_2) \tag{176}$$

$$\zeta_b\dot{x}_2 = -\frac{3k_BT}{a^*} + \zeta_b x_2\langle \mathbf{K} : \mathbf{S} \rangle + \frac{3k_BT}{Z_b a^{*2}}(x_1 - x_2). \tag{177}$$

These equations are entangled forms of the 'Rouse dumb-bell' toy model we looked at in section 4.1.1. Making the same coordinate change here we write for the stretch mode, $\lambda = (x_1 - x_2)/L$ and find

$$\dot{\lambda} = \langle \mathbf{K} : \mathbf{S} \rangle \lambda - \frac{1}{\tau_s}(\lambda - 1) \tag{178}$$

with the stretch relaxation time

$$\tau_s = \frac{1}{3}\frac{q\phi_b^{\alpha}\tau_a}{p^2}$$

(note that in earlier publications a different prefactor arises due to the cleaner definition of $M_e$ adopted here). Just as in the calculation of damping function, we must override the dynamical equation for the stretch by the non-analytic BPW process as soon as the tension in the crossbar equals the sum of equilibrium tensions of the dangling arms. This is just when $\lambda = q$, so equation (178) operates only until it would violate $\lambda < q$, in which case the maximal stretch is maintained until the driving flow would cause stretch relaxation below $q$. The non-analyticity arises, as usual in statistical physics, when the dynamics result from integrating out many microscopic variables.

*Local branch-point displacement*. The exponential sensitivity of the branch-point drag on the effective entangled arm length requires a careful treatment of

the displacement of the branch-points in strong flows [333]. The topological confining field cannot allow escape of the branch-point along the crossbar tube until the critical stretch is reached, but as we have seen, before then local displacement of order $a^*$ would be expected towards the crossbar tube, reducing the effective value of $Z_a$ by a number of order $\phi_b^{-\alpha}$. This can have large effects on the stretch and reptation timescales, since we have generally

$$\tau_a \sim \exp(\nu' Z_a). \tag{179}$$

As a first guess at the form of the confining field $U_b(x)$ for displacements $x$ of a branch-point (as opposed to the tube field for the chain itself), we write a quadratic form

$$U_b(x) = k_B T(q-1)k_* \left(\frac{x}{a}\right)^2,$$

where $k_*$ is a new dimensionless constant of the tube model, appearing for the first time in the nonlinear response of branched polymers. We might expect it to be of order unity, since the penalty to displace the branch point one tube diameter must be of order $k_B T$. The dependence on $q-1$ rather than $q$ corrects reference [333]: the localization must disappear for the linear case of $q = 1$. By equating the tension from the crossbar $\lambda f_{eq}$ to the force from the branch-point localization potential $\partial U_b/\partial x$, a displacement $\Delta x(\lambda)$ results, which in turn subtracts $\Delta x(\lambda)/a$ from $Z_a$ in equation (179) for the current arm terminal time $\tau_a$. The renormalization

$$\tau_a \rightarrow \tau_a \exp[-\nu^*(\lambda - 1)] \tag{180}$$

with $\nu^*$ related to $k_*$, introduces important nonlinearities in the stretch equation (178), and the orientation equation (172) as it carries through to $\tau_s$ and $\tau_d$. In its effect on the stretch, it moderates the degree of extension-hardening predicted, and proved essential in accounting for the maximum hardening observed in experiments on H-polymers [50] (see figure 13). The reason for this connects the molecular process of BPW directly with a macroscopic observable—in this case the strain at which a LCB melt measured in uniaxial extension will always break. When the crossbars of a pom-pom polymer (or generally high priority segments of a more complex molecule) stop stretching near-affinely due to BPW, the rate of increase of extensional stress with further strain rapidly reduces. The effect of this extreme retraction on an extending free fibre of the material, is that it is no longer stable to perturbations of its width, rapidly forming necks and breaking soon thereafter [335]. The consequences for the localizing potential $U_b(x)$ of large withdrawal of arms is that beyond a single tube diameter, it assumes a *linear* rather than *quadratic* form, so that further retraction occurs at the constant force generated by dragging all outer arms into the crossbar tube. Possible model forms for this potential have been proposed, such as

$$U_b(z) = \frac{3k_B T}{a}(q-1)\left\{z - \mu a\left[1 - \exp\left(-\frac{z}{\mu a}\right)\right]\right\}, \tag{181}$$

with $\mu$ an $O(1)$ constant [336]. This rather detailed prediction of molecular theory awaits the application of simulation: tests would not require the prohibitively long simulation runs that full viscoelastic simulations do, yet the consequences of branch point localization potentials such as (181) for rheological flows are very important.

5.2.3. *Assessment of the pom-pom equations*

The set of equations (171), (172), (178), (180) determine the constitutive behaviour of the pom-pom model. Remarkably, for the physically relevant ordering of $\tau_s < \tau_d$, it exhibits strong shear softening (yet with overshoots in shear and normal stress), and equally strong extension hardening, up to a maximum set by the degree of branching, $q$. These are all the special qualitative features observed in the extensive studies of the much more topologically polydisperse LDPE [17]. Significantly the hardening is shared equally in uniaxial and planar extension, also the case in branched melts generally [138]. The lack of the small but significant second normal stress difference, the poor degree of quantitative approximation of the differential version to the integral form for **S**, and the poor degree of recovery of time–strain separability in the polydisperse case has been criticized [330], but the model investigated at that point did not carry the BPW-induced nonlinearity in the relaxation times, which has proved all-important when comparing with experimental data.

Tests on monodisperse architectures have to date been limited to studies on H-polymers, but the nonlinear transients in extension and shear together with their overshoots and maxima were quantitatively accounted for using a value of $k_* \simeq 0.36$. Partially-deuteriated H PI molecules were additionally given large step-extensions and rapidly quenched in order to probe the spatial consequences of BPW. Qualitatively the effect on spatial correlations of the chain ends are particularly remarkable: at high strains beyond the critical value for BPW the ends are drawn *together* by further strain (affine deformation would in general separate them). The prediction of an extension of the 'random phase approximation' to non-equilibrium states [337] is that very strong scattering should appear in the strain direction as the arm relaxation proceeds following the step strain. Qualitatively this is exactly what is seen [50, 338], but with about twice the magnitude predicted! These observations remain a challenge for the future, and underline the importance of supplementing rheological observations with direct structural probes such as SANS.

But perhaps the most important legacy of this model study, that led to the pom-pom equations, is their use as elements in mathematical models for LDPE and other polydisperse LCB polymers. The insights gained in studies of the model architectures above may be applied to commercial, random branched polymers, even without detailed knowledge of their architectures. Of course, an eventual goal of this programme of work is the ability to predict the rheological response of any melt of topologically complex polymers if their distribution of structures is known. However, the insights we have gained in to the H (and in general 'pom-pom') family of structures are informative straight away in that they point to a generic feature of the rheology of branched polymers not reproduced by phenomenological constitutive equations. This is that:

> *An entangled segment of a branched polymer in the melt will contribute to the bulk stress via both its orientation (tensor property) and stretch (scalar property). These quantities will relax with different characteristic timescales. The segment will stretch in flow, but only up to a maximum ratio, given by the effective number of free ends attached to its delimiting branch points.*

The 'pom-pom' constitutive equation was based on these assumptions and showed how such a structure could lead to a polymer melt that was simultaneously extension-hardening and shear-thinning. To model existing random branched

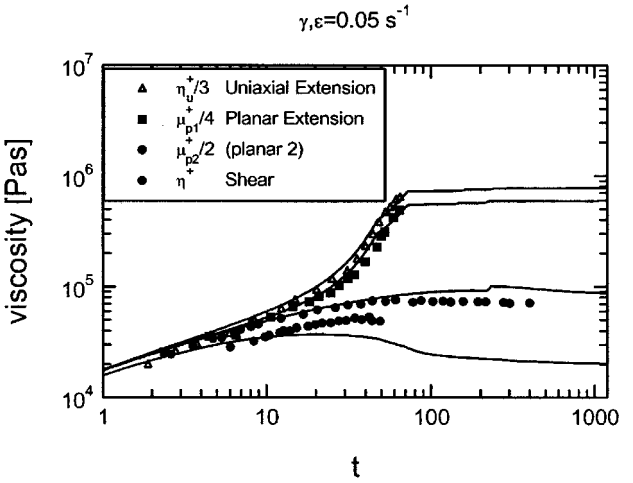


Figure 48. A 'multimode pom-pom' model simultaneously fitting transients in uniaxial and planar extension as well as shear for the LDPE IUPAC X [332].

polymers such as LDPE in this way one can take the linear relaxation spectrum $G(t) = \sum_i g_i \exp(-t/\tau_i)$ as an indication of the distribution of segment orientation times, and 'decorate' each mode $i$ with the nonlinear parameters of a 'buried' branched segment, i.e. a stretch relaxation time $\tau_{si}$ and a maximum stretch ratio $q_i$. This has been done recently by several groups [153, 332, 333]. Figure 48 shows the results for one deformation rate in a range of transient flow geometries for the LDPE IUPAC X. With the same set of parameters, the weaker response in shear and the second normal stress in planar extension are modelled, as well as the stiffer response in the first normal stress of the extensional flows. Similar fits are achieved at a range of deformation rates. Of particular note is the consequence of the $q_i$ distribution: the extensional curves typically show a rapid change of gradient when the dominant segments for that extension rate reach their maximum extension. As we have seen, this would cause a free extending film to break—and end the experiment. So a possible consequence is that the break points in an extensional data set are direct measures of the molecular distributions of the 'priority' distribution $q_i$. Such 'spectra' of nonlinear parameters with timescale might be a very useful way of 'fingerprinting' a branched polymer.

Finally we note that another use of this constitutive scheme is as a local viscoelastic stress calculator in a flow solver for complex geometries. Do the special features of these molecular constitutive equations capture any of the corresponding special phenomena observed with LDPE, for example, in complex flows? An important example is the large recirculating vortex growth seen in contracting flows. Another level of calculation is required, that takes the local physics embodied in a molecular constitutive equation and computes the consequences under the additional imposition of conservation of mass and momentum together with the boundary conditions of a complex flow. This is not the place to review the great range of methods that have been used to attack this challenging problem of non-Newtonian fluid mechanics, particularly as most of this work has been directed to the solution of phenomenological models. However, there have recently been a number of considerable advances in a particularly appropriate type of flow solver for molecular

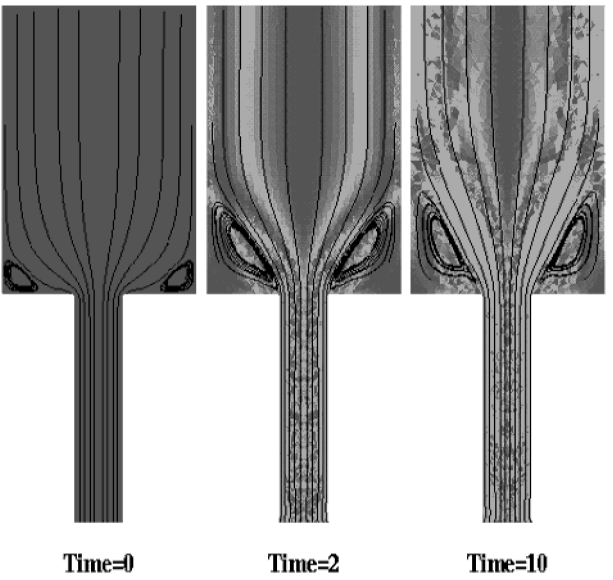


Figure 49. Simulations of a commercial LDPE modelled with a multi-mode pom-pom ensemble in transient start-up flow into a contraction. The development of the vortex structure seen in experiments is clear. The shading indicates regions of high segment stretch. [Courtesy of Dr T. Nicholson.]

approaches, namely Lagrangian solvers [339–341]. Rather than discretize the spatial domain by a fixed grid, the lattice of finite elements moves and deforms with the flow. Careful application of this technique seems to permit the attainment of high deformation rates (in terms of the fluid relaxation time) without numerical instability, and compares well with fixed-grid methods. A great advantage is that its data structure is easily adapted to carry physical 'hidden' variables (such as the orientation and stretch of the pom-pom molecules) on the co-moving fluid elements themselves. Simulations of flows such as the contraction flow of figure 3 by these and more standard [153, 342] methods have recently been attempted. An example of a simulation of a LPDE into a contraction is shown visualized in figure 49. As well as capturing the famous vortex structure of branched polymers, this technique has predicted a previously unseen stretch pattern in the outflow of a contraction [152], and the very high stress distribution in the vicinity of a stagnation point [153]. There is clearly a great deal of potential in using flow simulation, together with molecular constitutive equations, to relate phenomena linked across a huge gulf of spatial scales. But it is unsatisfactory to employ structures such as the pom-pom equations in a purely phenomenological way, even if one claims that they contain the essence of the right physics. Just a few more complex architectures have been investigated in a more fundamental way.

### 5.2.4. *Application to other topologies*

In many ways the success of the multi-mode version of the pom-pom model in accounting quantitatively for the nonlinear rheology of commercial LCB polymers is a great surprise. After all, we have seem time and again that the exponential

hierarchy jointly imposed on the melt by the topological constraints and the presence of branching, mean that the effective topology of the molecules depends on the *timescale* with which they are observed. An H-polymer melt, for example, may behave as a linear polymer at low frequency. Such 'topological renormalization' would appear to militate against any constitutive formulation that used a fixed set of priority parameters $q_i$ at all flow rates. A second concern is that in practice, the elements of the pom-pom ensemble with different relaxation times occupy typically positions of seniority within the same molecules, so will be directly coupled in a flow. A study aimed at investigating how these effects would emerge from a more rigorous application of the tube model considered the case of a melt of monodisperse Cayley tree molecules of three levels [298]. The coupling of segments of the three different seniorities that emerges is of two kinds. Firstly, *orientation* is advected by the flow from inner to outer segments. This is responsible for a much longer time to achieve steady-state in a shear flow than in a decoupled model, since very high strains are required to deform tube segments originally around high-seniority chain to the outside of the molecule. But secondly, information on chain *stretch* is convected in the reverse sense. It is the time-dependent stretch of the outer segments, rather than their nominal priorities, that determines the maximum stretch of deeper segments. In consequence, although it is possible to approximate the behaviour of such a melt by a decoupled ensemble of pom-pom modes, the elements used are not typically identifiable with particular seniorities in the molecules, and much of the agreement is possible due to the necking instability in extension, hiding later behaviour that would otherwise distinguish the models.

Such calculations are a useful caution when pursuing more advanced goals, such as the prediction of nonlinear rheology from polydisperse LCB melts. From the LCB metallocene ensemble we reviewed above in section 4.3.4, it is possible to derive not only the seniority, but also the priority distributions of the ensemble at any timescale of observation [72]. Using the two parameters of plateau modulus $G_N^{(0)}$ and entanglement segment Rouse time $\tau_e$, an estimation of the rheology may be made by mapping the bivariate distribution of seniority and priority onto a pom-pom ensemble with the identical bivariate distribution. Only the physics of seniority and priority coupling is omitted. Initial results are promising, correctly predicting, for example, that the regime of extension hardening switches from low extension rates to high at a value of the branching parameter $b_U$ of 0.1. An example of the quality of prediction by this technique is given in figure 50, where the lighter, non-hardening set of curves result from topological renormalization of the ensemble by one level. The surprising apparent lack of the topological renormalization at lower flow rates, when one would have naïvely thought it necessary (see figure 50) is a current challenge. The effective amplification of local (tube scale) deformation rates greatly above the bulk rate identified in [298] may be a clue.

There is a need for experiments on well-defined architectures intermediate in complexity between the simple H and pom-pom materials and the fully polydisperse commercial melts currently available. Nonlinear measurements on well defined combs will probably be the next step.

## 6. Current challenges

There are a number of pressing issues that the research programme we have reviewed is currently grappling with, that are worth pointing out. Some fall under the

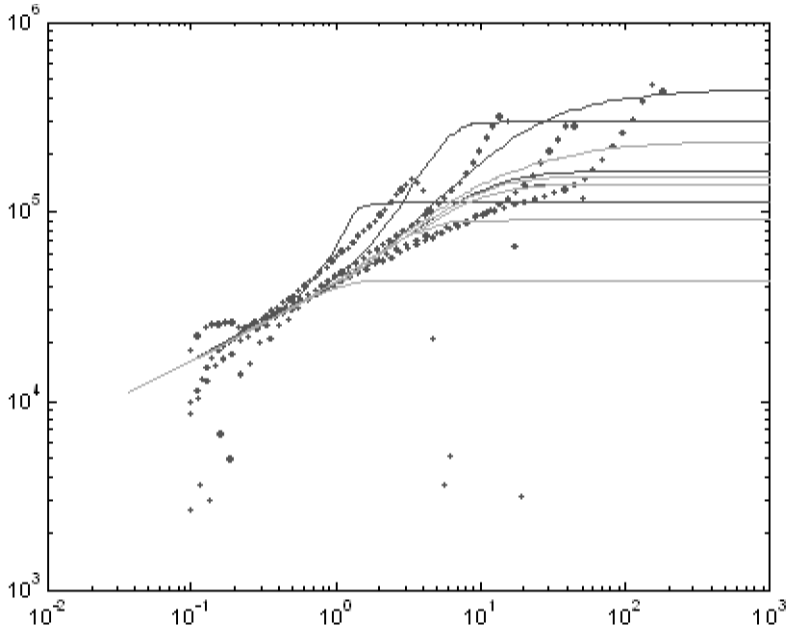


Figure 50. Data on extensional transient flow (stress growth coefficient in pascals with time in seconds) for a LCB metallocene melt with $b_U \simeq 0.1$. Predictions with the full priority distribution are the dark lines, with the outer branched relaxed in light. Extension rates are 0.03, 0.1, 0.3 and $1.0\,s^{-1}$.

category of the incremental addition of dynamical processes that has been the great fruitfulness of the tube model. There is every reason to hope that the series: reptation, contour length fluctuation, constraint release, branch-point withdrawal, local branch-point displacement ... will terminate (many more terms and the underlying model will cease to be useful), but as one of our themes has been the close relation of experiment and theory in this field, it will not be a surprise if new physics emerges with, for example, the increasing use of SANS and NSE on entangled dynamics. Other problems open up the field to a greater appreciation of the molecular structure underlying our coarse-grained picture. Yet others touch on fundamental conservation laws and guard against dangers lurking in the approximations inherent in a coarse-grained approach.

### 6.1. *Pre-averaged chain dynamics*

Before considering physical effects so far discounted, it is worth reminding ourselves how accustomed we are to writing constitutive equations for polymers in terms of the behaviour of the average chain rather than averaging the reponses of many chains with stochastic variation in their behaviour. In dilute solutions the dynamically pre-averaging approach can lead to qualitatively poor approximations. This has been carefully investigated by comparing the pre-averaged closures for 'dumb-bell' models with explicit stochastic simulations of ensembles of them [343]. In this case the spread of molecular properties such as stretch can be very wide compared with the mean, a behaviour that in turn arises from the very different histories of molecular deformation that arise from the

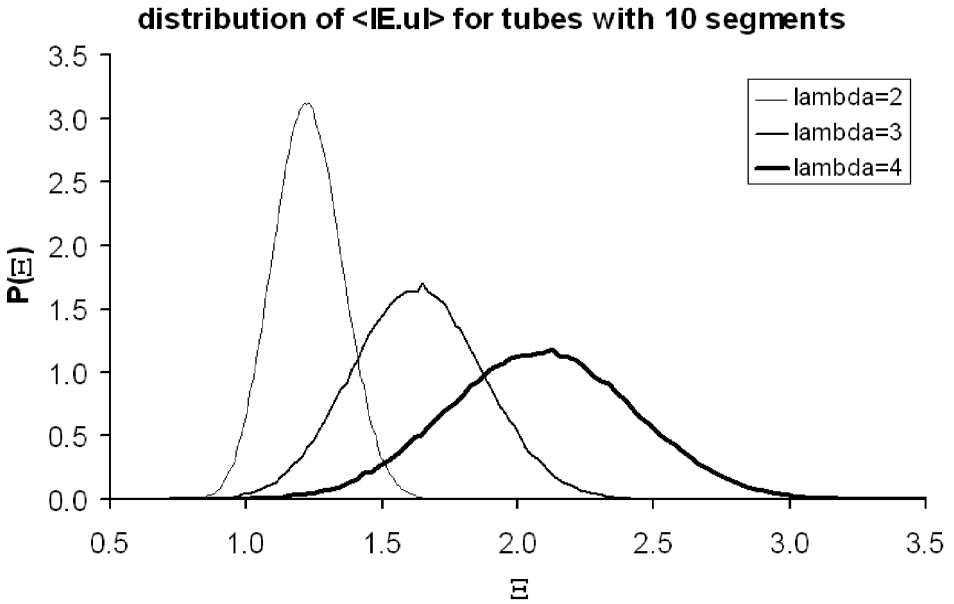


Figure 51. The distribution of total stretch of primitive path $\langle|\mathbf{E}\cdot\mathbf{u}|\rangle$ calculated for chains of $Z = 10$ at three different bulk deformations. The approximation of a single effective average value becomes increasingly poor, even at this degree of entanglement. [Figure and calculation courtesy of Dr D. J. Read.]

geometry of presentation of individual molecules to the axes of an extensional flow. The unassailable spread of 'molecular individuality' has been observed and modelled in single-molecule observations of DNA in dilute solutions under extensional flow [344].

In entangled solutions the situation is not so bad: the pre-averaging is better at the level of individual molecules because orientations are sampled by individual tube segments, rather than by entire molecules. So a large number of entanglements per molecule generates an average over orentations that in the limit of large $Z = N/N_e$ constrains all molecules in the melt to adopt mean segmental orientations and stretches that are closely distributed about the mean. However, the approach to this convenient limit is not as fast in practical cases as is often tacitly assumed. In figure 51, to take a concrete example, we show the distribution of primitive path length increases on a bulk uniaxial extension, $\langle|\mathbf{E}\cdot\mathbf{u}|\rangle$, where in this case the average is taken only over the segments of single representations of the chains. In each chain the orientation of tube segments is chosen at random from an isotropic distribution. Even at $Z = 10$, it is clear that the pre-averaging approximation is not a very good one, and moreover that it becomes worse with increasing stretch. This could be very important when molecular strains lead to local critical behaviour such as the branch point withdrawal of highly branched polymers. At intermediate levels of entanglement, some molecules will be well into a BPW transition while others will not yet have reached it. It is possible that in the rather smeared response of rheology, this distinction is not severe, but the approximation is not likely to be benign for calculations of scattering functions [338, 345]. In any case, the examination of

pre-averaging assumtions in entangled rheology is likely to be an important topic in the near future [346].

### 6.2. *Tube deformation*

It is of interest to think about relaxing the assumption that the local tube confining field is unchanged even in nonlinear flow, although hard experimental tests for specific assumptions of the deformation of the tube constraint itself can never be confined to rheology alone, but will involve at least careful analysis of neutron-scattering experiments [311, 338]. Not only might the tube diameter depend on the local strain, but the localizing field described by the tube may well take on an anisotropy consistent with the symmetry of the bulk strain. Two recent models for deformation of networks containing both crosslinks and entanglements reach the conclusion that the entanglement constraints do deform, but sub-affinely with the strain [312, 313].

Reasons have been advanced for both an increase and a decrease of the tube diameter with strain. A justification of the former view might be the retraction process itself [222]. If it acts in a similar way to the dynamic dilution, and the effective concentration of entanglement network $c_e$ follows the retraction, then $c_e \sim \langle|\mathbf{E}\cdot\mathbf{u}(s)|\rangle$ so that $a \sim \langle|\mathbf{E}\cdot\mathbf{u}(s)|\rangle^{1/2}$. On the other hand one might guess that at large strains the tube deforms at constant tube volume $La^2$ [74, 310]. The tube length must increase as $\langle|\mathbf{E}\cdot\mathbf{u}(s)|\rangle$, so from this effect $a \sim \langle|\mathbf{E}\cdot\mathbf{u}(s)|\rangle^{-1/2}$. Indeed, Marrucci has recently proposed that both these effects exist and remain unnoticed in step strain because they cancel [57]! The same author has recently pointed out that the ratio of the normal stress differences in shear is very sensitive to any anisotropy in the tube that develops in deformation [347].

A corresponding effect may occur at junctions of tube segments, or 'entanglement points', if these really exist in any sense. It has been pointed out that two-body topological interactions of chains cannot deform affinely if distant connections of the entangling chains do [75, 348]. These modifications allow relative displacement of the entanglement points to maintain a local stress balance. The form of the $\mathbf{Q}$ tensor is modified quite strongly in these models. Simulation [313] and carefully-chosen scattering experiments [338] in consort with optical rheology will be needed to advance these questions of tube and entanglement deformation.

### 6.3. *Thermodynamic consistency*

Theories of hydrodynamics of complex fluids containing slow structural variables are, of course, much older than the advent of molecular models for entangled polymers. Liquid crystalline order parameters and demixing fluids have a longer history [349]. When both reactive and dissipative processes are at work in a flow, it is important that any coarse-grained theory (i) maintains a positive entropy production, and (ii) contains an expression for the stress that is consistent with the equations of motion [65]. This is not always obvious, and terms can be omitted from the stress if a careful accounting is not made, or if a clear virtual work calculation is not tractable [31]. Application of this programme in various formalisms has been more recently applied to polymer rheology [66, 350, 351]. For example, the pom-pom equation set can be shown to obey the consistency conditions (i) and (ii) (as do various possible extensions of the model without immediate molecular motivation).

These tools, although no substitute for molecular derivations of equations of motion, are a useful complement to them, especially when purely mathematical approximations such as decoupling high order correlations for closure, or the IAA approximation, are required. Often there is a choice of approximation. If only a subset of these meets the thermodynamic criteria then further evaluation can be greatly speeded up.

### 6.4. *The tube diameter*

There has been a long history of attempts to derive the existence of the tube confining field from fundamental properties of Gaussian chains, rather than simply to work with it as an *anzatz*. The difficulties facing a rigorous topological approach [352] is that entangled melts (rather than simple rings) do not posses true global topological invariants such as those that can be defined for closed knots and braids. Instead, locally defined topological states are the best that one can achieve [15, 353, 354]. In addition, only the simplest invariant of the 'winding number' bears representation in terms of the familiar spatial arc coordinate representation of a polymeric fluid [355, 356]. One can, however, show that forces can be transmitted via Brownian motion between chains that are only linked but not crosslinked [352]. Calculations that restrict the huge number of possible topological structures and invariants to the winding numbers can be made to produce results for the power-law with which an emergent confining field scales with polymer concentration. The conceptual tool used in most approaches is the function $f_N(r)$, defined as the probability that two rings of $N$ links, whose centres of mass are separated by a distance $r$, are linked. A good approximation to this function is [357]

$$f_N(r) \simeq 0.6 \exp\left(-0.3 \frac{r^3}{R_L^3}\right),$$

where $R_L$ is the 'linking radius', close to $R_g$ of the chains. The model of Graessley and Pearson, for example [15], predicts that the elastic modulus of a rubber can be separated into a simple sum of a crosslink ('phantom') contribution, and a linking contribution $a[f_N(r)]$ that is an integral functional of $f(r)$ and the chain density:

$$G = G_{\text{phant}} + b \cdot a[f_N(r)]\rho_{\text{link}}.$$

A recent simulation confirmed the effectiveness of the approximation that linking numbers are the dominant topological invariant for rubber elasticity [313] in the case of random networks, but found a strong underprediction of the entanglement contribution to the modulus in specially designed regular networks. This reference also gives a good summary of the field, including the opportunities now offered by computer simulation.

Clearly these fundamental considerations are at the point where they can sharpen the questions posed in the last section about tube deformation, as well as perhaps answer some of them.

### 6.5. *Limits to universality: the packing length*

At some point the universal picture presented here, arising from the happy circumstance that entanglement strands even in melts are already polymers, will find its limitations. $N_e$ is a large, but not a very large, number, and we have already seen how in one case at least (star arm retraction), local bond properties control large scale topological disentanglements. We also know that when $N_e$ becomes small in the

case of persistent chains, the picture changes completely as the source of stress becomes bending energy of the chains rather than configurational entropy [76]. But for flexible chains we believe that the hierarchy of entangled processes of reptation, CLF, CR and so-on give rise to the classic regimes of the viscosity function $\eta(M)$ of $\sim M$, (for $M < M_c$), $\sim M^{3.4}$ (for $M_c < M < M_\rho$) and finally $\sim M^3$ (for $M > M_\rho \simeq 10^3 m_0$ for common flexible polymers) when CLF are no longer important. It was a considerable surprise, therefore, when a recent very careful study of the rheological properties of many tens of different chemistries [78, 79] came to the conclusion that this sequence does *not* take place in a universal way, but that $M_e$, $M_c$ and $M_\rho$ all scale in a different way with the packing length of the polymer, $p$. This length, independent of the molecular weight of the chain, is defined as

$$p = \frac{\Omega(N)}{R_g^2(N)}$$

where $\Omega(N)$ is the volume of melt occupied by the monomers of a chain of degree of polymerization $N$. Both $\Omega$ and $R_g^2$ are proportional to $N$, so $p$ is independent of molecular weight, and is usually between 2 and 10 Å. In a simple model of monomers in which they have a length $l$ and a width $w$, $p = w^2/l$, the monomer width moderated by its aspect ratio. The observation that $M_e \sim p^3$ is consistent with the suggestion that an entanglement length is defined by a fixed number of other chains passing through the volume it spans [253]. But the other critical molecular weights scale in a different way: $M_c$ is about twice $M_e$ at low packing length, but falls proportionately as $p$ rises. On the other hand, the molecular weight at which pure reptation is seen to dominate, $M_\rho$, falls from a high value of $10^3$ at low packing length. The extrapolation at present is that all three molecular weights converge at $p \simeq 10$ Å!

Although at first sight a shock, there is one grain of consistency with what we know about the underlying physics. The relative strength of CLF is responsible for the separate existence of both $M_c$ and $M_\rho$ from $M_e$, so if CLF is suppressed by increasing $p$, then this would indeed produce the observed effect. No more can be said at present without detailed rheological or dielectric experiments on monodisperse melts of high $p$, or without some inkling of the mechanism by which increasing packing length might suppress CLF in flexible chains.

## 7. Conclusions

This is probably a good point to conclude our account of this story to date. We have made one iteration of a loop in the qualitative comparison of observed vortex growth in commercial branched polymers and the simulation of figure 49, and made contact with the industrial world of the new polyolefins. Underlying this is a theoretical development that has made a marriage of the two idealized cases of polymer dynamics. The free-chain Rouse theory and the purely-entangled reptation mode now combine in a picture that sees the confining tubes themselves as Rouse objects self-consistently guiding their chains. The topological foundation of the phenomena have emerged most clearly in the enormous effects of very small topological changes to the molecules themselves by long chain branching.

There is of course much still to do. There has yet to be a proper consideration of the role of convective constraint release in branched polymers. The ubiquitous strong stretch of these materials seems to suppress it to some extent, but the lesson

from the linear case is certainly that it cannot be ignored with impunity. Clearly there is also a long way to go before we can apply these tools and ideas to a stochastically branched and polydisperse polymer melt with confidence. However, the molecular approach to the dynamics of entangled polymers outlined in this chapter has proved remarkably fruitful, and has accounted for a very wide range of phenomena, some initially very puzzling. The central role of molecular topology continues to grow in its appeal. There are still many open challenges of which a few might be the following questions:

(1) What is the nature of the entanglement field, and why does the tube diameter scale in the way it does with concentration?
(2) What is the nature of the anomalous terminal region of star polymers, where tube dilation breaks down?
(3) What is the general relation between local constraint release and tube dilation?
(4) What is the physics underlying the packing length problem?
(5) Why is topological renormalization experimentally so weak in highly branched polymers under strong flows?
(6) Are inhomogeneities in the entanglement field important for dynamics, and are they behind the strange H-polymer scattering anisotropies?
(7) What is the correct nonlinear physics of local tube geometry and CR in strong flows?

We could go on, but a final exercise for the reader is the most important and creative scientific work of all: to ask the really important questions!

**Acknowledgements**

I have benefited hugely from discussions with many colleagues in the preparation of this article and its background, but in particular would like to thank Sam Edwards, Masao Doi, Ron Larson, Scott Milner, Michael Rubinstein, Ralph Colby, Robin Ball, Mike Cates, Lew Fetters, Oliver Harlen, Kevin O'Connor, Nigel Clarke, Graeme Bishko, David Bick, Daniel Read, Richard Blackwell, Sasha Semenov, Alexei Likhtman, Tam Sridhar and Hiroshi Watanabe. I am very grateful to Mark Warner, Ron Larson, Mike Rubinstein and Alexei Likhtman for their careful reading of the manuscript.

## Appendix: Brownian barrier-hopping in a potential well

Consider a potential $U(x)$ with a single minimum at $x = 0$ (the mean position of the diffusers). We want to calculate the average first passage time of a particle through position $s > 0$, given that it is introduced at $x = 0$ at $t = 0$. This is equivalent to the mean lifetime of the particle if an absorbing barrier is placed at $x = s$ (see figure 52). To solve this problem we consider introducing a steady current $j\delta(x)$ of diffusers at the origin, and waiting until a steady-state number density $n(x)$ of diffusers has been established. Then the total number of particles in the distribution is just the supply current multiplied by the mean survival time $\tau_{\text{esc}}$. So

$$\tau_{\text{esc}} = \frac{1}{j}\int_{-\infty}^{s} n(x)\,\mathrm{d}x.$$

We assume that the scaled diffusion constant is $D$ and work in units of $k_{\text{B}}T$ for the

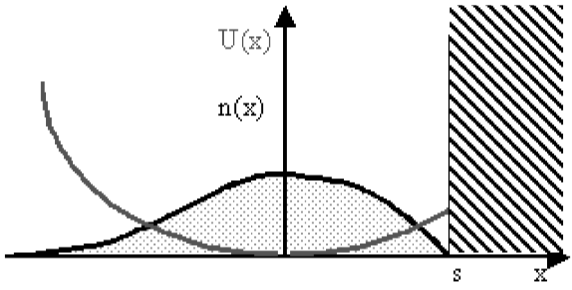


Figure 52. Potential and steady-state distribution function for particles diffusing over the barrier at $x = s$.

energy. Then in the diffusive limit, $n(t, x)$ satisfies

$$\frac{\partial n}{\partial t} = -\frac{\partial}{\partial x} D\left(-\frac{\partial n}{\partial x} - n\frac{\partial U}{\partial x}\right) + j\delta(x) = 0$$

in the steady state. In $x > 0$ we may integrate this once directly to give

$$\frac{\partial n}{\partial x} + \frac{\partial U}{\partial x} = \frac{-j}{D}$$

and once more by using the integrating factor $\exp(U)$ throughout:

$$\frac{\partial}{\partial x}[n\exp(U)] = \frac{-j\exp(U)}{D} \Longrightarrow n(x) = \frac{j}{D}\exp[-U(x)]\int_x^s \exp[U(x')]\,dx' \quad \text{for} \quad x > 0.$$

In $[-\infty, 0]$, there is no current (all the introduced flux ends up at the absorbing boundary at $x = s$) so the population distribution is just proportional to the equilibrium distribution, with the prefactor chosen to match with the solution in $x > 0$. So

$$n(x) = \frac{j}{D}\exp[-U(x)]\int_0^s \exp[U(x')]\,dx' \quad \text{for} \quad x < 0.$$

Now integrating $n(x)$ over all $x$ (it is sensible to reverse the order of integration between $x$ and $x'$ so that the two pieces in $x < 0$ and $x > 0$ can be joined in one initial integration from $-\infty$ to $x'$), and using the relation for the mean lifetime we find

$$\tau(s) = \frac{1}{D}\int_0^s dx' \exp[U(x')]\int_{-\infty}^{x'} dx \exp[U(x)].$$

This exact solution for the mean lifetime can be further approximated when the barrier is high ($U(s) \gg 1$). For now the inner integral is completely dominated by the contribution near the origin where $U$ is at its minimum—a good approximation is the consequent Gaussian integral. The outer integral is likewise dominated by the contribution near the upper limit. This may be expanded in $U'(s)$ (or $U''(s)$ if the first derivative is zero at $s$) to give an exponential integral. The final result is

$$\tau(s) \simeq \frac{1}{DU'(s)}\left(\frac{2\pi}{U''(0)}\right)^{1/2}\exp[U(s)],$$

so the prefactor of the dominant $\exp(U)$ is not necessarily close to unity, especially when the potential is large.

## References


[1] Flory, P. J., 1953, *Principles of Polymer Chemistry* (Ithaca, NY: Cornell University Press).
[2] Zimm, B. H., and Stockmayer, W. H., 1949, *J. chem. Phys.*, **17,** 1301.
[3] Edwards, S. F., 1976, Configurations and dynamics of the polymer chain. *Molecular Fluids*, edited by R. Balin and G. Weill (London: Gordon & Breach), pp. 151–208.
[4] Kuhn, W., 1934, *Kolloid Z.*, **68,** 2.
[5] Zimm, B. H., 1956, *J. chem. Phys.*, **24,** 269.
[6] Rouse, P. E., 1953, *J. chem. Phys.*, **21,** 1272.
[7] Zinn-Justin, J., 1993, *Field Theory and Critical Phenomena* (Oxford: Clarendon Press).
[8] De Gennes, P. G., 1986, *Scaling Concepts in Polymer Physics* (Ithaca, NY: Cornell University Press).
[9] Edwards, S. F., 1966, *Proc. phys. Soc. London*, **88,** 265.
[10] Adam, M., and Delsanti, M., 1984, *J. Phys. Fr.*, **45,** 1513.
[11] Verdier, P. H., and Stockmayer, W. H., 1962, *J. chem. Phys.*, **36,** 227.
[12] Ferry, J. D., 1986, *Viscoelastic Properties of Polymers* (Wiley).
[13] Treloar, L. R. G., 1975, *The Physics of Rubber Elasticity* (Oxford: Clarendon Press).
[14] Ball, R. C., Doi, M., Edwards, S. F., and Warner, M., 1981, *Polymer*, **22,** 1010.
[15] Graessley, W. W., and Pearson, D. S., 1997, *J. chem. Phys.*, **66,** 3363.
[16] Small, P. A., 1975, *Adv. polym. Sci.*, **18,** 1.
[17] Meissner, J., 1975, *Pure appl. Chem.*, **42,** 551.
[18] Hansen, D. R., Williams, M. C., and Shen, M., 1976, *Macromolecules*, **9,** 345.
[19] Edwards, S. F., 1967, *Proc. Soc. London*, **92,** 9.
[20] De Gennes, P. G., 1971, *J. chem. Phys.*, **55,** 572.
[21] De Gennes, P. G., 1975, *J. Phys. (Paris)*, **36,** 1199.
[22] Doi, M., and Edwards, S. F., 1978, *J. chem. Soc. Faraday Trans 2*, **74,** 1789; Doi, M., and Edwards, S. F., 1978, *J. chem. Soc. Faraday Trans 2*, **74,** 1802; Doi, M., and Edwards, S. F., 1978, *J. chem. Soc. Faraday Trans. 2*, **74,** 1818; Doi, M., and Edwards, S. F., 1979, *J. chem. Soc. Faraday Trans 2*, **75,** 38.
[23] For a lighthearted and alternative view of this story see: McLeish, T. C. B., 2000, *Rheol. Bull.*, **43,** 8.
[24] Kaye, A., 1962, College of Aeronautics, Cranfield, Note no. 134.
[25] Berstein, B., Kearsley, E. A., and Zapas, L. J., 1963, *Trans. Soc. Rheol.*, **7,** 391.
[26] Larson, R. G., 1990, *Constitutive Equations for Polymer Melts and Solutions* (Stoneham, MA: Butterworths).
[27] McLeish, T. C. B., and Ball, R. C., 1986, *J. polym. Sci.* B, *polym. Phys. Edn*, **24,** 1755; McLeish, T. C. B., 1987, *J. polym. Sci. polym. Phys. Edn*, **25,** 2253.
[28] Watanabe, H., and Kotaka, T., 1984, *Macromolecules*, **17,** 2316.
[29] Pearson, D. S., and Helfand, E., 1984, *Macromolecules*, **17,** 888.
[30] Graessley, W. W., 1974, *Adv. polym. Sci.*, **16,** 1.
[31] Doi, M., and Edwards, S. F., 1986, *The Theory of Polymer Dynamics* (Oxford University Press).
[32] Pearson, D. S., 1987, *Rubber Chem. Tech.*, **60,** 439.
[33] Klein, J., 1986, *Macromolecules*, **19,** 105.
[34] Lodge, T. P., Rotstein, N. A., and Prager, S., 1990, *Adv. chem. Phys.*, **79,** 1.
[35] Rubinstein, M., and McLeish, T. C. B., 1997, *Theoretical Challenges in the Dynamics of Complex Fluids*, edited by T. C. B. McLeish (Dordrecht: Kluwer), p. 21.
[36] McLeish, T. C. B., and Milner, S. T., 1998, *Adv. polym. Sci.*, **143,** 195.
[37] Watanabe, H., 1999, *Prog. polym. Sci.*, **24,** 1253.
[38] Bird, R. B., Curtiss, C., Armstrong, R., and Hassager, O., 1977, *Dynamics of Polymeric Liquids*, Vols. I and II (New York: Wiley).
[39] Larson, R. G., 1999, *The Structure and Dynamics of Complex Fluids* (Oxford: Clarendon Press).
[40] Brown, E. F., and Burghardt, W. R., 1996, *J. Rheol.*, **40,** 37.
[41] Kornfield, J., Fuller, G., and Pearson, D. S., 1989, *Macromolecules*, **22,** 1334.
[42] Higgins, J. S., and Roots, J. E., 1985, *J. chem. Soc. Faraday Trans.*, **81,** 757.
[43] Richter, D., Ewen, B., Farago, B., and Wagner, T., 1989, *Phys. Rev. Lett.*, **62,** 2140.

[44] Schleger, P., Farago, B., Lartigue, C., Kollmar, A., and Richter, D., 1998, *Phys. Rev. Lett.*, **81,** 124.
[45] Komlosh, M. E., and Callaghan, P. T., 1998, *J. chem. Phys.*, **109,** 10053.
[46] Klein, P. G., Adams, C. H., Brereton, M. G., Ries, M. E., Nicholson, T. M., Hutchings, L. R., and Richards, R. W., 1998, *Macromolecules*, **31,** 8871.
[47] Kimmich, R., Kopf, M., and Callaghan, P., 1991, *J. polym. Sci.* B, *polym. Phys. Edn.*, **29,** 1025.
[48] Adams, C. H., Brereton, M. G., Hutchings, L. R., Klein, P. G., McLeish, T. C. B., Richards, R. W., and Ries, M. E., 2000, *Macromolecules*, **33**, 7101.
[49] Muller, R., Pesce, J. J., and Picot, C., 1993, *Macromolecules*, **26,** 4356.
[50] McLeish, T. C. B., Allgaier, J., Bick, D. K., Bishko, G., Biswas, P., Blackwell, R., Blottière, B., Clarke, N., Gibbs, B., Groves, D. J., Hakiki, A., Heenan, R., Johnson, J. M., Kant, R., Read, D. J., Young, R. N., 1999, *Macromolecules*, **32,** 6734.
[51] Boué, F., Nierlich, M., Jannink, G., and Ball, R. C., 1982, *J. Phys. (Fr.)*, **43,** 137; Boué, F., Nierlich, M., Jannink, G., and Ball, R. C., 1982, *J. Phys. Lett. (Fr.)*, **43,** L585; Boué, F., Nierlich, M., Jannink, G., and Ball, R. C., 1982, *J. Phys. Lett. (Fr.)*, **43,** L593.
[52] Lodge, T. P., 1999, *Phys. Rev. Lett.*, **83,** 3218.
[53] Vlassopoulos, D., Pakula, T., Fytas, G., Roovers, J., Karatasos, K., and Hadjichristidis, N., 1997, *Europhys. Lett.*, **39,** 617.
[54] Pütz, M., Kremer, K., and Grest, G. S., 2000, *Europhys. Lett.*, **49,** 735.
[55] Skolnick, J., and Yaris, R., 1988, *J. chem. Phys.*, **881,** 1418.
[56] Milner, S. T., and McLeish, T. C. B., 1998, *Phys. Rev. Lett.*, **81,** 725.
[57] Marrucci, G., 1996, *J. non-Newt. Fluid Mech.*, **62,** 279.
[58] Mead, D. W., Doi, M., and Larson, R. G., 1998, *Macromolecules*, **31,** 7895.
[59] Likhtman, A. E., McLeish, T. C. B., and Milner, S. T., 2000, *Phys. Rev. Lett.*, **85,** 4550.
[60] Ronca, G., 1983, *J. chem. Phys.*, **79,** 1031.
[61] Schweizer, K. S., Fuchs, M., Szamel, G., Gueanza, M., and Tang, H., 1997, *Macromol. Theory Simul.*, **6,** 1037.
[62] Hess, W., 1986, *Macromolecules*, **19,** 1395; Hess, W., 1987, *Macromolecules*, **20,** 2589.
[63] Pattamaprom, C., Larson, R. G., and Van Dyke, T. J., 2000, *Rheol. Acta.*, **39,** 517.
[64] Wagner, M. H., and Schaeffer, J., 1994, *Rheol. Acta.*, **33,** 506.
[65] Martin, P. C., Parodi, G., and Pershan, P. S., 1972, *Phys. Rev.* A, **6,** 2401.
[66] Öttinger, H. C., 1996, *Stochastic Processes in Polymeric Fluids* (Berlin: Springer-Verlag).
[67] See for example Framework IV EU projects ART and LCBPolyolefins at CORDIS.
[68] Leonardi, F., Allal, A., and Marin, G., 1998, *Rheol. Acta.*, **37,** 199.
[69] Thimm, W., Friedrich, C., Marth, M., and Honerkamp, J., 1999, *J. Rheol.*, **43,** 1663.
[70] Thimm, W., Friedrich, C., Marth, M., and Honerkamp, J., 2000, *J. Rheol.*, **44,** 429.
[71] Janzen, J., and Colby, R. H., 1999, *J. mol. Structure*, **486,** 569.
[72] Read, D. J., and McLeish, T. C. B., 2001, *Macromolecules*, **34,** 1928.
[73] Wagner, M. H., Bastien, H., Ehreckhe, P., Kraft, M., Hachmann, P., and Meissner, J., 1998, *J. non-Newt. Fluid Mech.*, **79,** 283.
[74] Mhetar, V. R., and Archer, L. A., 1999, *J. non-Newt. Fluid Mech.*, **81,** 71.
[75] Marrucci, G., Greco, F., and Ianniruberto, G., 2000, *J. Rheol*, **44,** 845.
[76] Morse, D. C., 1998, *Macromolecules*, **31,** 7030.
[77] Morse, D. C., 1998, *Macromolecules*, **31,** 7044.
[78] Fetters, L. J., Lohse, D. J., and Graessley, W. W., 1999, *J. polym. Sci.* B, *polym. Phys. Edn.*, **37,** 1023.
[79] Fetters, L. J., Lohse, D. J., Milner, S. T., and Graessley, W. W., 1999, *Macromolecules*, **32,** 6847.
[80] Guth, E., and Mark, H., 1934, *Monats. Chim.*, **65,** 93.
[81] James, H., and Guth, E., 1947, *J. chem. Phys.*, **15,** 669.
[82] Agarwal, R., Horsk, J., Stejskal, J., Quadrat, O., and Kratochvil, P., 1983, *J. Appl. poly. Sci*, **28,** 3453.

[83] QUACK, G., HADJICHRISTIDIS, N., FETTERS, L. J., and YOUNG, R. N., 1980, *Ind. Eng Chem. Prod. Res. Dev*, **19,** 587.
[84] ROOVERS, J. E. L., and BYWATER, S., 1972, *Macromolecules*, **4,** 385.
[85] FETTERS, L. J., KISS, A. D., PEARSON, D. S., QUACK, G. F., and VITUS, F. J., 1993, *Macromolecules*, **26,** 647.
[86] FERNEYHOUGH, C. M., YOUNG, R. N., POCHE, D., DEGROOT, A. W., and BOSSCHER, F., 2001, *Macromolecules*, **34,** 7034.
[87] ARCHER, L. A., and VARSHNEY, S. K., 1998, *Macromolecules*, **31,** 6348.
[88] HEMPENIUS, M. A., MICHELBERGER, W., and MÖLLER, M., 1997, *Macromolecules*, **30,** 5602.
[89] STOCKMAYER, W. H., 1943, *J. chem. Phys.*, **11,** 45; STOCKMAYER, W. H., 1944, *J. chem. Phys.*, **12,** 125.
[90] RUBINSTEIN, M., COLBY, R. H., and GILLMOR, J., 1989, *Space-Time Organization in Macromolecular Fluids*, edited by F. Tanaka, T. Ohta, and M. Doi (Berlin: Springer-Verlag).
[91] LUISIGNAN, C. P., MOUREY, T. H., WILSON, J. C., and COLBY, R. H., 1999, *Phys. Rev.* E, **60,** 5657.
[92] KASEHAGEN, L. J., and MACOSKO, C. W., 1998, *J. Rheol.*, **42,** 1303.
[93] SOARES, J. B. P., and HAMILEC, A. C., 1995, *Polymer*, **36,** 2257.
[94] SOARES, J. B. P., and HAMILEC, A. C., 1996, *Macromol. Theory Simul.*, **5,** 547.
[95] IEDEMA, P. D., WULKOW, M., and HOEFSLOOT, H., 2000, *Macromolecules*, **33,** 7173.
[96] FREDRICKSON, G. H., and BATES, F., 1996, *Curr. Opin. Colloid Interface Sci.*, **1,** 472.
[97] HONERKAMP, J., and WEESE, J., 1993, *J. Rheol.*, **32,** 65.
[98] MEAD, D. W., 1994, *J. Rheol.*, **38,** 1769.
[99] BOUCHAUD, J. P., 2000, *Soft and Fragile Matter*, edited by M. E. Cates and M. R. Evans (Bristol: IOP), p. 285.
[100] FIELDING, S., SOLLICH, P., and CATES, M. E., 2000, *J. Rheol.*, **44,** 277.
[101] DOI, M., 1981, *J. polym. Sci.* B, *polym. Lett. Edn.*, **19,** 265.
[102] DOI, M., 1983, *J. polym. Sci.* B, *polym. Lett. Edn.*, **21,** 667.
[103] CATES, M. E., 1994, *Structure and Flow in Surfactant Solutions*, edited by C. A. Herb and R. K. Prud'homme (Washington, DC: ACS Books), Chap. 2.
[104] REHAGE, H., and HOFFMAN, H., 1991, *Mol. Phys.*, **74,** 933.
[105] MATSUDA, T., KITAGAWA, K., INOUE, T., and ONOGI, S., 1970, *Macromolecules*, **3,** 116.
[106] MONTFORT, J.-P., MARIN, G., and MONGE, PH., 1984, *Macromolecules*, **17,** 1551.
[107] WATANABE, H., and KOTAKA, T., 1984, *Macromolecules*, **17,** 2316.
[108] KOTAKA, T., and WATANABE, H., 1985, *Macromol. Chem. Suppl.*, **14,** 179.
[109] STRUGLINSKI, M. J., and GRAESSLEY, W. W., 1985, *Macromolecules*, **18,** 2630.
[110] RUBINSTEIN, M., and COLBY, R. H., 1988, *J. chem. Phys.*, **89,** 5291.
[111] WATANABE, H., YAMAZAKI, M, YOSHIDA, H., and KOTAKA, T., 1991, *Macromolecules*, **24,** 5573.
[112] TUMINELLO, W. H., 1986, *Polym. Eng. Sci.*, **26,** 1339.
[113] TSENOGLU, C., 1991, *Macromolecules*, **24,** 1762.
[114] DES CLOISEAUX, J., 1990, *Macromolecules*, **23,** 3992.
[115] DES CLOISEAUX, J., 1990, *Macromolecules*, **23,** 4678.
[116] DE GENNES, P. G., 1975, *J. Phys. (Paris)*, **36,** 1199.
[117] GRAESSLEY, W. W., 1982, *Adv. polym. Sci.*, **47,** 68.
[118] DANIELS, D. R., MCLEISH, T. C. B., KANT, R., CROSBY, B. J., YOUNG, R. N., PRYKE, A., ALLGAIER, A., GROVES, D. J., and HAWKINS, R. J., 2001, *Rheol. Acta*, **40,** 403.
[119] KRAUS, G., and GRUVER, J. T., 1965, *J. polym. Sci.*, **A3,** 105.
[120] GRAESSLEY, W. W., MASUDA, T., ROOVERS, J. E. L., and HADJICHRISTIDIS, N., 1976, *Macromolecules*, **9,** 127.
[121] GRAESSLEY, W. W., and ROOVERS, J. E. L., 1979, *Macromolecules*, **12,** 959.
[122] ROOVERS, J. 1984, *Macromolecules*, **17,** 1196.
[123] ROOVERS, J., and GRAESSLEY, W. W., 1981, *Macromolecules*, **14,** 766.
[124] ISLAM, M. T., JULIANI, ARCHER, L. A., and VARSHNEY, S. K, 2001, *Macromolecules*, **34,** 6438.

[125] Gabriel, C., and Münstedt, H., 1999, *Rheol. Acta.*, **38,** 393.
[126] Menezes, E. V., and Graessley, W. W., 1982, *J. polym. Sci.* B, *polym. Phys. Edn.*, **20,** 1817.
[127] Osaki, K., Inoue, T., and Isomura, T., 2000, *J. polym. Sci.* B, *polym. Phys. Edn.*, **38,** 1917.
[128] Pattamaprom, C., and Larson, R. G., 2001, *Macromolecules*, **34,** 5229.
[129] Osaki, K., Inoue, T., and Isomura, T., 2000, *J. polym. Sci.* B, *polym. Phys. Edn.*, **38,** 2043.
[130] Bercea, M., Peiti, C., Dimionescu, B., and Navard, P., 1993, *Macromolecules*, **26,** 7095.
[131] Petrie, C. J. S., 1979, *Extensional Flows* (London: Pitman).
[132] Münstedt, H., 1979, *J. Rheol.*, **23,** 421.
[133] Sridhar, T., Tirtaatmadja, V., Nguyen, D. A., and Gupta, R. K., 1991, *J. non-Newtonian fluid Mech.*, **40,** 271.
[134] Spiegelberg, S. H., and McKinley, G. H., 1996, *J. non-Newt. fluid Mech.*, **67,** 49.
[135] Anna, S. L., McKinley, G. H., Nguyen, D. A., Sridhar, T., Muller, S. J., Huang, J., and James, D. F., 2001, *J. Rheol.*, **45,** 83.
[136] Meissner, J., 1997, *Rheology*, **5,** 120.
[137] Schulze, J. S., Lodge, T. P., Macosko, C. W., Hepperle, J., Münstedt, H., Bastian, H., Ferri, D., Groves, D. J., Kim, Y. H., Lyon, M., Schwiezer, T., Virkler, T., Wassner, E., and Zoetelief, W., 2001, *Rheol. Acta*, **40,** 457.
[138] Laun, H. M., and Schuch, H., 1989, *J. Rheol.*, **33,** 119.
[139] Wagner, M. H., Ehrecke, P., Hachmann, P., and Meissner, J., 1998, *J. Rheol.*, **42,** 621.
[140] Pearson, D. S., Herbolzheimer, E., Grizutti, N., and Marrucci, G., 1991, *J. polym. Sci.* B, *polym. Phys. Edn.*, **29,** 1589.
[141] McLeish, T. C. B., and Larson, R.G., 1998, *J. Rheol.*, **42,** 81.
[142] Osaki, K., 1993, *Rheol. Acta.*, **32,** 429.
[143] Osaki, K., Nishizawa, K., and Kurata, M., 1982, *Macromolecules*, **15,** 1068.
[144] Fukuda, M., Osaki, K., and Kurata, M., 1975, *J. polym. Sci.* B, *polym. Phys. Edn.*, **13,** 1563.
[145] Archer, L. A., 1999, *J. Rheol.*, **43,** 1555.
[146] Osaki, K., Takatori, E., Kurata, M., Watanabe, H., Yoshida, H., and Kotaka, T., 1990, *Macromolecules*, **23,** 4392.
[147] Wagner, M. H., and Ehrecke, P., 1998, *J. non-Newtonian fluid Mech.*, **67,** 183.
[148] Osaki, K., Kimura, S., Kimura, M., and Kurata, M., 1981, *J. Rheol.*, **25,** 549.
[149] Doi, M., 1980, *J. polym. Sci.* B, *polym. Phys. Edn.*, **18,** 2055.
[150] Janeschitz-Kriegl, H., 1983, *Polymer Melt Rheology and Flow Birefringence* (New York: Springer).
[151] Venerus, D. C., Zhu, S.-H., and Öttinger, H. C., 1999, *J. Rheol.*, **43,** 795.
[152] Lee, K., Mackley, M. R., McLeish, T. C. B., Nicholson, T. M., and Harlen, O. G., 2001, *J. Rheol.*, **45,** 1261.
[153] Verbeeten, W. M. H., Peters, G. W. M., and Baaijens, F. P. T., 2001, *J. Rheol.*, **45,** 823.
[154] Macosko, C. W., 1994, *Rheology Principles, Measurements and Applications* (New York: Wiley).
[155] Marrucci, G., and Hermans, J. J., 1980, *Macromolecules*, **13,** 380.
[156] Magda, J. J., Lee, C.-S., Muller, S. J., and Larson, R. G., 1993, *Macromolecules*, **26,** 1696.
[157] Tassin, J. F., Monnerie, L., and Fetters, L. J., 1986, *Polym. Bull.*, **15,** 165.
[158] Lantman, C. W., Tassin, J. F., Monnerie, L., Fetters, L. J., Helfand, E., and Pearson, D. S., 1989, *Macromolecules*, **22,** 1184.
[159] Ylitalo, C. M., Kornfield, J., Fuller, G., and Pearson, D. S., 1991, *Macromolecules*, **24,** 749.
[160] Ekanayake, P., Menge, H., Korner, S., Schneider, H., Ries, M. E., Brereton, M. G., 2001, *Macromolecules*, **34,** 4683.

[161] Doi, M., Pearson, D. S., Kormfield, J., and Fuller, G., 1989, *Macromolecules*, **22,** 1488.
[162] Doi, M., and Watanabe, H., 1991, *Macromolecules*, **24,** 740.
[163] Wignall, G. D., Ballard, D. G. H., and Schelten, J., 1974, *Eur. polym. J.*, **10,** 861.
[164] Cotton, J. P., Decker, D., Benoit, H., Farnoux, B., Higgins, J. S., Jannink, G., Ober, R., Picot, C., and Des Cloiseaux, J., 1974, *Macromolecules*, **7,** 863.
[165] Debye, P., 1947, *J. Phys. Colloid Chem.*, **51,** 18.
[166] Higgins, J. S., and Benoit, H., 1994, *Polymers and Neutron Scattering* (Oxford: Clarendon Press).
[167] De Gennes, P. G., 1967, *Physics*, **3,** 37.
[168] De Gennes, P.-G., 1981, *J. Physique*, **42,** 735.
[169] Wischnewski, A., Monkenbusch, M., Willner, L., Richter, D., Likhtman, A. E., McLeish, T. C. B., and Farago, B., 2001, *Phys. Rev. Lett.* (submitted).
[170] Brochard, F., and De Gennes, P. G., 1977, *Macromolecules*, **10,** 1157.
[171] Adam, M., and Delsanti, 1985, *Macromolecules*, **18,** 1760.
[172] Brown, W., and Nicolai, T., 1993, *Dynamic Light Scattering. The Method and Some Applications*, edited by W. Brown (Oxford).
[173] Doi, M., and Onuki, A., 1992, *J. Phys. II Fr.*, **2,** 1631.
[174] Semenov, A. N., 1990, *Physica A*, **166,** 263; Semenov, A. N., 1997, *Theoretical Challenges in the Dynamics of Complex Fluids*, edited by T. C. B. McLeish (Dordrecht: Kluwer), p. 77.
[175] Jian, T., Vlassopoulos, D., Fytas, G., Pakula, T., and Brown, W., 1996, *Colloid polym. Sci.*, **274,** 1033.
[176] Buhler, E., Munch, J. P., and Candau, S. J., 1995, *J. Phys. II Fr.*, **5,** 765.
[177] Watanabe, H., 2001, *Macromol. rapid commun.*, **22,** 172.
[178] Stockmayer, W. H., 1967, *Pure appl. Chem.*, **15,** 539.
[179] Watanabe, H., Urakawa, O., and Kotaka, T., 1993, *Macromolecules*, **26,** 5073.
[180] Yoshida, H., Adachi, H., Watanabe, H., and Kotaka, T., 1989, *Polym. J.*, **21,** 863.
[181] Matsumia, Y., Watanabe, H., and Osaki, K., 2000, *Macromolecules*, **33,** 499.
[182] Watanabe, H., Urakawa, O., and Kotaka, T., 1994, *Macromolecules*, **27,** 3525.
[183] Adachi, K., Yoshida, H., Fukui, F., and Kotaka, T., 1990, *Macromolecules*, **23,** 3138.
[184] Watanabe, H., Urakawa, O., Yamada, H., and Yao, M.-L., 1996, *Macromolecules*, **29,** 755.
[185] Matsumiya, Y., Watanabe, H., Osaki, K., and Yao, M.-L., 1998, *Macromolecules*, **31,** 7538.
[186] Yoshida, H., Watanabe, H., Adachi, H., and Kotaka, T., 1991, *Macromolecules*, **24,** 2981.
[187] Matsumiya, Y., Watanabe, H., Osaki, K., and Yao, M.-L., 1998, *Macromolecules*, **31,** 7528.
[188] Watanabe, H., Matsumiya, Y., and Osaki, K., 2000, *J. polym. Sci.* B, *polym. Phys. Edn.*, **38,** 1024.
[189] Watanabe, H., Matsumiya, Y., and Osaki, K., 2002, *Macromolecules*, **35,** 2339.
[190] Milner, S. T., and McLeish, T. C. B., 1997, *Macromolecules*, **30,** 2159.
[191] Frischknecht, A., and Milner, S. T., 2002, *Macromolecules*, **33,** 9764.
[192] McLeish, T. C. B., *J. Rheol.* (submitted).
[193] Shanbhag, S., Larson, R. G., Takimoto, J., and Doi, M., 2001, *Phys. Rev. Lett.*, **87,** 195502.
[194] Cohen Addad, J. P., and Dupreyre, R., 1983, *J. Phys. I, Fr.*, **24,** 400.
[195] Brereton, M., 1990, *Macromolecules*, **23,** 1119.
[196] Brereton, M., 1991, *J. chem. Phys.*, **94,** 213.
[197] Ball, R. C., Callaghan, P. T., and Samulski, E. T., 1997, *J. chem. Phys.*, **106,** 7352.
[198] Callaghan, P. T., Kilfoil, M. L., and Samulski, E. T., 1998, *Phys. Rev. Lett.*, **81,** 4524.
[199] Cormier, R. J., Kilfoil, M. L., and Callaghan, P. T., 2001, *Phys. Rev.* E, **64,** 051908.

[200] KLEIN, J., 1978, *Macromolecules*, **11,** 852.
[201] BARTELS, C. B., CRIST, B., FETTERS, L. J., and GRAESSLEY, W. W., 1986, *Macromolecules*, **19,** 785.
[202] MILS, P. J., GREEN, P. F., PALMSTR9M, C., MAYER, J. W., and KRAMER, E. J., 1984, *J. appl. Phys. Lett.*, **45,** 957.
[203] WHITLOW, S. J., and WOOL, R. P., 1989, *Macromolecules*, **22,** 2648.
[204] WELP, K. A., WOOL, R. P., SATIJA, S. K., PISPAS, S., and MAYS, J., 1998, *Macromolecules*, **31,** 4915.
[205] BACHUS, R., and KIMMICH, R., 1983, *Polymer*, **24,** 964.
[206] ANTONIETTI, M., COUTANDIN, J., and SILLESCU, H., 1986, *Macromolecules*, **19,** 793.
[207] WHEELER, L. M., and LODGE, T. P., 1989, *Macromolecules*, **22,** 3399.
[208] NEMOTO, N., KOJIMA, T., INOUE, T., KISHINE, M., KIRAYAMA, T., and KURATA, M., 1989, *Macromolecules*, **122,** 3793.
[209] GREEN, P. F., and KRAMER, E. J., 1986, *Macromolecules*, **19,** 1108.
[210] KLEIN, J., and FLETCHER, D., 1983, *Nature*, **304,** 5926.
[211] ANTONIETTI, M., and SILESCU, H., 1986, *Macromolecules*, **19,** 798.
[212] WHITTINGTON, S. G., 1998, *Numerical Methods for Polymeric Systems*, The IMA Volumes in Mathematics and its Applications (New York: Springer).
[213] KREMER, K., and BINDER, K., 1988, *Comp. Phys. Rep.*, **7,** 259.
[214] KREMER, K., 2000, *Soft and Fragile Matter*, edited by M. E. Cates and M. R. Evans (Bristol: IOP), p. 145.
[215] EVANS, K. E., and EDWARDS, S. F., 1981, *J. chem. Soc., Faraday Trans.*, **2,** 1891.
[216] KREMER, K., and GREST, G. S., 1990, *J. chem. Phys.*, **92,** 5057.
[217] KRÖGER, M., and HESS, S., 2000, *Phys. Rev. Lett.*, **85,** 1128.
[218] SCHAFFER, J. S., 1995, *J. chem. Phys.*, **103,** 761.
[219] KREER, T., BASCHNAGEL, J., MÜLLER, M., and BINDER, K., 2001, *Macromolecules*, **34,** 1105.
[220] BROWN, S., LENCZYCKI, T., and SZAMEL, G., 2001, *Phys. Rev.* E, **63,** 052801.
[221] RUBINSTEIN, M., 1987, *Phys. Rev. Lett.*, **59,** 1946.
[222] DEUTSCH, J. M., and MADDEN, T. L., 1989, *J. chem. Phys.*, **91,** 3252.
[223] O'CONNOR, N. P. T., and BALL, R. C., 1992, *Macromolecules*, **25,** 5677.
[224] KETZMERICK, R., and ÖTTINGER, H.-C., 1989, *Continuum Mech Thermodyn*, **1,** 113.
[225] HUE, C. C., and SCHIEBER, J. D., 1998, *J. chem. Phys.*, **109,** 10018; HUA, C. C., and SCHIEBER, J. D., 1998, *J. chem. Phys.*, **109,** 10028.
[226] HUA, C. C., SCHIEBER, J. D., and VENERUS, D. C., *J. Rheol.*, **43,** 701.
[227] HUA, C. C., and KUO, H. Y., 2000, *J. polym. Sci.* B, *polym. Phys. Edn.*, **38,** 248.
[228] MASUBUCHI, Y., TAKIMOTO, J.-I., KOYAMA, K., IANNIRUBERTO, G., GRECO, F., and MARRUCCI, G., 2001, *J. chem. Phys.*, **115,** 4387.
[229] SHANBHAG, S., LARSON, R. G., TAKIMOTO, J., and DOI, M., 2001, *Phys. Rev. Lett.*, **87,** 195502.
[230] MCLEISH, T. C. B., 1988, *Macromolecules*, **21,** 3639.
[231] WATANABE, H., URAKAWA, O., and KOTAKA, T., 1993, *Macromolecules*, **26,** 5073.
[232] PAUL, P. E., SMITH, G. D., YOON, D. Y., FARAGO, B., RATHGEBER, S., ZIRKEL, A., WILNER, L., and RICHTER, D., 1998, *Phys. Rev. Lett.*, **80,** 2346.
[233] STÜHN, B., EWEN, B., and RICHTER, D., 1986, *Z. Phys.* B, **58,** 305.
[234] RICHTER, D., MONKENBUSCH, M., ALLGEIER, J., ARBE, A., COLMENERO, J., FARAGO, B., CHEOL BAE, Y., and FAUST, R., 1999, *J. chem. Phys.*, **111,** 6107.
[235] INOUE, T., and OSAKI, K., 1996, *Macromolecules*, **29,** 1595.
[236] EDWARDS, S. F., 1977, *Polymer*, **6,** 143.
[237] DOI, M., and KUZUU, N. Y., 1980, *J. polym. Sci., polym. Lett. Edn.*, **18,** 775.
[238] HELFAND, E., and PEARSON, D. S., 1983, *J. chem. Phys.*, **79,** 2054.
[239] RUBINSTEIN, M., and HELFAND, E., 1985, *J. chem. Phys.*, **82,** 2477.
[240] MEHTA, A., NEEDS, R. J., and THOULESS, D. J., 1991, *Europhys. Lett.*, **14,** 113.
[241] KHOKHLOV, A. R., and NECHAEV, S. K., 1985, *Phys. Lett.*, **112A,** 156.
[242] SEMENOV, A. N., and YURASOVA, T. A., 1987, *Visokomol. Soed.*, **29B,** 175.
[243] ZHELIGOVSKAYA, E. A., TERNOVSKII, F. F., and KHOKHLOV, A. R., 1988, *Theo. Math. Phys.*, **75,** 461.
[244] NECHAEV, S. K., SEMENOV, A. N., and KOLEVA, M. K., 1987, *Physica* A, **140,** 506.

[245] LEVINE, A. J., and MILNER, S. T., 1998, *Macromolecules*, **31,** 8623.
[246] CATES, M. E., 1987, *Macromolecules*, **20,** 2289; CATES, M. E., 1990, *J. Phys. Chem.*, **94,** 371.
[247] LIKHTMAN, A. E., and MCLEISH, T. C. B., 2002, *Macromolcules*, **35,** DOI 10.1021/ma0200219 (to be published).
[248] CLARKE, N., and MCLEISH, T. C. B., 1993, *Macromolecules*, **26,** 5264.
[249] KLEIN, P. G., ROBERTSON, M. B., DRIVER, M. A. N., WARD, I. M., and PACKER, K. J., 1998, *Polym. Int.*, **47,** 76.
[250] WATANABE, H., and TIRRELL, M., 1989, *Macromolecules*, **22,** 927.
[251] RICHTER, D., personal communication.
[252] WISCHNEWSKI, A., and RICHTER, D., 2000, *Europhys. Lett.*, **52,** 719; PÜTZ, M., KREMER, K., and GREST, G. S., 2000, *Europhys. Lett.*, **52,** 721.
[253] KAVASSALIS, T. A., and NOOLANDI, J., 1988, *Macromolecules*, **21,** 2869.
[254] ROOVERS, J., 1987, *Macromolecules*, **20,** 148.
[255] WATANABE, H., YOSHIDA, H., and KOTAKA, T., 1992, *Macromolecules*, **25,** 2442.
[256] DAOUD, M., and DE GENNES, P. G., 1979, *J. polym. Sci.* B, *polym. Phys. Edn.*, **17,** 1981.
[257] GRAESSLEY, W. W., and STRUGLINSKI, M. J., 1986, *Macromolecules*, **19,** 1754.
[258] RUBINSTEIN, M., HELFAND, E., and PEARSON, D. S., 1987, *Macromolecules*, **19,** 1754.
[259] DOI, M., GRAESSLEY, W. W., HELFAND, E., and PEARSON, D. S., 1987, *Macromolecules*, **20,** 1900.
[260] VIOVY, J. L., RUBINSTEIN, M., and COLBY, R. H., 1991, *Macromolecules*, **24,** 3587.
[261] MARRUCCI, G., 1985, *J. polym. Sci.* B, *polym. Phys. Edn.*, **23,** 159.
[262] BROCHARD-WYART, F., AJDARI, A., LEIBLER, L., RUBINSTEIN, M., and VIOVY, J. L., 1994, *Macromolecules*, **27,** 803.
[263] DEAN, P., 1964, *Proc. phys. Soc.*, **84,** 727.
[264] SCHAUSBERGER, A., SCHNINDLAUER, G., and JANESCHITZ-KRIEGL, H., 1986, *Rheol. Acta.*, **24,** 1985.
[265] ROOVERS, J. E. L., 1981, *Polymer*, **22,** 1603.
[266] PAKULA, T., VLASSOPOULOS, D., FYTAS, G., and ROOVERS, J., 1998, *Macromolecules*, **31,** 8931.
[267] ROOVERS, J., 1994, *Macromolecules*, **27,** 5359.
[268] KRAMERS, H. A., 1940, *Physica (Amsterdam)*, **7,** 284.
[269] HANGGI, P., TALKNER, P., and BORKOVEC, M., 1990, *Rev. mod. Phys.*, **62,** 251.
[270] LIKHTMAN, A. E., 2001, personal communication.
[271] PEARSON, D. S., and HELFAND, E., 1984, *Macromolecules*, **19,** 888.
[272] BALL, R. C., and MCLEISH, T. C. B., 1989, *Macromolecules*, **22,** 1911.
[273] MILNER, S. T., and MCLEISH, T. C. B., 1998, *Macromoleules*, **31,** 7479.
[274] VEGA, D. A., SEBASTIAN, J. M., RUSSEL, W. B., and REGISTER, R. A., 2002, *Macromolecules*, **35,** 169.
[275] MILNER, S. T., MCLEISH, T. C. B., JOHNSON, J., HAKIKI, A., and YOUNG, R. N., 1998, *Macromolecules*, **31,** 9345.
[276] ADAMS, C. H., HUTCHINGS, L. R., KLEIN, P. G., MCLEISH, T. C. B., and RICHARDS, R. W., 1996, *Macromolecules*, **29,** 5717.
[277] BLOTTIÈRE, B., MCLEISH, T. C. B., HAKIKI, A., YOUNG, R. N., and MILNER, S. T., 1998, *Macromolecules*, **31,** 9295.
[278] STRUGLINSKI, M. J., GRAESSLEY, W. W., and FETTERS, L. J., 1988, *Macromolecules*, **21,** 783.
[279] FRISCHKNECHT, A. L., and MILNER, S. T., 2000, *Macromolecules*, **33,** 5273.
[280] RUBINSTEIN, M., 1986, *Phys. Rev. Lett.*, **57,** 3023.
[281] SHULL, K. R., KRAMER, E. S., and FETTERS, L. J., 1990, *Nature*, **345,** 790.
[282] GELL. C. B. GRAESSLEY, W. W., EFSTRATIADIS, V., PITSIKALIS, M., and HADJICHRISTIDIS, N., 1997, *J. polym. Sci.* B, **35,** 1943.
[283] FRISCHKNECT, A., MILNER, S. T., PRYKE, A., YOUNG, R. N., HAWKINS, R., and MCLEISH, T. C. B., 2002, *Macromolecules*, **35,** 4801.
[284] PORTER, R. S., KNOX, J. P., and JOHNSON, J. F., 1968, *Trans. Soc. Rheol.*, **12,** 409.
[285] RAJU, V. R., RACHAPUDY, H., and GRAESSLEY, W. W., 1979, *J. polym. Sci.* B, *polym. Phys. Edn.*, **17,** 1223.

[286] Graessley, W. W., and Raju, V. R., 1984, *J. polym. Sci.* B, *polymer Symposium*, **17,** 1981.
[287] Carella, J. M., Gotro, J. T., and Graessley, W. W., 1986, *Macromolecules*, **19,** 659.
[288] Fetters, L. J., Graessley, W. W., Krishnamoorti, R., and Lohse, D. J., 1997, *Macromolecules*, **30,** 4973.
[289] Santagelo, P. G., and Roland, C. M., 1998, *J. non-cryst. Solids*, **235–237,** 709.
[290] Graessley, W. W., 1982, *Macromolecules*, **15,** 1164.
[291] Hakiki, A., Young, R. N., and McLeish, T. C. B., 1996, *Macromolecules*, **29,** 6348.
[292] Bick, D. K., and McLeish, T. C. B., 1996, *Phys. Rev. Lett.*, **76,** 2587.
[293] Larson, R. G., 2001, *Macromolecules*, **34,** 4556.
[294] Roovers, J., and Toporowski, P. M., 1987, *Macromolecules*, **20,** 2300.
[295] Yurasova, T. A., McLeish, T. C. B., and Semenov, A. N., 1994, *Macromolecules*, **27,** 7205.
[296] Rubinstein, M., Zurek, S., McLeish, T. C. B., and Ball, R. C., 1990, *J. Phys. (Fr.)*, **51,** 757.
[297] McLeish, T. C. B., 1988, *Europhys. Lett.*, **6,** 511.
[298] Blackwell, R. J., Harlen, O. G., and McLeish, T. C. B., 2001, *Macromolecules*, **34,** 2579.
[299] Curro, J. G., and Pincus, P., 1983, *Macromolecules*, **16,** 559.
[300] Stauffer, D., 1985, *Introduction to Percolation Theory* (Philadelphia: Taylor and Francis).
[301] Cates, M. E., 1985, *J. Phys. (Paris)*, **46,** 1059.
[302] Martin, J. E., Adolf, D., and Wilcoxon, J. P., 1988, *Phys. Rev. Lett.*, **76,** 2587.
[303] Durand, D., Delsanti, M., Adam, M., and Luck, J. M., 1987, *Europhys. Lett.*, **3,** 297.
[304] Vales, E. M., and Macosko, C. W., 1979, *Macromolecules*, **12,** 521.
[305] Mours, M., and Winter, H. H., 1996, *Macromolecules*, **29,** 7221.
[306] Nicol, E., Nicolai, T., and Durand, D., 2001, *Macromolecules*, **34,** 5205.
[307] Gasilova, E., Benyahia, L., Durand, D., and Nicolai, T., 2002, *Macromolecules*, **35,** 141.
[308] Crosby, B. J., Mangnus, M., Poche, D., De Groot, W., Daniels, D. R., and McLeish, T. C. B., 2002, *J. Rheol.*, **46,** 401.
[309] Islam, M. T., Sanchez-Reyes, J., and Archer, L. A., 2001, *J. Rheol.*, **45,** 61.
[310] Wagner, M., 1994, *J. Rheol*, **38,** 655.
[311] Straube, E., Urban, V., Pyckhout-Hinzen, W., Richter, D., and Glinka, C. J., 1995, *Phys. Rev. Lett.*, **74,** 4464.
[312] Rubinstein, M., and Panyukov, S., 1997, *Macromolecules*, **30,** 8036.
[313] Everaers, R., 1998, *Eur. Phys. J.* B, **4,** 341.
[314] Osaki, K., Kimura, S., Nishizawa, K., and Kurata, M., 1981, *Macromolecules*, **14,** 456.
[315] Vrentas, C. M., and Graessley, W. W., 1982, *J. Rheol*, **26,** 359.
[316] Marrucci, G., and Grizzuti, N., 1983, *J. Rheol*, **27,** 433.
[317] Bray, A. J., 200, *Soft and Fragile Matter*, edited by M. E. Cates and M. R. Evans, (Edinburgh/Bristol: SUSSP/IoP).
[318] Wagner, M. H., 1976, *Rheol. Acta.*, **15,** 136; Wagner, M. H., 1977, *Rheol. Acta.*, **16,** 43.
[319] Fischer, E., and Callaghan, P. T., 2001, *Phys. Rev.* E, **63,** 6401.
[320] Doi, M., 1980, *J. polym. Sci.*, **18,** 2055.
[321] Helfand, E., and Pearson, D. S., 1982, *J. polym. Sci.*, **20,** 1249.
[322] Pearson, D. S., and Rochefort, W. E., 1982, *J. polym. Sci.* B, *polym. Phys. Edn.*, **20,** 83.
[323] Marrucci, G., and Grizzuti, N., 1988, *Gazz. Chim. Ital.*, **118,** 179.
[324] Ianniruberto, G., and Marrucci, G., 1996, *J. non-Newt. Fluid. Mechan.*, **65,** 241.
[325] Pattamaprom, C., and Larson, R. G., 2001, *Macromolecules*, **34,** 5229.
[326] Milner, S. T., McLeish, T. C. B., and Likhtman, A. E., 2001, *J. Rheol.*, **45,** 539.
[327] Graham, R. S., Likhtman, A. E., McLeish, T. C. B., and Milner, S. T., 2003, *J. Rheol.*, to be published.

[328] LARSON, R. G., 1987, *J. non-Newt. Fluid Mech.*, **23,** 249.
[329] SAMURKAS, T., LARSON, R. G., and DEALY, J. M., 1989, *J. Rheol*, **33,** 559.
[330] RUBIO, P., and WAGNER, M. H., 2000, *J. non-Newt. Fluid. Mech.*, **92,** 245.
[331] BISHKO, G., MCLEISH, T. C. B., HARLEN, O. G., and LARSON, R. G., 1997, *Phys. Rev. Lett.*, **79,** 2352.
[332] INKSON, N. J., MCLEISH, T. C. B., GROVES, D. J., and HARLEN, O. G., 1999, *J. Rheol.*, **43,** 873.
[333] BLACKWELL, R. J., MCLEISH, T. C. B., and HARLEN, O. G., 2000, *J. Rheol.*, **44,** 121.
[334] GRAHAM, R. S., MCLEISH, T. C. B., and HARLEN, O. G., 2001, *J. Rheol.*, **45,** 275.
[335] MCKINLEY, G. H., and HASSAGER, O., 1999, *J. Rheol.*, **43,** 1195.
[336] READ, D. J., and BLACKWELL, R. J., 2002, personal communication.
[337] READ, D. J., 1999, *Eur. J. Phys.* B, **12,** 431.
[338] HEINRICH, M., PYCKHOUT-HINZEN, W., RICHTER, D., STRAUBE, E., READ, D. J., MCLEISH, T. C. B., GROVES, D. J., BLACKWELL, R. J., WIEDENMANN, A., 2002, *Macromolecules*, **35,** DOI 10.1021/ma011923x (to be published).
[339] RASMUSSEN, H. K., and HASSAGER, O., 1993, *J. non-Newt. fluid Mech.*, **46,** 63.
[340] YUAN, X. F., BALL, R. C., and EDWARDS, S. F., 1993, *J. non-Newt. fluid Mech.*, **46,** 331.
[341] HARLEN, O. G., RALLISON, J. M., and SZABO, P., 1995, *J. non-Newt. fluid Mech.*, **60,** 81.
[342] WAPPEROM, P., KEUNINGS, R., *J. non-Newt. Fluid. Mech.*, 2001, **97,** 267.
[343] LIELENS, G., KEUNINGS, R., and LEGAT, V., 1999, *J. non-Newt. Fluid. Mech.*, **87,** 179.
[344] LARSON, R. G., HU, H., SMITH, D. E., and CHU, S., 1999, *J. Rheol.*, **43,** 267.
[345] READ, D. J., and MCLEISH, T. C. B., 1997, *Macromolecules*, **30,** 6376.
[346] ÖTTINGER, H. C., 2001, *Reol. Acta*, **40,** 317.
[347] MARRUCCI, G., and IANNIRUBERTO, G., 1999, *J. non-Newt. fluid Mech.*, **82,** 275.
[348] MILNER, S. T., 2001, *J. Rheol.*, **45,** 1023.
[349] HOHENBERG, P. C., and HALPERIN, B. I., 1977, *Rev. mod. Phys.*, **49,** 435.
[350] BERIS, A. N., and EDWARDS, B. J., 1990, *J. Rheol.*, **34,** 503.
[351] SCHIEBER, J. C., and ÖTTINGER, H. C., 1994, *Rheol. Acta*, **38,** 1909.
[352] PRAGER, S., and FRISCH, H. L., 1967, *J. chem. Phys.*, **46,** 1475.
[353] IWATA, K., 1982, *J. chem. Phys.*, **76,** 6363; IWATA, K., 1985, *J. chem. Phys.*, **83,** 1969.
[354] IWATA, K., and EDWARDS, S. F., 1989 *J. chem. Phys.*, **90,** 4567.
[355] BRERETON, M. G., and FILBRANDT, M., 1986, *Polymer*, **26,** 1134.
[356] MÜLLER-NEEDEBOCK, K. K., and EDWARDS, S. F., 1999, *J. phys.* A: *Math. Gen.*, **32,** 3301.
[357] VOLOGODSKII, A. V., LUKASHIN, A. V., and FRANK-KAMANETSKII, M. D., 1975, *Sov. Phys.–JETP*, **40,** 932.